Biosonar of narrow-band high-frequency toothed whales: Sampling a dynamic, multi-target world

Chloe Malinka

PhD Dissertation

Aarhus University 2021

Biosonar of narrow-band high-frequency toothed whales: Sampling a dynamic, multi-target world

PhD Dissertation

Chloe Malinka

Section for Zoophysiology,
Department of Biology,
Graduate School of Natural Sciences,
Aarhus University, Denmark

April 2021

Data Sheet

Title	Biosonar of narrow-band high-frequency toothed whales: Sampling a dynamic, multi-target world
Author	Chloe Malinka
Supervisor	Professor Peter Teglberg Madsen
Affiliation	Zoophysiology, Department of Biology Aarhus University, Denmark
Publication year	2021
Keywords	Echolocation, auditory scene analysis, spatial filtering, beam pattern, phantom targets, optimal localization, source parameter quantification, gain control, hydrophone array, biologging, dwarf sperm whale, *Kogia*, porpoise, *Phocoena*
Publisher	Aarhus University
Printed by	AU TRYK
Number of pages	206
Front page art	Catherine J. A. Williams
Cite as	Malinka, C. (2021). PhD Dissertation. Biosonar of narrow-band high-frequency toothed whales: Sampling a dynamic, multi-target world. Department of Biology, Aarhus University, Denmark

Table of Contents

The objective world simply is, it does not happen.
Only to the gaze of my consciousness,
crawling along the lifeline of my body,
does a section of this world come to life
as a fleeting image in space
which continuously changes in time.

– Hermann Weyl, 1949

Preface

This PhD dissertation is submitted to the Graduate School of Natural Sciences (GSNS) at Aarhus University to meet the partial requirements for the Doctor of Philosophy (PhD) degree. This thesis was carried out from March 2017 to April 2021 under the supervision of Professor Peter Teglberg Madsen at the Section for Zoophysiology, Dept. of Biology, Aarhus University. The findings have been produced in collaboration with [inter]national colleagues whose contributions as [co-]authors are recognized in the individual chapters. The degree of my contributions are clarified in the co-author statements.

I was introduced to bioacoustics through the acoustical oceanography lab at Dalhousie University, Canada, where I worked with industry to investigate passive acoustic technologies for tracking animals in the vicinity of marine renewable energy devices to work towards a net zero future that is respectful of the marine environment. My continual referral to related and advanced applied research coming out of Scotland prompted me to study and work with researchers at the Sea Mammal Research Unit within the University of St Andrews, who formalized my introduction to academic bioacoustic studies. Here, I worked on challenging projects involving using the latest technological advancements to track toothed whale movements and behaviours in fine-scale via their echolocation clicks. A proportional chunk of this work was informed by research on porpoise source parameters and biosonar behaviour coming out of what seemed to be a very fruitful lab in Denmark. Presenting some of this research at an SMM conference in San Francisco in 2015 lead to meeting Peter, and thereby to my PhD at AU.

In Peter's Bioacoustics AU research group, my focus shifted from how researchers can use echolocation clicks to understand what the animals are doing to how researchers can use echolocation clicks to understand how the animal can dynamically manipulate its perception of its surroundings. This dissertation picks up here, focusing on basic research questions with findings relevant for direct applications regarding passive acoustic monitoring accessibility and understanding by-catch. Specifically, this PhD includes the development of deep-sea acoustics kit, source parameter and beam pattern quantifications, biosonar behaviour compensation under acoustically complex, cluttered and noisy scenarios, as well as investigations into spatial filtering, auditory scene segregation, and localization strategies used by echolocating toothed whales.

This thesis comprises an introduction (**Ch. I**), where I review and discuss my findings in a broader context, followed by eight chapters (**Ch. II-IX**), four of which I am first-author, two of which I am second-author, and two on which I am a tertiary author. These are in the form of published research articles (four), submitted manuscripts (one), manuscripts drafted for international peer-reviewed journals and are close to submission (two), and a progress report of an on-going study (one). The Supplementary Materials accompanying published papers are available online, and those accompanying drafted manuscripts are included herein.

Aarhus, Denmark, April 2021

CHLOE ELIZABETH MALINKA

Acknowledgements

Big thanks are due to my supervisor, Professor Peter Teglberg Madsen, for his enthusiasm, research guidance, striking acoustic skills, and can-do attitude. I really appreciate his trust and encouragement, and aspire to having such a broadscale understanding of biology. Big thanks also to Dr Kristian Beedholm, who has provided helpful research support and sharpened my analysis skills.

I would like to extend gratitude to the Graduate School of Natural Sciences at Aarhus University, the Danish Council for Independent Research, and the Danish National Research Foundation (FNU) for funding my PhD. I am thankful to ONR, Oticon Fonden, the William Demant Foundation, the British Ecological Society, the Danish Acoustical Society, the Acoustical Society of America, the Society of Marine Mammalogy, and PeerJ, who have all supported me in conducting research, participating in conferences, and collecting data in the field. Thanks a bunch to my mentors Dr Doug Gillespie, Dr Carol Sparling, and Dr Mark Johnson, whose letters of support welcomed me into the PhD program at Aarhus University.

I would like to acknowledge the discussions with, and support of, all of my co-authors: Professor Peter T Madsen, Dr Kristian Beedholm, Dr Mark Johnson, Dr Doug Gillespie, Mr John Atkins, Dr Charlotte Dunn, Dr Diane Claridge, Dr Natacha Aguilar de Soto, Dr Jamie Macaulay, Dr Line Hermannsen, Dr Pernille Tønnesen, Dr Michael Ladegaard, Dr Laia Rojano-Doñate, Dr Jakob Tougaard, Dr Tess Gridley and Dr Simon H Elwen. Many thanks also to the workshop expertise of John Svane Jensen, Lasse Vestergaard Sørensen, Mehram Jahanara, and Niels Kristiansen for their help in gear preparations for lab experiments and field work.

I am grateful to the team at Fjord & Bælt, notably the research porpoises (Freja and the late Sif), Josefin Larsson, Fredrik Johansson, Mathilde Kjølby, and Jakob Højer Kristensen for their cooperation and assistance in conducting several experiments with me. Many thanks to Associate Professor Magnus Wahlberg for patiently allowing me (and my equipment) to occasionally overtake his SDU office in Kerteminde, and for his helpful and critical feedback as the opponent at my halfway PhD defence. Thanks to Dr Natacha Aguilar de Soto, Dr Jonas Teilmann and Dr Jakob Tougaard for lending me some of their research equipment along the way.

Thanks to Associate Professor Jeremy Goldbogen, for briefly hosting me at Stanford's Hopkins Marine Station, California, USA. Thanks to the professors and instructors of the 'SNAK' acoustics methods course in Denmark, the noise quantification workshop, and the inertial sensing workshop, both at Aarhus University, and those who taught the Sensory Ecology course at Lund University, Sweden. What a treat it has been to connect with the bioacoustic students across these courses.

Thanks to Professor Peter Tyack, Professor John R. Buck, and Dr. K Alex Shorter for constructive comments on early results from the spatial filtering and phantom targets studies, and to Dr Thomas Götz for guiding my attention to auditory attention. Hugs and thanks to Dr Charlotte Dunn and Dr Diane Claridge for their collaboration on the *Kogia* project and hosting me (and all of my gear) in their home for over a month; it was a pleasure to learn from you both. Thanks to the enthusiastic cooperation with the Canary-Island research team at Universidad de La Laguna: Natacha Aguilar de Soto, Jesus Alcazar, Raquel Vine Alfonso, Daniel Miranda Gonzalez, Agus Schiavi, Patricia Arranz, Olivia Marín, Chloe Yzoard, Alejandro Escánez, Adrian Martin Hernandez and Jacobo Marrero Perez. Thanks to Professor Cynthia Moss, Professor Paul Nachtigall, Professor Peter Narins, and Professor Lasse Jakobsen for helpful

feedback on presentations. Thanks to John Atkins for putting up with my persistence and opening SoundTrap feature development to the research community.

Thanks also to fruitful collaborations with students in the lab who headed projects using the autonomous deep water hydrophone array I developed in this PhD: notably, Ellen Jacobs with the Dominica Sperm Whale Project, and Michal Bjerre Pedersen for taking on the short-finned pilot whale click source parameter quantification that we collected during array testing in Tenerife.

I am thankful for the opportunities to share ideas and present my work at the following conferences during my PhD: the 30th European Cetacean Society Conference (April 2017, Denmark), the 6th Biologging Society Conference (September 2017, Germany), the 22nd Society of Marine Mammalogy Conference (October 2017, Halifax, Canada), the Danish Marine Mammal Symposium (March 2018, Denmark), the Odense Echolocation Symposium (October 2018, Denmark), the world marine mammal conference (SMM & ECS combination, December 2019, Barcelona, Spain), and the 2nd African Bioacoustics Community Conference (November 2020, virtual).

Not to be missed - thank you to the Danish state for recognizing the value in treating PhD fellows like the employees they are. I will forever be grateful for my maternity leave, which was generous in both duration and compensation. I also think it is so forward-thinking that financial coverage during such leave was not a burden to supervisor's personal research grants, but was instead covered by the University. This is an example of the kinds of actions that help to reduce a leaky pipeline and equalize gender equality at both the hiring stage and in retention beyond. Three cheers for setting a good example, Aarhus University!

Finally, thanks to the many friendly and clever students, postdocs and affiliates of the Bioacoustics lab: Laura, Laia, Siri, Ilias, Pernille T, 'old' Michael, 'young' Michael, Line, Simone, Karine, Fredrik, Jamie, Pernille M, Emily, Shane, Julie, and honorary Catherine, you too! Special thanks to Pernille, Laura, and Jamie for feedback on the introduction, and to Catherine for painting the beautiful cover art. A PhD takes a village, and gratitude is extended to friends and family for support all along the way. Warmest of thanks to the love and laughter of my own family – Jamie and Max. Two PhD theses submitted and one baby delivered, all within an 18 month period, all during a pandemic. What a wild finale!

Summary

The objective of this thesis was to gain insight into the constraints and flexibilities of toothed whale biosonar systems, with a focus on narrow-band high frequency echolocators. To better understand echolocation properties and the processes that guide target detection and interception, I have used both passive acoustic monitoring (PAM) hydrophone arrays and acoustic biologging devices, together and on their own, in captive experimental settings and in the wild.

The introductory **Chapter I** overviews the research findings presented in the subsequent chapters, and discuss these discoveries within the broader context of echolocation and sensory ecology research.

Chapter II presents a novel method for the acoustic monitoring of odontocetes in the deep sea via an autonomous hydrophone array. I designed this method to address the logistical and financial constraints of PAM at depth, with the aim of recording the echolocation clicks of the elusive dwarf sperm whale.

In **Chapter III**, I present on the biosonar of the dwarf sperm whale (*Kogia sima*). This includes a source parameter quantification, including beam pattern estimation, from clicks recorded using the aforementioned array at depth, as well as from clicks recorded in a rare shallow encounter. I show considerable variability in the click properties recorded in the shallow and in the deep, suggest that the lower than expected source levels mean that they forage in a reliable prey scattering layers, and speculate on a highly sensitive auditory system.

Chapter IV illustrates previously speculated upon energy in the back of the harbour porpoise biosonar beam (*Phocoena phocoena*) via a full 4π quantification of source parameters, relevant for PAM applications.

In **Chapter V**, I investigate the clutter interference zone via a psychoacoustic experiment that asked harbour porpoises to complete a target discrimination task. This allowed for quantifying the limits of the temporal and spatial resolutions of echo streams arising from targets and distractors. I propose that an evolutionary driver for the high directionality of their beam is the spatial filtering it allows for.

Chapter VI builds upon the previous chapter by exploring auditory stream segregation in harbour porpoises in a scenario in which they cannot capitalize on any spatial filtering benefits provided by their directional beam. This is achieved in a set-up novel for echolocation research: using a phantom echo generator with a freely moving echolocator in a target interception task.

Chapter VII addresses optimal localization hypothesis in a bottlenose dolphin (*Tursiops truncatus*) and a false killer whales (*Pseudorca crassidens*). Rather than the recently proposed hypothesis that toothed whales point their beam slightly askew of the target of interest to maximize localization precision, we instead observe that they use a strategy that renders high echo-to-noise ratios.

Chapter VIII demonstrates how high frequency masking noise impacts porpoise echolocation performance and biosonar sampling strategies.

Chapter IX explores drivers of range-dependent source level adjustments in harbour porpoises, and challenges the 'automatic' descriptor often tied to time-varying gain control.

In conclusion, this thesis explores how toothed whales adjust their echolocation behaviour to the task at hand, according to the surrounding environment, and in the presence of noise or distractors. The research findings presented are all relevant for the interpretation of acoustic behaviours recorded in PAM data.

Resumé (Danish summary)

Formålet med denne afhandling er at undersøge begrænsningerne og fleksibiliteten af tandhvalers biosonar med fokus på arter, der anvender højfrekvent og smalbåndet ekkolokalisering. For at forstå, hvordan tandhvaler bruger ekkolokalisering til at detektere og følge objekter i deres omgivelser, har jeg benyttet to forskellige metoder: passiv akustisk monitorering (PAM) og akustiske målepakker påsat både fritlevende og trænede hvaler.

Det indledende **kapitel I** giver en oversigt over forskningsresultaterne præsenteret i de efterfølgende kapitler og diskuterer disse opdagelser inden for en bredere kontekst af ekkolokalisering og sensorisk økologi.

Kapitel II præsenterer en ny metode til akustisk overvågning af tandhvaler i dybhavet via et autonomt hydrofonarray. Jeg designede denne metode til at tackle de logistiske og økonomiske begrænsninger af PAM på dybt vand og med det formål at optage ekkolokalisering af sky dværg-kaskelothvaler (*Kogia sima*).

I **kapitel III** præsenterer jeg ekkolokaliseringsadfærden hos dværg-kaskelothvalen. Dette inkluderer en kvantificering af kildeparametre, herunder estimering af deres lydkegle, opnået ved hjælp af optagelser med det førnævnte array på dybt vand samt en sjælden optagelse på lavt vand. Jeg viser, at kildestyrkerne er lavere end forventet, og at klikkene varierer betydeligt mellem lavt og dybt vand. Det antyder, at de søger føde i et pålideligt dybt byttelag og samtidig har udviklet en meget følsom hørelse.

Kapitel IV illustrerer lydenergien, der udsendes bagmarsvinets (*Phocoena phocoena*) lydkegle via en fuld 4π-kvantificering af de kildeparametre, som er relevante for PAM-applikationer.

I **kapitel V** har jeg lavet et psykoakustisk eksperiment, hvor marsvin blev trænet til at gennemføre en diskrimineringsopgave. Dette muliggjorde kvantificering af grænserne for de tidsmæssige og rumlige opløsninger af ekkostrømmene, der stammer fra specifikke mål og distraktorer. Jeg foreslår, at der har været en evolutionær selektion for deres smalle lydkegle, fordi den muliggør en rumlig filtrering.

Kapitel VI bygger på det foregående kapitel ved at udforske adskillelsen af auditive ekkostrømme hos marsvin i et scenarie, hvor de ikke kan udnytte fordelene ved deres lydkegle til at skabe en rumlig filtrering. Dette opnås i et set-up, som er nyt for ekkolokaliseringsforskning: et frit-bevægeligt ekkolokaliserende dyr, som skal finde en kugle, mens falske, computer-genererede ekkoer interfererer med dyrets ekkolokalisering.

Kapitel VII omhandler, hvordan lydkeglen hos et øresvin (*Tursiops truncatus*) og en falsk spækhugger (*Pseudorca crassidens*) bruges til at lokalisere objekter med. I stedet for den nyligt foreslåede hypotese om, at tandhvaler peger deres lydkegle lidt ved siden af deres sonar mål for at maksimere lokaliseringspræcision, observerer vi i stedet, at du bruger en strategi, der giver et højt ekko-støj-forhold.

Kapitel VIII viser, hvordan højfrekvent maskeringsstøj påvirker marsvins ekkolokaliseringsstrategi.

Kapitel IX udforsker afstandsrelateret kildeniveaujustering hos marsvin og udfordrer den 'automatiske' justeringsmekanisme publiceret i tidligere studier.

Denne afhandling undersøger, hvordan tandhvaler tilpasser deres ekkolokaliseringsadfærd til den aktuelle opgave i det givne miljø og ved tilstedeværelsen af støj eller distraktorer. De præsenterede forskningsresultater er alle relevante for fortolkningen af akustisk adfærd optaget ved hjælp af PAM.

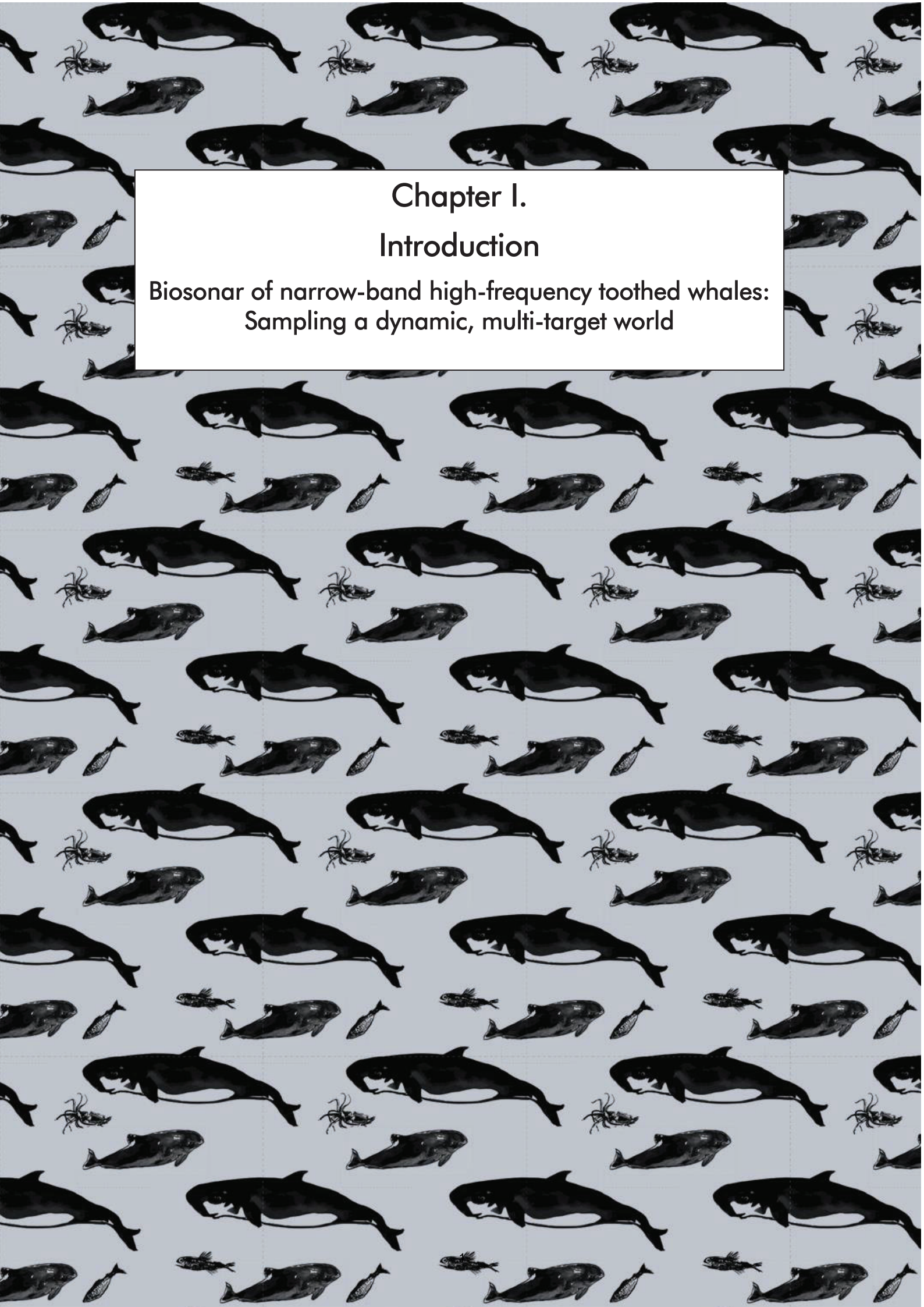

Chapter I.

Introduction

Biosonar of narrow-band high-frequency toothed whales: Sampling a dynamic, multi-target world

Overview

Echolocation is an active sensory modality that has evolved to guide foraging and navigation in light-limited environments. An echolocator emits a transient acoustic signal and interprets the timing, level and spectral content of the returning echoes to detect, locate, characterize and discriminate objects within their acoustic field of view. In this way, echolocation is of vital ecological importance for successfully finding and capturing escaping prey, and allows the sensory means for foraging under conditions of poor lighting. While speculated upon long before confirmation was available, evidence on both the production and hearing of ultrasonic sound waves was demonstrated in bats around 80 years ago (Pierce and Griffin, 1938; Galambos, 1942; Griffin, 1944, 1958) and in toothed whales around 60 years ago (Norris et al., 1961). Since then, a multitude of research has revealed how echolocating bats and odontocetes modify and control the high resolution acoustic sampling of their environment by adjusting the timing (*e.g.* DeRuiter et al., 2009; Moss et al., 2011), intensity (*e.g* Au and Benoit-Bird, 2003; Jensen et al., 2009; Brinkløv et al., 2010; Ladegaard and Madsen, 2019), and beamwidth (*e.g.* Moore et al., 2008; Jakobsen et al., 2013; Jensen et al., 2015; Wisniewska et al., 2015) of their biosonar to a given task. Studies have shown that echolocating animals can adjust their biosonar characteristics for acquiring, generating and modulating the information flow of their surroundings via an actively generated auditory scene to optimize information flow and guide successful foraging (Moss and Surlykke, 2001; Madsen and Surlykke, 2013).

Much of the research into toothed whale echolocation and their impressive target detection and discrimination abilities, branching from a focus on biomimetic military applications, has taken place with stationed animals in captive settings, presented with static auditory scenes and asked to perform very specific tasks (Au, 1993). Investigating odontocete echolocation in such a controlled manner enables the isolation variables of interest and exclusion of confounding variables, and has given rise to the fundamental quantitative concepts used in echolocation research today. However, they do not individually offer a full understanding of the flexibility, breadth, and ecological validity of biosonar behaviour in the wild under conditions for which this sensory modality evolved. However, one also has to acknowledge that ecological considerations were not the intention of these initial studies, and methods for adding this context were unavailable at the time.

Acoustic recordings made in the wild, on the other hand, allow us to gain an understanding of how toothed whales use their echolocation in ecologically relevant scenarios, but they offer little prospect for experimental manipulation nor control of the context. Additionally, owing to the high directionality of toothed whale echolocation clicks, what was known about biosonar behaviour in the wild has largely been limited to the interpretation of brief scans of biosonar beams across acoustic recording gear, often with little accompanying context. Only in the last 20 years or so have the combined advancements in the software and hardware of biologging and passive acoustic monitoring technologies enabled the recording and quantification of echolocation behaviour from free-swimming animals in their wild habitats accompanied by knowledge of the recording context. With these new technologies (*e.g.* including non-invasive sound-recording biologging tags (Johnson and Tyack, 2003), and autonomous hydrophone arrays (Barlow et al., 2018)), it is now possible to investigate the acoustic behaviours and fine-scale movements of these animals in unprecedented detail. This has lead to a wealth of knowledge disseminated in the literature in recent years. However there is still much to learn, especially regarding the more hard-to-reach species, and especially when investigating echolocation in more biologically meaningful contexts. In my PhD, I have used biologging and passive acoustic monitoring technologies, standalone and in tandem, in

both captive and wild settings, to gain insight into the operation, constraints and flexibilities of toothed whale biosonar systems, with a focus on narrow-band high frequency echolocators (porpoises and *Kogia*). Using tags and arrays have allowed me to tap into the sensory streams of animals by means of the biosonar signals they produce, the echoes they receive, and their behavioural response[s] to these. The objective of my PhD was to integrate lab and field studies to understand how echolocating toothed whales perform biosonar-mediated target interception using a fast vocal-motor feedback system in which echoes from powerful ultrasonic clicks inform the modulation of biosonar and behavioural changes.

This introductory chapter begins by outlining the sensory process of echolocation and the physical constraints imposed on acquiring and transmitting information via sound. I then move to a broadscale discussion of some of the topics that I have focused on in my PhD, including source parameter and beam pattern quantification, deep-sea hydrophone arrays, auditory scene analysis, masking effects of noise, and automatic gain control. Throughout this introduction, I focus on toothed whales, draw heavily upon the harbour porpoise as a model echolocator, and, where relevant, I present and discuss research findings discovered in this PhD and detailed in the later chapters. Studies that I have lead are referred to using "I", and studies that I have co-authored are referred to using "we".

The Active Sensing of Echolocation

Approximately one in every five mammal species echolocate as part of their sensory acquisition repertoire (~1,100 bats, and ~70 toothed whales; Griffin, 1958). Echolocators forage and navigate by emitting clicks and analysing the auditory scene generated by the returning echoes milliseconds later (Au, 1993). Such active sensing inherently means that echolocators only receive information when they actively probe their environment with ultrasonic pulses (Madsen and Surlykke, 2014) – similar to the active senses of electrolocation (*e.g.*. von der Emde et al., 1998) and perhaps haptic sensing via whiskers (*e.g.* Dehnhardt, et al., 1998; Knutsen et al., 2006). In this way, unlike most senses which operate using passively collected information, echolocation involves an animal actively producing the pulse and analysing the echoes after they have convolved with the surrounding environment (Nelson and MacIver, 2006). Echolocators have demonstrated dynamic control over the information flow rate and sound type, which in turn influences the temporal resolution and spatial extent (range and width) of their perceived surroundings (Moss and Surlykke, 2010; Moss et al., 2011). Specifically, echolocating animals have been shown to be able to adaptively adjust their beamwidth, source level, clicking rate, and direction of their beam to manage sensory loads from complex acoustic scenes (Moss et al., 2011; Wisniewska et al., 2015; Jensen et al., 2015; Yamada et al., 2016) and effectively manipulate their perception of the surrounding environment.

Such adjustments in biosonar are perhaps most dramatically striking and apparent when viewing an echogram (**Figure 1**). Echograms show a stacked time-series of the echoic signatures of reflectors positioned ahead of an echolocator out to a given range, as measured by an acoustic recorder mounted on the animal. The width of the each point sampled in time represents the inter-click interval (ICI), with the finer temporal sampling during the buzz, displayed as a finer resolution image in the echogram. Here, we see the porpoise actively adjusts its biosonar by reducing the output level of its clicks, as well as by clicking much faster and weaker in the buzz phase to provide for a simple echoic scene with high update rates (**Figure 1B**). The prey capture attempts are also indicated by signatures in the tag's accelerometry data (**Figure 1C**).

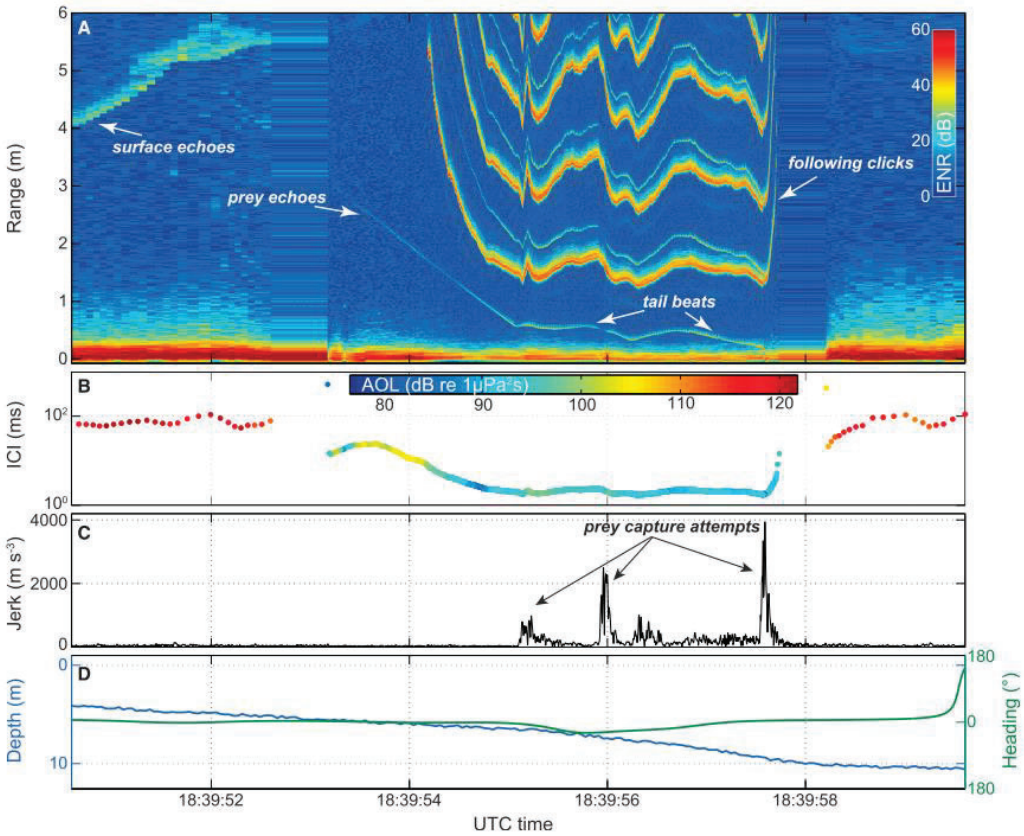

***Figure 1**. Example of data streams collected by a tag (DTAG3) mounted behind the blowhole on a wild harbour porpoise (Phocoena phocoena) as it approached a prey item. A) An echogram, created using acoustic recordings collected by a tag. The y-axis is a range conversion of the elapsed time between emitting a click to receiving an echo, assuming a sound speed of 1,500 m/s. Colour denotes the echo-to-noise ratio (ENR). When the clicking rate is fast, as it is in the buzz, the echogram also displays the next set of emitted clicks. B) Inter-click interval (ICI) and apparent output level (AOL) both reduce as the porpoise approaches the prey item. C) Rate of change of acceleration of the tag, indicating the porpoise attempting to capture a prey item. D) Depth and heading of the porpoise during the prey capture attempt. (From Wisniewska et al., 2016).*

Sound Production and Reception

Echolocation involves both the production of a click that travels through a medium and ensonifies a given target (*e.g.* a prey item), as well as the processing of the returning echoes reflecting off of a target and objects in the surrounding environment. Echolocation clicks produced by odontocetes are brief and ultrasonic transients. These clicks are produced by the pneumatic actuation of the right pair of phonic lips and are projected via the melon in a directional beam enabled by air sacs and the morphology of the skull (Au et al., 2012; Madsen et al., 2013a; Ames et al., 2020). There is a remarkable convergence of high-directionality across all toothed whale clicks (Jensen et al., 2018) with transmitting directivity indices ($DI_{transmitting}$) converging at around 26 $\pm$ 2 dB. The DI is the calculated difference between an on-axis SL of a directional source and a theoretical SL if the same energy was radiated equally in all directions, and thus provides a quantification of how directional a biosonar beam is. A directional beam offers benefits to the echolocators in terms of a facilitating auditory stream segregation (see *Acoustic Field of View* section below).

Each returning echo holds an intermittent sonic "snapshot" (Ghose and Moss, 2006). Sound reception in toothed whales occurs through fat in the lower jaw conducting sound energy to the middle and inner ear (Brill et al., 1988; Ketten, 1997; Møhl et al., 1999). The inter-aural difference in the EL, along with small delays in the arrival times of the echo across the pan bones, can cue the echolocator to the location of the sound reflecting target (Aytekin et al., 2004). There is a pattern of a wider receiving beam (and so a lower DI of ~10-20 dB) than a transmitting beam (of ~26 dB) in several species of toothed whales (Au and Moore, 1984; Kastelein et al., 2005; Jensen et al., 2018). This means that the sound reception pathway is attuned to receiving sounds from the narrow cone in front of the echolocating animal, such that the echolocator's hearing is directionally aligned with the most powerful part its biosonar beam swath (Kastelein et al., 2005). Thus, the receiving and transmitting DIs serve as a spatial filter to improve the detectability of objects ensonified near the acoustic axis of the beam (see **Chapter V**, Malinka et al., *submitted*, and **Chapter VIII**, Hermannsen et al., *in prep.*).

Ranges of Biosonar Inspection

This process of transmission and reflection is illustrated in **Figure 2**. The source level (SL) describes the sound level of the click back-calculated to one meter ahead of the animal on the beam axis. A fraction of the energy that reaches a given target will be reflected; the difference between the received level (RL) on the target and the EL one meter back on the same axis is referred to as the target strength (TS). Target strength is greater (and so reflects more of the impinging energy) if the target is large, and also if the impedance mismatch between the target and the propagation medium is large (*e.g.* as would be the case for the swim bladder of a fish in seawater). The outgoing click and the incoming echo are both subject to spreading and absorption losses which combine to form the overall transmission loss (TL). The magnitude of this TL will increase with increasing range (R) to the target. Specifically, these can – for the ranges relevant for echolocation – be calculated as $20\log_{10}(R)$ for geometric spreading, and αR for frequency-dependent absorption, where α is the absorption coefficient (in dB/m). The sound pressure level of the echo, as received at the echolocator, is described as the backscattered, received echo level (EL). The overall performance of a given biosonar, including the detection range, can be estimated using the *active sonar equation*, originally established for naval sonars (Urick, 1983). The active sonar equation is demonstrated graphically in **Figure 2**, and formulaically below. Note that this sonar equation assumes the center of the biosonar beam ensonified the target (a topic discussed further in **Chapter VII**, Beedholm et al., 2021).

$$\mathbf{EL = SL - 2TL + TS}$$

where $\mathbf{TL = 20\log_{10}(R) + \alpha R}$

In addition to echo level, the echo contains other cues that can inform the echolocator of the composition and/or species (*e.g.* spectral cues; Au et al., 2009; Wisniewska et al., 2012) and size of the prey or prey school (*e.g.* level and duration of echo; Johnson et al., 2008). These cues arise because the physical attributes of the target modify the waveform of the echolocation click/call, and in turn, return a unique echo (Arditi et al., 2015) convolved with the impulse response of the target[s]. The behaviour of the prey can also be inferred by the rate of change in ELs, as the undulations in TS arising from, for example, the undulating tail of an escaping prey item, can indicate prey size and swim speed (Wisniewska et al., 2016; **Figure 1**). Similarly, as the density of a prey school can be evaluated from echosounder data (as in Benoit-Bird et al., 2017), I would imagine toothed whale biosonar to similarly be capable of evaluating distances between neighbouring prey items in a school.

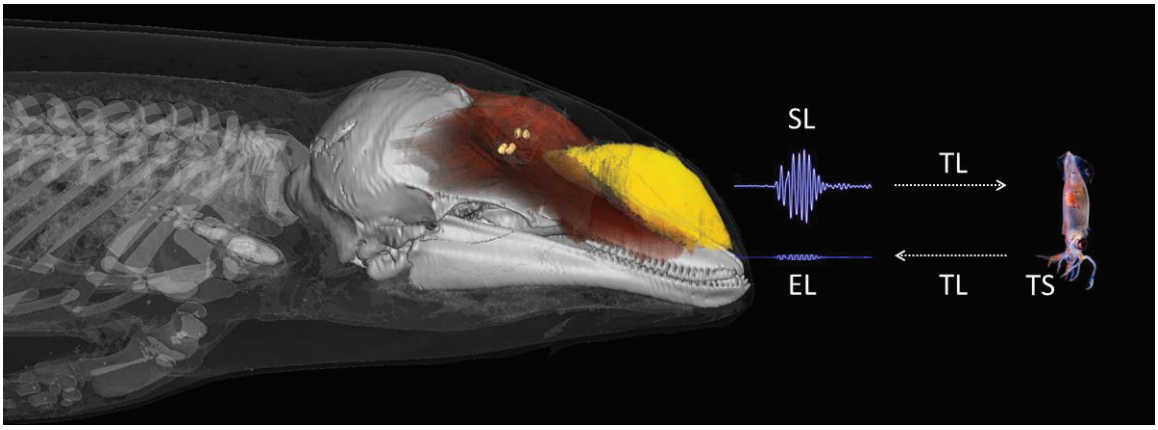

Figure 2*. Active sonar equation illustration with magnetic resonance image (MRI) scan of a harbour porpoise, showing source level (SL), two-way transmission loss (TL), target strength (TS), and received echo level (EL). Target range is estimated from echo delay, target size is estimated from echo level and duration, and target properties are estimated from the echo time-frequency structure. Image courtesy of Peter Teglberg Madsen.*

Beyond SL, several other factors inform the range limits to which a biosonar system can effectively operate. These include the ambient noise levels (NL) in relevant frequency, as well as the animal's hearing detection threshold (DT). The DT defines the level at which the weakest stimulus can be detected and is therefore a measure of an animal's auditory sensitivity for a given frequency. Factors affecting the DT include an animal's age (*e.g.* compare Yuen et al., 2005 with Kloepper et al., 2010) and history of noise exposures causing temporary (*e.g.* Finneran et al., 2005) and/or permanent threshold shifts (*e.g.* Reichmuth et al., 2019). Furthermore, increasing amounts of reverberation and/or clutter (unwanted echoes from non-target objects which happen to be ensonified by the biosonar) affect the DT, if these levels are higher than the absolute detection threshold of the auditory system. An echo can only be detected if the signal-to-noise (SNR) ratio – or specifically, the echo-to-noise (ENR) ratio – exceeds the DT. Any sound that reduces SNRs or ENRs, including clutter and reverberation, is called a masking noise, defined as sound atop the ambient noise that reduces or eliminates the perception of a signal (Richardson et al., 1995). The relationship of these is shown with the *active sonar equation* (under noise-limited conditions):

$$\mathbf{ENR = SL + TS - 2TL - (NL - DI_{Receiving})}$$

Source Parameters

The constraints of sound production and sound reception systems shape the echolocator's sensory perception. The source parameters of biosonar signals and the rate at which they are emitted directly influence the spatial and temporal resolution extent of an echolocator's umwelt (Moss et al., 2006). Furthermore, as the source parameters and the click rates can be dynamically adjusted by the echolocator to suit the specific environment or task at hand in order to meet the behavioural objective (Schnitzler and Kalko, 2001; Moss et al., 2011), quantifying the echolocation click source parameters from free-ranging, wild animals has the potential to convey information about their acoustic behaviours and the foraging ecologies that they allow (Madsen et al., 2004; Kyhn et al., 2009).

The acoustic parameters of biosonar clicks/calls, and the rates at which they are sequentially produced, are the outcome of various trade-offs in sensory perception. Such trade-offs could include acoustic crypsis from predators: for example, a high frequency click may be beyond the most sensitive hearing range of a predator (*e.g.* Morisaka and Connor, 2007; Branstetter et al., 2017; **Chapter III**, Malinka et al., 2021). Additionally, the ensuing high directionality of a high frequency click means that off-axis

acoustic clutter is reduced (Jensen et al., 2018), and the click may be subject to less masking by overlapping in frequency within ambient noise minima in the ocean (Møhl and Andersen, 1973). Furthermore, high frequency signals have shorter wavelengths and therefore are able to provide finer resolution for smaller prey items. However, producing high frequency clicks comes at the cost of having a shorter operational biosonar range due to inherently high levels of sound absorption at high frequencies (Urick, 1983). A high frequency echolocator, such as a species of *Kogia*, would then be expected to compensate for this and extend their biosonar operational range by producing clicks with high SLs – a logical hypothesis that runs counter to my results presented in **Chapter III** (Malinka et al., 2021). The probing range of a biosonar increases with increased SLs under noise-limited conditions, and the degree to which the biosonar range can be increased depends on the frequency of the outgoing signal. However the benefits of a farther biosonar inspection range enabled by high SLs are only realized in environments that are not reverberant, as any high SL clicks produced there would be accompanied by high intensity reverberation of sound reflecting off multiple surfaces (Au, 1993). Nevertheless, dolphins have been shown to detect targets [with low ENRs] close to the reflective surface that is the seafloor, and do so at ranges of tens of meters (Houser et al., 2005).

Click rate also plays a role in sensory perception. If an echolocator clicks too quickly, echoes from distant objects will only arrive after the emission of the next click, leading to ambiguity in target range. Emerging research has pointed out that the issue of range ambiguity from non-target items can be addressed by the echolocator clicking weaker, so that the ELs of the non-target echo stream[s] fall below the detection threshold (Stidsholt et al., 2021; **Chapter IX**, Ladegaard et al., *in prep.*). On the other hand, if an echolocator clicks too slowly, the poor temporal resolution of their auditory scene may lead to them missing out on detecting and/or tracking moving targets (*e.g.* prey). In **Chapter VI** (Malinka et al., *in prep.*), I explore click rate as a function of acoustic complexity when porpoises are subjected to two simultaneously presented auditory scenes, and observe that, the porpoises tend to not accommodate the additional, distracting echo stream in their clicking rates; however, these results, which run counter to predictions, are preliminary and should be treated with caution. The source parameters of biosonar clicks thus seem to have evolved as a compromise of mechanistic and physical factors (*e.g.* sound absorption, ambient noise levels, and any constraints arising from the size and/or morphology of the sound-producing apparatuses (Jensen et al., 2018)) and biological factors (*e.g.* amount of clutter, detectability by and acoustic crypsis from predators, prey size and dynamics).

The source parameters of toothed whale echolocation clicks have revealed four general categories, grouped by a click's bandwidth, frequency, and number of cycles in the waveform (**Figure 3**, from Jensen et al., 2018). These biosonar signal types include: (1) the broadband and multi-pulsed clicks of sperm whales (**Figure 3**, red; Møhl et al., 2003), (2) frequency-modulated clicks of beaked whales (**Figure 3**, blue; Johnson et al., 2004, 2006), (3) broadband clicks produced by most delphinids (**Figure 3**, yellow; Au, 1993), and (4) narrow-band high-frequency (NBHF; Kyhn et al., 2009, 2010, 2013; Madsen et al., 2005a; **Chapter III**, Malinka et al., 2021) clicks produced by porpoises, dwarf and pygmy sperm whales, Franciscana dolphins (*Pontoporia*), as well as six species of coastal dolphin in the genera *Lagenorhynchus* and *Cephalorhynchus* (**Figure 3**, purple). Such different sound types probably arose as a combination of evolutionary history and ecological pressures.

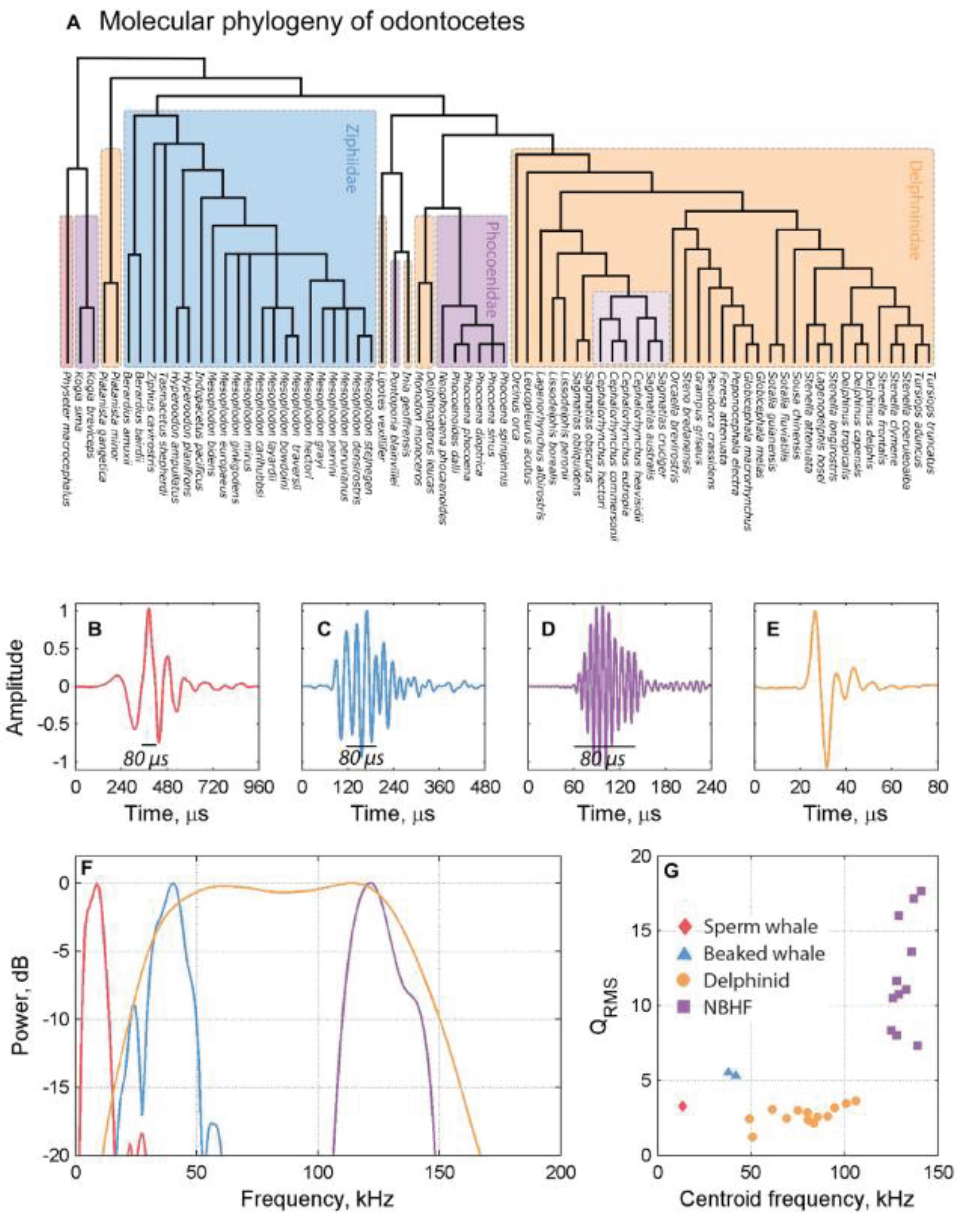

***Figure 3**. Biosonar click types in toothed whales (from Jensen et al., 2018). A shows the molecular phylogeny of toothed whales, and highlights the convergent evolution of narrowband high frequency clicks. B-E show waveforms of on-axis clicks from sperm whales (red), beaked whales (blue), NBHF odontocetes (purple), and delphinids (yellow). F compares the normalized power spectra of each click type. G shows the Q-factor (a measure of the rate at which waveform oscillations diminish, calculated by dividing the centroid frequency by the root-mean-square bandwidth) as a function of the centroid frequency of the click, and highlights clear groupings of click type.*

Recording Echolocation Clicks and Array Design

Beyond opening a window into their sensory ecology, source parameter quantifications are relevant for species detection and classification in passive acoustic monitoring (PAM) efforts used to monitor species presence, distribution and abundance. Many toothed whales, including a dozen or more beaked whale species, remain to have their source parameters adequately quantified. For example, while the acoustic behaviour of pilot whales has been described from tag data (*e.g.* Aguilar de Soto et al., 2008 details the foraging depths, diel patterns in diving, and echolocation sequences leading up to prey capture, *etc.*), it was only recently that we provided an acoustic quantification of their on-axis clicks (Pedersen et al., 2021).

To bridge this knowledge gap in other species, several chapters of this PhD cover source parameterization of toothed whale echolocation clicks.

Clicks need to be recorded along their acoustic axis for on-axis source parameters quantifications, as highly directional clicks are distorted when recorded off of the acoustic axis of the biosonar beam (Au, 1993; Madsen and Wahlberg, 2007). Several established criteria are often used to identify on-axis clicks (see: Au and Benoit-Bird, 2003; Kyhn et al., 2009, 2010, 2013; Madsen and Wahlberg, 2007; Jensen et al., 2013; Ladegaard et al., 2015). Such criteria often include finding clicks that are detected on multiple channels and are acoustically localized. The small time of arrival differences (TOADs) of a single click as recorded on several dispersed channels (along with the known relative position of the hydrophones and a known speed of sound) allow for back-calculating the position of the clicking animal relative to each of the channels, allowing for [A]SL ([apparent] source levels) calculations. More confidence in whether a click has been recorded on-axis is enabled with the use of an array of multiple time-synchronized hydrophones because in addition to enabling acoustic localization, they also allow for the same click to be recorded at several different aspects, with the highest ASL in a scan serving as the best proxy for SL (*e.g.* Ladegaard et al., 2015; Pedersen et al., 2021; **Chapter III**, Malinka et al., 2021). Further criteria include restricting analysis to localized positions occurring at ranges of approximately no greater than five to ten times the aperture of the array, beyond which localization accuracy deteriorates, depending on the design of the array (**Chapter II**; Malinka et al., 2020). The criteria that the click has the highest RL in a series of clicks scanning across the array, with the highest RL occurring on a central channel, both increase the likelihood that the click was recorded on-axis in the vertical and horizontal planes.

Several factors can inform the design of an array of hydrophones used for quantifying the source properties of a target species of toothed whale. Design considerations include the number of hydrophones, the spacing between them, whether the array is 2D or 3D, the rigidity of the array, whether the deployment is short-term or long-term, and whether the recording unit is autonomous or supervised. Factors that influence array design include the predicted features of the target species' echolocation click, their acoustic and diving behaviours, as well as the research question itself. Hydrophone spacing is a balance between having hydrophones close enough so that enough are consistently ensonified (allowing for localization, a greater likelihood that a click is actually recorded on-axis, and favouring a highly directional beam), versus having peripheral hydrophones spaced far enough apart to favour greater localization range and accuracy (because errors in the measurements of both time delays and hydrophone positions would become proportionally smaller; *e.g.* a 950 m long vertical array was developed to target sperm whale sounds in Heerfordt et al., 2007). For example, if a species is anticipated to closely approach an array near the surface, a small aperture Y-shaped (or star-shaped) planar array suspended from a boat may be appropriate (*e.g.* Au and Benoit-Bird, 2003), and if a species is deep-diving and rarely observed, a large-aperture (widely-spaced), moored array may be more appropriate (*e.g.* Gassman et al., 2015). Source level estimates of the animal can be used to estimate the maximal ranges at which a sound could be recorded. If a click is high in frequency and therefore subject to greater levels of frequency-dependent absorption loss, it may be wise to have closer spacing between at least some of the hydrophones, perhaps in a nested fashion, to increase the likelihood of a click being detected on multiple channels). Further array design considerations include the research question itself: if only concerned with knowing the range to the animal, a linear array (which gives rotational ambiguity in localized positions around the axis of the array, whereby the radius of the circle corresponds to the range of the localized animal) is suitable, as would be the case for an acoustic line-transect survey using a towed array (*e.g.* Barlow and Taylor, 2005). If unambiguous animal tracks are instead of interest, as would be the case for tracking the 3D movements of an echolocating animal in its

foraging habitat (*e.g.* Wiggins et al., 2012) or around a manmade structure (*e.g.* Malinka et al., 2018), then a 3D array would be appropriate as it would remove ambiguity in localizations. The energetic qualities of the recording environment should also be considered: if placing an array in a turbulent tidal rapid, for example, rigid arrays, or flexible linear arrays with rigid components (*e.g.* as in Macaulay et al., 2017), may be beneficial for the fidelity of localizations.

In **Chapter II** (Malinka et al., 2020), I detail the methodological development of a deep-sea hydrophone array I built specifically to capture, record, and quantify the clicks of deep-diving toothed whales. This array was, amongst other objectives, planned to enable the recording and source parameter quantification of the elusive NBHF species dwarf sperm whales (*Kogia sima*) and/or pygmy sperm whales (*Kogia breviceps*). *Kogia spp.* are a remarkable outlier when considering the high frequency of their clicks (Madsen et al., 2005a) in relation to their proportional size (see Jensen et al., 2018), and it is counterintuitive to use an echolocation click subject to such high levels of absorption in the open seas. A first step to investigate their paradoxical acoustic ecology was to quantify the source parameters of on-axis clicks. The apparently skittish surface behaviour of *Kogia spp.* near boats/people meant that an autonomous device was desirable, and our chosen recording site along an abruptly dropping continental shelf in the Bahamas near far-ranging oceanic currents dictated that we had to focus on short-term recordings on the order of several hours. Furthermore, as prey items in the stomach contents of stranded individuals indicated deep-diving behaviour (Plön, 2004), an array depth of down to several hundred meters was thought to be ideal for recording their clicks.

In **Chapter III** (Malinka et al., 2021), I present the echolocation click parameters and biosonar behaviour of the NBHF-producing dwarf sperm whale (*Kogia sima*), as recorded using both a single-channel recorder in shallow water and the aforementioned vertical hydrophone array at depth, both in the wild. I report highly directional and narrowband biosonar signals with much lower source levels than predicted, based on their presumed deep-diving foraging behaviour in open seas, and suggest that they instead exploit a reliable and dense prey strata in which a highly directional click would facilitate the generation of an easier auditory scene in an acoustically cluttered environment.

Source parameters and array design are also explored more throughout the thesis, including in **Chapter IV** (Macaulay et al., 2020). Here, we had the goal of providing a detailed spatial quantification of the source parameters of harbour porpoise clicks to uniquely describe the full 360° beam profile in both horizontal and vertical planes ("4π"), so as to inform acoustic detection probabilities using PAM. To do this, we lined the perimeter of a sea pen enclosure with an array of time-synchronized hydrophones, as inspired by investigations on the horizontal beam pattern of *Tursiops* by Finneran et al. (2014). We then tasked a tagged porpoise to click whilst rolling and approaching a target near the centre of a star array (**Figure 4**). The combination of using 27 channels (varying in being widely spaced along the perimeter and closely spaced in the nested 7-channel planar star array), all with known relative positions, allowed for the identification of on-axis clicks, along with recording a variety of clicks at known ranges and known off-axis angles on the other hydrophones. Together, these measurements were able to form a spatial map of

Figure 4*. The recording set-up used to measure the 4π porpoise beam profile in Kerteminde, Denmark. The set-up included a 27-channel hydrophone array lining the perimeter of a sea pen (marked with arrows), within which there was a nested 7-channel star-array (marked with a star) that the porpoise (Freja) was tasked to approach. Some locations marked with an arrow have two hydrophones at different depths. The blocks on the pontoon indicate positions of peripheral hydrophones (See:* ***Chapter IV****, Macaulay et al., 2020).*

Phases of Echolocation

Source parameters of clicks can vary according to the behavioural phase of an echolocation sequence, and so tracking the source parameters (including beamwidth and intensity) and click emission rate throughout a click sequence can reveal the echolocator's vocal-motor adjustments as it homes in on a prey item. Echolocation sequences have classically been parsed into *search*, *approach*, and *terminal buzz* phases, with each phase having distinctive characteristics concerning the click intervals and intensities (**Figure 5**). Borrowing from the bat echolocation literature where this pattern was initially described (Griffin, 1958), clicks in the search phase are generally of higher intensity and produced at a slow rate, resulting in larger inter-click intervals (ICIs). These are often (but not always, see: Madsen et al., 2005b; Johnson et al., 2006; Fais et al., 2016) followed by approach-phase clicks (**Figure 5**), whereby reductions in the ICI, often accompanied by reduced output levels, indicate that a detected prey item is being pursued. As the echolocator closes in on a prey item, clicks of extremely high repetition are produced in the terminal phase (recorded down to <2 ms, corresponding to 500 clicks per second in porpoises; Wisniewska et al., 2016). These buzz clicks are of markedly lower intensity and can be broader in beamwidth, in an apparent trade-off between temporal resolution and output (Madsen and Surlykke, 2013). In this way, buzzing enables a superior temporal resolution with which to track evasive prey; This could be viewed as occurring at the cost of a short-range biosonar due to low source levels (Wisniewska et al., 2016), or as a benefit as it would beget a simpler auditory scene. Even within the buzz, toothed whales have been demonstrated to adjust their ICIs to the movements of escaping prey, often over-compensating the depth of view (Vance et al., *submitted*). This phenomenon has recently been proposed to serve as a spatial anchor for orientation (Stidsholt et al., 2021). Such rapid vocal-motor adjustments to prey are likely facilitated by keeping multiple echo streams within the acoustic field of view.

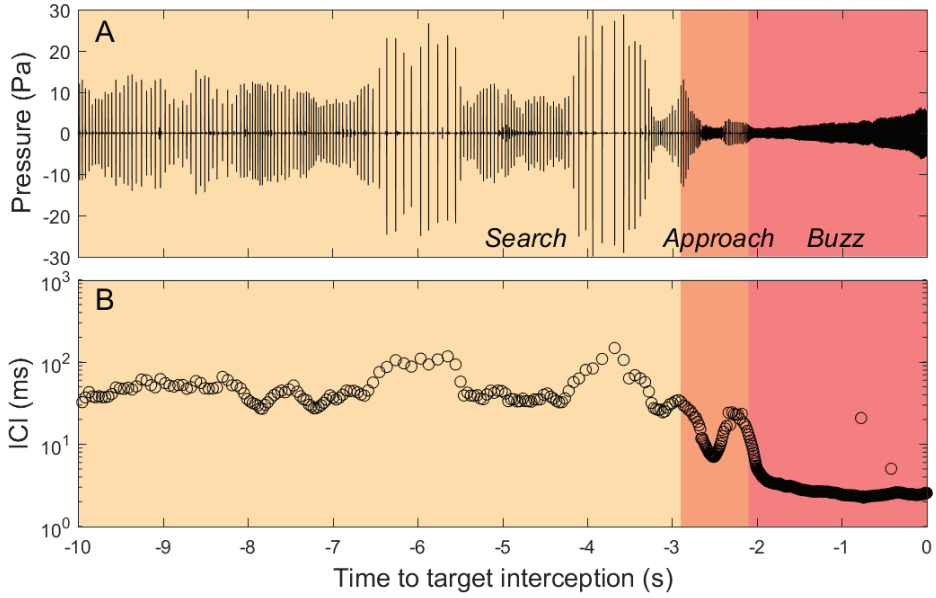

Figure 5. *Example of search, approach and buzz phases of echolocation as recorded on a porpoise-mounted tag, with phases denoted by colour: search (yellow), approach (orange), and terminal buzz (salmon). Note that the exact bounds of what is considered the approach phase are somewhat arbitrary. A) shows the waveform, and B) shows the variation in the inter-click intervals (ICI) during the echolocation sequence. This example is from one target approach trial performed by Freja (12/7/2017, session 1, trial 6), an echolocating harbour porpoise (Phocoena phocoena), and is part of the data presented in* ***Chapter V*** *(Malinka et al., submitted).*

The sampling rate of the clicks effectively allows for the expansion and contraction of the acoustic depth of field (~ICI x sound speed/2), which echolocators often adjust with the range to the target of interest (Madsen and Surlykke, 2013). The ICI generally just exceeds the two-way-travel-time (TWTT), with a short lag time for processing (Cahlander et al., 1964; Au, 1993). While ICIs have been used to estimate the inspection range that a biosonar is attending to (Penner, 1988; Thomas and Turl, 1990), the assumption of a fixed lag time (*e.g.* Akamatsu et al., 2005) is contradicted with evidence of either variable lag times (*e.g.* Verfuß et al., 2005; Wisniewska et al., 2012; Ladegaard et al., 2019) or the near absence of range-dependent ICI adjustments for large portions of target approaches (*e.g.* DeRuiter et al., 2009). Thus, while inspection ranges garnered from ICIs can be used as a proxy for maximal inspection ranges (as discussed in **Chapter III**, Malinka et al., 2021, and Pedersen et al., 2021), their relationship to target range is not always straightforward (Ladegaard and Madsen, 2019). Additionally, clicks have been assumed to be emitted after receiving the echo from the previous click, in a manner that presumably avoids ambiguity in the range estimate of targets of interest (Kadane and Penner, 1983; Surlykke and Nachtigall, 2014). This assumption, too, is muddled by findings from recent experiments measuring acoustically-evoked electric potentials in porpoises, which showed higher order brain processing at intervals of 80-100 ms, exceeding the average ICI (**Figure 6**; Beedholm et al., *in prep.*). This observation suggests that porpoise clicks seem to be emitted before higher order auditory processing of echoes from the previous click.

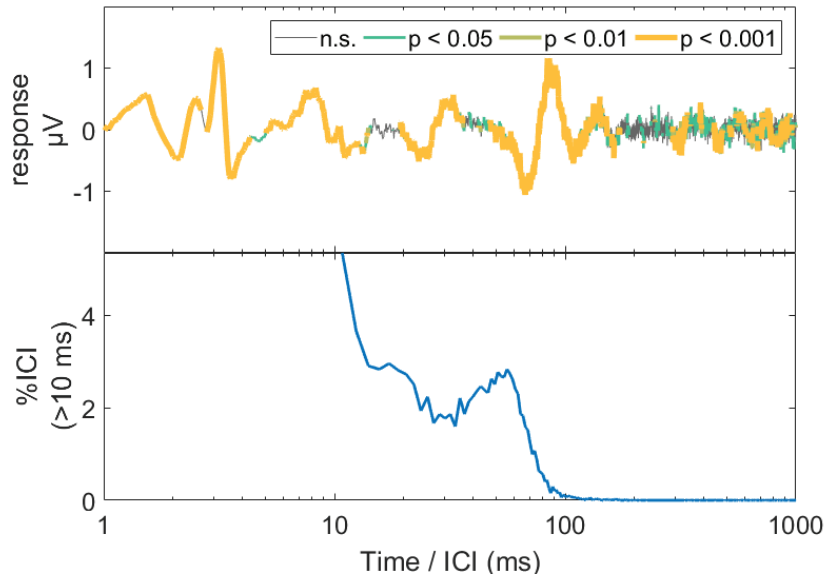

Figure 6*. Auditory evoked potential (AEP) latencies and inter-click interval (ICI) distribution of a porpoise presented echoes at 100 ms intervals. A) Average time series of 2000+ full bandwidth AEP recordings (10-2000 Hz). Significance shows fidelity in the auditory response to the same stimulus, and was determined at each sample as a Monte Carlo permutation test for either the real or the imaginary part of the analytical AEP signals. B) Density distribution of ICIs produced by two porpoises during a target approach experiment. (Data collected by Michael Ladegaard; Figure from the drafted manuscript: Beedholm et al., in prep.).*

The extremely fast clicking rate during buzzing has brought into question the temporal processing capability of acoustic information in toothed whales (Vance et al., *submitted*.), with suggestions that echo information is not processed on a click-by-click basis (Au, 1993; and consistent with **Figure 6**), but is instead integrated over several consecutive clicks (Kothari et al., 2018; Ladegaard et al., 2019). **Figure 6** clearly shows that such an integration happens over at least two consecutive clicks. In **Chapter V** (Malinka et al., *submitted*), I show that each scan across a target in a discrimination task consists of some 4-6 clicks; perhaps such series of clicks is a more useful grouping for representing the 'actual' information package, rather than one click-echo pair.

In several chapters herein, I investigate how porpoises control the timing and output parameters of their echolocation clicks to match the biosonar task at hand, and explore the behavioural factors that drive changes in sonar sampling rates in echolocating porpoises. Specifically, I investigate how porpoises modulate acoustic gaze (here defined as the spatial extent of echoic information as controlled by the beam pattern, sampling rate, and output energy) to inform changes in motor behaviour during search, approach and interception of targets in noise and clutter. These studies, detailed in the following sections, are done under various conditions: with a spatially and temporally separated acoustic distractor (**Chapter V**; Malinka et al., *submitted*), with only a temporally separated acoustic distractor (**Chapter VI**; Malinka et al., *in prep.*), and with varying levels of noise to explore masking effects (**Chapter VIII**; Hermannsen et al., *in prep.*). In this last-mentioned chapter (**Chapter VIII;** Hermannsen et al., *in prep.*), we find that the porpoises adjusted their SLs to compensate for high frequency noise, but this was only partially effective as target discrimination success was poor in these instances where high-level, high frequency masking combined with spatial masking.

Gain Control

Owing to both the diversity in the source parameters of toothed whale clicks (**Figure 3**), and the breadth of biologically relevant contexts under which this sensory system operates, there is a large variation in the maximal ranges to which toothed whales can echolocate prey targets, ranging from tens to hundreds of meters (Madsen et al., 2007). This variation in operating range is driven by SLs, click frequencies and TS differences, and is mitigated by time-varying gain control. For the same SL, returning echo levels may vary by more than 100 dB, depending on target strength and range to the target (Supin and Nachtigall, 2013). This is thought to be greater than the dynamic range of odontocete auditory systems, and so could have lead to the evolution of mechanisms that reduce the perceived magnitude of echo levels (Supin et al., 2010). Indeed, stabilizing perceived echo levels to a smaller dynamic range are thought to facilitate auditory processing (Neuweiler, 1990; Moss and Schnitzler, 1995), perhaps via cortical auditory neurons that are tuned to target distance and optimized for managing echo-level compensation (Macías et al., 2016).

Echo level stabilization can be achieved in two manners: via adjustments on either the receiving and/or transmitting side of the biosonar feedback loop, both of which act as gain control mechanisms to compensate for changing transmission losses over the ranges to the target. A combination of transmitting and receiving gain control mechanisms have been demonstrated in toothed whales and bats alike. If perceived echo levels were to be perfectly stabilized, a $\sim 20\log_{10}(R)$ one-way adjustment would be observed in both the transmitting and receiving sides of the biosonar feedback loop, combining to form a $\sim 40\log_{10}(R)$ compensation to offset two-way geometric spreading losses.

The receiving-side of the biosonar feedback loop can be adjusted as a gain control mechanism whereby the intensity of the outgoing signal remains the same, and the sensitivity of the receiver decreases as the range to the target decreases, due to gain increasing with time after an emitted pulse. Receiving-side gain control is the mode of operation for human-made sonar, including some echosounder systems. Some bats similarly use a receiving-side gain control to partially compensate for transmission losses (Kick and Simmons, 1984) via a stapedial reflex in the middle ear (Henson et al., 1965). It has been debated whether this is to protect the ears and keep more neurons out of the refractory state, or instead to provide receiving-side gain control (Schrøder et al., 2017). On the other hand, recent auditory brainstem response studies have shown an echolocating bat (*Tadarida brasilienasis*) to enhance its receiving gain in a short time window immediately following pulse emission (Smotherman and Bakshi, 2019). In toothed whales, time-varying auditory gain control is thought to be achieved via forward-masking whereby hearing is less sensitive in a short time window after a click is emitted (Supin and Nachtigall, 2013; Schrøder et al., 2017). However, there are also examples of active changes to hearing sensitivity that cannot be explained by forward-masking (*e.g.* Nachtigall et al., 2018). Either way, echo delay and SL could act as drivers of adjustments for auditory gain control (as suggested in **Chapter IX,** Ladegaard et al., *in prep.*).

The transmitting end of the biosonar feedback loop can also be adjusted as a gain control mechanism: some bats have been shown to reduce their SLs as range-to-target decreases, thereby employing a time-varying gain control on the transmission side via intensity compensation (Boonman and Jones, 2002; Hiryu et al., 2007; Fenton et al., 2014; Stidsholt et al., 2020). This pattern has also been reported in toothed whales (Rasmussen et al., 2002; Au and Benoit-Bird, 2003; Jensen et al., 2009; Wisniewska et al., 2012), with many wild odontocetes seeming to adjust the output level of their clicks in a $20\log_{10}(R)$ manner as a function of range to the target. However, there are also studies in the toothed whale echolocation literature in which this pattern is absent (*e.g.* Jensen et al., 2013), and while this could be due to assumptions of the recording hydrophone[s] being the target that the echolocator's biosonar is

adjusting to, it could alternatively call into question the 'automatic' descriptor in "automatic gain control" (AGC). AGC in odontocetes was originally proposed to occur automatically as a consequence of having a pressurized nasal system that produces clicks in quicker succession when at close range to a target and hence be produced at lower output levels (Au and Benoit-Bird, 2003), but our data from (**Chapter IX**; Ladegaard et al., *in prep.*) show this view may be too simplistic as porpoises echolocating in noise can click faster and louder when masked.

Furthermore, there is uncertainty in the mechanism[s] for how SL is controlled beyond the mechanics of pneumatic sound production: perhaps SL changes are driven by echo delays, or driven by received echo levels. In **Chapter IX** (Ladegaard et al., *in prep.*), we explore the drivers of range-dependent adjustments in SL by measuring porpoise echolocation behaviour with both target-mounted hydrophones and biologging devices attached to the porpoise as it freely swims to solve a target detection, localization and interception task of a target of various strengths. We find that porpoises adjust their SL in a logarithmic function of range to target (from 15* to 21*$\log_{10}$(R)), and we propose that echo level drives the intensity compensation. We find that the porpoises adjust their source levels to range in a way that renders EL in a dynamic range from around their detection threshold and some 30 dB up; therefore porpoises do not seek to stabilize ELs but rather to receive them in a fairly narrow dynamic range likely to facilitate auditory processing. Our proposed functional dynamic range in the porpoise auditory system (of ~30 dB) would allow for the variability in ELs arising from a moving prey target.

Acoustic Field of View and Spatial Filtering

Echolocators have also demonstrated control over not just the levels of the echoes they receive, but also the amount of echoes themselves. This example curation of sensory acquisition facilitates the perceptual distinction between relevant and distracting cues (Dukas 1999; Niven and Laughlin, 2008). The capability of selectively focusing attention on targeted stimuli while ignoring or filtering out irrelevant stimuli is key for organizing and disambiguating sensory scenes (Lavie, 2005), and such sensory gating (on incoming streams of echoic information, for example) can reduce the load on neural processing (Dukas and Kamil, 2000; Carylon et al., 2001). The active sense of echolocation provides a means of doing so, as an echolocator has control over its sensory input and the information processing on its receiving auditory system. A directional biosonar beam can similarly pre-filter the surrounding environment to render an acoustic field of view.

Biosonar beamwidths are conventionally quantified by their half-power (-3 dB) beamwidth, equivalent to the width over which the power of the beam is halved. During regular echolocation, harbour porpoise clicks are narrow in beamwidth, with a -3 dB beamwidths of ~12° (Au et al., 1999; Koblitz et al., 2012; **Chapter IV**; Macaulay et al., 2020). While buzzing during the final phase of target approach, the area ensonified by a given click can increase by ~200% (Wisniewska et al., 2015), translating to a greater half-power beamwidth of ~15°. Describing these changes in terms of -3 dB (or -10 dB) beamwidths is set by convention, but it remains to be understood if they are fully biologically relevant. Indeed, in my opinion, these numbers are insufficient unless they are combined with knowledge on the limits on the spatial extent of the biosonar field (Moore et al., 2008). Toothed whales can steer their acoustic gaze to include and exclude information, but it is unknown what the functional beamwidth is, *i.e.* how far off-axis can information still be collected, and how far off-axis should an interfering target be to not provide clutter in the same delay window? What space in front of an echolocator contains useful echoic information?

The functional beamwidth has been somewhat quantified for one free-swimming odontocete species in its natural environment. Specifically, Madsen et al. (2013b), tagged Blainville's beaked whales (*Mesoplodon densirostris*) with dual-hydrophone sound-and-movement biologging devices (DTAG3; Johnson and Tyack 2003). Here, the acoustic field of view of was estimated by computing the angle-of-arrival of emitted clicks and their corresponding echoes. These measurements can indicate the area ensonified ahead of the whale, as a function of range and angle. The majority (~95%) of echoes recorded by the tag were ±10° of the beam center, suggesting a functional beamwidth of 20° (**Figure 8**) and agreeing with previous beamwidth estimations on the same species, as calculated using widely-spaced seafloor mounted hydrophone arrays (Shaffer et al., 2013).

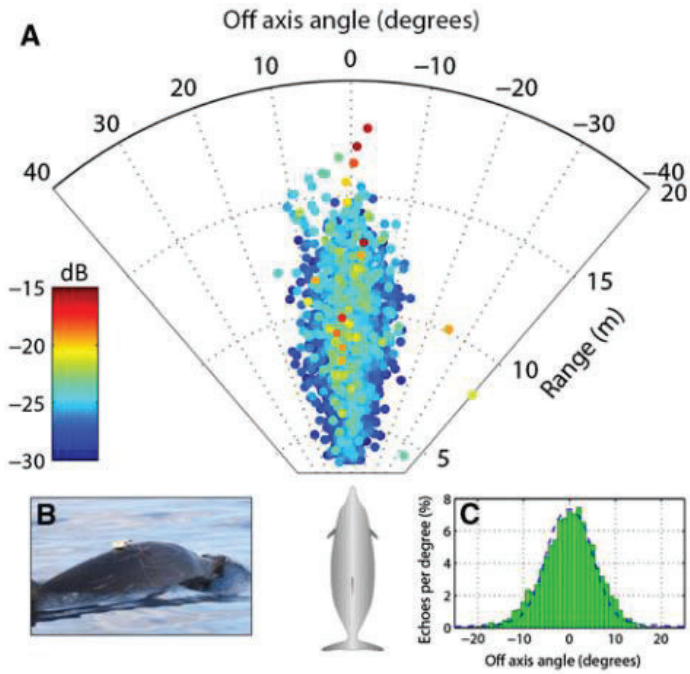

Figure 7. *Representation of the "functional beamwidth" from Madsen et al., 2013b. A,B) Here, we see a 2D view of the angles of echoes from targets ensonified by echolocation clicks produced by and recorded on a tagged Blainville's beaked whale (Mesoplodon densirostris), with colour denoting echo level. Here, we see that the strongest echoes are received within a narrow space ahead of the animal. C) Histogram showing 95% of returning echoes were within ±10° of the beam axis.*

In several chapters, I consider the acoustic field of view, here defined as the spatial extent of echoes returning from objects ensonified by the biosonar beam. Biosonar beamwidths are highly directional across odontocetes (Jensen et al., 2018), meaning that there is high intensity along the acoustic axis and reduced ensonification of items off-axis. Narrow beamwidths of the highly directional echolocation clicks have been interpreted as an evolutionary adaptation enabling greater source levels (SLs) for the same power ($SL_{directional\ source}$ = SL omnidirectional source with same power + DI), thus allowing for the detection and tracking of distant prey (Surlykke et al., 2009; Au, 2014). The correlated high directionality also restricts the width of what is ensonified, and therefore restricts the spatial swath of the returning echoes that provide information to the echolocator (Simmons et al., 1988). This high directivity inherently means that the biosonar beam itself inherently acts as a "spatial filter" for acoustic information, defined by Moss and Surlykke (2010) to be constituted by the beamwidth and constraining the "…limited region of space sampled at a given point in time."

In **Chapter V** (Malinka et al., *submitted*), I explore this notion by quantifying the echo level differences in multiple simultaneous echo streams received by a porpoise to suggest that a reason their beams evolved to be so directional was due, in part, to the spatial filtering advantages that it allows for. A directional beam aids with acoustic clutter rejection since objects outside the directional beam do not generate loud echoes in the same delay bin as targets of interest. In other words, this clutter rejection occurs via spatial release from temporal masking at short target ranges via large contrasts in the levels of echoes from on- and off-axis objects within the echolocator's acoustic field of view (Koblitz et al., 2012; Moss and Surlykke, 2001), which would be especially useful in cluttered environments. How directional a beam is exists in a trade-off with the sensory volume (that is, the spatial volume that an echolocator ensonifies with a given click; see Stidsholt et al., 2021). Further benefits of a directional beam are discussed in the *Head Scanning* section below.

Auditory scene analysis / auditory stream segregation

Even while the directionality of a biosonar beam offers spatial filtration that effectively simplifies an auditory scene (**Chapter V**, Malinka et al., *submitted*), echolocators must still be adept at retrieving, processing, and perceptually organizing information obtained from an often complex mosaic of echoes (Madsen and Surlykke, 2013), often within an already narrow acoustic field of view. To effectively manage the sensory load from an acoustically cluttered environment, echolocators must use this information to guide their motor and vocal behaviour (Bregman, 1990; Kothari et al., 2014). Foraging toothed whales must be able to distinguish between targets and selectively keep track of prey items whilst in multi-target and acoustically cluttered, dynamic environments (Johnson et al., 2008; Verfuß et al., 2009). The perceptual organisation of sound is thus necessary for the disambiguation of echo streams. This is often referred to as 'auditory scene analysis' (Bregman, 1990), and describes the parsing of a complex acoustic environment into discrete auditory streams (Barber et al., 2003).

However, much remains to be understood regarding how toothed whales negotiate acoustic scenes filled with unwanted echoes. How do they segregate multiple incoming auditory streams and selectively focus their attention on those which are relevant? Inversely, how do they minimise perceptual emphasis on irrelevant information? There is still much open area for research into the principles that guide and govern active auditory scene analysis. For example, clutter echoes can mask the reception of target-echoes if they both exist within the auditory integration time (Simmons et al., 1988), and this is anticipated to be an nearly omnipresent challenge for those who echolocate.

Auditory Integration Time

Toothed whales echolocate with water as the propagation medium where sounds travel fast (at ~1500 m/s). This means that whenever there are targets that are closely spaced, echoes from different targets will arrive back at the echolocating animal with small differences in the time delays between them. For example, consider objects that are spaced 15 cm apart – a biologically reasonable spacing between small intraspecific prey items in a school (Benoit-Bird et al., 2017). Echoes from neighbouring prey items at this spacing, for example, would arrive at the echolocator with a maximum time delay of ~200 μs. This is below the temporal threshold at which toothed whales are reportedly able to parse independent echo streams, the so-called 'auditory integration time' of ~264 μs (Vel'min and Dubrovskiy, 1975; Vel'min, 1976; Moore et al., 1984; Au et al., 1988). It is not understood how echolocators can handle clutter echo streams when interfering targets are in the same delay windows and beam angles as the target of interest. How do echolocators process and act on such rapid and dense sensory information with sampling intervals much shorter than the processing times in their auditory systems? Indeed, for the echoes to arrive at the

echolocator with a timing difference that exceeds this threshold, they would have to be spaced at least 40 cm apart. How is biosonar-mediated prey capture carried out using an auditory system whose resolution is apparently impaired when it is needed most?

When predators are absent, the spacing between individual prey within a prey school has been found to increase as a function of prey length, whereby inter-individual distances of prey are about double that of individual body length (Benoit-Bird et al., 2017). The conundrum of resolving individual prey items using toothed whale echolocation is further compounded by echosounder observations that prey items school into tighter clusters in the presence of toothed whale predators (**Figure 8**; Benoit-Bird et al., 2017). In the presence of Risso's dolphins (*Grampus griseus*), squid prey aggregate tighter, from mean nearest neighbour distances decreasing from ~110 cm to ~50 cm (Benoit-Bird et al., 2017). Is schooling with a density that is near the boundary of a predator's auditory integration time (50 cm ~= 333 µs) sufficient enough to achieve evasion? Has the difficulty in the auditory stream segregation task of distinguishing between closely-spaced prey items contributed to shaping the schooling behaviour of pelagic prey?

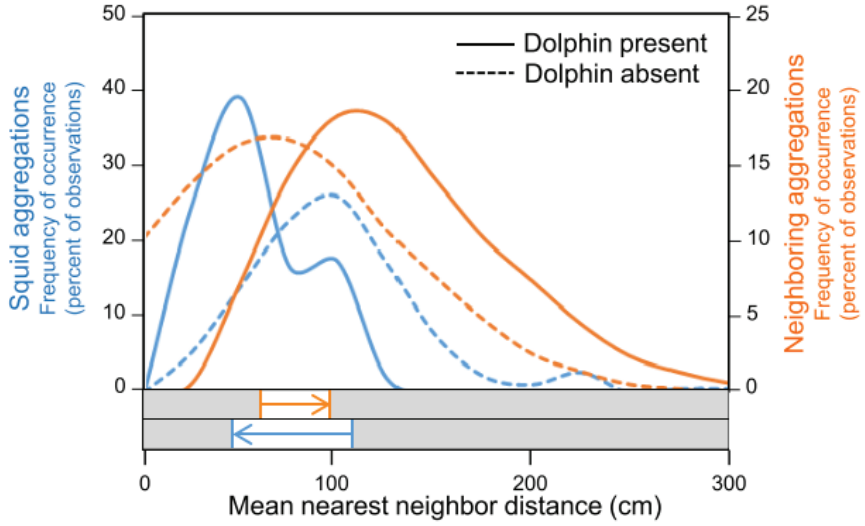

***Figure 8**. Prey aggregation changes in presence and absence of Risso's dolphins. In the presence of a dolphin predator within the aggregation, the distance between squid in the aggregation decreases so that the aggregation tightens (blue). Meanwhile, the spacing of squid aggregations to adjacent groups of other taxa increase their spacing (orange). (From Benoit-Bird et al., 2017).*

Such predator/prey behavioural interaction observations in the wild, combined with findings from psychophysical experiments, have set the stage for several chapters in this thesis exploring the dynamism of odontocete biosonar. On what basis do toothed whales adjust their acoustic gaze to focus on distinct targets in a dynamic and time-varying echoic scene? In **Chapter V** (Malinka et al., *submitted*), I tasked harbour porpoises with a two-alternative forced-choice target discrimination task under scenarios of varying acoustic complexity. By examining their biosonar behaviour and echolocation adjustments made when discriminating between closely-spaced targets of varying inter-target distances, I explore how spatial filtering and temporal filtering can perceptually separate auditory streams. In doing so, I find that the porpoises make successful discrimination decisions with very small echo time delays; These were often much smaller than both the widely reported auditory integration time of ~264 µs (Vel'min and Dubrovskiy, 1975; Vel'min, 1976; Moore et al., 1984; Au et al., 1988), as well as the smaller, but less widely reported auditory time resolution constant of 20 µs for bottlenose dolphins and 50 µs for porpoises (Zaslavski,

2008, 2012; **Figure 9**). Owing to different methodological approaches of pulse-pair discrimination (as in the studies converging on ~264 μs) and target identification near a clutter screen (as in Zaslavski, 2008, 2012), the reported auditory integration times are difficult to reconcile or compare with one another.

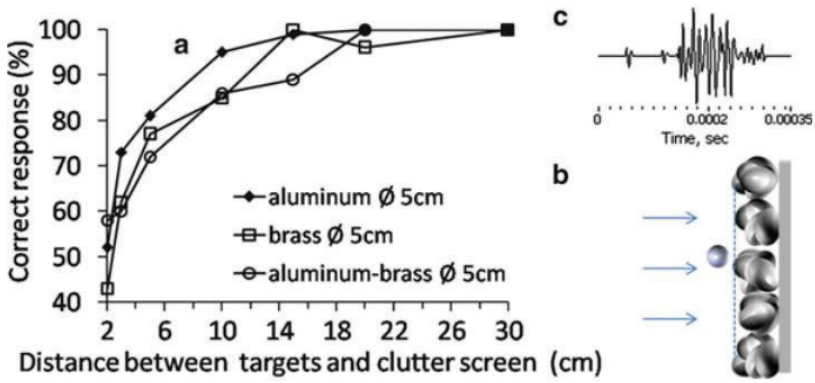

***Figure 9**. Discrimination performance by an echolocating Tursiops truncatus (from Zaslavski, 2012). A) Performance success as a function of the separation between the target and the clutter screen; B) schematic of the clutter screen; and C) a small echo from the target followed by a larger echo from the clutter screen.*

Nevertheless, I find porpoises make low error rate discrimination decisions with time delays between echoes that are less than all reported auditory integration times. I find in **Chapter V** (Malinka et al., *submitted*) that as long as there is about 2 dB of echo level difference in the spatial separation of the target of interest and the distractor, the porpoise could successfully perform biosonar-based target discrimination despite echo delays of down to only 4 μs. When faced with greater acoustic complexity via distracting clutter, often within the clutter interference zone (here defined as the region where echoes from prey overlap with echoes from other non-target objects in the environment, and produce a masking effect on the echolocator), the porpoises adjusted their biosonar by clicking faster, clicking with lower amplitude at close range, buzzing for a longer duration, scanning across the targets more, and delaying discrimination decision-making. Our results demonstrate the spatial filtering provided by using the directional biosonar beam as an amplitude gradient (via high contrasts in echo levels from auditory streams on- and off-axis), and call into question the interpretation of the reported auditory integration time as a hard delay limit for when echoes from close objects can be resolved.

In **Chapter VI** (Malinka et al., *in prep.*), I examine this same conundrum, but instead build on **Chapter V** (Malinka et al., *submitted*) to create an experimental set-up that denies that porpoise of any benefits reaped by the spatial filter provided by its directional beam. To further investigate how echolocators segregate overlapping and simultaneous auditory streams, one can conduct an experiment with "phantom targets." Phantom echo generator experiments have previously been used to study bat and toothed whale echolocation (*e.g.* Simmons, 1973; Au et al., 1988; Aubauer et al., 2000; Finneran et al., 2019), but have never (to my knowledge) been applied in a more biologically relevant set-up that uses a freely moving animal in an active target interception task. When additional, artificial ("phantom") echoes are projected into the environment, an echolocating animal would perceive these as simulated echo streams representing real objects, thus allowing for manipulation of the acoustic scene experienced by an echolocating animal. When the phantom echoes are projected from the location of a real target (as is the case in **Chapter VI**, Malinka et al., *in prep*) the echo streams can only be disambiguated on the range axis and hence delay axis, as the auditory steam of the phantom target will always be perceived as being directly

in line with the real target. In other words, in tasking a free-swimming porpoise to approach and intercept a target connected to a phantom-echo generator, I have essentially put the porpoise in a situation where it receives echo streams from both a real target, as well as from a distracting target that cannot be spatially separated with beam filtering.

The experiment was thus designed in such a way that the beam could not be used as an amplitude gradient for returning echoes, because the distracting acoustic clutter was always perceived to come from directly behind the target, and so the porpoise is forced to make any biosonar-guided decisions (regarding target discrimination or selection) without the aid of the spatial filter. In the preliminary investigation of the in-progress **Chapter VI**, I find that the porpoises click quieter when confronted with more clutter (as in **Chapter V**, Malinka et al., *submitted*, and Ladegaard and Madsen, 2019) in an attempt to reduce the ELs of the phantom stream (**Chapter IX**; Ladegaard et al., *in prep.*). Additionally, counter to predictions on click rate arising in the literature on other echolocators in cluttered scenarios, the porpoises do not seem to accommodate the extra (phantom) stream by clicking slower, for example. However, as this study is still in progress, conclusions are not set and much remains to be determined in this study on auditory stream segregation.

Head Scanning

Even without the ability to gain spatial filtering advantages of a directional beam (**Chapter V**, Malinka et al., *submitted*) on an individual click basis, as was the case in the experimental design of **Chapter VI** (Malinka et al., *in prep.*), echolocators can make use of the amplitude gradient provided via the scanning of several consecutive clicks that move across an item of interest. Bats, porpoises and dolphins have been observed continuously scanning their head horizontally and vertically over targets during an approach (Ghose and Moss, 2003; Schevill and Lawrence, 1956; Norris et al., 1961; Wisniewska et al., 2012). Head scanning behaviour could facilitate binaural localization by constantly modulating the phase and intensity differences of echoes reaching both ears (Kellog, 1961). This combination of echolocation and binaural localization has been referred to as 'auditory scanning' (Kellog, 1961). When buzzing is coupled with head movements, the sensory volume in which prey can be searched for effectively increases (Norris et al., 1961). Note that porpoises, with documented beamwidth broadening during buzzing (Wisniewska et al., 2015), have been observed using head scanning movements during the final phases of target approach, even when the contrast in the returning echo levels would be less pronounced when emitting clicks with a broader beamwidth (Wisniewska et al., 2015).

Head scanning behaviour could also facilitate exploitation of the beam gradient, thus facilitating the fine-scale localization of a target. The 'optimal localization hypothesis' (whereby an echolocator places the peak of the slope of its beam, rather than the axis of its beam, on the target of interest) was reported in Egyptian fruit bats (*Rousettus aegyptiacus*; Yovel et al., 2010). Placing the peak of the beam slightly askew of the target of interest would be beneficial in that it would could indicate prey escape direction, and some toothed whale research has speculated that the gradients of a directional beam (or even, the gradients between apparent dual peaks of beams, see Starkhammer et al., 2011) could help with target localization. This benefit to prey localization (and hunting) could act alongside the benefits associated with the widening of the biosonar beam during the final phases of prey capture that allow for keeping a fast-moving, evasive prey item within the field of view at close range (Ratcliffe et al., 2013). These reports prompted me to experimentally investigate whether this phenomenon existed in toothed whales. However, while these experiments on porpoises were underway (see next paragraphs), optimal localization hypothesis was reported as a biosonar strategy employed by bottlenose dolphins, at least in a static target detection task

(Kloepper et al., 2018). The occurrence of the predictions precisely matching the results in this study – along with the serendipity of our lab having data on the same animal, at the same facility, conducting the same task with a similar target – prompted us to dig into our previously collected data, collected alongside a different research project in the lab (that presented in Wisniewska et al., 2014).

In doing so (see **Chapter VII**; Beedholm et al., 2021), we found that rather than the recently proposed hypothesis that toothed whales point their beam slightly askew of the target of interest to maximize localization precision (Kloepper et al., 2018), they are instead observed to perform a strategy that renders high echo-to-noise ratio. The opposing conclusions presented by Kloepper et al. (2018) and Beedholm et al. (2021) highlight errors arising from interpolations of data collected by non-linear hydrophone arrays. In **Chapter VII**, we discuss this, and also caution biological interpretations that seem too good to be true, and/or may appear to be on-trend with research disseminated in high-impact journals. However, scientific debate aside, I suspect that both sets of authors (Kloepper et al., 2018 and Beedholm et al., 2021) can agree that it is not ideal to use a static target detection experiment to investigate localization strategies used by echolocators. Indeed, both sets of authors used existing 'datasets of opportunity' with a stationed animal to test for evidence of optimal localization hypothesis.

In a pilot study not included in the following chapters, I tried to investigate head scanning behaviour using active target approaches and in relation to the hypothesis that the biosonar beam gradient facilitates target localization. I explored this with blindfolded harbour porpoises as they approached a target (an aluminium rod) suspended by a microfilament line in either a horizontal or vertical orientation. I hypothesized that head scanning movements would primarily be from left-to-right when the rod was oriented vertically, and be in the dorsal-ventral direction when the rod was oriented horizontally, so as to maximize the exploitation of the beam gradient for target localization. This technique of using the beam gradient for localization is analogous to sector scanning used in radars or when radio-tracking to localize an object (a lost biologging tag, for example). Oscillating the target placement on and off of the biosonar beam axis would maximise the changes in reflected energy from the target, thereby enhancing contrast in cues useful for fine-scale localization. In my pilot study, the porpoises were given a fish reward for approaching and touching their rostrum on the center of the rod. However, while they consistently targeted the rod, they were often doing so at the tip of the rod, which outsmarted the experimental set-up since the strongest echo level contrasts were provided along 3 sides (left/right/tip, or up/down/tip) of the target edge, rather than just two (left/right, or up/down). It proved to be a difficult animal training task to get the porpoises to target the center of the rods, even when rod length was increased (from 25 cm, to 40 cm, to 3 m) and rod thickness decreased (from diameters of 1.5 cm, to 1 cm, to 0.3 cm). Furthermore, as the biologging tag was placed immediately posterior to the blowhole, its accelerometers could not measure the degree to which head scanning occurred.

In acknowledgement of this unfruitful pilot study, I flipped the research question around: rather than ask how the porpoises used their biosonar to optimally localize and intercept a target, I designed an experiment that asked them how they ignore, or downplay the perception of, a distractor. In **Chapter V** (Malinka et al., *submitted*), I placed spherical targets at varying inter-target distanced and put the porpoises in a two-alternative forced choice task. The acoustic scene became more complex when the targets were closely spaced, as, in this situation, echoes from both targets would be more similar in level, and the time delays at which they were received would be small. Thus, the porpoises were always confronted with a target and a distractor (of varying prominence) throughout their free-swimming target discriminations. While I still could not comment on the degree of head-scanning due to the aforementioned tag placement,

I could quantify a host of other, related variables to assess their biosonar performance in scenarios with varied clutter, including: number of scans across targets, trial duration, total buzz duration, ranges to targets at both buzz onset and at the discrimination decision. In **Chapter V** (Malinka et al., *submitted*), for example, I found that the number of head scans across targets increased with more closely spaced auditory streams, lending some credence at least to the idea behind my pilot study. Furthermore, I could also quantify the time delay of target echoes, the differences in echo levels, the bearing offset to the distractor, the SLs and the ICIs for all on-axis clicks, as these cues likely provide the echolocator with information that influences the degree of any head scanning behaviour.

Had more research time been available, I would have liked to explore optimal localization hypothesis in porpoises (akin to the Yovel et al., 2010 study) using a dataset collected using a 48-channel planar hydrophone array (presented in Wisniewska et al., 2015). Here, free-swimming, tagged porpoises intercepted a target placed at the center of a large array. Preliminary analysis shows a time series of one trial during which a porpoise scanned her beam around a target throughout an active target approach (**Figure 10**). This figure shows that the beam repeatedly scans near and sometimes across the target, and is consistent with the hypothesis that target localization is facilitated by the gradient of the biosonar beam as in sector scanning. This observation is worth noting, as it is often assumed (as when using the active sonar equation, **Figure 2**) that the target is on-axis. Several examples in this thesis, including **Figure 9**, show that leading up to successful target interception, porpoises glance at targets but do not always scan across them. Indeed, that peaks in the received levels of clicks are used (along with other criteria) to indicate that a click was recorded on-axis can result in false positives of clicks that scan near, but not across a target (see additional criteria used in **Chapter V** to disentangle this; Malinka et al., *submitted*).

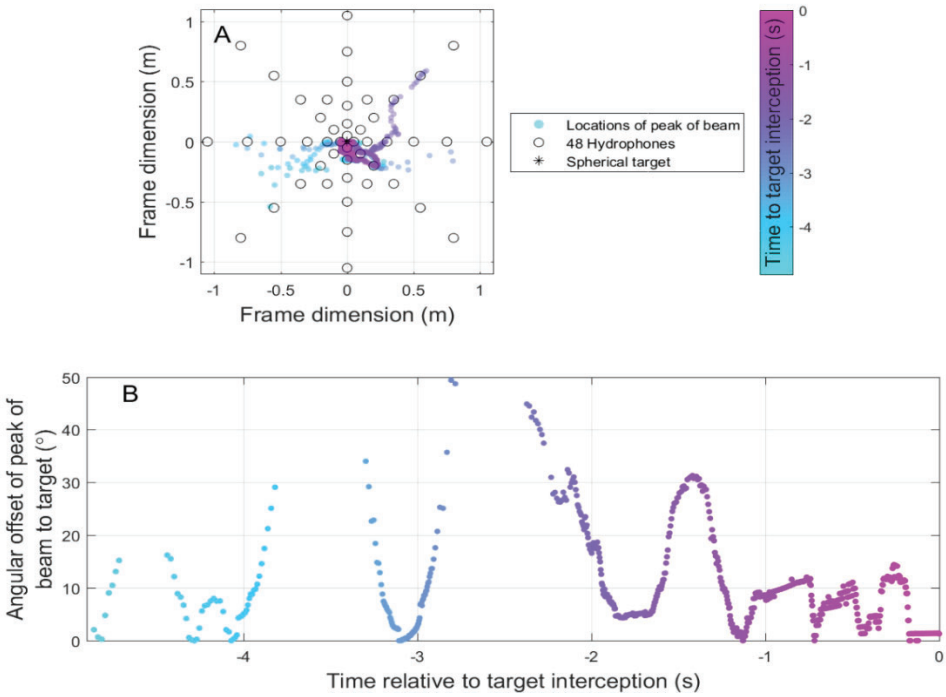

Figure 10. Example porpoise scanning behaviour during active target interception. *A) 2D plot of planar 48-channel hydrophone array, overlaid with the locations of the peak of the beam; B) Time series of angular offset of the peak of the beam to the target, with calculated angles accounting for the variable range to target. The colour denotes time relative to target interception. Data is shown from one trial with Freja (25/7/2021, session 1, trial 6), collected by Danuta M. Wisniewska, and is a subset of the data presented in Wisniewska et al., 2015.*

Implications for Applied Science

Most of the chapters in this PhD thesis focus on blue skies research, exploring curiosity-driven, academic questions. While this is of course important and valuable, it cannot be denied that we are in the midst of a climate crisis and a biodiversity crisis, both of which threaten ecosystem stability (IPBES, 2019). Marine inhabitants, such as the toothed whales focused upon in this thesis, are subject to increasing amounts of anthropogenic disturbance (*e.g.* chemical and noise pollution, overfishing, bycatch, habitat fragmentation and loss, *etc.*) all of which are agents that can drive biodiversity loss. If we have the privilege as a society to fund and research the basic biology of these animals, then, in my opinion, we also have the duty of using our expanding knowledge to protect these animals and their ecosystems. As such, to close the gap between the research bench and the everyday person, and to recognize that much of science is publically funded, I think we scientists owe explanations of how our research is relevant. With all of this in mind, it is valuable to also remember that the findings of blue skies research often critically enable or filter into applied science in ways that are often not initially anticipated, as was the case for the porpoise literature produced by the Bioacoustics Aarhus lab (*e.g.* DeRuiter et al., 2009; Wisniewska et al., 2012) which informed the interpretation of wild behaviours recorded using PAM (*e.g.* Macaulay et al., 2017; Malinka et al., 2018). Another example of knowledge trickling from blue skies to applied research, includes a recent tandem analysis of passive acoustic monitoring data and biologging data: Oestreich et al., (2020) revealed distinct bioacoustic features of blue whale calls useful for distinguishing between migrating and foraging individuals – relevant for monitoring their post-whaling population rebound. I hope here to provide some concrete examples of how my research is relevant to the conservation of wild toothed whales.

There are some obvious applications of the research presented in this PhD thesis. For example, the development of methods used for acoustic monitoring can spread from the academic realm into more applied research. There is an ongoing dialogue about using the array I developed in **Chapter II** (Malinka et al., 2020) to be used in an upcoming iteration of a large scale acoustic density estimation project, 'SAMBAH' (Static Acoustic Monitoring of the Baltic Sea Harbour Porpoise; www.SAMBAH.org, SAMBAH 2016). Here, the array would be used to obtain detection probabilities for the existing network of acoustic monitoring instruments. Acoustic monitoring projects, especially when widespread (as in SAMBAH) or long term, allow us to understand seasonal variations in site usage patterns, identify possible hotspots of habitat preference, and propose areas of conservation (*e.g.* marine Natura 2000 sites).

Acoustic species identification is the first step for using acoustics to assess species presence, abundance, and density, and confidence in this is improved with improved classifiers (Marques et al., 2013). Therefore, another application of the research presented in this PhD thesis is the source parameter quantifications that can inform both the interpretation of PAM data and the design of future PAM arrays targeting specific species. The source parameters of *Kogia* (**Chapter III**, Malinka et al., 2021), for example, immediately lets us design better acoustic classifiers, and also lets us appreciate the short ranges that *Kogia* clicks can be recorded using PAM. Making the raw waveform data accessible further contributes to this, as such data can be used as training data for acoustic classifiers, as well as in the latest generation of deep-learning techniques (*e.g.* Shiu et al., 2020). Indeed, this motivated my publishing of the accompanying dataset of all on- and off-axis *Kogia* clicks (Malinka, 2020). Additionally, acoustic detection probabilities can be modelled using a variety of data inputs, including the source parameters and biosonar beam profiles presented in **Chapter III** (Malinka et al., 2021) and **Chapter IV** (Macaulay et al., 2020). Results of such model can facilitate acoustic density estimations where it might otherwise not be possible (*e.g.* Hildebrand

et al., 2019). Furthermore, taking the full 360° horizontal and vertical (or "4π") beam profile is into account (as presented in **Chapter IV**, Macaulay et al., 2020) will result in significant increases in the accuracy of a detection probability model, and thus the density estimation itself.

Understanding echolocation behaviour, and the biomechanical and processing constraints under which it operates, contribute to the interpretation of animal behaviours captured in acoustic recordings made in the wild. For example, investigating the auditory segregation of multiple, simultaneous echo streams in relation to the auditory integration time in **Chapter V** (Malinka et al., *submitted*) suggests that the ongoing incidence of toothed whale bycatch in nets that are acoustically detectable (*e.g.* Kastelein et al., 2000) is an issue of auditory attention rather than a lack of capability to track both a net and a fish in it or close to it. The hindered hunting performance of bats exposed to the distraction and/or masking of noise has recently been reported (Allen et al., 2021), and it is plausible that the attention demanded by porpoise to keep track of multiple echo streams near a net is made further difficult under noisy conditions. Furthermore, that different auditory streams can be resolved by echolocating porpoises, even when no spatial filtering benefits of a directional biosonar beam can be employed (see **Chapter VI**, Malinka et al., *in prep.*), better equips researchers with interpreting acoustic events that precede entanglement events on a gill net (*e.g.* Maeda et al., 2021).

Reactions and risk factors associated with potential anthropogenic interactions are also explored within this thesis, mostly notably in **Chapter VIII** (Hermannsen et al., *in prep.*) and in **Chapter IX** (Ladegaard et al., *in prep.*). These investigations were prompted by findings that even weak high-frequency vessel noise elicits strong, stereotyped behavioural responses in harbour porpoises (Dyndo et al., 2015). This high-frequency vessel noise is underreported, widespread, and can pose a masking problem (**Figure 11**; Hermannsen et al., 2014). Current in-progress studies that are measuring the auditory brainstem response in harbour porpoises subjected to masking noise suggest that there is little spatial release from masking (Kyhn et al., *in prep.*). In **Chapter VIII** (Hermannsen et al., i*n prep.*), we demonstrate that high frequency masking noise impacts porpoise echolocation performance and output. Such findings, especially when considered alongside their metabolic requirements (Rojano-Doñate et al., 2018), can directly feed into the PCoD/PCaD (Population Consequence of [Acoustic] Disturbance) frameworks (King et al., 2015; Pirotta et al., 2018). These can then inform models on the ecological impacts of human activities (*e.g.* Nabe-Nielsen et al., 2018), as well as inform noise exposure criteria (*e.g.* Southall et al., 2007; Tougaard et al., 2015).

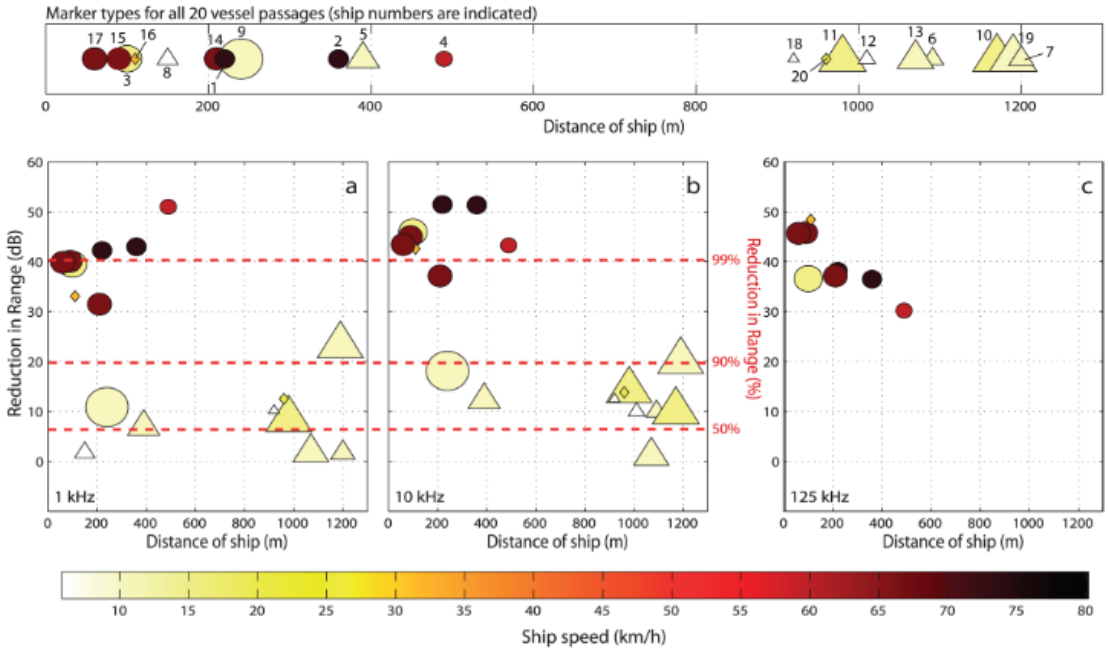

Figure 11. *Acoustic masking impacts of vessel noise on harbour porpoises at third-octave bands centered at a) 1 kHz, b) 10 kHz, and c) 125 kHz, modelled as the reduction in effective porpoise hearing range. Shapes show ship type (with circles as ferries, triangles as freight ships, and diamonds as navy ships), size shows relative ship size, and colour shows ship speed (see colourbar). (From Hermannsen et al., 2014).*

Perspectives

Given the above discussion of conducting research within a degrading environment, I here discuss suggested priorities for related research on toothed whales in the anthropocene. In the future, I think the research community and regulators alike would benefit from specific investigations on the effects of noise on animals that rely on sound from the host of unregulated and widespread noise pollutants that are often overlooked. For example, while the acute but potentially devastating effects of mid-frequency active naval sonars (*e.g.* Wensveen et al., 2019), pile-driving (*e.g.* Tougaard et al., 2009), and seismic air-guns for oil exploration (*e.g.* Madsen et al., 2006) have rightfully garnered much research attention, much less is known about more chronic noise pollutants that are much more widespread in time and space, hence potentially constituting a much bigger problem. These include the less impulsive but more pervasive sounds from vessels, which can dominate soundscapes (Hermannsen et al., 2019), and have been reported to disrupt foraging behaviour in beaked whales (Aguilar de Soto et al., 2006) and porpoises (Wisniewska et al., 2018). Similarly, the use of echosounders is ubiquitous on fishing and research vessels alike, and has recently been reported to drive changes in the acoustic behaviour of beaked whales, with the cessation of echolocating potentially reflecting reduced opportunities for foraging (Cholewiak et al., 2017). Additionally, the use of acoustic harassment/deterrent devices (intended to ward off predators such as seals from the perimeter of salmon aquaculture sites, for example) can be widespread (Findlay et al., 2018) and recent reports on the physiological responses brought about by these noise exposures as demonstrated in porpoises (Elmegaard, 2020) are worrying.

I would be keen to see more research into the effects of masking on toothed whales, both in the context of communication (*e.g.* Branstetter et al., 2021) and echolocation (*e.g.* **Chapter VIII**, Hermannsen et al., *in prep.*). Much research remains to be done in determining the threshold levels at which noise elicits

masking effects. Even if noise does not mask echolocation, it may act as auditory distractor. What is the attentional load of extra noise? How does this relate to absolute noise levels? Does this relate at all to bycatch rates? How are auditory scene segregation tasks impacted by noise?

The effects of noise exposures are likely to depend on the context in which the noises are received. Recent calls for the precautionary principle to be applied to underwater noise emissions (Risch et al., 2021) need to be balanced by both knowledge on the impacts of noise levels from natural sources (*e.g.* ice), which can be acoustically similar to anthropogenic noises (*e.g.* vessels), and by an understanding of the degree of plasticity in any risk/profit balancing behaviours exhibited by the animals. For example, noise exposures [to continuous tidal turbine noise] were tolerated by grey seals when high prey density was available (Hastie et al., 2019). In is important to keep note of the presence and magnitude of realized fitness consequences of noise effects. Knowing the context in which noise is received improves the accuracy in the dose-response curves used to estimate fitness consequences.

Collecting high-resolution, multi-sensor biologging data in environments with varying noise levels allows for context to be explored, with findings able to be fed into population consequences of [acoustic] disturbance models (Nabe-Nielsen et al., 2018). Furthermore, the continuingly evolving technological developments have enabled longer-term acoustic recording tags (on the order of months instead of hours) which will open up opportunities to quantify these effects and provide insight into variations in behavioural responses (*e.g.* Mikkelsen et al., 2019; Parks et al., 2019). Temporal budgets of noise exposures at different TOLs derived from different wild tagged animals will facilitate a contextual understanding of noise exposures. Alongside this, long term PAM efforts will facilitate a better understanding of the ambient soundscapes of natural environments, providing further context to the data provided by animal-borne acoustic sensors.

In addition to the aforementioned noise-related research directions, I also foresee a fruitful future in the findings arising from passive acoustic monitoring datasets as hardware becomes less expensive, software becomes more accessible, acoustic classifiers evolve, recording longevity increases, memory constraints are relieved so that it is easier to record at higher sample rates, and as recording devices become more autonomous. I strongly suspect that these advancements will reveal unexpected bioacoustic features of animals where group-think has perhaps constrained our understanding of their acoustic ecologies – a notable recent example being the ultrasonic pulses produced by Weddell seals and their suspected abilities to use echo-based acoustic spatial perception (Cziko et al., 2020). I look forward especially to hearing about or facilitating bioacoustic findings in EDGE species (Evolutionary Distinct and Globally Endangered); like the *Kogia* presented in this thesis, investigating species that are outliers in general patterns (*e.g.* as in the bioacoustic meta-analysis presented in Jensen et al., 2018) offers us the opportunity to challenge and adjust our ever-evolving understanding of these fascinating creatures.

References

Aguilar Soto, N., Johnson, M., Madsen, P. T., Tyack, P. L., Bocconcelli, A., and Fabrizio Borsani, J. (2006). Does intense ship noise disrupt foraging in deep-diving cuvier's beaked whales (*Ziphius cavirostris*)? **Mar Mamm Sci**, 22(3), 690-699.

Aguilar Soto, N., Johnson, M. P., Madsen, P. T., Díaz, F., Domínguez, I., Brito, A., and Tyack, P. (2008). Cheetahs of the deep sea: deep foraging sprints in short-finned pilot whales off Tenerife (Canary Islands). **J Anim Ecol**, 77(5), 936-947.

Akamatsu, T., Wang, D., Wang, K., and Naito, Y. (2005). Biosonar behaviour of free-ranging porpoises. **Proc Roy Soc B**, 272(1565), 797-801.

Allen, L. C., Hristov, N. I., Rubin, J. J., Lightsey, J. T., and Barber, J. R. (2021). Noise distracts foraging bats. **Proc Roy Soc B**, 288 (1944), 20202689.

Ames, A. E., Beedholm, K., and Madsen, P. T. (2020). Lateralized sound production in the beluga whale (*Delphinapterus leucas*). **J Exp Biol**, 223(17).

Au, W. W. (1993). The Sonar of Dolphins. Springer-Verlag, New York.

Au, W. W. L. (2014). Dolphin biosonar target detection in noise: Wrap up of a past experiment. **J Acoust Soc Am**, 136 (1), 9-12.

Au, W. W., and Moore, P. W. (1984). Receiving beam patterns and directivity indices of the Atlantic bottlenose dolphin *Tursiops truncatus*. **J Acoust Soc Am**, 75(1), 255-262.

Au, W. W., and Benoit-Bird, K. J. (2003). Automatic gain control in the echolocation system of dolphins. **Nature**, 423 (6942), 861-863.

Au, W. W., Moore, P. W., and Pawloski, D. A. (1988). Detection of complex echoes in noise by an echolocating dolphin. **J Acoust Soc Am**, 83 (2), 662-668.

Au, W. W., Kastelein, R. A., Rippe, T., and Schooneman, N. M. (1999). Transmission beam pattern and echolocation signals of a harbor porpoise (*Phocoena phocoena*). **J Acoust Soc Am**, 106 (6), 3699-3705.

Au, W. W., Branstetter, B. K., Benoit-Bird, K. J., and Kastelein, R. A. (2009). Acoustic basis for fish prey discrimination by echolocating dolphins and porpoises. **J Acoust Soc Am**, 126(1), 460-467.

Aubauer, R., Au, W. W., Nachtigall, P. E., Pawloski, D. A., and DeLong, C. M. (2000). Classification of electronically generated phantom targets by an Atlantic bottlenose dolphin (*Tursiops truncatus*). **J Acoust Soc Am**, 107(5), 2750-2754.

Arditi, G., Weiss, A.J., and Yovel, Y. (2015). Object localization using a biosonar beam: how opening your mouth improves localization. **R Soc Open Sci**, 2 (8).

Aytekin, M., Grassi, E., Sahota, M., and Moss, C. F. (2004). The bat head-related transfer function reveals binaural cues for sound localization in azimuth and elevation. **J Acoust Soc Am**, 116 (6), 3594-3605.

Barber, J., Razak, K., and Fuzessery, Z. (2003). Can two streams of auditory information be processed simultaneously? Evidence from the gleaning bat Antrozous pallidus. **J Comp Phys A**, 189(11), 843-855.

Barlow, J., and Taylor, B. L. (2005). Estimates of sperm whale abundance in the northeastern temperate Pacific from a combined acoustic and visual survey. **Mar Mamm Sci**, 21(3), 429-445.

Barlow, J., Griffiths, E. T., Klinck, H., and Harris, D. V. (2018). Diving behavior of Cuvier's beaked whales inferred from three-dimensional acoustic localization and tracking using a nested array of drifting hydrophone recorders. **J Acoust Soc Am**, 144(4), 2030-2041.

Beedholm, K., Madsen, P. T., and Tyack, P. L. (*In prep*). Properties and utilization of mid- to long-latency auditory potentials for the study of hearing in the harbour porpoise.

Benoit-Bird, K. J., Moline, M. A., and Southall, B. L. (2017). Prey in oceanic sound scattering layers organize to get a little help from their friends. **Limnol Oceanog**, 62 (6), 2788-2798.

Boonman, A., and Jones, G. (2002). Intensity control during target approach in echolocating bats; stereotypical sensori-motor behaviour in Daubenton's bats, *Myotis daubentonii*. **J Exp Biol**, 205(18), 2865-2874.

Branstetter, B. K., Leger, J. S., Acton, D., Stewart, J., Houser, D., Finneran, J. J., and Jenkins, K. (2017). Killer whale (*Orcinus orca*) behavioral audiograms. **J Acoust Soc Am**, 141(4), 2387-2398.

Branstetter, B. K., Felice, M., and Robeck, T. (2021). Auditory masking in killer whales (*Orcinus orca*): Critical ratios for tonal signals in Gaussian noise. **J Acoust Soc Am**, 149(3), 2109-2115.

Bregman, A. (1990) Auditory stream analysis: The perceptual organization of sound. MIT Press, Cambridge, MA.

Brill, R. L., Sevenich, M. L., Sullivan, T. J., Sustman, J. D., and Witt, R. E. (1988). Behavioral evidence for hearing through the lower jaw by an echolocating dolphin (*Tursiops truncatus*). **Mar Mamm Sci**, 4(3), 223-230.

Brinkløv, S., Kalko, E. K., and Surlykke, A. (2010). Dynamic adjustment of biosonar intensity to habitat clutter in the bat *Macrophyllum macrophyllum* (*Phyllostomidae*). **Behav Ecol Sociobiol**, 64 (11), 1867-1874.

Cahlander, D., McCue, J., and Webster, F. (1964). The determination of distance by echolocating bats. **Nature**, 201 (4919), 544-546.

Carlyon, R. P., Cusack, R., Foxton, J. M., and Robertson, I. H. (2001). Effects of attention and unilateral neglect on auditory stream segregation. **J Exp Psychol Hum Percept Perform**, 27:115-127.

Cholewiak, D., DeAngelis, A. I., Palka, D., Corkeron, P. J., and Van Parijs, S. M. (2017). Beaked whales demonstrate a marked acoustic response to the use of shipboard echosounders. **Roy Soc Open Sci**, 4(12), 170940.

Cziko, P. A., Munger, L. M., Santos, N. R., and Terhune, J. M. (2020). Weddell seals produce ultrasonic vocalizations. **J Acoust Soc Am**, 148(6), 3784-3796.

Dehnhardt, G., Mauck, B., and Bleckmann, H. (1998). Seal whiskers detect water movements. **Nature**, 394(6690), 235-236.

DeRuiter, S. L., Bahr, A., Blanchet, M.-A., Hansen, S. F., Kristensen, J. H., Madsen, P. T., Tyack, P. L., and Wahlberg, M. (2009). Acoustic behaviour of echolocating porpoises during prey capture. **J Exp Biol**, 212 (19), 3100-3107.

Dukas, R. (1999). Costs of memory: ideas and predictions. **J Theor Biol**, 197 (1), 41-50.
Dukas, R., and Kamil, A. C. (2000). The cost of limited attention in blue jays. **Behav Ecol**, 11 (5), 502-506.
Dyndo, M., Wiśniewska, D. M., Rojano-Doñate, L., and Madsen, P. T. (2015). Harbour porpoises react to low levels of high frequency vessel noise. **Sci Rep**, 5, 11083.
Elmegaard, S. L. (2020). Ecophysiology of echolocating toothed whales, PhD thesis, Aarhus University.
Fais, A., Johnson, M., Wilson, M., Soto, N. A., and Madsen, P. T. (2016). Sperm whale predator-prey interactions involve chasing and buzzing, but no acoustic stunning. **Sci Rep**, 6, 28562.
Fenton, B. M., Jensen, F. H., Kalko, E. K., and Tyack, P. L. (2014). Sonar signals of bats and toothed whales. *In*: A. Surlykke, P. E. Nachtigall, R. R. Fay, and A. N. Popper (Eds.), Biosonar (pp. 11-59): Springer.
Findlay, C. R., Ripple, H. D., Coomber, F., Froud, K., Harries, O., van Geel, N. C. F., . . . and Wilson, B. (2018). Mapping widespread and increasing underwater noise pollution from acoustic deterrent devices. **Mari Poll Bull**, 135, 1042-1050.
Finneran, J. J., Carder, D. A., Schlundt, C. E., and Ridgway, S. H. (2005). Temporary threshold shift in bottlenose dolphins (*Tursiops truncatus*) exposed to mid-frequency tones. **J Acoust Soc Am**, 118(4), 2696-2705.
Finneran, J. J., Branstetter, B. K., Houser, D. S., Moore, P. W., Mulsow, J., Martin, C., and Perisho, S. (2014). High-resolution measurement of a bottlenose dolphin's (*Tursiops truncatus*) biosonar transmission beam pattern in the horizontal plane. **J Acoust Soc Am**, 136(4), 2025-2038.
Finneran, J. J., Jones, R., Mulsow, J., Houser, D. S., and Moore, P. W. (2019). Jittered echo-delay resolution in bottlenose dolphins (*Tursiops truncatus*). **J Comp Phys A**, 205(1), 125-137.
Galambos, R. (1942). Cochlear potentials elicited from bats by supersonic sounds. **J Acoust Soc Am**, 14(1), 41-49.
Gassmann, M., Wiggins, S., & Hildebrand, J. (2015). Three-dimensional tracking of Cuvier's beaked whales' echolocation sounds using nested hydrophone arrays. **J Acoust Soc Am**, 138(4), 2483-2494.
Ghose, K., and Moss, C. F. (2003). The sonar beam pattern of a flying bat as it tracks tethered insects. **J Acoust Soc Am** 114 (2), 1120-1131.
Ghose, K., and Moss, C. F. (2006). Steering by hearing: a bat's acoustic gaze is linked to its flight motor output by a delayed, adaptive linear law. **J Neurosci**, 26(6), 1704-1710.
Griffin, D. R. (1944). Echolocation by blind men, bats and radar. **Science**, 100(2609), 589-590.
Griffin, D. R. (1958). Listening in the dark: the acoustic orientation of bats and men.
Hastie, G., Merchant, N. D., Götz, T., Russell, D. J., Thompson, P., and Janik, V. M. (2019). Effects of impulsive noise on marine mammals: investigating range-dependent risk. **Ecol Appl**, 29(5), e01906.
Heerfordt, A., Møhl, B., and Wahlberg, M. (2007). A wideband connection to sperm whales: A fiber-optic, deep-sea hydrophone array. **Deep Sea Res I**, 54(3), 428-436.
Henson Jr, O. (1965). The activity and function of the middle-ear muscles in echo-locating bats. **J Physiol**, 180(4), 871-887.
Hermannsen, L. (2019). Anthropogenic underwater noise pollution and its impacts on marine mammals, PhD thesis, Aarhus University.
Hermannsen, L., Mikkelsen, L., Tougaard, J., Beedholm, K., Johnson, M., and Madsen, P. T. (2019). Recreational vessels without Automatic Identification System (AIS) dominate anthropogenic noise contributions to a shallow water soundscape. **Sci Rep**, 9(1), 1-10.
Hermannsen, L., Tønnesen, P., Ladegaard, M., Malinka, C. E., Tougaard, J., and Madsen, P. T. (*In prep*). Porpoise echolocation can be masked by weak high-frequency vessel noise
Hildebrand, J. A., Frasier, K. E., Baumann-Pickering, S., Wiggins, S. M., Merkens, K. P., Garrison, L. P., Soldevilla, M. S., and M. A. McDonald. (2019). Assessing seasonality and density from passive acoustic monitoring of signals presumed to be from pygmy and dwarf sperm whales in the Gulf of Mexico. **Front Mar Sci**, 6, article 66.
Hiryu, S., Hagino, T., Riquimaroux, H., and Watanabe, Y. (2007). Echo-intensity compensation in echolocating bats (*Pipistrellus abramus*) during flight measured by a telemetry microphone. **J Acoust Soc Am**, 121(3), 1749-1757.
Houser, D., Martin, S. W., Bauer, E. J., Phillips, M., Herrin, T., Cross, M., . . . and P. W. Moore. (2005). Echolocation characteristics of free-swimming bottlenose dolphins during object detection and identification. **J Acoust Soc Am**, 117(4), 2308-2317.
IPBES. 2019. Summary for policymakers of the global assessment report on biodiversity and ecosystem services of the Intergovernmental Science Policy Platform on Biodiversity and Ecosystem Services. (S. Diaz, J. Settele, E. Brondizio, H. T. Ngo, M. Gueze, J. Agard, A. Arneth, et al., eds.). Bonn, Germany.
Jakobsen, L., Ratcliffe, J. M., and Surlykke, A. (2013). Convergent acoustic field of view in echolocating bats. **Nature**, 493:93-96.

Jensen, F. H., Bejder, L., Wahlberg, M., and Madsen, P. T. (2009). Biosonar adjustments to target range of echolocating bottlenose dolphins (*Tursiops sp.*) in the wild. **J Exp Biol**, 212, 1078-1086.

Jensen, F. H., Rocco, A., Mansur, R. M., Smith, B. D., Janik, V. M., and Madsen, P. T. (2013). Clicking in shallow rivers: short-range echolocation of Irrawaddy and Ganges river dolphins in a shallow, acoustically complex habitat. **PloS one**, 8(4), e59284.

Jensen, F. H., Wahlberg, M., Beedholm, K., Johnson, M., Aguilar de Soto, N., and Madsen, P. T. (2015). Single-click beam patterns suggest dynamic changes to the field of view of echolocating Atlantic spotted dolphins (*Stenella frontalis*) in the wild. **J Exp Biol**, 218:1314-1324.

Jensen, F. H., Johnson, M., Ladegaard, M., Wisniewska, D., Madsen, P. T. (2018). Narrow acoustic field of view drives frequency scaling in toothed whale biosonar. **Curr Biol**, 28, 1-8.

Johnson, M. (2014). On-animal methods for studying echolocation in free-ranging animals. *In*: A. Surlykke, P. E. Nachtigall, R. R. Fay, and A. N. Popper (Eds.), Biosonar (pp. 195-229): Springer.

Johnson, M. P., and Tyack, P. L. (2003) A digital acoustic recording tag for measuring the response of wild marine mammals to sound. **IEEE J Ocean Eng,** 28:3-12.

Johnson, M., Madsen, P. T., Zimmer, W. M., Aguilar de Soto, N., and Tyack, P. L. (2004). Beaked whales echolocate on prey. **Proc Roy Soc B** 271:S383-S386.

Johnson, M., Madsen, P. T., Zimmer, W., Aguilar de Soto, N., and Tyack, P. (2006). Foraging Blainville's beaked whales (*Mesoplodon densirostris*) produce distinct click types matched to different phases of echolocation. **J Exp Biol,** 209 (24), 5038-5050.

Johnson, M., Hickmott, L., Aguilar de Soto, N., and Madsen, P. T. (2008). Echolocation behaviour adapted to prey in foraging Blainville's beaked whale (*Mesoplodon densirostris*). **Proc Roy Soc B**, 275 (1631), 133-139.

Kadane, J., and Penner, R. (1983). Range ambiguity and pulse interval jitter in the bottlenose dolphin. **J Acoust Soc Am**, 74(3), 1059-1061.

Kastelein, R., Au, W., De Haan, D. (2000). Detection distances of bottom-set gillnets by harbour porpoises (*Phocoena phocoena*) and bottlenose dolphins (*Tursiops truncatus*). **Mar Environ Res**, 49 (4), 359-375.

Kastelein, R. A., Janssen, M., Verboom, W. C., and de Haan, D. (2005). Receiving beam patterns in the horizontal plane of a harbor porpoise (Phocoena phocoena). **J Acoust Soc Am**, 118(2), 1172-1179.

Kellogg, W. N. (1961). Porpoises and sonar: University of Chicago Press.

Ketten, D. R. (1997). Structure and function in whale ears. **Bioacoustics**, 8(1-2), 103-135.

Kick, S. A., and Simmons, J. A. (1984). Automatic gain control in the bat's sonar receiver and the neuroethology of echolocation. **J Neurosci**, 4(11), 2725-2737.

King, S. L., Schick, R. S., Donovan, C., Booth, C. G., Burgman, M., Thomas, L., and Harwood, J. (2015). An interim framework for assessing the population consequences of disturbance. **Meth Ecol Evol**, 6(10), 1150-1158.

Kloepper, L., Nachtigall, P., Gisiner, R., and Breese, M. (2010). Decreased echolocation performance following high-frequency hearing loss in the false killer whale (*Pseudorca crassidens*). **J Exp Biol**, 213(21), 3717-3722.

Kloepper, L. N., Buck, J. R., Liu, Y., and Nachtigall, P. E. (2018). Off-axis targets maximize bearing Fisher Information in broadband active sonar. **J Acoust Soc Am**, 143(1), EL43-EL48.

Koblitz, J. C., Wahlberg, M., Stilz, P., Madsen, P. T., Beedholm, K., Schnitzler, H.-U. (2012). Asymmetry and dynamics of a narrow sonar beam in an echolocating harbor porpoise. **J Acoust Soc Am**, 131:2315-2324.

Kothari, N. B., Wohlgemuth, M. J., Hulgard, K., Surlykke, A., and Moss, C. F. (2014). Timing matters: sonar call groups facilitate target localization in bats. **Front Physiol**, 5, 168.

Knutsen, P. M., Pietr, M., and Ahissar, E. (2006). Haptic object localization in the vibrissal system: behavior and performance. **J Neurosci**, 26(33), 8451-8464.

Kyhn, L. A., Tougaard, J., Jensen, F., Wahlberg, M., Stone, G., Yoshinaga, A., Beedholm, K., and Madsen, P. T. (2009). Feeding at a high pitch: Source parameters of narrow band, high-frequency clicks from echolocating off-shore hourglass dolphins and coastal Hector's dolphins. **J Acoust Soc Am**, 125(3), 1783-1791.

Kyhn, L. A., Jensen, F. H., Beedholm, K., Tougaard, J., Hansen, M., and Madsen, P. T. (2010). Echolocation in sympatric Peale's dolphins (*Lagenorhynchus australis*) and Commerson's dolphins (*Cephalorhynchus commersonii*) producing narrow-band high-frequency clicks. **J Exp Biol**, 213(11), 1940-1949.

Kyhn, L. A., Tougaard, J., Beedholm, K., Jensen, F. H., Ashe, E., Williams, R., and Madsen, P. T. (2013). clicking in a killer whale habitat: narrow-band, high-frequency biosonar clicks of harbour porpoise (*Phocoena phocoena*) and Dall's porpoise (*Phocoenoides dalli*). **PloS one**, 8(5), e63763.

Kyhn, L.A., Beedholm, K., Smith, A. and Madsen, P. T. (*In prep.*) In-band noise masks auditory responses to echo-like clicks at low SNR levels with limited spatial release due to angle of arrival.

Ladegaard, M., Jensen, F. H., de Freitas, M., da Silva, V. M. F., and Madsen, P. T. (2015). Amazon river dolphins (*Inia geoffrensis*) use a high-frequency short-range biosonar. **J Exp Biol**, 218(19), 3091-3101.

Ladegaard, M., and Madsen, P. T. (2019). Context-dependent biosonar adjustments during active target approaches in echolocating harbour porpoises. **J Exp Biol**, 222, jeb. 206169.

Ladegaard, M., Beedholm, K., Johnson, M., Malinka C. E., and Madsen, P. T. (*In prep.*) Sensory-motor control of output levels as a function of range and target strength in echolocating harbour porpoises.

Lavie, N. (2005). Distracted and confused?: Selective attention under load. **Trends Cog Sci**, 9 (2), 75-82.

Macaulay, J. D. J., Gordon, J. C. D., Gillespie, D., Malinka, C. E., and Northridge, S. (2017). Passive acoustic methods for fine-scale tracking of harbour porpoises in tidal rapids. **J Acoust Soc Am**, 141(2), 1120-1132.

Macaulay, J. D. J., Malinka, C. E., Gillespie, D., and Madsen, P. T. (2020). High resolution three-dimensional beam radiation pattern of harbour porpoise clicks with implications for passive acoustic monitoring. **J Acoust Soc Am**, 147 (6): 4175-4188.

Macías, S., Mora, E. C., Hechavarría, J. C., & Kössl, M. (2016). Echo-level compensation and delay tuning in the auditory cortex of the mustached bat. **Eur J Neurosci**, 43(12), 1647-1660.

Madsen, P. T., and Surlykke, A. (2013). Functional convergence in bat and toothed whale. **Physiol,** 28, 276-283.

Madsen, P. T., and Surlykke, A. (2014). Echolocation in air and water. In: A. Surlykke, P. E. Nachtigall, R. R. Fay, and A. N. Popper (Eds.), Biosonar (pp. 257-304): Springer.

Madsen, P. T., and Wahlberg, M. (2007). Recording and quantification of ultrasonic echolocation clicks from free-ranging toothed whales. **Deep Sea Res I**, 54(8), 1421-1444.

Madsen, P. T., Kerr, I., and Payne, R. (2004). Echolocation clicks of two free-ranging, oceanic delphinids with different food preferences: false killer whales *Pseudorca crassidens* and Risso's dolphins *Grampus griseus*. **J Exp Biol**, 207(11), 1811-1823.

Madsen, P., Johnson, M., de Soto, N. A., Zimmer, W., and Tyack, P. (2005a). Biosonar performance of foraging beaked whales (*Mesoplodon densirostris*). **J Exp Biol**, 208(2), 181-194.

Madsen, P. T., Carder, D., Bedholm, K., and Ridgway, S. (2005b). Porpoise clicks from a sperm whale nose—Convergent evolution of 130 kHz pulses in toothed whale sonars? **Bioacoustics**, 15 (2), 195-206.

Madsen, P. T., Johnson, M., Miller, P. J. O., Aguilar Soto, N., Lynch, J., and Tyack, P. (2006). Quantitative measures of air-gun pulses recorded on sperm whales (*Physeter macrocephalus*) using acoustic tags during controlled exposure experiments. . **J Acoust Soc Am**, 120, 2366–2379

Madsen, P. T., Wilson, M., Johnson, M., Hanlon, R. T., Bocconcelli, A., Aguilar de Soto, N., and Tyack, P. L. (2007). Clicking for calamari: toothed whales can echolocate squid *Loligo pealeii*. **Aquat Biol**, 1(2), 141-150.

Madsen, P. T., Lammers, M., Wisniewska, D., and Beedholm, K. (2013a). Nasal sound production in echolocating delphinids (*Tursiops truncatus* and *Pseudorca crassidens*) is dynamic, but unilateral: clicking on the right side and whistling on the left side. **J Exp Biol**, 216(21), 4091-4102.

Madsen, P. T., Aguilar de Soto, N., Arranz, P., and Johnson, M. (2013b). Echolocation in Blainville's beaked whales (*Mesoplodon densirostris*). **J Comp Phys A,** 199:451-469.

Maeda, S., Sakurai, K., Akamatsu, T., Matsuda, A., Yamamura, O., Kobayashi, M., and Matsuishi, T. F. (2021). Foraging activity of harbour porpoises around a bottom-gillnet in a coastal fishing ground, under the risk of bycatch. **PloS One**, 16(2), e0246838.

Malinka, C. E., Atkins, J., Johnson, M., Tønnesen, P. H., Dunn, C., Claridge, D., Aguilar de Soto, N., and Madsen, P. T. (2020). An autonomous hydrophone array to study the acoustic ecology of deep-water toothed whales. **Deep Sea Res I,** 158C: 103233.

Malinka, C. E., Tønnesen, P., Dunn, C., Claridge, D., Gridley, T., Elwen, S. H., and Madsen, P. T. (2021). Echolocation click parameters and acoustic behaviour of wild dwarf sperm whale (*Kogia sima*). **J Exp Biol**, 224, jeb240689.

Malinka, C. E. (2020). Dataset accompanying: Echolocation click parameters and biosonar behaviour of the dwarf sperm whale (*Kogia sima*). http://doi.org/10.5281/zenodo.4273697

Malinka C. E., Rojano-Donate, L., and Madsen, P. T. (*Submitted*). Directional biosonar beams allow echolocating harbour porpoises to actively discriminate and intercept closely-spaced targets.

Malinka, C. E., Beedholm, K., and Madsen, P. T. (*In prep.*). Auditory stream segregation in echolocating porpoises during active target approaches.

Marques, T. A., Thomas, L., Martin, S. W., Mellinger, D. K., Ward, J. A., Moretti, D. J., Harris, D., and P. L. Tyack (2013). Estimating animal population density using passive acoustics. **Biol Rev**, 88(2), 287-309.

Mikkelsen, L., Johnson, M., Wisniewska, D. M., van Neer, A., Siebert, U., Madsen, P. T., and Teilmann, J. (2019). Long-term sound and movement recording tags to study natural behavior and reaction to ship noise of seals. **Ecol Evol**, 1-14.

Møhl, B., and Andersen, S. (1973). Echolocation: high-frequency component in the click of the Harbour Porpoise (*Phocoena ph.* L.). **J Acoust Soc Am**, 54(5), 1368-1372.

Moore, P., Hall, R., Friedl, W., and Nachtigall, P. (1984). The critical interval in dolphin echolocation: What is it? **J Acoust Soc Am**, 76 (1), 314-317.

Moore, P. W. B., Dankiewicz, L. A., and Houser, D. S. (2008). Beamwidth control and angular target detection in an echolocating bottlenose dolphin (*Tursiops truncatus*). **J Acoust Soc Am**, 124:3324-3332.

Morisaka, T., and Connor, R. (2007). Predation by killer whales (*Orcinus orca*) and the evolution of whistle loss and narrow-band high frequency clicks in odontocetes. **J Evol Biol**, 20(4), 1439–1458.

Moss, C. F., and Schnitzler, H.-U. (1995). Behavioral studies of auditory information processing. *In*: Hearing by bats (pp. 87-145): Springer.

Moss, C. F., and Surlykke, A. (2001). Auditory scene analysis by echolocation in bats. **J Acoust Soc Am**, 110 (4), 2207-2226.

Moss, C. F., and Surlykke, A. (2010). Probing the natural scene by echolocation in bats. **Front Behav Neurosci**, 4, 33.

Moss, C. F., Bohn, K., Gilkenson, H., and Surlykke, A. (2006). Active listening for spatial orientation in a complex auditory scene. **PLoS Biol**, 4 (4), e79.

Moss, C. F., Chiu, C., and Surlykke, A. (2011). Adaptive vocal behavior drives perception by echolocation in bats. **Curr Opinion Neurobiol**, 21 (4), 645-652.

Nabe-Nielsen, J., van Beest, F. M., Grimm, V., Sibly, R. M., Teilmann, J., and P. M. Thompson (2018). Predicting the impacts of anthropogenic disturbances on marine populations. **Conserv Lett**, 11(5), e12563.

Nachtigall, P. E., Supin, A. Y., Pacini, A. F., and Kastelein, R. A. (2018). Four odontocete species change hearing levels when warned of impending loud sound. **Integr Zool**, 13(2), 160-165.

Nelson, M. E., and MacIver, M. A. (2006). Sensory acquisition in active sensing systems. **J Comp Phys A,** 192 (6), 573-586.

Neuweiler, G. (1990). Auditory adaptations for prey capture in echolocating bats. **Physiol Rev**, 70(3), 615-641.

Niven, J. E., and Laughlin, S. B. (2008). Energy limitation as a selective pressure on the evolution of sensory systems. **J Exp Biol**, 211, 1792-1804.

Norris, K. S., Prescott, J. H., Asa-Dorian, P. V., and Perkins, P. (1961). An experimental demonstration of echo-location behavior in the porpoise, *Tursiops truncatus* (Montagu). **Biol Bull**, 120(2), 163-176.

Oestreich, W. K., Fahlbusch, J. A., Cade, D. E., Calambokidis, J., Margolina, T., Joseph, J., … and J. P. Ryan. (2020). Animal-borne metrics enable acoustic detection of blue whale migration. **Curr Biol**, 30(23), 4773-4779.e4773.

Parks, S. E., Dombroski, J. R. G., Shorter, K. A., Wiley, D. N., Ross, M., and Johnson, M. (2019). Extended duration acoustic tags provide insight into variation in behavioral response to noise by marine mammals. **Proceedings of Meetings on Acoustics**, 37(1), 010013.

Pedersen, M. B., Tønnesen, P. H., Malinka, C. E., Ladegaard, M., Johnson, M., Aguilar de Soto, N., and Madsen, P. T. (2021). Echolocation click parameters of short-finned pilot whales (*Globicephala macrorhynchus*) in the wild. **J Acoust Soc Am**, 149(3), 1923-1931.

Penner, R. H. (1988). Attention and detection in dolphin echolocation. *In*: Animal Sonar (pp. 707-713): Springer.

Pierce, G. W., and Griffin, D. R. (1938). Experimental determination of supersonic notes emitted by bats. **J Mamm**, 19(4), 454-455.

Pirotta, E., Booth, C. G., Costa, D. P., Fleishman, E., Kraus, S. D., Lusseau, D., . . . Schwarz, L. K. (2018). Understanding the population consequences of disturbance. **Ecol Evol**, 8(19), 9934-9946.

Plön, S. (2004). The status and natural history of pygmy (*Kogia breviceps*) and dwarf (*K. sima*) sperm whales off Southern Africa. PhD thesis, Rhodes University Grahamstown, South Africa.

Rasmussen, M. H., Miller, L. A., and Au, W. W. (2002). Source levels of clicks from free-ranging white-beaked dolphins (*Lagenorhynchus albirostris* Gray 1846) recorded in Icelandic waters. **J Acoust Soc Am**, 111(2), 1122-1125.

Ratcliffe, J. M., Elemans, C. P., Jakobsen, L., and Surlykke, A. (2013). How the bat got its buzz. **Biol Lett**, 9(2), 20121031.

Reichmuth, C., Sills, J. M., Mulsow, J., and Ghoul, A. (2019). Long-term evidence of noise-induced permanent threshold shift in a harbor seal (*Phoca vitulina*). **J Acoust Soc Am**, 146(4), 2552-2561.

Richardson, W., Greene Jr, C., Malme, C., and Thomson, D. (1995). Marine mammals and noise. San Diego, USA: Academic Press.

Risch, D., Calderan, S., Leaper, R., Weilgart, L., & Werner, S. (2021). current knowledge already justifies underwater noise reduction. **Trends Ecol Evol**, 2802.

Rojano-Doñate, L., McDonald, B. I., Wisniewska, D. M., Johnson, M., Teilmann, J., Wahlberg, M., . . . Madsen, P. T. (2018). High field metabolic rates of wild harbour porpoises. **J Exp Biol**, 221(23), jeb185827.

SAMBAH (2016) Static Acoustic Monitoring of the Baltic Sea Harbour Porpoise (SAMBAH). Final report under the LIFE+ project LIFE08 NAT/S/000261. Kolmårdens Djurpark AB, Kolmården.

Schevill, W. E., and Lawrence, B. (1956). Food-finding by a captive porpoise (*Tursiops trucatus*). **Brevorica**, (53), 1-15.

Schnitzler, H.-U., and Kalko, E. K. (2001). Echolocation by Insect-Eating Bats We define four distinct functional groups of bats and find differences in signal structure that correlate with the typical echolocation tasks faced by each group. **Bioscience**, 51 (7), 557-569.

Schrøder, A. E. M., Beedholm, K., and Madsen, P. T. (2017). Time varying auditory gain control in response to double pulse stimuli in harbour porpoises is not mediated by a stapedial reflex. **Biol Open**, bio. 021469.

Shaffer, J. W., Moretti, D., Jarvis, S., Tyack, P., and Johnson, M. (2013). Effective beam pattern of the Blainville's beaked whale (*Mesoplodon densirostris*) and implications for passive acoustic monitoring. **J Acoust Soc Am**, 133:1770-1784.

Shiu, Y., Palmer, K. J., Roch, M. A., Fleishman, E., Liu, X., Nosal, E.-M., Helble, T., Cholewiak, D., Gillespie, D., and H. Klinck. (2020). Deep neural networks for automated detection of marine mammal species. **Sci Rep**, 10(1), 607.

Simmons, J. A. (1973). The resolution of target range by echolocating bats. **J Acoust Soc Am**, 54(1), 157-173.

Simmons, J. A., Kick, S. A., Moffat, A. J., Masters, W. M., and Kon, D. (1988). Clutter interference along the target range axis in the echolocating bat, *Eptesicus fuscus*. **J Acoust Soc Am,** 84:551-559.

Smotherman, M., and Bakshi, K. (2019). Forward masking enhances the auditory brainstem response in the free-tailed bat, *Tadarida brasiliensis*, during a critical time window for sonar reception. **J Acoust Soc Am**, 145(1), EL19-EL24.

Southall, B. L., Bowles, A. E., Ellison, W. T., Finneran, J. J., Gentry, R. L., Greene, C. R., . . . and P. L. Tyack (2007). Marine mammal noise exposure criteria: Initial scientific recommendations. **Aquat Mamm**, 33(4), 411-414.

Starkhammar, J., Moore, P. W., Talmadge, L., and D. S. Houser. (2011). Frequency-dependent variation in the two-dimensional beam pattern of an echolocating dolphin. **Biol Lett**, 7(6), 836-839.

Stidsholt, L., Müller, R., Beedholm, K., Ma, H., Johnson, M., and Madsen, P. T. (2020). Energy compensation and received echo level dynamics in constant-frequency bats during active target approaches. **J Exp Biol**, 223 (2), jeb.217109.

Stidsholt, L., Greif, S., Goerlitz, H. R., Beedholm, K., Macaulay, J., Johnson, M., and Madsen, P.T. (2021). Hunting bats adjust their echolocation to receive weak prey echoes for clutter reduction. **Sci Adv**, 7 (10), eabf1367.

Supin, A. Y., Nachtigall, P. E., and Breese, M. (2010). Target distance-dependent variation of hearing sensitivity during echolocation in a false killer whale. **J Acoust Soc Am**, 127(6), 3830-3836.

Supin, A. Y., and Nachtigall, P. E. (2013). Gain control in the sonar of odontocetes. **J Comp Phys A**, 199(6), 471-478.

Surlykke, A., Ghose, K., and Moss, C. F. (2009). Acoustic scanning of natural scenes by echolocation in the big brown bat, *Eptesicus fuscus*. **J Exp Biol**, 212(7), 1011-1020.

Surlykke, A., and Nachtigall, P. E. (2014). Biosonar of bats and toothed whales: an overview. In: Biosonar (pp. 1-9): Springer.

Thomas, J. A., and Turl, C. W. (1990). Echolocation characteristics and range detection threshold of a false killer whale (*Pseudorca crassidens*). In: Sensory abilities of cetaceans (pp. 321-334): Springer.

Tougaard, J., Carstensen, J., Teilmann, J., Skov, H., and Rasmussen, P. (2009). Pile driving zone of responsiveness extends beyond 20 km for harbor porpoises (*Phocoena phocoena*). **J Acoust Soc Am**, 126(1), 11-14.

Tougaard, J., Wright, A. J., and Madsen, P. T. (2015). Cetacean noise criteria revisited in the light of proposed exposure limits for harbour porpoises. **Mar Poll Bull**, 90, 196– 208.

Urick, R. J. (1983). Principles of underwater sound (3rd ed.). Peninsula, Los Altos: McGraw-Hill.

Vance, H., Madsen, P. T., Aguilar de Soto, N., Wisniewska, D., Ladegaard, M., Hooker, S., and Johnson, M. (*Submitted*). Echolocating whales use ultra-fast echo-kinetic responses to track evasive prey.

Vel'min, V., and Dubrovsky, N. (1975). Auditory analysis of sound pulses in dolphins. **Doklady Akademii Nauk SSSR** 225, 470-473.

Vel'min, V. (1976). The critical interval of active hearing in dolphins. **Soviet Physics and Acoustics**, 2, 351-352.

Verfuß, U. K., Miller, L. A., and Schnitzler, H.-U. (2005). Spatial orientation in echolocating harbour porpoises (*Phocoena phocoena*). **J Exp Biol**, 208(17), 3385-3394.

Verfuß, U. K., Miller, L. A., Pilz, P. K., and Schnitzler, H.-U. (2009). Echolocation by two foraging harbour porpoises (*Phocoena phocoena*). **J Exp Biol**, 212(6), 823-834.

von der Emde, G., Schwarz, S., Gomez, L., Budelli, R., and Grant, K. (1998). Electric fish measure distance in the dark. **Nature**, 395(6705), 890-894.

Wensveen, P. J., Isojunno, S., Hansen, R. R., von Benda-Beckmann, A. M., Kleivane, L., van IJsselmuide, S., . . . and Curé, C. (2019). Northern bottlenose whales in a pristine environment respond strongly to close and distant navy sonar signals. **Proc Roy Soc B**, 286(1899), 20182592.

Wiggins, S. M., McDonald, M. A., and Hildebrand, J. A. (2012). Beaked whale and dolphin tracking using a multichannel autonomous acoustic recorder. **J Acoust Soc Am**, 131(1), 156-163.

Wisniewska, D. M., Johnson, M., Beedholm, K., Wahlberg, M., and Madsen, P. T. (2012). Acoustic gaze adjustments during active target selection in echolocating porpoises. **J Exp Biol**, 215:4358-4373.

Wisniewska, D. M., Johnson, M., Nachtigall, P. E., and Madsen, P. T. (2014). Buzzing during biosonar-based interception of prey in the delphinids *Tursiops truncatus* and *Pseudorca crassidens*. **J Exp Biol**, 217(24), 4279-4282.

Wisniewska, D. M., Ratcliffe, J. M., Beedholm, K., Christensen, C. B., Johnson, M., Koblitz, J. C., Wahlberg, M., and Madsen, P. T. (2015). Range-dependent flexibility in the acoustic field of view of echolocating porpoises (*Phocoena phocoena*). **eLife**:e05651.

Wisniewska, D. M., Johnson, M., Teilmann, J., Rojano-Doñate, L., Shearer, J., Sveegaard, S., Miller, L., Siebert, U., and Madsen, P. T. (2016). Ultra-high foraging rates of harbor porpoises make them vulnerable to anthropogenic disturbance**. Curr Biol**, 26, 1441–1446.

Wisniewska, D. M., Johnson, M., Teilmann, J., Siebert, U., Galatius, A., Dietz, R., and Madsen, P. T. (2018). High rates of vessel noise disrupt foraging in wild harbour porpoises (*Phocoena phocoena*). **Proc Roy Soc B**, 285(1872), 20172314.

Yamada, Y., Hiryu, S., and Watanabe, Y. (2016). Species-specific control of acoustic gaze by echolocating bats, *Rhinolophus ferrumequinum nippon* and *Pipistrellus abramus*, during flight. **J Comp Phys A**, 202(11), 791-801.

Yuen, M. M., Nachtigall, P. E., Breese, M., and Supin, A. Y. (2005). Behavioral and auditory evoked potential audiograms of a false killer whale (Pseudorca crassidens). **J Acoust Soc Am**, 118(4), 2688-2695.

Yovel, Y., Falk, B., Moss, C. F., and Ulanovsky, N. (2010). Optimal localization by pointing off axis. **Science**, 327(5966), 701-704.

Zaslavski, G. L. (2008). The auditory time resolution in bottlenose dolphins: Behavioral experiments versus auditory evoked potential methods. **J Acoust Soc Am** conference, Paris, France.

Zaslavski, G. (2012). High auditory time resolution in bottlenose dolphins is effective protection against reverberation. *In*: The effects of noise on aquatic life (Vol. 730, pp. 37-40): Springer.

Chapter II.

Deep-sea Vertical Hydrophone Array

Malinka, C. E., Atkins, J., Johnson, M., Tønnesen, P. H., Dunn, C., Claridge, D., Aguilar de Soto, N., & P. T. Madsen. (2020). "An autonomous hydrophone array to study the acoustic ecology of deep-water toothed whales," *Deep Sea Research I,* 158C: 103233. doi: 10.1016/j.dsr.2020.103233

Deep–Sea Research I 158 (2020) 103233

Contents lists available at ScienceDirect

Deep-Sea Research Part I

journal homepage: http://www.elsevier.com/locate/dsri

An autonomous hydrophone array to study the acoustic ecology of deep-water toothed whales

Chloe E. Malinka [a,*], John Atkins [b], Mark P. Johnson [a,d], Pernille Tønnesen [a], Charlotte A. Dunn [c,d], Diane E. Claridge [c,d], Natacha Aguilar de Soto [e], Peter Teglberg Madsen [a,f]

[a] Marine Bioacoustics Lab, Zoophysiology, Dept. Biology, Aarhus University, Aarhus, Denmark
[b] Ocean Instruments, Auckland, New Zealand
[c] Bahamas Marine Mammal Research Organization (BMMRO), Sandy Point, Abaco, Bahamas
[d] Sea Mammal Research Unit, Scottish Oceans Institute, University of St Andrews, St Andrews, Scotland, UK
[e] University of La Laguna, Tenerife, Canary Islands, Spain
[f] Aarhus Institute of Advanced Studies, Aarhus University, Denmark

ARTICLE INFO

Keywords:
Bioacoustics
Echolocation
Passive acoustics
Localisation
Hydrophone array
Source level

ABSTRACT

For vocal animals with distinctive calls, passive acoustic monitoring can be used to infer presence, distribution, and abundance provided that the calls and calling behaviour are known. Key to enabling quantitative acoustic surveys are calibrated recordings of identified species from which the source parameters of the sounds can be estimated. Obtaining such information from free-ranging aquatic animals such as toothed whales requires multi-element hydrophone arrays, the use of which is often constrained by cost, the logistical challenge of long cables, and the necessity for attachment to a boat or mooring in order to digitise and store multiple channels of high-sample rate audio data. Such challenges are compounded when collecting recordings or tracking the diving behaviour of deep-diving animals for which the array must be deployed at depth. Here we report the development of an autonomous drifting deep-water vertical passive acoustic array that uses readily available off-the-shelf components. This lightweight portable array can be deployed quickly and repeatedly to depths of up to 1000 m from a small boat. The array comprises seven ST-300 HF SoundTrap autonomous recorders equally spaced on an 84 m electrical-mechanical cable. The single-channel digital sound recordings were configured to allow for synchronisation in post-processing using an RS-485 timing signal logged by all channels every second. We outline how to assemble the array, and provide software for time-synchronising the acoustic recorders. To demonstrate the utility of the array, we present an example of short-finned pilot whale clicks localised on the deep-water (700 m) array configuration. This array method has broad applicability for the cost-effective study of source parameters, acoustic ecology, and diving behaviour of deep diving toothed whales, which are valuable not only to understand the sensory ecology of deep-diving cetaceans, but also to improve passive acoustic monitoring for conservation and management.

1. Introduction

Toothed whales are the largest toothed predators on the planet and rely on sound to mediate vital functions from foraging to courtship (Goldbogen and Madsen, 2018). However, relatively little is known about their acoustic ecology due to the challenges inherent to systematic sampling of the acoustic emissions of highly mobile free-ranging and deep-diving marine megafauna in offshore and pelagic environments. One approach to learn more about how these animals use sound is to tag them with sound and movement recording tags (*e.g.* Johnson and Tyack, 2003). While a biologging approach can provide unprecedented insights into the diving patterns, fine-scale movements, predator-prey dynamics and echolocation behaviours of individual animals, some toothed whale species are difficult to tag, and ethical issues can arise surrounding the tagging of protected species (Johnson et al. 2009). Additionally, audio recordings from tags on echolocating toothed whales cannot provide

* Corresponding author. Zoophysiology, Dept. Biology, Aarhus University, C. F. Møllers Allé 3, building 1131, DK-8000, Aarhus C, Denmark.
E-mail addresses: chloe.e.malinka@gmail.com (C.E. Malinka), john@oceaninstruments.co.nz (J. Atkins), markjohnson@st-andrews.ac.uk (M.P. Johnson), pernille-t@bios.au.dk (P. Tønnesen), cdunn@bahamaswhales.org (C.A. Dunn), dclaridge@bahamaswhales.org (D.E. Claridge), naguilar@ull.edu.es (N. Aguilar de Soto), peter.madsen@bios.au.dk (P.T. Madsen).

https://doi.org/10.1016/j.dsr.2020.103233
Received 23 August 2019; Received in revised form 27 December 2019; Accepted 7 February 2020
Available online 14 February 2020

information about the source properties of the biosonar signals of the tagged animal, because these signals are focused into a narrow forward-directed beam and yet are collected by a tag that is attached behind the head and so out of the main beam (Johnson et al. 2009). In order to quantify the source parameters (such as source level, bandwidth, duration, *etc.*) of such directional signals, it is essential that these are measured close to the acoustic axis, since both spectral content and signal amplitude vary with aspect (Au et al. 1986).

The quantification of animal sounds is important for several reasons. Passive acoustic monitoring (PAM) methods to study the occurrence, distribution, density and relative abundance of vocal animals rely on descriptions of species-specific sounds in order to classify detections (Zimmer, 2011). Estimates of source parameters can be used to calculate maximum detection ranges and infer the acoustic detection function (Marques et al. 2009), both of which are essential for the planning and interpretation of data from PAM surveys (Zimmer et al. 2008). Knowledge about an echolocator's beamwidth is useful for informing optimal hydrophone array configurations (Zimmer et al. 2005), indicating the volume over which their biosonar system can operate to detect prey (Madsen et al. 2007; Jensen et al. 2018), estimating acoustic detection probabilities, and inferring density (Fraiser et al. 2016). Also, the directionality of a biosonar beam reveals the acoustic field of view of echolocating animals, providing insight into their sensory ecology (Madsen et al. 2013).

Recordings from moored, drifting, or boat-deployed hydrophones are typically used to characterise the powerful clicks produced by echolocating toothed whales. Single hydrophone recordings can be used to quantify the occurrence rate and general characteristics of biosonar sounds, but rarely give unambiguous information about the range to the clicking animal, or whether the sound was recorded close to the animal's acoustic axis. Both of these are needed to estimate the source level and therefore infer the detection range of biosonar sounds. By using an array of synchronised hydrophones at known locations it is possible to calculate the location of the animal, and therefore its range, from the time-difference-of-arrival (TDoA) of signals at each hydrophone (Watkins and Schevill, 1972; Spiesberger and Fristrup, 1990; Wahlberg et al. 2001). With this set-up it is also possible to distinguish on-axis clicks by comparing the relative amplitudes of clicks recorded on different receivers. As animals manoeuvre, they occasionally scan their biosonar across the array giving rise to recordings of sequences of clicks with increasing and then decreasing amplitude; the highest amplitude click in these sequences is then the closest exemplar of the on-axis click (Au, 2004; Madsen et al. 2004a, 2004b). The source level of the clicks can be estimated using the range to the animal and the received level of putative on-axis clicks combined with known transmission properties of the medium (Møhl et al. 1990). Thus, accurate identification and quantification of the spectral and temporal properties of on-axis clicks requires the deployment of a calibrated and time-synchronised hydrophone array in front of the echolocating animal (Madsen et al. 2004a; Madsen and Wahlberg, 2007).

It is critical to quantify biosonar sounds produced by animals in their natural habitat. Sonar signals recorded in small tanks in captivity have been shown to be of lower amplitude and lower frequency than those recorded from wild cetaceans (Au, 1993; Wahlberg et al. 2011; Ladegaard et al. 2019). However, when recording at sea it can be difficult to obtain on-axis clicks from animals vocalising at depth with a hydrophone array near the surface, because animals may rarely point upwards towards the array. This problem is relevant when using arrays that must be closely tethered to a vessel to both power the recording system and digitise the sound. The use of tethered hydrophone arrays to study marine animals was pioneered by Whitney (1968), Dunn (1969), and Watkins and Schevill (1971), amongst others. These authors used linear hydrophone arrays suspended from a boat or sonobuoy to localise toothed whales and to investigate the spectral content, intensity, and duration of echolocation clicks, as well as to quantify inter-click intervals (ICIs). Using a 4-hydrophone array, Watkins (1980) reported the depths at which sperm whales start clicking, and inferred their vertical dive angles and swim speeds during dives. Towed linear arrays have also been used to identify the vocal individual in a group of diving whales using beam-forming (*e.g.* Miller and Tyack, 1998; Zimmer et al. 2005), or to identify the range and bearing of vocal whales in acoustic surveys. Such tethered arrays, often in a star configuration, are useful for studying shallow-swimming wild odontocetes and, in particular, species that are prone to approach vessels. They have been used to quantify the source properties of echolocation clicks and to investigate how animals adjust their biosonar signals as they approach targets (*e.g.* Rasmussen et al. 2002; Au and Herzing, 2003; Au and Benoit-Bird, 2003; Au et al. 2004; Ladegaard et al. 2017). More recent tethered arrays have also reported on the beam pattern of biosonar clicks (*e.g.* Koblitz et al. 2016).

An alternative to maintaining recording synchrony on a hydrophone array, while relieving the constraint to be tethered to a boat, is by distributing the array and synchronising it with a universal timing signal. This approach has been implemented via radio-linking hydrophones to record simultaneous signals on a single recorder (Møhl et al. 2000; Hayes et al. 2000; Wahlberg et al. 2001). Another implementation is using a distributed horizontal array of GPS-synchronised receivers (Møhl et al. 2001, 2003; Miller and Dawson, 2009). Such an array has been used to calculate the source level and radiation patterns of clicks produced by sperm whales (Madsen et al. 2002; Møhl et al. 2003). However, the large spacing of elements needed to accurately estimate the range of distant animals makes beam directivity difficult to resolve with high accuracy, since it was rare for the narrow beam of sperm whales, for example, to simultaneously ensonify multiple channels that were up to 2000 m apart (as in Møhl et al. 2003). To increase the chances of a given click ensonifying multiple hydrophones on the array at once, Heerfordt et al. (2007) proposed an array with several closely spaced hydrophones. The number of hydrophones and the spacing between them is therefore a compromise between having hydrophones close enough for several channels to be consistently ensonified by a highly directional biosonar beam, and of having a large enough aperture to accurately measure the range to vocalising animals (Wahlberg et al. 2001). Deploying an array for a longer duration, increasing the number of hydrophones, and deploying elements at the foraging depths of the target species also increase the probability of recording on-axis clicks (Møhl et al. 2000; Heerfordt et al. 2007).

Recording sounds in the habitat in which they are produced presents a challenge when studying whales that echolocate at depth (Heerfordt et al. 2007). Deploying a tethered hydrophone array to the foraging depths of deep-diving animals has been rare, as it necessitates a long, multi-core cable connected to the research boat. This cable transmits the analogue signals received by the hydrophones to an on-board multi--channel high sample-rate data acquisition system. Such cables for deep sea applications are heavy, expensive, and difficult to deploy, especially from smaller vessels, largely restricting this approach to projects for which large oceanographic vessels are available. To simplify the cable requirements, Heerfordt et al. (2007) developed a 10-element, 950 m long vertical hydrophone array using fibre optic cables which was used to study the biosonar beam patterns of deep-diving odontocetes. Individual elements in this array digitised data at depth and transmitted these data on a time-division basis to a recording system on a boat. This approach enabled the use of a thin lightweight fibre optic cable which could be deployed from a 45 ft sailing vessel. While this array design overcomes some of the challenges of deep sea bioacoustics, including the requirements for a wide aperture and high bandwidth, the implementation required cabling to a vessel and faced the problem that failing opto-couplers affected data transmission from lower nodes of the array. The tough conditions encountered at sea dictate that a practical hydrophone array should be robust to the failure of individual receivers if it is to be used repeatedly.

The need for a cable tethered to a vessel is a major impediment to achieving a robust, easily deployed deep hydrophone array. A key improvement would therefore be to make the array record

autonomously. Macaulay et al. (2015, 2017) developed such a system for a different but equally challenging recording environment: energetic tidal rapids that form in narrow channels between islands. The autonomous recorder in this case was housed in a drifting float with a surface-suspended rigid array of 4 hydrophones and a vertical array of 6–8 hydrophones. Movement sensors spaced regularly along the vertical axis of the array produced a time series of the precise 3D locations of the hydrophones, used to interpret the TDoA. This array was used to track the high frequency echolocation signals of porpoises as it drifted through the rapids. The array was not built for deep water applications (maximum depth 30 m) but it represents a step towards autonomy in multichannel recorders. Similarly, Barlow et al. (2018) simultaneously deployed a series of two-channel vertical drifting acoustic spar buoy recorders (DASBRs) to depths of ~100 m, and achieved localisation using the TDoAs between two hydrophones on the same drifter, or by using the TDoAs between the direct path and the surface-reflected echolocation click. Such a nested-array configuration, with smaller aperture arrays nested within a larger aperture array, has also been employed by Gassmann et al. (2015) to track beaked whales. Each small aperture array provided a bearing to the sound, and where these bearings crossed indicated the 3D location of the whale, thus eliminating the need for precise synchronisation between recorders on their widely spaced array. However, none of these implementations have enough receivers to properly quantify the source properties of biosonar clicks

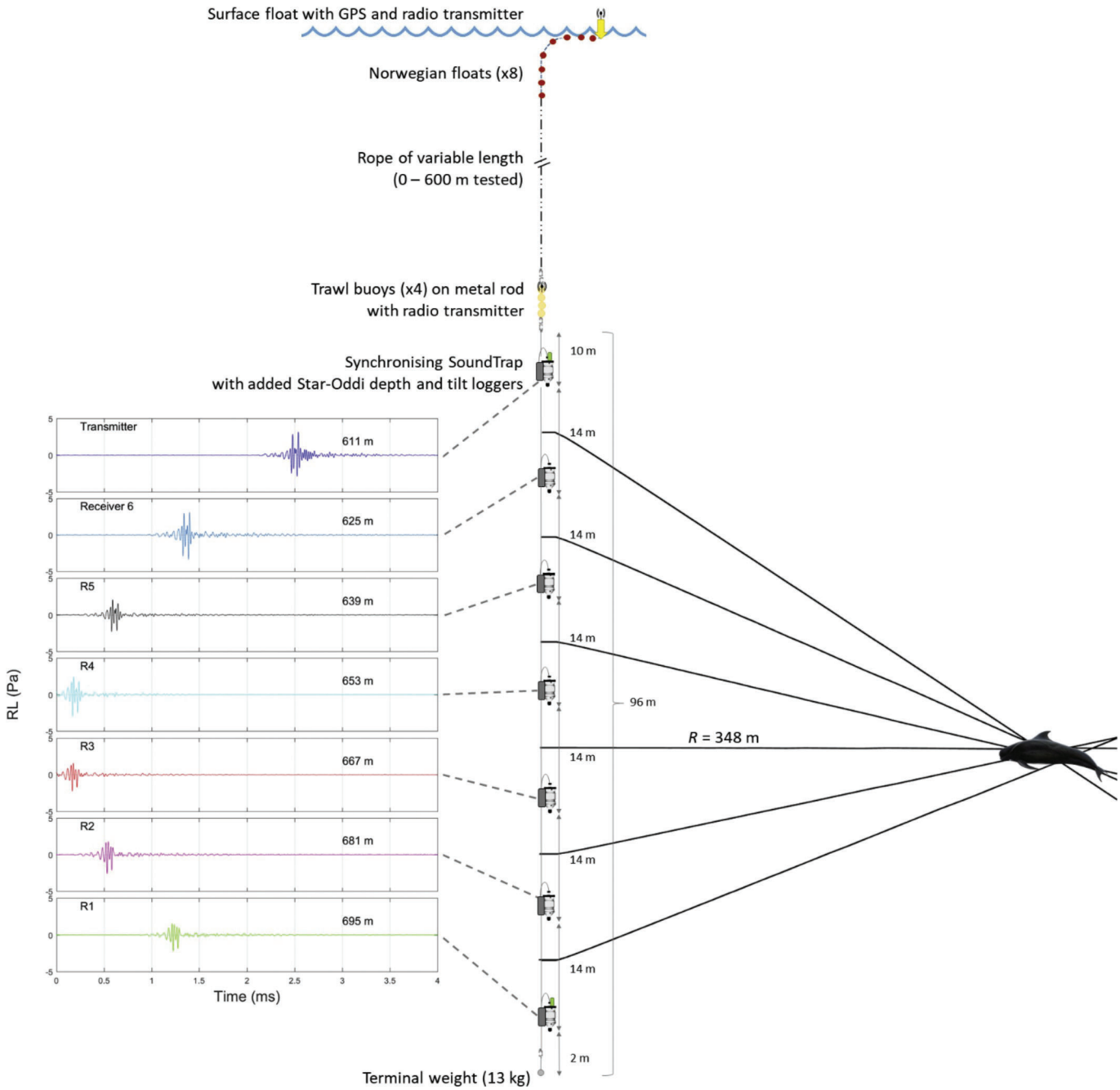

Fig. 1. Diagram (not to scale) of the 7-channel vertical hydrophone array. Star-Oddi depth and tilt loggers are attached to upper and lower recorders. Waveforms of a single pilot whale click, as received on all time-aligned channels, are shown on the left. Hyperbolae, which appear here as straight lines due to the relatively long range to the whale, indicate the loci of source locations that give the measured TDoAs between pairs of consecutive recorders. These loci intersect at a range of 348 m from the 4th recorder. The estimated whale depth for this click was 661 m.

from deep-diving toothed whales. Thus, there exists an equipment gap requiring the creation of a multi-hydrophone, deep-water vertical array which can be deployed for longer periods of time, autonomously, from a small boat.

Here we report on the development and performance of such an autonomous, drifting, large-aperture, deep-water vertical hydrophone array, designed to quantify the acoustic parameters of echolocation clicks from odontocetes in the deep sea. The array uses off-the-shelf high performance autonomous recorders to eliminate the need for expensive and cumbersome cables. The approach combines the benefits of multi-channel, high sample rate recordings that usually require cabled attachment to a boat for digitisation, with the autonomous ability and longer recording durations (up to about 1 week, battery-limited) more typical of deep-water single-channel recorders. This paper describes the array design, how it can be deployed from a small vessel, and demonstrates array recordings from short-finned pilot whales. An accompanying set of software tools enable the creation of multi-channel time aligned audio files from independent but synchronised recordings, effectively turning a set of autonomous recorders into an ad hoc array.

2. Materials and methods

2.1. Array design

The vertical linear array comprises 7 SoundTraps (ST300-HF, Ocean Instruments, Auckland, New Zealand, www.oceaninstruments.co.nz). The ST300-HF are self-contained digital sound recorders with a sampling rate of up to 576 kHz with 16-bit resolution and a low self-noise level (~30 dB re 1 μPa/Hz). The broadband (160 kHz) dynamic range is 90 dB and clipping occurs at a received level (RL) of either ~172 dB re 1 μPa (high gain) or ~186 dB re 1 μPa (low gain). The high dynamic range of the low-gain setting accommodates for the large variations in received levels that are expected from odontocetes with a narrow beamwidth, and the high gain setting, with its low clipping level, enables ambient noise measurement. The ST300-HF are single-channel recorders and so require external equipment to enable synchronisation of multiple units. The seven recorders are accordingly linked together by a cable which extends for the length of the array. The array is then deployed at the desired depth by suspending it with a rope from a drifting buoy (Fig. 1).

2.1.1. Synchronisation

A firmware modification for the recorders allows synchronisation of multiple devices connected to a common cable, to sample-level accuracy. This firmware employs one SoundTrap (set to be the 'transmitter') to generate an RS-485 timing message every second, which is received on the other SoundTraps (configured as 'receivers'). Upon receiving a message, all receivers record their respective current audio sample numbers, and save the timing message along with sample number to a log file. After data collection, single-channel wave files are time-aligned using information stored in this log file.

The synchronising protocol corrects for the variable and inevitable clock drifts of the individual instruments. The maximal clock drift of an individual SoundTrap is ~2 s per day (~2 × 10^-5). At a sampling rate of 576 kHz, this corresponds to a potential timing error of ~13 samples/s. To maintain localisation accuracy it is advisable that the synchronisation pulses occur frequently (here we used 1 Hz). Custom software in MATLAB (The Mathworks Inc., Natick, MA) was developed to synchronise the recordings from the SoundTrap array (provided in Supplementary Material A). This software is applicable to any array of sound recorders that log an external synchronisation pulse.

2.1.2. Cable and breakouts

All array components are commercially available and can be readily assembled using low-cost laboratory equipment. Step-by-step directions for building the array are provided in Supplementary Material B. The cable used to distribute the time-synchronisation signals (Cortland Cable Co., diameter = 0.7 cm) contains 4 insulated wires reinforced with braided liquid-crystal polymer (Vectran®) to give an overall breaking strength of ~900 kg. Of the four wires, only two are used to transmit the differential (RS-485) synchronisation message; the other two wires are unneeded (in our implementation one is wired as a common ground) and so a two-wire cable would suffice. The mass of the 96 m cable is 11.5 kg, including the seven SoundTraps, and it is slightly negatively buoyant in seawater.

Each SoundTrap connects to the cable via a SubConn connector pigtail (MacArtney Underwater Technology, MCIL8M) which is tied electrically to the two active wires of the cable. These attachments are secured in waterproof breakouts made of Scotchcast™ epoxy resin (3M-2131). This flexible resin was chosen to allow bending of the cable near the join and prevent salt water ingress without compromising adhesion of the breakout. The resin was poured into custom 3D prints which were designed to provide a consistent mounting point for the SoundTraps, so that the hydrophone element position remained constant between deployments and field seasons (see Supplementary Material B). Cable ties, aligned over the flanges of the breakouts and the SoundTraps, secure the recorders, preventing their detachment from the cable at sea.

The hydrophone elements on each SoundTrap are protected with custom-built cages of 2.5 mm stainless steel wire. The wires do not interfere with the received waveforms for tested frequencies up to 150 kHz; This would only problematically impact sound propagation at very high frequencies where λ approaches the wire diameter. Small LED lights, built into the SoundTrap to confirm operation, are taped over, in order to not intentionally attract any animals to the array at depth.

2.1.3. Array dimensions

2D localisation (*i.e.* depth and range) of a clicking animal is possible with a vertical array if at least 3 elements detect a click, but the accuracy of localisation depends on the hydrophone spacing. In the chosen configuration, the array comprises 7 evenly-spaced hydrophones, ~14 m apart, resulting in an overall aperture of ~84 m (distance between the top and bottom recorders). This spacing accommodates a directional narrow-band high frequency click, ensuring that an animal with a half-power beamwidth of 10° will ensonify at least 3 sequential hydrophones. Specifically, the dimensions of the array are designed to provide sufficient spatial resolution to be able to measure the biosonar beam of a deep water, high frequency echolocator, such as dwarf/pygmy sperm whales (*Kogia* spp*)*. A range of estimated source levels projected from a range of distances from the centre of the array assuming a half power beamwidth of 10° and appropriate absorption at 130 kHz were simulated, and the maximum range at which the simulated received level exceeded a signal-to-noise ratio (SNR) of at least 10 dB above estimated background noise levels was considered. For the chosen configuration, this meant that for the lowest considered source level of 175 dB re 1 μPa (Madsen et al. 2005), a minimum of 3 hydrophones were ensonified with sufficient SNR at a range approximately 10x the array aperture. The relatively large time delays between these widely-spaced hydrophones enable more accurate localisations of distant sound sources while reducing the sensitivity to timing errors. Applying the rule-of-thumb that localisation accuracy becomes poor at a range of ~5-10x the aperture of the array (*e.g.* Kyhn et al. 2009; Macaulay et al. 2017), this means that animals could be localised with moderate accuracy at a range of up to ~840 m from the array, if both the top and bottom recorders receive the signal.

2.1.4. Buoyancy, weight, depth and tilt

To deploy the array to different depths, a single cross-braided polyester rope (6 mm diameter, with 650 kg breaking strength) connects the top of the hydrophone array cable to a surface float (Fig. 1). A series of 8 Norwegian floats (15 cm diameter) at 2 m intervals below the surface float provide distributed buoyancy to decouple surface wave movement from the array. The highly visible surface float contains both a radio

transmitter (MM150, Advanced Telemetry Systems) and a GPS device (Tractive GPS pet tracker, www.tractive.com) to provide real-time positioning of the array, viewable on a mobile phone app. This GPS can operate for a maximum of 5 days, but a range of similar devices are commercially available to accommodate longer deployments.

Between the array and the rope are four U70 trawler buoys (18 cm diameter, Daconet), depth rated to 2000 m, mounted on a stainless steel rod. These buoys are tightly spaced with rubber padding between them to avoid any movement noise. Similarly, all metal-to-metal contacts (*i.e.* between the stainless steel thimbles and shackles that connect the cable array, trawl buoy rod, rope, and surface float) are wrapped with clear PVC tubing (Tygon®, Saint-Gobain Performance Plastics) to prevent clinking noises that could contaminate acoustic recordings. As a precaution, a radio transmitter (MM150, Advanced Telemetry Systems, depth rated to 2000 m) is attached to the rod of trawler buoys. The purpose of buoyancy in this location (between the cable array below and the rope extension above) is two-fold: to allow for the array to come to the surface should the rope be cut, and to increase tension, and therefore straightness, on the cable section of the array below.

Weights (sand in biodegradable cotton bags) are attached at the bottom of the array to keep the array vertical and linear. The amount of weight added is adjusted slightly according to deployment location (as varying temperature and salinity affect water density) as well as the amount of rope added to the top of the array (*e.g.* 13 kg of weight was used for an array with 600 m of rope). Of this weight, 10 kg are attached via a galvanic magnesium timed release (Neptune Marine Products), so that, should the extension rope become cut/entangled, or the weight become stuck on the seafloor, the array would float to the surface once the release corrodes. The release time (determined by the circumference of the magnesium coupling) is chosen to be significantly longer than the intended deployment duration.

Two autonomous inclinometer, depth, and temperature data loggers (Star-Oddi DST tilt, Reykjavik, Iceland) are attached to SoundTraps at the top and bottom of the array, and sampled at 1 Hz. These are roughly synchronised with the SoundTraps by tapping them against one of the SoundTraps at the beginning and end of each deployment. Having the array close to vertical facilitates quantifying the depth of localised animals, but the array only needs to be straight (and not necessarily vertical) in order to resolve acoustic parameters such as source level, peak frequency, beam pattern, *etc.* (Heerfordt et al. 2007). Known deviations from verticality, recorded with the Star-Oddi loggers, can be used in calculations of the localisation errors. For example, if localisations are calculated assuming that the array is vertical, but it in fact is θ degrees off vertical, the depth of a localisation point will be subject to a error of $sin(\theta)*range$. Thus greater tilt angles introduce larger errors in depth.

2.2. Calibrations and performance assessment

2.2.1. Instrument calibrations

All SoundTraps were individually calibrated against a Reson 4034 hydrophone (Teledyne, Slangerup, Denmark) in a 3 m deep cedar tank. A series of pure tones (in 10 kHz steps, from 10 to 200 kHz) were projected to each device at a range of 2 m. In addition, artificial clicks were projected at different angles to a SoundTrap attached to the cable in an open water environment to investigate the degree of acoustic shading introduced by the cable. This resulted in a maximal nominal loss of 1.5 dB, which would only be problematic at very high frequencies (where λ approaches the cable diameter). Star-Oddis were individually calibrated for depth (in a pressure tank, from 20 to 300 m in steps of 10 m, and from 300 to 1000 m in steps of 100 m) and tilt (at 0, 20, 45, 70 and 90°) using a protractor.

2.2.2. Performance assessment of time synchronisation

Time synchronisation performance was tested in air for a duration similar to that of a field deployment (2 h 44 m). As an independent timing check, an acoustic tone burst (10 kHz sine wave, 100 μs duration, 1 V_{pp}), generated by a signal generator (Agilent), was projected every 10 s to a string of parallel-connected custom-made pingers, with each pinger taped to the hydrophone of a SoundTrap in the array. Thus each recorder received an external synchronising ping with no transmission delay, as well as the cable-borne electrical timing message pulse. The electrical timing signals were used to align the sound data recorded on the different devices (see section 2.1.1), and the relative timing of the external pings across the recorders was used to assess the accuracy of this alignment procedure as a function of time.

Time synchronisation performance was also tested in deep water using a modified version of the array with built-in piezo ceramic discs (SMD10T2R111WL, STEMiNC, FL, USA) sealed in epoxy resin, positioned 5 cm from each hydrophone element. These elements emitted synchronous acoustic tone bursts (215 kHz sine wave, 23 μs duration) every 110 ms. The tone bursts were generated by a custom-made pinger board molded into the top of the array and transmitted via one of the unused wires in the array cable. The high frequency of these synchronisation signals was chosen so as to be inaudible to toothed whales and also to ensure that the signals are only weakly detected by neighbouring recorders on the array, making the time of arrival of each signal unambiguous. The arrival time of each acoustic synchronisation ping relative to the preceding electrical timing message was calculated for each recorder. This produced a record of time synchronisation errors for each receiver with which to assess the time alignment of all devices on the array.

2.2.3. Localisation error due to time synchronisation errors

Despite the use of a common timing signal to synchronise recorders, some time alignment jitter is inevitable. This jitter is due to processor latency, as transmission and reception of the common timing signal requires processor time which must be interleaved with other tasks. A simulation was constructed in MATLAB to investigate how much extra error this jitter adds to localisation errors. Simulated toothed whale signals were generated on a grid of ranges and depths around a simulated array at ~600–700 m depth. Points on the grid were spaced at 10 m intervals in range and depth and extended up to a maximum of 420 m (5x the total array aperture of 84 m) above and below the array, and 840 m (10 x the aperture) in horizontal range from the array. For each point (in the 94 × 84 m grid), the received time delays on the array elements were calculated assuming a homogenous sound speed.

Two types of time delay error were considered: (1) errors generated by the small observed time alignment jitter of the SoundTraps, and (2) cross correlation errors which typically occur when calculating TDoAs of narrow band high frequency (NBHF) clicks, such as those produced by *Kogia*. To simulate the synchronisation errors, time errors were randomly drawn from the empirical distribution of time synchronisation errors observed during the timing validation trial and added to the simulated time delay measurements at each receiver. To examine cross correlation errors, *Kogia* clicks were used as an example as they are narrow band with a slowly varying waveform envelope. For this type of signal, there are multiple peaks in the cross-correlation function used to measure TDoAs, and even small amounts of noise can lead to the selection of a peak on either side of the true peak (Weinstein and Weiss, 1984; Gillespie and Macaulay, 2019). It was therefore assumed that a TDoA error corresponding to one cycle of a typical *Kogia* click was equally likely, so that each TDoA between channel pairs was accordingly modified by adding, with equal probability, +/- 9 μsec (the duration of one wavelength of a *Kogia* click (Madsen et al. 2005)).

Two scenarios were then considered: (1) perfectly time-synchronised SoundTraps for which the only error in TDoA was due to cross correlation errors, and (2) SoundTraps with time delay errors arising from both cross correlation errors and time synchronisation errors. Localisations were then run on the resulting simulated time delays using a Simplex optimisation method for localisation (Nelder and Mead, 1965; Press et al. 1988) and the errors in depth and range were recorded. The complete simulation was run 100 times through every possible grid

position (7896 grid points) and median absolute values of depth and range errors, were plotted. The median absolute errors for each range bin, across all depths, was also plotted to visualise the impact that the time synchronisation errors had on localisation accuracy, and contextualise these errors by comparing them with errors that would be observed when cross correlating NBHF signals.

2.3. Field deployments

The vertical array was deployed and recovered from several small vessels to test its feasibility. These included a 4 m rigid-hull inflatable boat (RHIB) and a sport fishing boat (10.4 m), both in a maximum of sea state 5. The array was deployed by hand which took as little as 2 min when deployed without additional rope, and 14 min with 600 m of rope. Although recovery by hand-hauling was initially done, an electrical winch (North Lift line hauler LH200, running on 12 V and lifting up to 90 kg) greatly improved recovery time and effort, and made it comfortable to recover the array in sea states beyond 3. Retrieval time ranged from 4 min with no rope, to 18–27 min with 600 m of rope. The final ~96 m of cable array was always hand-hauled to avoid the recorders hitting the gunwale. The array was re-located for recovery using either positions sent by the GPS on the float, or by radio-tracking the VHF signal using a 3-element Yagi antenna and an R-1000 radio (Communication Specialists Inc.).

An example of a field recording demonstrating the array performance is taken from fieldwork in March 2019, in the waters southwest of Tenerife, in the Canary Islands of Spain (~28°N/16°W). Our configuration used high gain settings to improve the probability of getting on-axis clicks from deep diving whales with often unpredictable movements. An example from this fieldwork is shown to demonstrate the efficacy of the array. Bioacoustic descriptions emerging from this dataset will form publications of their own. Visual sightings of odontocetes at the surface prompted this deep-water deployment (with 600 m of rope, so that the deepest channel was ~696 m deep) and recorded signals from short-finned pilot whales (*Globicephala macrorhynchus*).

2.4. Analysis

2.4.1. Acoustic localisation and parameter quantification

Acoustic localisation of individual clicks was carried out on the synchronised multi-channel acoustic recordings based on the TDoAs of the click on each hydrophone. A simplified estimator can be used if it can be assumed that the array is vertical and the sound speed is constant, yielding an estimate of the range and depth of the sound source (Zimmer, 2011). A more complex iterative analysis is needed if the sound speed varies significantly over the sound propagation paths from the animal to each array element (Spiesberger and Fristrup, 1990). A vertical array is only able to resolve range and depth, *i.e.*, a 2D localisation points. If the array is straight but not vertical, the sound source is localised to a circle perpendicular to the array axis, leading to errors in the depth estimate. However, neither the tilt of the array nor the exact depths of the hydrophones impact measurements of acoustic parameters and beam directivity (Heerfordt et al. 2007), provided that the array is straight.

To determine the acoustic parameters of clicks, the following steps must be performed on the synchronised audio recordings for each detected click: i) identification of the same click in each hydrophone recording, ii) measurement of arrival times of the click, iii) measurement of received sound pressures on each device, iv) measurement of the sound velocity, and v) localisation of the whale (Wahlberg et al. 2001). Click examples shown here were detected, classified, and localised in PAMGuard (www.pamguard.org; Gillespie et al. 2008) using the Large Aperture 3D Localiser module, which used the hybrid time-delay based algorithm described in Macaulay et al. (2017). Sequences of clicks with slowly-varying inter-click interval and consistent localisations were presumed to come from single individuals. The most intense clicks in these sequences were identified as potential exemplars of on-axis clicks (Møhl et al. 2000). These potential on-axis clicks were only selected if they were recorded by the middle elements in the array, *i.e.* if the strongest version of the click was not recorded on either of the top or bottom channel (*sensu* Au and Benoit Bird, 2003; Ladegaard et al. 2017). The received levels of the presumed on-axis clicks were combined with the distance between the localised whale and the strongest receiving hydrophone to back-calculate apparent source levels (*e.g.* Møhl et al. 2003). Assuming that the whale was pointing directly at the strongest receiving hydrophone, the off-axis angle to each other receiver was inferred from the localised range and depth in order to estimate the biosonar beam radiation pattern (*e.g.* Zimmer et al. 2005; Nosal and Frazer, 2007; Shaffer et al. 2013).

2.4.2. Ambient noise quantification

The array can be used to quantify ambient noise provided that this is more than 6 dB above the noise floor of the recorders. Self noise spectra were measured from recordings made in air in an anechoic room at Aarhus University, Aarhus, Denmark. During deployments, third octave levels (TOLs) of ambient noise from the lowest channel of the array in its deep-water configuration were measured to quantify the deep noise level in the study location. Measurements were computed over 30 s analysis windows, in third octave bands centred from 24.8 Hz to 161 kHz. Percentiles (5, 50, 95) of these 30 s measurements within each third octave band were calculated over a 5 h interval in which the array was drifting free of the vessel. Note that TOL measurements (in dB re 1 μPa) differ in unit from the reported spectral level of self noise, in power per Hertz. To obtain the noise level within a given TOL band (in dB re 1 μPa), add the nominal spectral level of self noise (here, 30 dB re 1 μPa/Hz) to $10*\log_{10}$(bandwidth of any third octave band, in Hertz).

3. Results

3.1. Field deployments

The array was deployed 23 times in the deep configuration, in a variety of sea-states. In the half-hour deployment in Tenerife shown here, the sea-state was low and the depth and tilt sensors on the upper and lower recorders confirmed that the array was oriented nearly vertically (mean tilt of 5.5–8.8° off vertical), and was close to straight, with a small difference in the tilt at the top and bottom of the array (STD 1.7–2.4°) which was within the ±3° accuracy of the tilt sensors. In less optimal deployment conditions with strong surface currents, the deep-water array was shallower by ~100 m than expected with the 600 m rope extension, indicating that the rope had a catenary, however the cabled part of the array still appeared to remain straight (mean array tilt of 7.4° off vertical, STD 2.8°) due to sufficient buoyancy and weights at the ends of the tensioned cable.

3.1.1. Globicephala example

An example recording of a short-finned pilot whale click received on all hydrophones of the 7-channel array is shown in Fig. 1. The pilot whale was localised to a depth of 661 m that overlapped with the depth of the array in its deep-water configuration (spanning 611–695 m). The whale's biosonar beam was first received on receiver 4 (highest RL at 137 dB re 1 μPa_{pp}), at a calculated range of 348 m from this channel. This click is suspected to be off-axis due to the low variation in RLs across the recorders and the double-pulse waveforms recorded by all elements. Localisations of preceding and following clicks ($n = 42$) are comparable in range (STD 12 m) and depth (STD 6 m), and therefore likely come from the same animal.

3.1.2. Other applications

Localisations of multiple successive clicks from the same animal can be used to reconstruct diving tracks of animals at depth (Freitag and Tyack, 1993). Localisations of 20 clicks spanning 12 s from a

short-finned pilot whale, shown in Fig. 2, indicate that this animal was approaching the array in approximately horizontal swimming with a closing speed of about 1.6 m/s. This is most probably an underestimation of the actual speed of the animal because circumferential movements around the array axis cannot be resolved with a vertical array.

To demonstrate the use of the array to record deep sea ambient noise, a third octave level (TOL) analysis was conducted for the deepest channel (depth of ~695 m) from a longer duration (5 h) field deployment (Fig. 3). During this deployment, several odontocete species were visually observed at the surface: short-finned pilot whales, sperm whales (*Physeter macrocephalus*), and bottlenose dolphins (*Tursiops truncatus*). Peaks in the 95th percentile of ambient noise correspond to the frequencies of bioacoustic signals from these odontocetes, while variations at lower frequencies are likely due to traffic from a ferry and recreational boats. Note that this application does not use the features of the array, but is an added bonus of recording at depth.

3.2. Array calibrations

3.2.1. Time synchronisation calibration

Laboratory testing in air and a deep-water field test confirmed that alignment of multiple channels into a time-synchronised multi-channel WAV file was accurate over the duration of the deployments (maximum duration of 10 h). Raw data from the laboratory test and graphs demonstrating time alignment at the beginning and end of the deployment can be found in Supplementary Material A and in the Research Data.

The distribution of time synchronisation errors between the transmitter and all six receivers during the field test is shown in Fig. 4 (mean error = 0.5 samples, STD = 16.1 samples). Each node has similar distributions and are stable with time. The 90th percentile of this distribution is 27 samples, corresponding to an error in TDoA of 47 μs and a ranging error of ~7 cm. These are close to the expected per second drifts if the receivers have a clock drift of 2 s/day.

3.2.2. Localisation error from time synchronisation errors

Simulated localisation errors due to time synchronisation errors (Fig. 4) and potential errors in cross correlation increase with increasing range from the array (Fig. 5). This is a consequence of the increasingly small differences in TDoAs at long ranges which are therefore more susceptible to errors. Similarly, as a whale moves closer to the axis of the array, large change in range produce smaller changes in time delays, generating larger errors; when the whale is exactly above or below the array, TDoAs are the same regardless of range, thus error is infinite. Localisation errors arising from cross-correlation of NBHF clicks are comparable to the additional range and depth errors that arise due to SoundTrap time synchronisation, with range errors of <2% at ranges 10x the aperture of the array (Fig. 5). This simulation does not account for array bending, ignores off-axis click distortions by not considering how waveforms change with aspect to the array, assumes that sound speed is constant, and assumes that there is a good signal to noise ratio of clicks on all receivers on the array, so actual localisations will likely be less accurate.

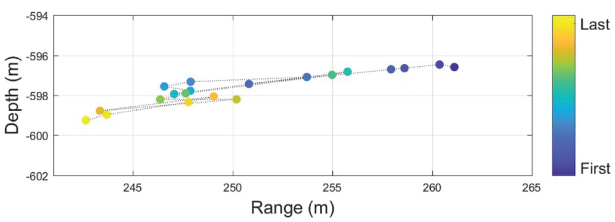

Fig. 2. Range-depth track constructed from localised clicks ($n = 20$) in a pilot whale click train over a 12 s period, demonstrating that the array can be used to track the diving behaviour of deep-diving toothed whales. Range shown is relative to the central channel on the array.

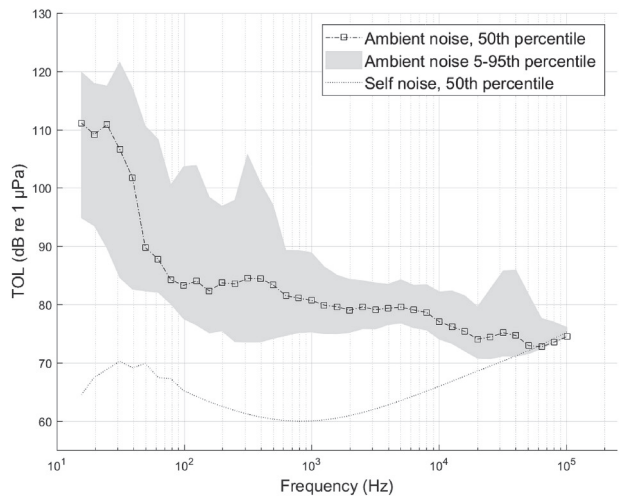

Fig. 3. Third octave levels of deep-water ambient noise from the deepest channel (~695 m) of one deep water deployment lasting 5 h. TOLs were calculated over 30 s intervals. The self noise of the SoundTrap is also shown, illustrating that ambient noise measurements were limited by self noise above about 30 kHz in this location.

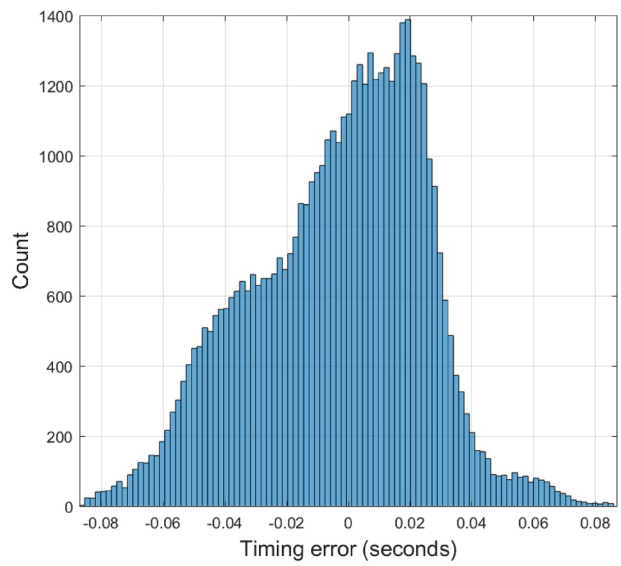

Fig. 4. Time synchronisation errors for six SoundTraps on the array with respect to the seventh recorder which acted as the timing master. This distribution was taken from one field deployment (n = ~43,800 acoustic timing pings) recording at a sample rate of 576 kHz.

4. Discussion

Studying the sounds of deep-diving, echolocating toothed whales is challenging in the marine environment. Specifically, collecting multi-channel, high sample rate data of sufficient quality for acoustic parameter quantification has typically required expensive specialised equipment deployed from a large vessel making such studies inaccessible to many researchers. Here, an autonomous deep-water vertical hydrophone array was designed to obtain high quality deep water array recordings from a small boat with a relatively small budget of ~$31K USD (see Supplementary Materials, Table B1), compared to the cost of deploying a deep water array from an oceanographic research vessel.

The major advantages of this array are that it is autonomous, thereby

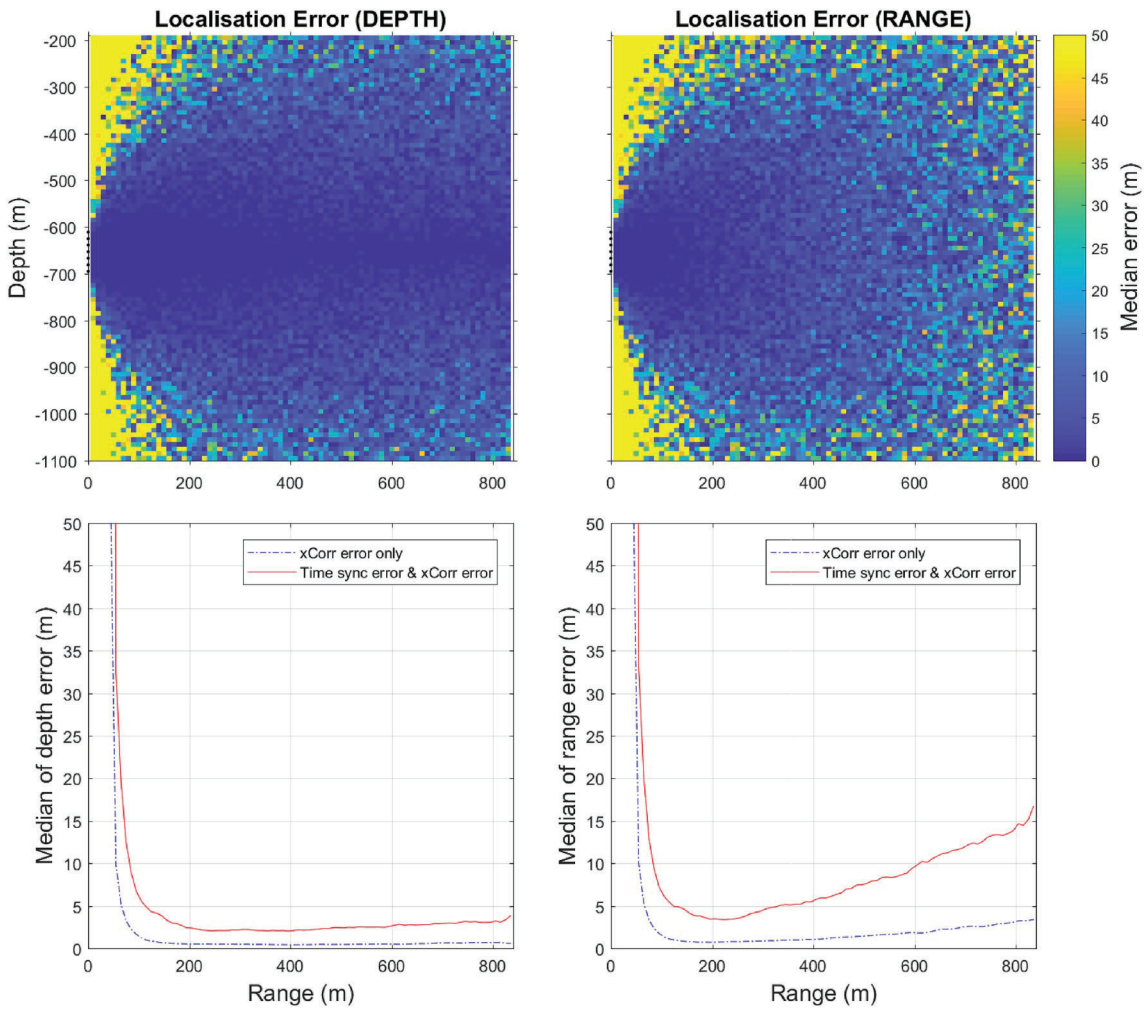

Fig. 5. Simulated source localisation errors for a 7-hydrophone array, showing errors in depth (left) and range (right). (Top): Simulated localisation error surfaces. Small black points at range of 0 m and depth between ~600-700 m represent the locations of each of the recorders on the array. Each 10 m grid point shows the median error value from 100 simulations. For each run, the localised position calculated from manipulated time errors are compared to the known source location. (Bottom): The median depth (left) and range (right) errors across 100 simulations and across all depths as a function of horizontal range to the array.

eliminating an expensive multi-conductor cable to a ship-based recorder, and that it is capable of recording at depth (up to ~700 m tested here). While some toothed whales dive deeper than the maximum depth at which this array was deployed (~700 m), tagging studies have demonstrated important echolocation behaviours, such as the foraging buzzes of sperm and beaked whales, to occur at these depths (Watwood et al. 2006; Johnson et al. 2006). If deep-water SoundTraps are used (depth rated to 1000 m), the array can be deployed even deeper. It can be deployed and retrieved rapidly from a small boat using a low-cost battery-powered winch. It is also resistant: a total of 34 deployments to maximum depths ranging from 100 to 700 m were carried out without mechanical failure of the cable or failure of the electrical connections. The SoundTraps that comprise the array have low self-noise and a large dynamic range, and can sample at high rates (up to 576 kHz) making them well-suited for the target application but, in principal, any compact autonomous recorder could be used provided that it has the capability of being synchronised with an external signal. The large aperture (~84 m presented here) allows for accurate localisations at distances of several hundred metres. The array requires an electrical-mechanical cable to distribute a timing signal to the recorders but this can be a small diameter, inexpensive cable and need be no longer than the aperture of the array itself easing the practicalities of array transport, deployment, and recovery. As a result, the array is highly portable (total shipping weight of ~14 kg, excluding sand for the weights, which is locally-sourced), enabling its deployment from small boats (*e.g.* a RHIB). This portability and autonomy permit flexibility in fieldwork scheduling, because the array can be deployed and recovered relatively opportunistically alongside other at-sea data collection or when animals are sighted in the vicinity of the vessel. An additional advantage of using autonomous recorders is that these can be separated from the array and used for other projects when the array is not needed, making the most of a limited equipment inventory, indeed some of the recorders used here were borrowed from other researchers. While our maximum field deployment duration was 10 h, the battery endurance of the ST-300HF SoundTraps sampling at 576 kHz is about a week, enabling longer deployments if the challenges of tracking and recovering a drifting array over longer intervals can be resolved.

A fundamental limitation of any acoustic array is that animals can only be tracked accurately up to ranges of about 10x the length of the array. Although the array design presented here could be readily extended to track animals at greater ranges, there are some limitations associated with a longer array. The longer the array, the heavier and less portable it becomes, thereby making it less practical for deployment from small boats. Moreover, additional electronics (*e.g.*, a line driver) may be required to transmit timing messages over a longer cable. Longer arrays are also more difficult to keep straight and vertical. The straightness and verticality of the array also depend on deployment conditions: although the typically low water currents at depths of

hundreds of metres make it possible to achieve a straight and vertical array with relatively little weight and buoyancy, high surface currents and sea-state can pull the array up to shallower depths and away from verticality. Array straightness, but not verticality, is critical when quantifying acoustic parameters such as source level, peak frequency or beam pattern (Heerfordt et al. 2007). Array verticality matters when it is important to minimising errors in estimating the depths of localised animals, *i.e.* when describing their depth distributions and diving patterns. To achieve a more vertical array, greater buoyancy and weight are required at the terminal ends of the array, and these increase the difficulty of deploying and recovering the array.

Localisation errors introduced by the SoundTrap time synchronisation method developed here are of the order of 10–20 μs and so are comparable in magnitude with timing errors that arise in the cross correlation of multi-cycle NBHF clicks (Fig. 5). This means that localisation errors for species producing these high frequency clicks are not greatly increased due to inaccuracies in the synchronisation. In other words, the effect of the timing errors observed between channels on the array (Fig. 4) is comparable to the effect of errors in time delays calculated for multi-cycle clicks on a perfectly time-synchronised array (Fig. 5). This effect would be slightly smaller for other deep-diving echolocators, such as beaked whales and sperm whales; Even though these whales have fewer cycles in their clicks and thus the magnitude of timing errors arising from cross correlation errors are expected to be smaller, the reduced error would make very little practical difference in terms of localisation errors. Increasing the array aperture will tend to decrease the impact of synchronisation errors as the time differences of arrival of clicks impinging on the array increase for an animal in a given location. Additionally, localisation accuracy is a function not only of range to the source, but also of the aspect of the source to the array (Madsen and Wahlberg, 2007).

Conversely, time synchronisation errors become increasingly dominant as the array aperture is reduced setting a practical lower limit on the size of the array. In the array described here, the 90th percentile of timing errors was less than 27 samples at 576 kHz, or 47 μs, which effectively means an uncertainty in the relative location of recorders of <7 cm. In a small aperture array this distance is a larger proportion of the inter-hydrophone spacing, increasing the impact of timing errors on localisation accuracy. The timing synchronisation method presented here is therefore not suitable for a small aperture array, such as an autonomous star-array configuration. In this case, a single multi-channel recorder is a better solution (e.g. a 4-channel SoundTrap). Note that 4-channel SoundTraps were not used on our array because their sample rate is limited to 374 kHz, greater latency problems in time synchronisation are expected due to the higher loading of its processor, and with each hydrophone requiring its own cable, the array would be thicker and more delicate. Additionally, with hydrophones spliced at each node, this would preclude their use in other applications.

Within the constraints on array size discussed above, an important advantage of building the array, as opposed to buying a complete commercial solution, is that it can be readily adapted to the intended application and research question. The number of hydrophones and their spacing can be adjusted as desired (see section 2.1.3 and Supplementary Material B), depending, for example, on the intended localisation range, in concert with the desired beam pattern resolution for directional clicks. To modify the distances between hydrophones, additional cable would be required for larger node spacing, and alternatively, coiling up the cable between nodes would allow for smaller node spacing. For example, the array could be built to be 500 m long, extending the localisation range to several km, if interested in more distant loud sound sources of lower frequency, whose propagation is less subject to frequency-dependent absorption losses. However, it is important to consider the accuracy required by the research question, prior to considering array geometry. For example, localisation range errors resulting in <2 dBs of error in apparent source level are rarely critical (Madsen et al. 2007). However, the same errors in range of some 20% on a linear scale can result in larger errors in biosonar beam pattern estimation (up to ±3°), as the aspect angles measured between receivers to the localised whale are impacted on a linear scale, not a logarithmic scale. Thus there are a number of practical design trade-offs that must be considered when adapting the array to different applications.

It is possible, in principle, to have no surface expression (*i.e.*, no float), so that the array is not only autonomous, but independent of the surface. To do this, additional weight would be added so that the array is slightly negatively buoyant and so slowly descends upon deployment, collecting a vertical acoustical profile of the water column. With sufficient tension on the array, the array will sit vertically on the seafloor. Weights may be attached with magnesium releases as used here or with acoustic releases. When the ballast is dropped, the array would become positively buoyant and rise to the surface. This approach has the benefits of complete decoupling from wave movement and avoids the risk of boats colliding or tampering with the surface floats. However, there is an increased risk that the array would drift far or become snagged and not return to the surface. On steep terrain, such as that found at the edge of the continental shelf, the array may also travel down the slope and into water depths that exceed the ratings of the recorders, radio-transmitters, trawl buoys, and depth/tilt sensors.

The example shown here demonstrate the use of the array for characterising the signals from deep-diving toothed whales. The array could also be used with no rope extension, in a shallow-water configuration. Additional information collected by the array can also be exploited to improve tracking and to assess the acoustic context in which animal sounds are produced. Echoes following echolocation clicks, for example, are likely generated by surface reflections, offering the opportunity for an additional virtual hydrophone for each surface reflection for each recorder, positioned above the water surface at a height equivalent to the depth of the receiver (Urick, 1983; Møhl et al. 1990). Usage of these surface bounces can improve the vertical resolution of localisations (*e.g.* Barlow et al. 2018) and effectively increase the aperture of the array (Wahlberg et al. 2001; Madsen and Wahlberg, 2007).

The array has the potential to study sounds beyond biosonar. For example, the array can be used to study sound production in the many deep sea fishes and invertebrates whose bioacoustics remain largely unquantified (Hawkins and Popper, 2017). Additionally, ambient noise (Fig. 4) can be quantified along the drift trajectory of the array potentially enabling studies of how deep sea animals adjust vocal output to accommodate changing noise levels (*e.g.* Parks et al. 2007) or react to vessel passes (*e.g.* Wisniewska et al. 2018). Knowledge of ambient noise is also relevant when defining baseline levels in acoustic impact studies, estimating the zone of acoustic influence of an anthropogenic sound, and monitoring levels of rising anthropogenic noise (Richardson et al. 1995; Hildebrand, 2009). To obtain reliable recordings of low frequency ambient noise it is critical to decouple recorders from wave motion and avoid vessel noise, both of which are achieved by the drifting array described here. Recently, eco-acoustic monitoring applications (*e.g.* acoustic complexity indices) have been used to provide insight into the presence and abundance of marine life (*e.g.* Bolgan et al. 2018; Kaplan et al. 2018), and have been suggested to assist with the detection of cryptic, soniferous species (Staaterman et al. 2017). Using the array to localise such sound sources can establish whether one or several animals are vocalising. As such, the array could be used to remotely monitor the largely unquantified soundscapes of deep marine habitats that are otherwise difficult to sample, and estimate the biodiversity therein.

5. Conclusions

We have reported on the design and performance of a large multi-element, vertical array that addresses a number of challenges facing studies of deep sea bioacoustics. Critically, the array overcomes the high cost and difficulty of deployment of conventional cabled arrays by using commercially-available single channel autonomous recorders. A robust synchronisation method is described that effectively turns these

independent recorders into a multi-channel synchronised acoustic array capable of recording with a wide dynamic range at a high sample rate. The lightweight array is portable and can be deployed from small platforms of opportunity. Data collected with the array can be used to quantify the source parameters of toothed whale clicks, which is valuable both for understanding the acoustic ecology of these species and for informing the design of passive acoustic monitoring systems. The array design presented here can be used as is, or modified, to record the largely undescribed sounds of other marine taxa, and/or to quantify deep sea ambient noise levels and estimate biodiversity at different depths of the water column.

Ethics statement

Fieldwork in Tenerife was under the authorisation of the Spanish Ministry for Ecological Transition MITECO, permit SGPM/BDM/AUTSPP, and with an animal experimentation ethics authorisation from CEIBA of the University of La Laguna (CEIBA2017-0276).

Author contributions

- CEM and PTM designed the array.
- CEM built the array, with help from PHT.
- CEM, PHT, CAD, DEC, MJ, NAS, and PTM collected the data.
- CEM analysed the acoustic data.
- PHT and CEM analysed the depth and tilt sensor data.
- JA provided the SoundTrap firmware modification for synchronisation.
- JA and MJ provided analysis support.
- CEM and PTM wrote the manuscript.
- All authors revised the manuscript, and approved of the final version.

Declaration of competing interest

None.

Acknowledgements

Array development and PhD funding for CEM were supported by the Danish Council for Independent Research (FNU) to PTM (grant 27125). Fieldwork for CEM was funded by the Oticon Foundation (grant 18-0340), the William Demant foundation (grant 19-0386), and the Danish Acoustical Society. NAS was funded by a Ramón y Cajal fellowship from the Spanish Government. Many thanks to the researchers who generously lent us their SoundTraps: Jonas Teilmann, Magnus Wahlberg, and Jakob Tougaard. Thanks to the Zoophysiology workshop at Aarhus University (Niels Kristiansen, John Svane Jensen, Mehran Jahanara, and Lasse Vestergaard Sørensen) for preparing trawl floats, and designing both the 3D-printed moulds for the breakouts and the ping-board in the vertical array. Thanks to the collaborating students and researchers of the University of La Laguna for their help in the field, and to the crew and owners of the vessel Punta Umbría, where we navigated to find pilot whales off Tenerife. Jamie Macaulay (University of St Andrews), Magnus Wahlberg (University of Southern Denmark), Michael Ladegaard and Kristian Beedholm (both Aarhus University) are kindly acknowledged for helpful feedback and discussions.

Appendix A. Supplementary data

Supplementary data to this article can be found online at https://doi.org/10.1016/j.dsr.2020.103233.

References

Au, W.W., 1993. The Sonar of Dolphins. Springer-Verlag, New York. https://doi.org/10.1007/978-1-4612-4356-4.
Au, W.W., Moore, P.W., Pawloski, D., 1986. Echolocation transmitting beam of the Atlantic bottlenose dolphin. J. Acoust. Soc. Am. 80 (2), 688–691. https://doi.org/10.1121/1.394012.
Au, W.W., Benoit-Bird, K.J., 2003. Automatic gain control in the echolocation system of dolphins. Nature 423 (6942), 861–863. https://doi.org/10.1038/nature01727.
Au, W.W., Herzing, D.L., 2003. Echolocation signals of wild Atlantic spotted dolphin (Stenella frontalis). J. Acoust. Soc. Am. 113, 598–604. https://doi.org/10.1121/1.1518980.
Au, W., 2004. Echolocation signals of wild dolphins. Acoust Phys. 50 (4), 454–462. https://doi.org/10.1134/1.1776224.
Au, W.W., Ford, J.K., Horne, J.K., Allman, K.A.N., 2004. Echolocation signals of free-ranging killer whales (Orcinus orca) and modeling of foraging for chinook salmon (Oncorhynchus tshawytscha). J. Acoust. Soc. Am. 115 (2), 901–909. https://doi.org/10.1121/1.1642628.
Barlow, J., Griffiths, E.T., Klinck, H., Harris, D.V., 2018. Diving behavior of Cuvier's beaked whales inferred from three-dimensional acoustic localization and tracking using a nested array of drifting hydrophone recorders. J. Acoust. Soc. Am. 144 (4), 2030–2041. https://doi.org/10.1121/1.5055216.
Bolgan, M., Amorim, M.C.P., Fonseca, P.J., Di Iorio, L., Parmentier, E., 2018. Acoustic Complexity of vocal fish communities: a field and controlled validation. Sci. Rep. 8 (1), 10559. https://doi.org/10.1038/s41598-018-28771-6.
Dunn, J.L., 1969. Airborne measurements of the acoustic characteristics of a sperm whale. J. Acoust. Soc. Am. 46 (4B), 1052–1054. https://doi.org/10.1121/1.1911803.
Frasier, K.E., Wiggins, S.M., Harris, D., Marques, T.A., Thomas, L., Hildebrand, J.A., 2016. Delphinid echolocation click detection probability on near-seafloor sensors. J. Acoust. Soc. Am. 140 (3), 1918–1930. https://doi.org/10.1121/1.4962279.
Freitag, L.E., Tyack, P.L., 1993. Passive acoustic localization of the Atlantic bottlenose dolphin using whistles and echolocation clicks. J. Acoust. Soc. Am. 93 (4), 2197–2205. https://doi.org/10.1121/1.406681.
Gassmann, M., Wiggins, S., Hildebrand, J., 2015. Three-dimensional tracking of Cuvier's beaked whales' echolocation sounds using nested hydrophone arrays. J. Acoust. Soc. Am. 138 (4), 2483–2494. https://doi.org/10.1121/1.4927417.
Gillespie, D., Mellinger, D.K., Gordon, J.C.D., Mclaren, D., Redmond, P., Mchugh, R., Trinder, P., Deng, X.Y., Thode, A., 2008. PAMGUARD: semiautomated, open source software for real-time acoustic detection and localisation of cetaceans. J. Acoust. Soc. Am. 30 (5), 54–62. https://doi.org/10.1121/1.4808713.
Gillespie, D., Macaulay, J., 2019. Time of arrival difference estimation for narrow band high frequency echolocation clicks. J. Acoust. Soc. Am. 146 (4), EL387–EL392. https://doi.org/10.1121/1.5129678.
Goldbogen, J.A., Madsen, P.T., 2018. The evolution of foraging capacity and gigantism in cetaceans. J. Exp. Biol. 221 (11), 1–9. https://doi.org/10.1242/jeb.166033.
Hawkins, A.D., Popper, A.N., 2017. A sound approach to assessing the impact of underwater noise on marine fishes and invertebrates. ICES J. Mar. Sci. 74 (3), 635–651. https://doi.org/10.1093/icesjms/fsw205.
Hayes, S.A., Mellinger, D.K., Croll, D.A., Costa, D.P., Borsani, J.F., 2000. An inexpensive passive acoustic system for recording and localizing wild animal sounds. J. Acoust. Soc. Am. 107 (6), 3552–3555. https://doi.org/10.1121/1.429424.
Heerfordt, A., Møhl, B., Wahlberg, M., 2007. A wideband connection to sperm whales: a fiber-optic, deep-sea hydrophone array. Deep Sea Res. Part I 54 (3), 428–436. https://doi.org/10.1016/j.dsr.2006.12.003.
Hildebrand, J.A., 2009. Anthropogenic and natural sources of ambient noise in the ocean. Mar. Ecol. Prog. Ser. 395, 5–20. https://doi.org/10.3354/meps08353.
Jensen, F.H., Johnson, M., Ladegaard, M., Wisniewska, D., Madsen, P.T., 2018. Narrow acoustic field of view drives frequency scaling in toothed whale biosonar. Curr. Biol. 28, 1–8. https://doi.org/10.1016/j.cub.2018.10.037.
Johnson, M.P., Tyack, P.L., 2003. A digital acoustic recording tag for measuring the response of wild marine mammals to sound. IEEE J. Ocean. Eng. 28 (1), 3–12. https://doi.org/10.1109/JOE.2002.808212.
Johnson, M., Madsen, P.T., Zimmer, W., De Soto, N.A., Tyack, P., 2006. Foraging Blainville's beaked whales (Mesoplodon densirostris) produce distinct click types matched to different phases of echolocation. J. Exp. Biol. 209 (24), 5038–5050. https://doi.org/10.1242/jeb.02596.
Johnson, M.P., Aguilar de Soto, N., Madsen, P.T., 2009. Studying the behaviour and sensory ecology of marine mammals using acoustic recording tags: a review. Mar. Ecol. Prog. Ser. 395, 55–73. https://doi.org/10.3354/meps08255.
Kaplan, M.B., Lammers, M.O., Zang, E., Mooney, T.A., 2018. Acoustic and biological trends on coral reefs off Maui, Hawaii. Coral Reefs 37 (1), 121–133. https://doi.org/10.1007/s00338-017-1638-x.
Koblitz, J.C., Stilz, P., Rasmussen, M.H., Laidre, K.L., 2016. Highly directional sonar beam of Narwhals (Monodon monoceros) measured with a vertical 16 hydrophone array. PloS One 11 (11), e0162069. https://doi.org/10.1371/journal.pone.0162069.
Kyhn, L.A., Tougaard, J., Jensen, F., Wahlberg, M., Stone, G., Yoshinaga, A., Beedholm, K., Madsen, P.T., 2009. Feeding at a high pitch: source parameters of narrow band, high-frequency clicks from echolocating off-shore hourglass dolphins and coastal Hector's dolphins. J. Acoust. Soc. Am. 125 (3), 1783–1791. https://doi.org/10.1121/1.3075600.
Ladegaard, M., Jensen, F.H., Beedholm, K., da Silva, V.M.F., Madsen, P.T., 2017. Amazon river dolphins Inia geoffrensis modify biosonar output level and directivity during prey interception in the wild. J. Exp. Biol. 220, 2654–2665. https://doi.org/10.1242/jeb.159913.

Ladegaard, M., Madsen, P.T., 2019. Context-dependent biosonar adjustments during active target approaches in echolocating harbour porpoises. J. Exp. Biol. https://doi.org/10.1242/jeb.206169.
Macaulay, J.D.J., Gordon, J.C.D., Gillespie, D., Malinka, C.E., Johnson, M.P., Northridge, S., 2015. Tracking Harbor Porpoises in Tidal Rapids: a Low Cost Autonomous Platform to Track the Movement of Harbor Porpoises in Tidal Rapids. Sea Mammal Research Unit, NERC Knowledge Exchange Report, p. 32 no DOI available. See. https://risweb.st-andrews.ac.uk/portal/en/research output/tracking-harbor-porpoises-in-tidal-rapids (59db2edc-84f2-4060-98e3-c207b78ca008)/export.html.
Macaulay, J.D.J., Gordon, J.C.D., Gillespie, D., Malinka, C.E., Northridge, S., 2017. Passive acoustic methods for fine-scale tracking of harbour porpoises in tidal rapids. J. Acoust. Soc. Am. 141 (2), 1120–1132. https://doi.org/10.1121/1.4976077.
Madsen, P., Wahlberg, M., Møhl, B., 2002. Male sperm whale (Physeter macrocephalus) acoustics in a high-latitude habitat: implications for echolocation and communication. Behav. Ecol. Sociobiol. 53 (1), 31–41. https://doi.org/10.1007/s00265-002-0548-1.
Madsen, P.T., Kerr, I., Payne, R., 2004a. Echolocation clicks of two free-ranging, oceanic delphinids with different food preferences: false killer whales Pseudorca crassidens and Risso's dolphins Grampus griseus. J. Exp. Biol. 207 (11), 1811–1823. https://doi.org/10.1242/jeb.00966.
Madsen, P.T., Kerr, I., Payne, R., 2004b. Source parameter estimates of echolocation clicks from wild pygmy killer whales (Feresa attenuata)(L). J. Acoust. Soc. Am. 116 (4), 1909–1912. https://doi.org/10.1121/1.1788726.
Madsen, P.T., Carder, D., Beedholm, K., Ridgway, S., 2005. Porpoise clicks from a sperm whale nose—convergent evolution of 130 kHz pulses in toothed whale sonars? Bioacoust 15 (2), 195–206. https://doi.org/10.1080/09524622.2005.9753547.
Madsen, P.T., Wahlberg, M., 2007. Recording and quantification of ultrasonic echolocation clicks from free-ranging toothed whales. Deep Sea Res. Part I 54 (8), 1421–1444. https://doi.org/10.1016/j.dsr.2007.04.020.
Madsen, P.T., Wilson, M., Johnson, M., Hanlon, R.T., Bocconcelli, A., Aguilar de Soto, N. A., Tyack, P.L., 2007. Clicking for calamari: toothed whales can echolocate squid Loligo pealeii. Aquat. Biol. 1 (2), 141–150. https://doi.org/10.3354/ab00014.
Madsen, P.T., de Soto, N.A., Arranz, P., Johnson, M., 2013. Echolocation in Blainville's beaked whales (Mesoplodon densirostris). J. Comp. Physiol. A Neuroethol Sensory, Neural, Behav. Physiol. 199 (6), 451–469. https://doi.org/10.1007/s00359-013-0824-8.
Malinka, C., 2019. Example dataset for SoundTrap array. Mendeley Data, V1. https://doi.org/10.17632/xcs7y2wcph.1. https://data.mendeley.com/datasets/xcs7y2wcph/1.
Marques, T.A., Thomas, L., Ward, J., DiMarzio, N., Tyack, P.L., 2009. Estimating cetacean population density using fixed passive acoustic sensors: an example with Blainville's beaked whales. J. Acoust. Soc. Am. 125 (4), 1982–1994.
Miller, B., Dawson, S., 2009. A large-aperture low-cost hydrophone array for tracking whales from small boats. J. Acoust. Soc. Am. 126 (5), 2248–2256. https://doi.org/10.1121/1.3238258.
Miller, P.J., Tyack, P.L., 1998. A small towed beamforming array to identify vocalizing resident killer whales (Orcinus orca) concurrent with focal behavioral observations. Deep Sea Res. Part II 45 (7), 1389–1405. https://doi.org/10.1016/S0967-0645(98)00028-9.
Møhl, B., Surlykke, A., Miller, L.A., 1990. High Intensity Narwhal Clicks. Sensory Abilities of Cetaceans. Springer, pp. 295–303. https://doi.org/10.1007/978-1-4899-0858-2_18.
Møhl, B., Wahlberg, M., Madsen, P.T., Miller, L.A., Surlykke, A., 2000. Sperm whale clicks: directionality and source level revisited. J. Acoust. Soc. Am. 107 (1), 638–648. https://doi.org/10.1121/1.428329.
Møhl, B., Wahlberg, M., Heerfordt, A., 2001. A large-aperture array of nonlinked receivers for acoustic positioning of biological sound sources. J. Acoust. Soc. Am. 109 (1), 434–437. https://doi.org/10.1121/1.1323462.
Møhl, B., Wahlberg, M., Madsen, P.T., Heerfordt, A., Lund, A., 2003. The monopulsed nature of sperm whale clicks. J. Acoust. Soc. Am. 114 (2), 1143–1154. https://doi.org/10.1121/1.1586258.
Nelder, J.A., Mead, R., 1965. A simplex method for function minimization. Comput. J. 7 (4), 308–313. https://doi.org/10.1093/comjnl/7.4.308.
Nosal, E.-M., Frazer, L.N., 2007. Sperm whale three-dimensional track, swim orientation, beam pattern, and click levels observed on bottom-mounted hydrophones. J. Acoust. Soc. Am. 122 (4), 1969–1978. https://doi.org/10.1121/1.2775423.
Parks, S.E., Clark, C.W., Tyack, P.L., 2007. Short-and long-term changes in right whale calling behavior: the potential effects of noise on acoustic communication. J. Acoust. Soc. Am. 122 (6), 3725–3731. https://doi.org/10.1121/1.2799904.
Press, W.H., Teukolsky, S.A., Vetterling, W.T., Flannery, B.P., 1988. Minimization or Maximization of Functions. Numerical Recipes: the Art of Scientific Computing. Cambridge University Press, New York, pp. 408–412 [no DOI].
Rasmussen, M.H., Miller, L.A., Au, W.W., 2002. Source levels of clicks from free-ranging white-beaked dolphins (Lagenorhynchus albirostris Gray 1846) recorded in Icelandic waters. J. Acoust. Soc. Am. 111 (2), 1122–1125. https://doi.org/10.1121/1.1433814.
Richardson, W., Greene Jr., C., Malme, C., Thomson, D., 1995. Marine Mammals and Noise. Academic Press, San Diego, USA.
Shaffer, J.W., Moretti, D., Jarvis, S., Tyack, P., Johnson, M., 2013. Effective beam pattern of the Blainville's beaked whale (Mesoplodon densirostris) and implications for passive acoustic monitoring. J. Acoust. Soc. Am. 133 (3), 1770–1784. https://doi.org/10.1121/1.4776177.
Spiesberger, J.L., Fristrup, K.M., 1990. Passive localization of calling animals and sensing of their acoustic environment using acoustic tomography. Am. Nat. 135 (1), 107–153. https://doi.org/10.1086/285035.
Staaterman, E., Ogburn, M.B., Altieri, A.H., Brandl, S.J., Whippo, R., Seemann, J., Goodison, M., Duffy, J.E., 2017. Bioacoustic measurements complement visual biodiversity surveys: preliminary evidence from four shallow marine habitats. Mar. Ecol. Prog. Ser. 575, 207–215. https://doi.org/10.3354/meps12188.
Urick, R.J., 1983. Principles of Underwater Sound. McGraw-Hill, Peninsula, Los Altos.
Wahlberg, M., Møhl, B., Madsen, P.T., 2001. Estimating source position accuracy of a large-aperture hydrophone array for bioacoustics. J. Acoust. Soc. Am. 109 (1), 397–406. https://doi.org/10.1121/1.1329619.
Wahlberg, M., Jensen, F.H., Soto, N.A., Beedholm, K., Bejder, L., Oliveira, C., Rasmussen, M., Simon, M., Villadsgaard, A., Madsen, P.T., 2011. Source parameters of echolocation clicks from wild bottlenose dolphins (Tursiops aduncus and Tursiops truncatus). J. Acoust. Soc. Am. 130 (4), 2263–2274. https://doi.org/10.1121/1.3624822.
Watkins, W.A., 1980. Acoustics and the Behavior of Sperm Whales. Animal Sonar Systems. Springer, pp. 283–290. https://doi.org/10.1007/978-1-4684-7254-7_11.
Watkins, W.A., Schevill, W.E., 1971. Four Hydrophone Array for Acoustic Three-Dimensional Location. Woods Hole Oceanogr. Inst. Tech. Rep. Woods Hole Oceanographic Institution, p. 89. https://doi.org/10.1575/1912/76.
Watkins, W.A., Schevill, W.E., 1972. Sound source location by arrival-times on a non-rigid three-dimensional hydrophone array. Deep Sea Res. Oceanogr. Abstr. 691–706. https://doi.org/10.1016/0011-7471(72)90061-7.
Watwood, S.L., Miller, P.J., Johnson, M., Madsen, P.T., Tyack, P.L., 2006. Deep-diving foraging behaviour of sperm whales (Physeter macrocephalus). J. Anim. Ecol. 75 (3), 814–825. https://doi.org/10.1111/j.1365-2656.2006.01101.x.
Weinstein, E., Weiss, A., 1984. Fundamental limitations in passive time-delay estimation - Part II: wide-band systems. IEEE Trans. 32 (5), 1064–1078. https://doi.org/10.1109/TASSP.1984.1164429.
Whitney, W., 1968. Observations of Sperm Whale Sounds from Great Depths. MPL-U-11/68. Marine Physical Laboratory Scripps Institution of Oceanography, p. 8 [no doi].
Wisniewska, D.M., Johnson, M., Teilmann, J., Siebert, U., Galatius, A., Dietz, R., Madsen, P.T., 2018. High rates of vessel noise disrupt foraging in wild harbour porpoises (Phocoena Phocoena). Proc. Roy. Soc. B: Biol. Sci. 285 (1872) https://doi.org/10.1098/rspb.2017.2314.
Zimmer, W.M., 2011. Passive Acoustic Monitoring of Cetaceans. Cambridge University Press. https://doi.org/10.1017/CBO9780511977107.
Zimmer, W.M., Tyack, P.L., Johnson, M.P., Madsen, P.T., 2005. Three-dimensional beam pattern of regular sperm whale clicks confirms bent-horn hypothesis. J. Acoust. Soc. Am. 117 (3), 1473–1485. https://doi.org/10.1121/1.1828501.
Zimmer, W.M., Harwood, J., Tyack, P.L., Johnson, M.P., Madsen, P.T., 2008. Passive acoustic detection of deep-diving beaked whales. J. Acoust. Soc. Am. 124 (5), 2823–2832. https://doi.org/10.1121/1.298827.

Chapter III.

Kogia Echolocation

Malinka, C. E., Tønnesen, P., Dunn, C., Claridge, D., Gridley, T., Elwen, S. H., & P. T. Madsen. (2021). "Echolocation click parameters and acoustic behaviour of wild dwarf sperm whale (Kogia sima)," *Journal of Experimental Biology*. 224 (6), jeb250689. doi: 10.1242/jeb.240689

© 2021. Published by The Company of Biologists Ltd | Journal of Experimental Biology (2021) 224, jeb240689. doi:10.1242/jeb.240689

RESEARCH ARTICLE

Echolocation click parameters and biosonar behaviour of the dwarf sperm whale (*Kogia sima*)

Chloe E. Malinka[1,*], Pernille Tønnesen[1], Charlotte A. Dunn[2,3], Diane E. Claridge[2,3], Tess Gridley[4,5], Simon H. Elwen[4,5] and Peter Teglberg Madsen[1]

ABSTRACT

Dwarf sperm whales (*Kogia sima*) are small toothed whales that produce narrow-band high-frequency (NBHF) echolocation clicks. Such NBHF clicks, subject to high levels of acoustic absorption, are usually produced by small, shallow-diving odontocetes, such as porpoises, in keeping with their short-range echolocation and fast click rates. Here, we sought to address the problem of how the little-studied and deep-diving *Kogia* can hunt with NBHF clicks in the deep sea. Specifically, we tested the hypotheses that *Kogia* produce NBHF clicks with longer inter-click intervals (ICIs), higher directionality and higher source levels (SLs) compared with other NBHF species. We did this by deploying an autonomous deep-water vertical hydrophone array in the Bahamas, where no other NBHF species are present, and by taking opportunistic recordings of a close-range *Kogia sima* in a South African harbour. Parameters from on-axis clicks (*n*=46) in the deep revealed very narrow-band clicks (root mean squared bandwidth, BW_{RMS}, of 3±1 kHz), with SLs of up to 197 dB re. 1 µPa peak-to-peak (μPa_{pp}) at 1 m, and a half-power beamwidth of 8.8 deg. Their ICIs (mode of 245 ms) were much longer than those of porpoises (<100 ms), suggesting an inspection range that is longer than detection ranges of single prey, perhaps to facilitate auditory streaming of a complex echo scene. On-axis clicks in the shallow harbour (*n*=870) had ICIs and SLs in keeping with source parameters of other NBHF cetaceans. Thus, in the deep, dwarf sperm whales use a directional, but short-range echolocation system with moderate SLs, suggesting a reliable mesopelagic prey habitat.

KEY WORDS: Beam pattern, Bioacoustics, Hydrophone array, Narrow-band high-frequency, Passive acoustic monitoring, Source parameters

INTRODUCTION

Echolocating toothed whales navigate and detect prey by emitting powerful clicks and subsequently processing the returning echoes to form an actively generated auditory scene. This active sensory modality has allowed toothed whales to specialize in a range of aquatic food niches from mesopelagic depths to shallow rivers and estuaries (Madsen and Surlykke, 2013). The deep-diving sperm whales, pilot whales, belugas, narwhals and beaked whales are among the largest predators on the planet, and have evolved low (<30 kHz) to medium (~30-80 kHz) frequency, high-power biosonar systems sampling at low rates to find and target mainly cephalopod prey at mesopelagic and bathypelagic depths (Au et al., 1987; Møhl et al., 2003; Johnson et al., 2004, 2006; Aguilar de Soto et al., 2008; Koblitz et al., 2016; Pedersen et al., in review). Conversely, some of the smallest toothed whales, including river dolphins (e.g. *Inia*), small dolphins (e.g. *Cephalorhynchus*, *Lagenorhynchus*/*Sagmatius*) and porpoises (e.g. *Phocoena*, *Phocoenoides*), employ high-frequency, low-power biosonars, sampling at fast rates in keeping with finding small prey at short ranges in their often shallow, acoustically cluttered habitats (Jensen et al., 2013; Kyhn et al., 2009, 2010, 2013; Ladegaard et al., 2015). High-frequency signals are more suited to detecting/discriminating small prey items (Au, 1993), and may facilitate acoustic crypsis from eavesdropping killer whales (Møhl and Andersen, 1973). Thus, mounting evidence suggests that spectral emphasis, output levels and biosonar sampling rates have broadly co-evolved with foraging niche adaptations, predation pressure, body size and diving capabilities in toothed whales, similar to the sensory niche adaptation observed in the biosonar guilds of bats (Schnitzler and Kalko, 2001).

It has recently been argued that such inverse scaling of the spectral emphasis of clicks with body size serves to maintain a stable acoustic field of view of around 10 deg in echolocating toothed whales (Jensen et al., 2018). The narrowness of the acoustic field of view exists in a trade-off between high source levels (SLs) and clutter rejection on the one hand, and beamwidths wide enough to make prey search efficient on the other. Large toothed whales radiate lower-frequency clicks from their large melons and small toothed whales radiate high-frequency clicks from their small melons, resulting in broadly similar ratios between dominant wavelengths and radiating apertures across three orders of magnitude in body mass. Harbour porpoises (*Phocoena phocoena*), for example, are known to generally occupy coastal habitats and produce narrow-band high-frequency (NBHF) clicks centred on ~125 kHz at low SLs [150–190 dB re. 1 µPa peak-to-peak (μPa_{pp}) at 1 m) and short inter-click intervals (ICIs) below 100 ms. Such click properties are shared among the other porpoise species and have evolved convergently in dolphins in the *Cephalorhynchus* genus that are also often hunting in coastal habitats (Kyhn et al., 2009, 2010), leading to the proposition that NBHF clicks evolved to facilitate echolocation in cluttered habitats for small toothed whales (Ketten, 2000). Conversely, the deep-diving sperm whale (*Physeter macrocephalus*), which can reach a length of up to 18 m, employs a long-range echolocation system (of the order of hundreds of metres) via clicks with very high source levels (up to 240 dB re. 1 μPa_{pp}

[1]Zoophysiology, Department of Biology, Aarhus University, 8000 Aarhus, Denmark. [2]Bahamas Marine Mammal Research Organisation (BMMRO), Sandy Point, Abaco, Bahamas. [3]Sea Mammal Research Unit, University of St Andrews, St Andrews KY16 8LB, UK. [4]Department of Botany and Zoology, Stellenbosch University, Stellenbosch 7605, South Africa. [5]Sea Search Research and Conservation, Muizenberg, Cape Town 7945, South Africa.

*Author for correspondence (chloe.e.malinka@bio.au.dk)

C.E.M., 0000-0003-0138-8388; P.T., 0000-0002-0869-6490; C.A.D., 0000-0002-4274-7239; D.E.C., 0000-0002-9028-8647; T.G., 0000-0003-0925-5782; S.H.E., 0000-0002-7467-6121; P.T.M., 0000-0002-5208-5259

Received 18 November 2020; Accepted 11 February 2021

Journal of Experimental Biology (2021) 224, jeb240689. doi:10.1242/jeb.240689

List of abbreviations

ASL	apparent source level
BW	bandwidth
DI	directivity index
DT	detection threshold
EFD	energy flux density
EPR	equivalent piston radius
F_c	centroid frequency
F_p	peak frequency
ICI	inter-click interval
NBHF	narrow-band high-frequency
PAM	passive acoustic monitoring
pp	peak-to-peak
Q	resonant quality factor
RHIB	rigid hull inflatable boat
RL	received level
RMS	root mean square
SL	source level
TL	transmission loss
TOL	third octave level
TS	target strength

at 1 m), high directionality (directionality index of >27 dB), low absorption with peak frequencies at 15–20 kHz, and ICIs between 0.4 and 1 s (Møhl et al., 2000, 2003; Madsen et al., 2002, 2007; Tønnesen et al., 2020).

However, not all toothed whales conform to that scaling; a close relative of the sperm whale, the much smaller *Kogia*, the genus of both the dwarf [*Kogia sima* (Owen 1866)] and pygmy sperm whales [*Kogia breviceps* (Blainville 1838)], also produce NBHF clicks despite their presumed deep-sea foraging. Their deep-diving behaviour has been inferred from visual observations over continental slopes and shelf breaks (Caldwell and Caldwell, 1989; Baumgartner et al., 2001; MacLeod et al., 2004; Dunphy-Daly et al., 2008), and from deep-sea squid beaks and meso-benthopelagic fish otoliths in the stomach contents of stranded *Kogia* (Plön, 2004; Elwen et al., 2013; Staudinger et al., 2014). It is therefore puzzling and counterintuitive that *Kogia*, in evolutionary convergence with porpoises, also produce NBHF echolocation clicks (Madsen et al., 2005a), as this click type suffers from an absorption that is ∼40 times greater than that of clicks made by sperm whales foraging in the same environment. In the very different habitats of *Kogia*, porpoises and *Cephalorhynchus* dolphins, echolocators would be faced with different challenges in terms of prey ranges, reverberation, clutter and noise, yet *Kogia* have, in convergence with the shallow-diving species, evolved to produce NBHF biosonar clicks. Some acoustic parameters of *Kogia* clicks (e.g. peak frequency, bandwidth, duration, etc.) have been reported from stranded *Kogia* held in captivity for rehabilitation (Thomas et al., 1990; Ridgway and Carder, 2001; Marten, 2000; Madsen et al., 2005a) and from recent single-channel field recordings (Merkens et al., 2018; Merkens and Oleson, 2018; Hodge et al., 2018; Hildebrand et al., 2019; Griffiths et al., 2020). Here, we sought to obtain a deeper quantitative understanding of how *Kogia* can echolocate to find deep-sea prey using clicks with spectral properties suited for short-range echolocation.

The much larger body (4–6 times heavier) of *Kogia* compared with that of other NBHF odontocetes means that the aperture of its sound-producing head is expected to be 2–3 times larger with respect to the dominant wavelengths of a NBHF click. This suggests that their acoustic field of view should be narrower by the same factor on a linear scale, and the corresponding directivity index (DI) should be 6–9 dB higher than in other NBHF species (Au, 1993). From their deep-water prey, it is predicted that *Kogia* would search for prey over longer ranges (hundreds of metres) than shallow-diving NBHF species (tens of metres), making high directionality favourable. Such predictions prompt the hypotheses that they use higher SLs and longer ICIs to facilitate longer range echolocation. In this study, we tested these hypotheses by quantifying the biosonar source parameters and acoustic behaviour of wild *Kogia*. Specifically, we measured the SL, directionality and beam pattern of *Kogia* clicks, uniquely made possible via recordings made with a novel deep-water vertical hydrophone array deployed with concurrent visual sightings of *Kogia sima*. These data are presented in conjunction with visually validated and close-range, shallow-water, single-channel recordings of the same species.

MATERIALS AND METHODS

Clicks of *Kogia* were recorded in two locations with two methods: (1) using deep-water vertical arrays off the continental shelf edge in the Bahamas, and (2) opportunistically using a single-channel recorder in Cape Town harbour, South Africa.

Recording and calibration

Array recordings were made using two custom-built vertical hydrophone arrays, each composed of seven autonomously recording and sample-synchronized SoundTraps (ST300-HF, Ocean Instruments, Auckland, New Zealand; http://www.oceaninstruments.co.nz/) (see Malinka et al., 2020). The SoundTraps were spaced ∼14 m apart (13.82–14.21 m), as informed by simulations of predicted *Kogia* beam patterns, for an overall aperture of 84 m. Animals can theoretically be localized (with less than 30% range error) out to ∼840 m around the array (10× the array aperture), based on increasing deterioration in localization accuracy with increasing range (e.g. Kyhn et al., 2009; Macaulay et al., 2017; Malinka et al., 2020).

Prior to data collection, artificial porpoise-like clicks were projected at a SoundTrap attached to the array cable to quantify the degree of shading behind the cable, resulting in a maximal nominal loss of 1.5 dB. All SoundTraps on the arrays were calibrated against a Reson 4034 hydrophone (Teledyne Marine, Slangerup, Denmark) in a 3 m deep cedar tank (in 10 kHz steps up to 200 kHz). Each device sampled at 576 kHz with 16-bit resolution with a high gain setting (resulting in clip levels ranging from 174 to 180 dB re. 1 µPa at 130 kHz). The single SoundTrap used in South Africa was not available for calibration, and so an average from 19 other calibrated SoundTraps was applied to this recorder, for an estimated clip level of 174 dB re. 1 µPa at 130 kHz. All calibrated devices showed system clip levels varying ±2 dB, from 10 kHz to 90 kHz, and by ±1 dB in the 100–190 kHz range relevant to this study.

Two temperature and inclinometer sensors (Star Oddi DST tilt-and-depth sensors; www.star-oddi.com), attached to the body of the peripheral SoundTraps, confirmed that the arrays were straight throughout deployments with *Kogia* clicks. Deviations from hanging perfectly vertically (0 deg) were included in calculating error (sinθ×range) in the depth of the localizations. Temperature informed the sound speed used in transmission calculations.

Data collection

Shelf edge, Bahamas

Array data were collected in May–June 2018, in the NE Providence Channel, south of Great Abaco Island, in the Bahamas (∼25°54.0′N, ∼77°20.0′W) during daylight hours. This field site was chosen because *Kogia* are commonly observed there (MacLeod et al., 2004;

Claridge, 2006; Dunphy-Daly et al., 2008; Dunn and Claridge, 2014), and within 4 km from shore, the seafloor steeply drops to depths >3000 m, enabling daily fieldwork access with a small boat. Importantly, beyond the two species of *Kogia*, no other NBHF pulse-producing species are known to occur in Bahamian waters.

The vertical passive acoustic array was deployed from a rigid hull inflatable boat (RHIB) on 18 occasions. The array was suspended below a top float, with an optional rope (single cross-braid polyester) extension (of 100 or 200 m) between the top float and the array, making the depths of top and bottom hydrophones 11 m and 95 m, 111 m and 195 m, or 211 m and 295 m (for 16%, 15% and 69% of the total recording time, respectively). Both the top float and a rod of trawl buoys positioned between the extension rope and the array contained radio transmitters (MM150, Advanced Telemetry Systems) to facilitate recovery (for details, see Malinka et al., 2020). A ∼10 kg terminal weight was added to the bottom of the array to keep it vertical and linear in the water. One array was deployed at the start of a day in the absence of any visual or acoustic cues, and a combination of visual and acoustic observation was used to prompt the deployment of the second array. Acoustic observation entailed suspending a Reson TC4013 hydrophone a few metres below the RHIB, connected to a custom-built pre-filter (high pass 40 kHz) and click-detector box, connected to headphones. If clicks were heard on the headphones, the second array was deployed. Looking and listening stations were informed by past visual observations of *Kogia* presented in Dunphy-Daly et al. (2008).

A total of ∼20 min of *Kogia* echolocation clicks were recorded in the deep and natural habitat by the array over 74.6 h of effort. These were obtained in two ∼10 min continuous sections ('period A' and 'period B'), recorded on two consecutive days (10 and 11 May 2018), both when the array was at a maximum depth of ∼95 m. Period A coincided with visual observation of a pair of *Kogia sima* and no other odontocetes, with species identification visually confirmed by experienced local researchers. Period B had no visual detections of any odontocete. During other deployments, the only other odontocete species visually observed were Blainville's beaked whale (*Mesoplodon densirostris*) producing frequency-modulated clicks around 40 kHz (Madsen et al., 2013). For both periods A and B, the array was slightly tilted at 9 deg off vertical, but in both instances, the tilt measurement at the top and bottom of the array was <1 deg apart, indicating straightness, but translating to errors in the calculated depths of localizations of 4% or 15% for the localization ranges in periods A and B, respectively (Table 1). Within these two periods, a total of 8636 clicks were detected and classified as *Kogia* across all channels. As many of these click recordings represented the same click, a subset of 1492 clicks were available for ICI measurements (noting that each click was not necessarily detected on all channels). From these detections, 46 clicks (0.5%) fulfilled the on-axis criteria (detailed below), had localizations whose errors in apparent source level (ASL) were <3 dB, and were used in source parameter measurement. A subset of 21 clicks (0.2%) had localizations whose errors in angular incidence were <3 deg and were used in beam pattern estimation.

Sound speed was estimated to be 1535 m s^{-1} based on the mean water temperature measured by sensors attached to both peripheral SoundTraps on the array of 25.0°C (mean of 25.8°C at 11 m, and mean of 24.2°C at 95 m, for the two deployments in which *Kogia* clicks were detected), and a local salinity of 36.5 ppm (Medwin, 1975; Sato and Benoit-Bird, 2017). This constant sound speed was used in localization calculations. Accordingly, potential errors arising from surface propagation were investigated using the 'AcTUP' (Duncan and Maggi, 2006) MATLAB toolbox (2017a, Mathworks, Natick, MA, USA), which confirmed straightness of ray paths for the ranges considered here.

Cape Town harbour, South Africa

Opportunistic recordings (∼4 h) of a single wild *Kogia sima* were made during daylight hours (9 and 11 November 2016) in Cape Town harbour (depth of 6–8 m), South Africa (∼33°54′S, ∼18°26′E), with a single high-frequency digital recorder (SoundTrap HF300,

Table 1. Source parameters for all on-axis *Kogia* echolocation clicks

	Array recording, Bahamas		Single-channel recording, Cape Town harbour, South Africa		
Parameter	Mean±s.d.	Median (range) or [95% CI]	Mean±s.d.	Median (range)	Unit
SL_{pp}	186±6	185 (174–197)	158±12	157 (125–193)	dB re. 1 μPa at 1 m
SL_{RMS}	174±6	174 (162–186)	146±12	146 (113–181)	dB re. 1 μPa at 1 m
SL_{EFD}	135±6	134 (123–147)	105±11	104 (72–137)	dB re. 1 μPa^2 s at 1m
Duration (−10 dB)	142±37	142 (71–205)	77±29	68 (32–202)	μs
F_c	123±4	122 (118–129)	129±2	129 (120–142)	kHz
F_p	123±4	122 (117–130)	129±3	129 (118–140)	kHz
$BW_{-3\ dB}$	4±2	4 (2–9)	8±3	8 (2–18)	kHz
$BW_{-10\ dB}$	8±3	7 (5–16)	15±4	16 (6–31)	kHz
BW_{RMS}	3±1	2 (1–7)	5±2	5 (2–14)	kHz
Q_{RMS}	56±20	56 (19–94)	31±12	28 (10–82)	(unitless)
DI	27.0	[25.2–28.5]	n/a	n/a	dB
Equivalent piston radius	4.2	[3.7–5.5]	n/a	n/a	cm
Beamwidth	8.8	[7.0–10.3]	n/a	n/a	deg
ICI	209±75	228 (23–489)	51±34	43 (4–347)	ms
Range	405±189	479 (134–718)	9±7	7 (0.5–42)	m
Depth of localizations	94±113	47 (1–392)	n/a	n/a	m
Depth of recorder	11–95	n/a	∼3	n/a	m
Depth of water at recording site	(A) ∼400 (B) ∼900	n/a	∼7	6–8	m
N clicks (source parameters)	46		870		n/a
N clicks (beam pattern estimation)	21		n/a		n/a

Only those passing criteria and with reasonable localization errors are shown. Some measurements are indicated separately for the 2 array deployments with *Kogia* clicks (periods A and B; see Materials and Methods). SL, source level; pp, peak-to-peak; RMS, root mean square; EFD, energy flux density; F_c, centroid frequency; F_p, peak frequency; BW, bandwidth; *Q*, quality factor; DI, directivity index, ICI, inter-click interval; CI, confidence interval.

sampling at 576 kHz) suspended (depth of ∼3 m) from a moored RHIB. The close range to the animal facilitated species identification, which was based on the size and shape of the dorsal fin (Fig. S1). Audio recordings were made in conjunction with time-aligned voice notes detailing the orientation and distance of the visible and close-by animal relative to the recorder, as estimated by experienced observers. The animal was mostly slowly swimming in circles at the surface, but also regularly approached and came within metres of the hydrophone. The animal was clearly observed throughout recordings and no other cetaceans were observed. The harbour was active, and boats were motoring in and out of the harbour throughout the deployment. A total of 16,805 clicks were detected and classified as *Kogia*, of which 870 (5.2%) fulfilled on-axis criteria (detailed below).

Analysis

Detection, classification and localization

The click detection module in PAMGuard (www.pamguard.org, version 2.01.03; Gillespie et al., 2008) was used to detect and extract all transient signals above a 10 dB signal-to-noise ratio (SNR) threshold above background noise on filtered data (6-pole Chebyshev band-pass filter from 90 to 180 kHz). Small, unfiltered sound clips containing the full click waveform were saved upon each detection. Clicks were classified as *Kogia* based on peak frequency and by comparing energy in different frequency bands using the inbuilt click classifier. Manual supervision was applied to validate click detection and classification, including checking amplitude modulation and excluding echoes. Clips of raw WAV files of each classified click were then used in subsequent analysis. For the array data, clicks were localized using the Larger Aperture 3D Localizer module, using a time delay-based 'Mimplex' algorithm described by Macaulay et al. (2017). Only clicks that were detected on multiple channels and localized were considered in further analyses.

On-axis click selection

On-axis clicks, defined as being recorded at the centre of the sound beam, were selected using established criteria (Kyhn et al., 2009, 2010, 2013; Madsen and Wahlberg, 2007; Jensen et al., 2013; Ladegaard et al., 2015). It is important to use on-axis clicks for source parameter quantification given the high directionality of toothed whale biosonars, resulting in high distortion of clicks recorded off-axis. Specifically, on-axis clicks should be: (i) detected on multiple channels and localized; and (ii) part of a series of clicks scanning across the array; whereby (iii) the highest received level (RL) occurred on any of the central five channels, for the highest likelihood of being on-axis in the vertical plane; (iv) the click had the greatest RL within a scan, for the highest likelihood of being on-axis in the horizontal plane; and (v) localizations were within 10× the aperture of the array. Source parameters were extracted for clicks that met all of these criteria. Only criterion (ii) could be applied to the harbour recordings because of only using a single-channel recorder. Directionality of *Kogia* clicks is sufficiently high that even in a captive recording environment, clicks were only detected by Madsen et al. (2005a) when the animal was close to the hydrophone within the pool, or, if at a distance, was directly facing the hydrophone. This suspected high directionality of *Kogia* clicks means that of the clicks that were detected, a significant proportion are expected to be recorded on-axis.

Source parameter estimation

Pre-filtered (10 kHz high-pass 4-pole Butterworth) clips of click recordings were brought into MATLAB using the PamBinaries library for MATLAB (https://sourceforge.net/projects/pamguard/files/Matlab/). Click clips were digitally high-pass filtered (80 kHz, 4-pole Butterworth). Click source parameters from on-axis clicks were extracted following Au (1993), Madsen and Wahlberg (2007), and Ladegaard et al. (2015). ASLs were back-calculated (*sensu* Møhl et al., 2000) given the localized ranges (r, in metres), RLs and estimated transmission loss (TL), assuming spherical spreading losses (of $20\log_{10}r$) (Urick, 1983). The calculation for TL also relies on a range-dependent and frequency-specific absorption coefficient (α, in dB m^{-1}), but rather than assuming a single value of α based on, for example, the peak or centroid frequency, α was computed for each bin in the power spectrum (bin size ∼1 kHz; Ainslie and McColm, 1998) prior to inverse transformation back to a waveform from which all click parameter quantifications were drawn (*sensu* Pedersen et al., 2021). This compensation is especially important for broadband clicks, but is good practice to maintain for narrow-band clicks.

ASL values calculated for each hydrophone in the array were interpolated to determine the point along the array at which the acoustic axis was pointing. Therefore, it was not assumed that the channel that recorded the on-axis click candidate with the highest ASL was collected at exactly 0 deg relative to the beam axis. Clicks were rejected if the localization error resulted in a change in ASL of >3 dB on the on-axis channel (*sensu* Kyhn et al., 2013). ASL values for the single-channel recording were calculated using the RL and the visually observed ranges to the animal; recorded distances to the animal were interpolated, and if the time after the last sighting was greater than 5 s, then the click was discarded from further analysis as no reliable range estimation could be obtained.

Click clips were interpolated (MATLAB *interp* function) by a factor of 10 to better estimate signal window length (*sensu* Ladegaard et al., 2015), and click duration was calculated as the interval between the −10 dB points relative to the peak of the interpolated click envelope (Madsen et al., 2005b). The power spectrum of each click was computed (FFT size 1024 to provide a spectral resolution of 562 Hz). Peak frequency (F_p) was calculated as the highest value in the power spectra, and centroid frequency (F_c) divided a spectrum into two halves of equal energy on a linear scale. Bandwidth (BW), frequency minimum and frequency maximum were calculated at −3 dB and −10 dB thresholds around F_p in the power spectrum (*sensu* Au, 1993). The RMS of bandwidth (BW_{RMS}) was additionally measured by taking the standard deviation around the F_c. The resonant quality factor (Q_{RMS}) was calculated by dividing F_c by the BW_{RMS}, whereby a greater Q indicates a lower rate of energy loss relative to the resonator's energy, such that the oscillations diminish more slowly (Au, 1993). RLs were quantified as peak-to-peak amplitude (pp), root mean square amplitude (RMS) and energy flux density (EFD) level, where the last two were computed over the click duration. The RL EFD level was calculated as the RMS amplitude plus $10\log_{10}$(click duration) (measured in s) (*sensu* Madsen et al., 2005b). All clicks that were classified as *Kogia* and were within a scan, whether they were considered to be collected on-axis or not, contributed to measurements of ICI.

Beam pattern estimation

To resolve the beam pattern, the angles and intensities of on-axis clicks, as recorded on an array of hydrophones, were used to fit the transmission pattern of a flat and circular piston of varying diameter of 2–15 cm (in steps of 0.1 cm) (Strother and Mogus, 1970; Au et al., 1978; Beedholm and Møhl, 2006). The piston model describes the beam attenuation relative to the angle from the acoustic

axis, relying only on the waveform of an on-axis echolocation click and the functional aperture of the sound generator. It has previously been used as a model for the radiation of toothed whale biosonar (Au, 1993; Beedholm and Møhl, 2006; Kyhn et al., 2010; Koblitz et al., 2012; Jensen et al., 2015; Finneran et al., 2016) and can successfully model at ±30 deg around the beam axis (Macaulay et al., 2020).

For each on-axis and localized click, the location of the beam axis relative to each array channel is calculable. Therefore, the off-axis angle relative to the acoustic axis of the click, as recorded on all other hydrophones, is also calculable. The ASL of each on-axis click was normalized relative to the channel with the highest back-calculated ASL. Off-axis angles and normalized ASLs were used to resolve the biosonar transmission beam pattern (Madsen and Wahlberg, 2007). Clicks were not included in the beam pattern estimation if the localization error resulted in a change in angle of incidence of >3 deg. As we did not have a movement sensor on the animal, we could not measure the tilt of the emitter, and so rotational symmetry of the beam was assumed. The goodness of fit was calculated for each diameter and then bootstrapped for confidence intervals (*sensu* Jensen et al., 2015), including errors from cable shading. The half-power (−3 dB) beamwidth was calculated from the beam pattern and the transmission DI was fitted to this. The DI was calculated as $DI=20\log_{10}(185\ \text{deg}/BW_{3dB})$, following Zimmer et al. (2005).

Ambient noise

Third octave levels (TOLs) of ambient noise were measured on the deepest hydrophone (~95 m deep) for both array deployments which contained *Kogia* clicks, as well as on the harbour recordings. Measurements were computed over 1 s analysis windows, in third octave bands centred from 24.8 Hz to 256 kHz, and percentiles (5, 50, 95) within each band were calculated over deployment durations, excluding when the instrument(s) entered and left the water.

Ethics statement

Fieldwork in the Bahamas was conducted under a research permit issued by the Bahamas Department of Marine Resources to BMMRO (no.12a), under the Bahamas Marine Mammal Protection Act (2005). Recordings in South Africa were made under permit #RES2016/86 (Department of Environmental Affairs) to S.H.E.

RESULTS

Fig. 1 shows a waveform, spectrogram and spectrum from example on-axis *Kogia* clicks. A *Kogia* click, as received on all elements in the array, is also shown (Fig. 2). Spectra of the clicks were stereotyped in frequency and bandwidth (Fig. 3). The clicks recorded on the array were brief (~142±37 µs; ~15 cycles/click) narrow-band pulses (−3 and −10 dB bandwidths of ~4±2 kHz and 8±3 kHz, respectively) with high peak frequency (at 123±4 kHz) (Table 1). Localizations of on-axis clicks occurred at a range of 134–718 m, with mean and median depths of 94 and 47 m overlapping with the depth of the array (Table 1). No burst pulses, whistles or buzzes were detected on the array recordings, and no interleaving click trains during either period were observed. The modal ICI was 245 ms (with 5th and 95th percentiles at 55 and 313 ms, respectively) (Fig. 4). On-axis clicks revealed a narrow half-power (−3 dB) beamwidth of 8.8 deg (95% confidence interval, CI, 7.0–10.3 deg), with an equivalent piston radius (EPR) of 4.2 cm (95% CI 3.7–5.5 cm) and a directivity of 27 dB (95% CI 25.2–28.5 dB) (Fig. 5, Table 1). Source parameters are presented together (Table 1) and also split by observation period (Table S1), to address that a visual confirmation of species ID only existed in period A.

Ranges to on-axis clicks recorded in the harbour averaged 9±7 m (Table 1). A representative click shows that clicks are shorter and contain fewer cycles that the typical click from deep-water recordings (Fig. 1). Spectra of the clicks were also highly stereotyped, with a pronounced shoulder peak frequency at 156 kHz (Fig. 3). The modal ICI (37 ms) was lower than for the deep recordings (Table 1, Fig. 4). Echolocation click trains, closing with buzzes with ICIs as low as 4 ms, were also observed (Fig. 6). Note the varying peak frequency of clicks as the *Kogia* scanned across the recorder (Fig. 6).

In both recording settings, ambient noise in the TOL band (centred at 128 kHz) overlapping with the peak frequency of *Kogia* clicks, was immeasurably quiet, with the 50th percentiles of ambient noise equivalent to the noise floor of the instrument (at ~70–75 dB re. 1 µPa, RMS per third octave band) at frequencies >40 kHz (Fig. S2).

DISCUSSION

While the biosonar parameters and echolocation behaviour of most toothed whales, as for bats, conform to scaling predictions from size and broadscale niche segregation (Schnitzler and Kalko, 2001; Jensen et al., 2018), some toothed whales deviate from that general pattern. Here, we investigated one of the prime examples of that, *Kogia*, which are fairly small, yet deep-diving toothed whales that find their deep-sea food by using a high-frequency biosonar system. By using NBHF clicks, half of the power of their biosonar is lost to absorption in <40 m of target range, so how can these cryptic animals find their mesopelagic prey? In this study, we sought to address that question by quantifying the source parameters of *Kogia* echolocation clicks to test the hypotheses that their NBHF clicks are: (i) highly directional; (ii) emitted with long ICIs indicative of relatively longer prey search ranges; and (iii) of a higher SL than shallow diving NBHF species to compensate for the considerable absorption losses of their NBHF clicks.

Directivity

The NBHF clicks of *Kogia* were hypothesized to have a high DI and correspondingly narrow half-power beamwidth, as a result of the short wavelengths of their clicks and the larger aperture of their sound-producing apparatus in their head compared with other NBHF species (Fig. 5). Directionality increases with click frequency and aperture size (Urick, 1983; Madsen and Wahlberg, 2007), and the DI can, for a flat piston, be predicted from $20\log_{10}(ka)$, where ka is the wavenumber: $2\pi\text{radius}/\lambda$. The *Kogia* melon measures ~15 cm in diameter (Clarke, 2003; McKenna et al., 2012), which is roughly twice that of a harbour porpoise (Fig. 5), which produces clicks with similar peak frequency and has a DI of 22–25 dB (Au et al., 1999; Koblitz et al., 2012; Kyhn et al., 2013; Macaulay et al., 2020), suggesting that the DI of *Kogia* should be 6 dB higher. Our piston fitting suggests a DI of 27 dB for the equivalent flat piston aperture diameter of 8.4 cm (Fig. 5). The composite and presumed symmetric beam pattern, with a half-power (−3 dB) beamwidth of 8.8 deg (Fig. 5, Table 1), thus supports our hypothesis of higher directionality than harbour porpoises (at ~11–13 deg; Koblitz et al., 2012) and other small NBHF species (Jensen et al., 2018), but is not as high as the 28–31 dB predicted from the wavenumber. Our prediction of a higher DI for *Kogia* than for most odontocetes, based on the simple prediction concerning the ratio between the short dominant

Journal of Experimental Biology (2021) 224, jeb240689. doi:10.1242/jeb.240689

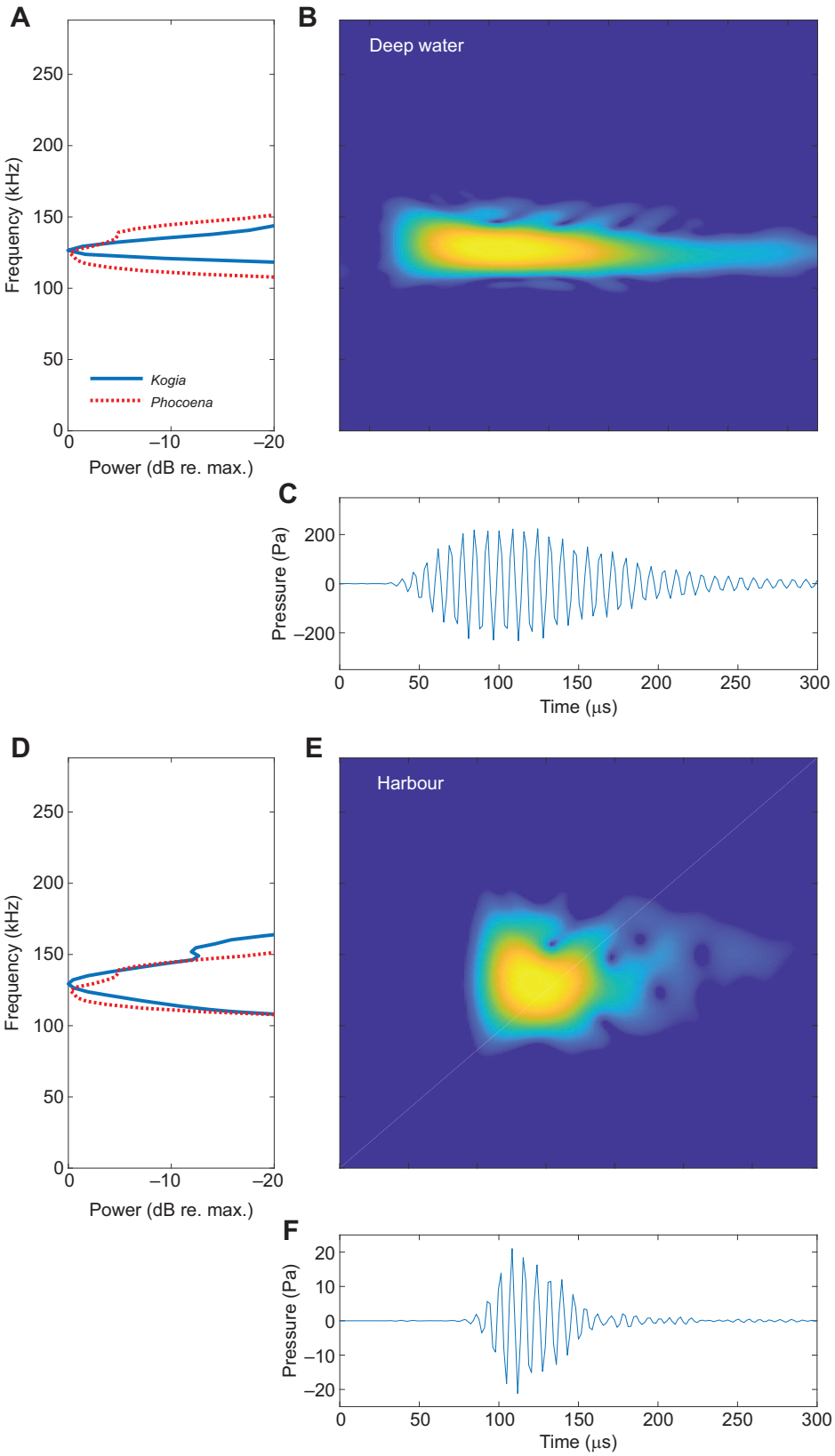

Fig. 1. Representative *Kogia sima* clicks from both recording environments. (A,D) Spectrum, (B,E) spectrogram, and (C,F) source level (SL) of waveform of representative *K. sima* click from deep water (Bahamas, left) and shallow harbour (Cape Town, South Africa, right) recordings (sampling at 576 kHz, FFT size of 2048 for a frequency resolution of 281 Hz). An average normalized spectrum of 65 on-axis harbour porpoise (*Phocoena phocoena*) clicks (from Macaulay et al., 2020, courtesy of J. Macaulay) is superimposed on A and D.

wavelength and larger head size (*sensu* Au et al., 1999), is therefore not supported by the composite beam pattern (Fig. 6). However, the composite DI of 27 dB matches well with the mean observed across toothed whales, lending support to the notion of a remarkable convergence on click directionality across echolocating toothed whales (Jensen et al., 2018), with smaller odontocetes producing

Journal of Experimental Biology (2021) 224, jeb240689. doi:10.1242/jeb.240689

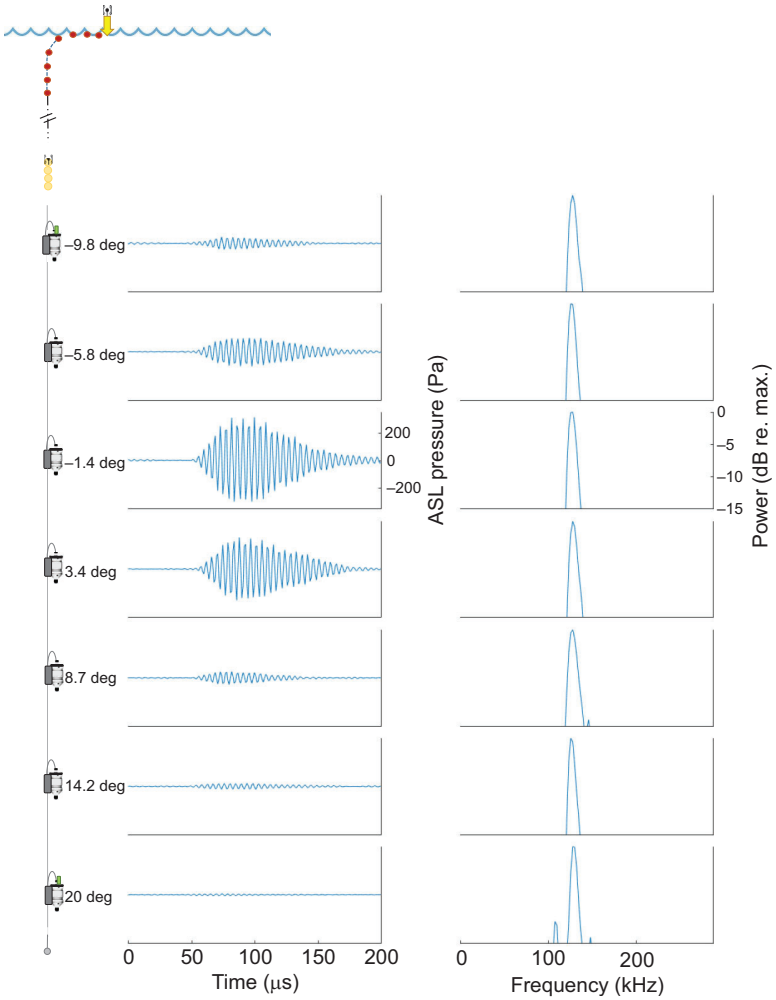

Fig. 2. Sample *K. sima* click recorded on all channels of the vertical hydrophone array. Waveform [apparent source level (ASL) pressure] and normalized power spectra of a representative on-axis *Kogia* click detected on all array elements. The angle indicates where the localization was relative to where the biosonar beam was pointing along the array.

clicks with higher frequencies to achieve the same acoustic field of view. The directional biosonar beam provides a narrow acoustic field of view, allowing for higher SLs and greater on-axis detection range, while facilitating the reduction of acoustic clutter through spatial filtering of off-axis echoes (Au, 1993; Moss and Surlykke, 2001; Jensen et al., 2018).

Despite *Kogia*'s larger head than other NBHF species, the surface through which sound exits the *Kogia* forehead over the melon (the 'oval face') is relatively narrow and flat (Goold and Clarke, 2000), and is comparable with the size of the derived equivalent piston radius (Fig. 5, Table 1; Clarke, 2003). Thus, it may be speculated that the anteriorly tapered melon of the *Kogia*, which is much narrower than the head itself (Fig. 5, inset), may have evolved to form an average acoustic field of view of around 9 deg to offer a balance between clutter rejection and acoustic field of view, as in most other toothed whales (Jensen et al., 2018). Some data points, however, in the radiation pattern of Fig. 5, imply that some *Kogia* NBHF clicks have a half-power beamwidth that is about half or double the mean (of 8.8 deg), suggesting that *Kogia*, similar to porpoises (Wisniewska et al., 2015), can potentially change the width of their sonar beam by changing the effective radiating aperture. Such adjustments are in addition to the demonstrated flexibility in click bandwidth observed in the shallow and deep-water recordings (Figs 1 and 2, Table 1). The complex sound-producing nasal structures of *Kogia*, with a single large phonic lip pair, intricately shaped air sacs, and a spermaceti organ preceding the melon (Clarke, 2003; Bloodworth and Odell, 2008; McKenna et al., 2012; Thornton et al., 2015), certainly offer the biomechanical potential for such changes in the degree of collimation (e.g. Au et al., 2006), as well as the possibility of the *Kogia* beam being asymmetric. Additionally, because the *Kogia* skull is canted downward (McKenna et al., 2012), it is possible that the beam is transmitted in a downwards direction, as has been found for biosonar beams radiating from Risso's dolphins (Philips et al., 2003). These hypotheses can potentially be tested on *Kogia* in rehabilitation to further our understanding of beam angles and biosonar-guided functional feeding morphology.

ICIs and inferred inspection ranges

Echolocators generally wait for the return of echoes of interest prior to emitting the next click, and ICI can therefore serve as a proxy for the maximum range an echolocating animal is expecting echoes of interest, the so-called inspection range (e.g. Au et al., 1974; Kadane and Penner, 1983; Akamatsu et al., 2005). From their deep-water food niche, we predicted *Kogia* would use ICIs longer than those of other NBHF toothed whales, to reflect longer-range biosonar-mediated foraging and navigation in the open ocean. The harbour porpoise, for example, has, on average, ICIs between 40 and 60 ms in the search phase of biosonar-based hunting (Villadsgaard et al., 2007; Verfuß et al., 2009; Fig. 4C). With a median ICI of 228 ms in

Journal of Experimental Biology (2021) 224, jeb240689. doi:10.1242/jeb.240689

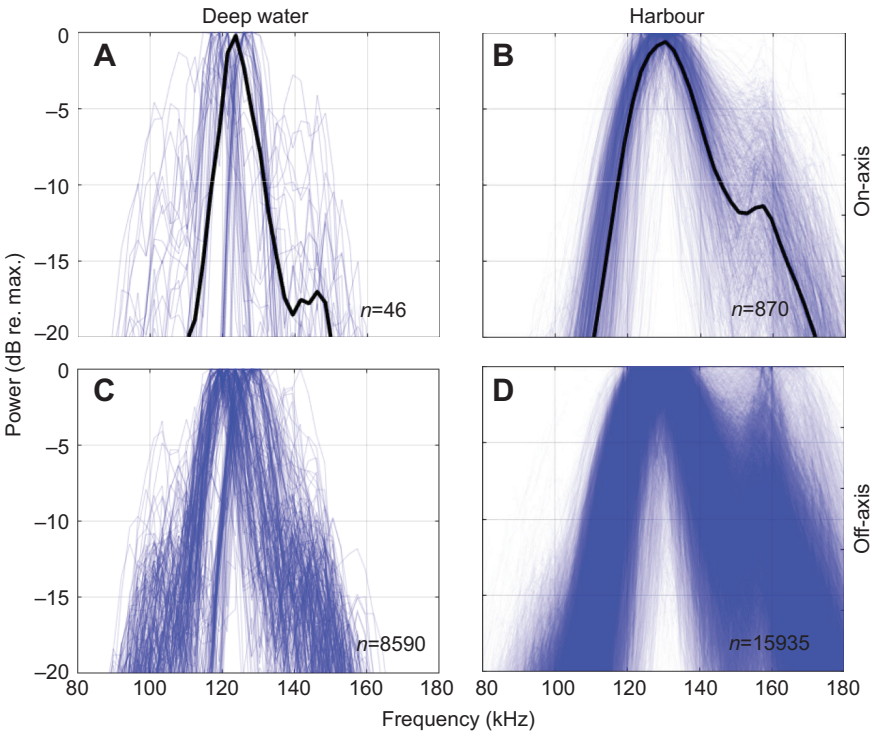

Fig. 3. Spectra of *K. sima* clicks. Clicks are shown from array recordings in the Bahamas (A,C) and single-channel recordings from Cape Town harbour, South Africa (B,D), separated into on-axis (A,B) and off-axis (C,D) clicks. Average spectra are shown as a black line for on-axis clicks.

deep water (Table 1, Fig. 4A), our data are consistent with the hypothesis that *Kogia* employ a longer inspection range (Fig. 4). The majority of *Kogia* ICIs in deep water are about 3–4 times longer than those of NBHF species in shallow water, including *Kogia* in shallow water (Fig. 4B), harbour porpoises (Fig. 4C) and *Cephalorhynchus* (Leeney et al., 2011), suggesting an inspection range that is ∼150 m longer. Alternatively, the long ICIs may be an upper bound on the time after each click at which reverberation from multiple scatters, on average, has faded enough to avoid interfering with the next click–echo pair and cause range ambiguity problems. Other deep-diving toothed whales, such as beaked whales, sperm whales and Risso's dolphins, also have long ICIs that suggest the perceptual organization of a long-range, complex multi-target environment is aided by avoiding range ambiguity (Madsen et al., 2005b, 2013; Fais et al., 2016; Jensen et al., 2020).

However, the long ICIs in *Kogia* are not hard-wired: the relatively long median ICI of >200 ms is over twice the ICI of *Kogia* observed by PAM in deep-water environments (e.g. Merkens et al., 2018; Merkens and Oleson, 2018; Hodge et al., 2018; Hildebrand et al., 2019). Note that the secondary peak in the ICI histogram (Fig. 4A) at ∼125 ms corresponds with ICIs from free-ranging *Kogia sima* reported by Merkens et al. (2018). Additionally, the harbour recordings demonstrate that this deep-water species, like other NBHF species (Ladegaard and Madsen, 2019) and bats (Surlykke and Moss, 2000), can adjust its biosonar behaviour to the conditions of the habitat, by emitting clicks with shorter ICIs in keeping with likely shorter ranges of inspection (Fig. 4). Shallow-water recordings in the harbour had ICIs comparable to those of porpoises (mode of 38 ms; Table 1, Fig. 4), indicating a maximum biosonar inspection range of ∼30 m. Furthermore, the ICIs of the *Kogia sima* recorded in the shallow harbour (51±34 ms; Table 1) overlap with the ICIs from a *Kogia breviceps* recorded in a shallow, concrete pool (40–70 ms; Madsen et al., 2005a). These are probably habitat-related adjustments in overall acoustic gaze.

Such adjustments in ICI and inspection range take their most extreme form in the buzz, where clicks with short ICIs serve the apparently ubiquitous role among toothed whales of providing high-resolution biosonar updates of a small auditory scene during the final phases of prey target interception (Madsen and Surlykke, 2013). Buzzes have not previously been reported for *Kogia*, with a lowest reported ICI of 25 ms (Merkens et al., 2018) exceeding the ICIs used for defining buzzing of ∼<15 ms for porpoise (DeRuiter et al., 2009; Wisniewska et al., 2014). It therefore begged the question of whether *Kogia* buzz at all, or whether they have simply not been recorded because of the weaker buzz click SLs. While no buzzes were recorded on the deep-water array recordings, with lowest ICIs of 23 ms (Table 1), the harbour recordings contained some echolocation buzzes during close range encounters, using the same sound recorder as the deep-water recordings, with ICIs as low as 4 ms (Table 1, Fig. 6). This buzzing click rate is comparable to those reported in porpoises (Wisniewska et al., 2012; DeRuiter et al., 2009) and dolphins (Wisniewska et al., 2014; Ladegaard et al., 2015; Martin et al., 2018). The pattern of buzzing initiated at a range of around 1–2 body lengths from a prey item appears consistent across a broad range of sizes of toothed whales, from large sperm whales (Fais et al., 2016; Tønnesen et al., 2020) and Blainville's beaked whales (Johnson et al., 2008) to porpoises (Wisniewska et al., 2012), and appears to be in agreement with the buzzing *Kogia sima* presented here. These 'hand-off distances' – from an approach phase to a buzzing interception phase – seem, along with maximum clicks rates, to be scaled with the whale's size and manoeuvrability (Madsen et al., 2013). Interestingly, the single phonic lip pair of the *Kogia* is large (1.8–3.8 cm; Thornton et al., 2015) compared with that of a harbour porpoise (0.8–1.3 cm; Huggenberger et al., 2009), and yet they can support fast click rates (Fig. 5, Table 1) of similar NBHF clicks (Fig. 1), highlighting both the difficulty of inferring acoustic outputs from anatomy and that much remains to be understood regarding the biomechanical details of pneumatic sound production in odontocetes.

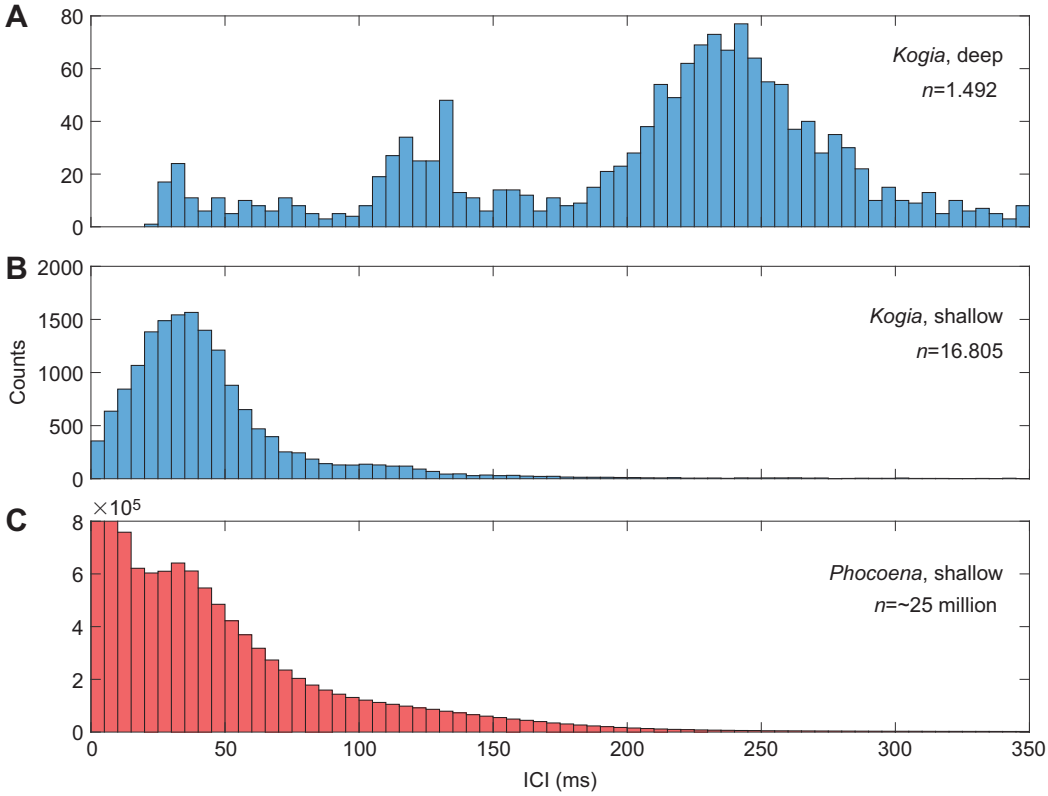

Fig. 4. Inter-click interval comparison. Inter-click intervals (ICIs; 5 ms bins) of narrow-band high-frequency (NBHF) toothed whales, as derived from on- and off-axis recordings of clicks. (A) *Kogia sima* recorded in deep water, Bahamas. (B) *Kogia sima* recorded in the shallow harbour, South Africa. (C) Data from 19 *P. phocoena* sound-and-movement tag recordings in shallow coastal Danish waters (courtesy of L. Rojano-Doñate). Note that *y*-axis is zoomed in to highlight non-buzz ICIs.

Source level and biosonar detection ranges

From the consistent observations of deep-water prey in the stomachs of *Kogia*, we hypothesized, like Kyhn et al. (2010), that *Kogia* hunting in the deep should produce higher SLs than shallow-water NBHF species to facilitate prey detection in their vast 3-dimensional foraging habitats. This notion is supported by their significantly longer ICIs than shallow-water NBHF species. Additionally, body size scaling with SL in toothed whales (Jensen et al., 2018) predicts that *Kogia*, with body sizes similar to those of bottlenose dolphins, should be able to produce SLs of more than 220 dB re. 1 μPa_{pp} (Au et al., 1974). However, the *Kogia* clicks we recorded in the open ocean environment have a mean SL of 186±6 dB re. 1 μPa_{pp} at 1 m and a maximum of 197 dB re. 1 μPa_{pp} at 1 m (Table 1). So, in contrast to our predictions and hypothesis, the moderate SLs reported here overlap with the SLs of clicks produced by harbour porpoises in shallow waters, with reported mean SL of ∼189–191 dB re. 1 μPa_{pp} at 1 m (Villadsgaard et al., 2007; Kyhn et al., 2013; Macaulay, 2020). These results are also at odds with the assumptions of Hildebrand et al. (2019), who used SL estimates of 212±5 dB re. 1 μPa_{pp} at 1 m to simulate acoustic density estimation of *Kogia*.

It may well be, of course, that we have not captured to the full capability of source outputs from *Kogia* and that they, in some contexts, use higher SLs than recorded here. Such flexibility is exemplified by our finding that the median SL of clicks emitted in the open environment was 28 dB greater than the median SL of those emitted in the harbour (Table 1). In deep water, the *Kogia* clicks were only recorded during two array deployments when the maximum hydrophone depth was ∼95 m, and during these periods, *Kogia* were localized to a maximum depth of 392 m (Table 1). As *Kogia* are thought to dive deeper than this, and have been recorded on PAM instruments at depths of ∼1000 m (Hodge et al., 2018), it is possible that higher SLs are instead employed at greater depths than those we recorded at, or when descending towards the prey layer, during which a vertical array may not receive powerful on-axis clicks. While the majority (69%) of our sampling effort was when the deepest channel on the array was at ∼300 m, no *Kogia* clicks were recorded on any of these deeper deployments, so perhaps our deployments were not deep enough, or our sampling effort of nearly 75 h was not enough to capture the full SL dynamic range. However, smaller datasets from similar-sized delphinids in oceanic waters consistently return SL estimates between 200 and 220 dB re. 1 μPa_{pp} at 1 m (e.g. Au et al., 1974; Au and Herzing, 2003; Madsen et al., 2004), much higher than those found here, in turn suggesting that perhaps these low SLs indeed are representative.

So what are the prey detection implications of the moderate SLs documented here? Because the NBHF *Kogia* clicks have durations of ∼100–200 µs in deep water (Table 1), they carry some 10 dB more energy for the same peak pressure compared with the short, broadband clicks of many delphinids and river dolphins, and 2–4 dB more energy than typical NBHF clicks of porpoises and dolphins of the *Cephalorhynchus* genus (Kyhn et al., 2009; 2010; Jensen et al., 2018). As the ear operates as an energy detector with a short integration time of around 260 µs in small toothed whales (Vel'min and Dubrovsky, 1975; Moore et al., 1984; Au et al., 1988; Supin and Popov, 1995), the appropriate measure for comparatively

Journal of Experimental Biology (2021) 224, jeb240689. doi:10.1242/jeb.240689

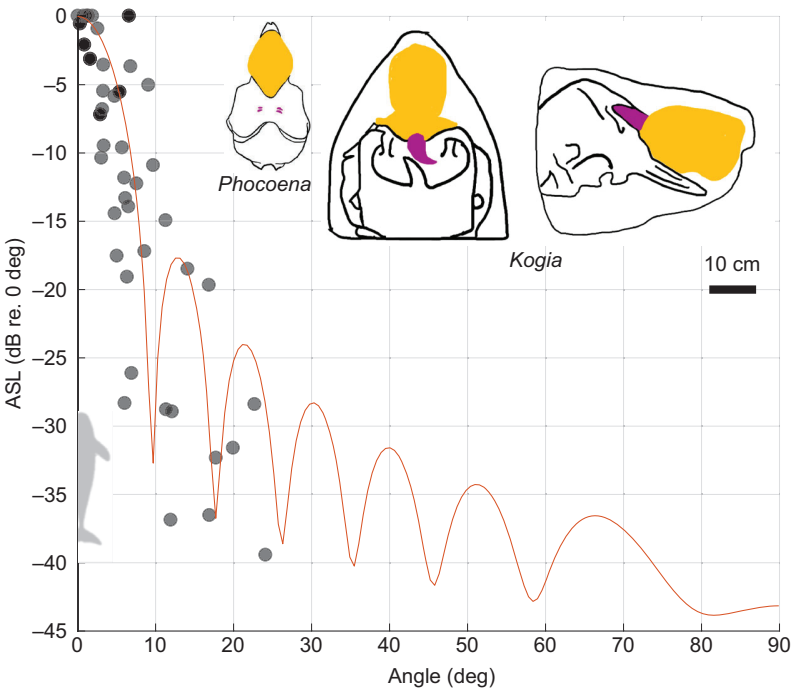

Fig. 5. Beam pattern of on-axis *K. sima* clicks. The line shows the theoretical beam pattern of a 8.4 cm diameter piston transmitting a *Kogia* click, and the dots show the ASL (relative to 0 deg) as a function of receiving angle of incidence for on-axis clicks (*n*=21), with each click contributing at least 3 points. The dots are partially transparent to emphasize that many clicks have half-power beamwidths narrower than the reported overall half-power beamwidth of 8.8 deg. Superimposed images of *Kogia breviceps* melon (adapted from McKenna et al., 2012) and *P. phocoena* melon (adapted from Huggenberger et al., 2009) are inset to emphasize differences in skull and melon sizes between *Kogia* and the harbour porpoise; yellow shows the melon and magenta shows the bursae/spermaceti organ complexes.

evaluating prey detection performance in *Kogia* is therefore not pp pressure, but rather the EFD (Au, 1993) of the returning echo. Target detection experiments with porpoises (Kastelein et al., 1999; Au et al., 2007) have not provided clear measures of detection threshold (DT) as performance as a function of measured SLs in target detection experiments was not logged. Therefore, we shall assume the DT of ∼33 dB re. 1 μPa^2 s, as measured for *Tursiops* during an unmasked detection experiment (Au et al., 2002). If we assume that threshold is valid for *Kogia* also, and assume a target strength (TS) range of ∼−35 to −45 dB of myctophid and cephalopod prey (Benoit-Bird and Au, 2001) typical of *Kogia*, we can, by using the sonar equation (Eqn 1), estimate the range over which they may be able to detect such prey under low-noise, clutter-free conditions with a median SL_{EFD} of 134 dB re. 1 μPa^2 s (Table 1):

$$DT = SL - 2TL + TS. \quad (1)$$

By inserting the relevant numbers (*sensu* Madsen et al., 2007), we find that a *Kogia*, in this scenario, will have ∼56–66 dB available for two-way TL which, under the assumption of spherical spreading and absorption at 125 kHz, corresponds to a maximum detection range of about ∼23–38 m. That TL number will increase to ∼69–79 dB, or some ∼43–68 m of target range if we use the highest measured SL_{EFD} of 147 dB re. 1 μPa^2 s.

It may well be that *Kogia* have evolved lower detection thresholds than dolphins, owing to their echolocation in a narrow high-frequency bandwidth down to a median of 2 kHz (BW_{RMS}, Table 1) under very low noise levels in the deep sea. We could not reliably measure third octave noise levels at the centre frequency of *Kogia* clicks in the recording habitats because they were consistently below the low self-noise of the SoundTrap recorders (Fig. S2). So, in the absence of actual numbers, we can only say that *Kogia* echolocate under very low noise conditions, perhaps approximated by the Wenz curve minima (Wenz, 1962) in a narrow bandwidth around 125 kHz. If indeed their DT has been shaped evolutionarily by the lowest ambient noise levels over the click, their DT may be the lowest for any odontocete, including dolphins and porpoises. We propose this by considering two potential sources of gain on the reception side of the biosonar feedback loop: a narrower bandwidth of their click than porpoises, and a narrower receiving DI. Firstly, a mean RMS bandwidth of 2–3 kHz (Table 1) is the narrowest bandwidth of any toothed whale echolocation click on record, 2–3 times narrower than for clicks of other NBHF species, and about 10 times narrower than the clicks of bottlenose dolphins. This reduction in bandwidth could potentially be driving the DT estimate for *Kogia* down by 3–4.5 dB compared with that of a porpoise (Au et al., 2007) and by 10 dB compared with that of a dolphin (Au, 1993), as calculated by $10\log_{10}$(factor of bandwidth reduction), if matched in narrowness by the auditory filters. Secondly, because the sound-receiving pan bones of the lower jaws in *Kogia*, acting as outer ears, are separated by twice the distance of the pan bones of a porpoise, the ambient noise-suppressing receiving DI is, all other things being equal, expected to be ∼6 dB better than for a porpoise (of ∼12 dB; Kastelein et al., 2005), and comparable to that of a bottlenose dolphin (of ∼18 dB; Au and Moore, 1984) (as calculated by $20\log_{10}2$). Combining these two potential noise suppressors, the DT of *Kogia* could be ∼10 dB lower than that of a dolphin, so that it is instead ∼23 dB re. 1 μPa^2 s. Thus, on purely physical grounds, it may be speculated that the DT of a *Kogia* is the lowest among all toothed whales. When assuming this and using, for example, the high SL_{pp} expected by Hildebrand et al. (2019) of 212 dB re. 1 μPa_{pp} at 1 m, corresponding to a SL_{EFD} of ∼163 dB re. 1 μPa^2 s, there is still, under these very ideal and probably unrealistic scenarios, ∼100 dB available for two-way TL, corresponding to a ∼155 m target range. Thus, our hypothesis that *Kogia* use high SLs for long-range echolocation of single prey is only tenuously supported: even under the best of scenarios, it is unlikely that *Kogia* detect their preferred prey at the ranges of 150 to 200 m inferred from their long ICIs, but are more likely to employ detection ranges in the tens of metres, on a par with other NBHF species. However, the long ICIs at moderate SLs will allow *Kogia* to

Journal of Experimental Biology (2021) 224, jeb240689. doi:10.1242/jeb.240689

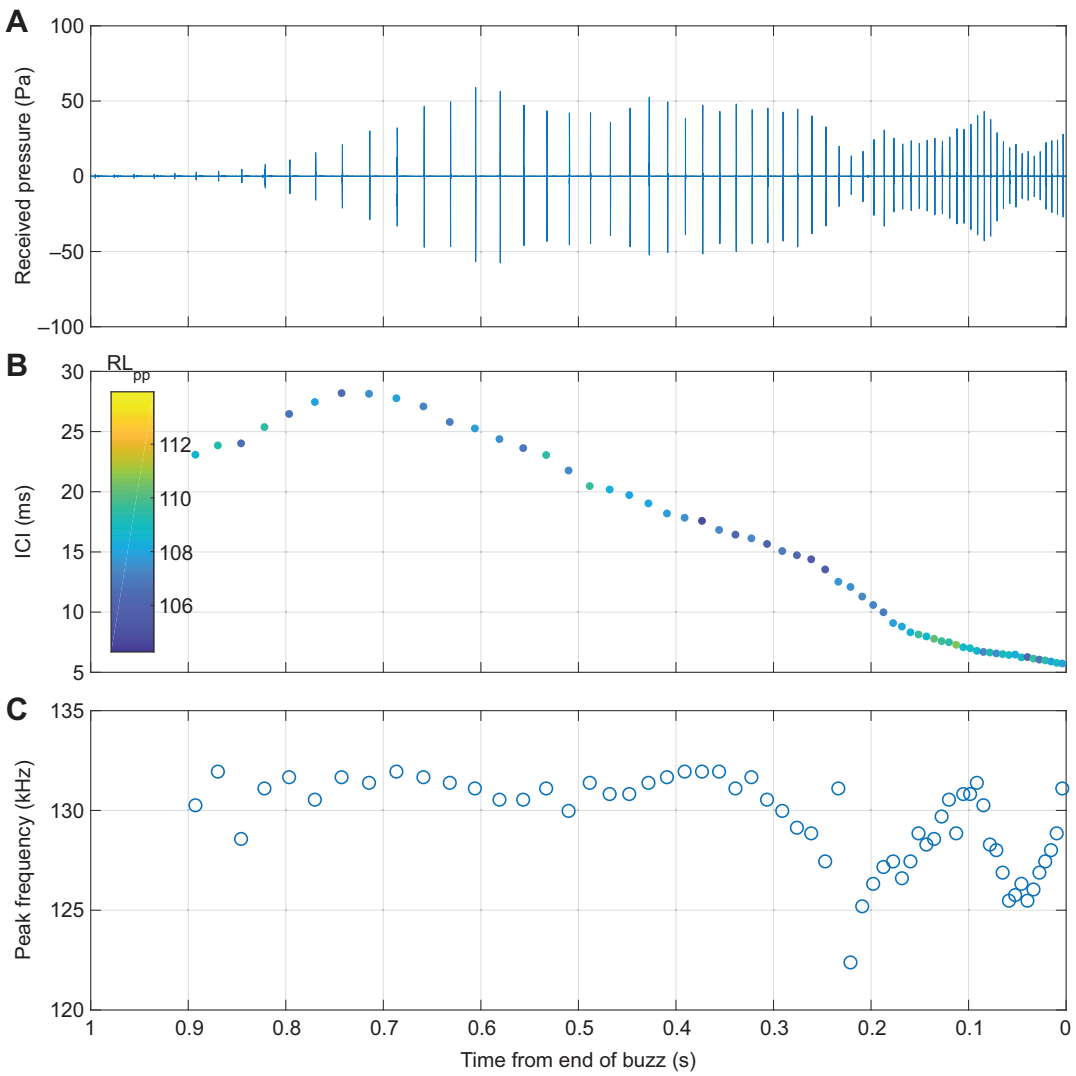

Fig. 6. *Kogia sima* buzz example. (A) Waveform, (B) ICI coloured by peak-to-peak received level (RL_{pp}) and (C) peak frequency displays of an example echolocation sequence ending with a buzz (down to 5.7 ms in this example), from a *K. sima* at a range of 9 m, from the single-channel, close-range harbour recording.

locate the deep scattering layer with volume scattering properties that allow for detection at much longer ranges than its single constituents (Wiebe et al., 1990). Further, in the deep scattering layer, many organisms are schooling (Madsen et al., 2013; Johnson et al., 2008; Benoit-Bird et al., 2017). In concert, these offer the means for a combined higher TS at long ranges, or, if prey schools are large enough relative to ensonification range, will also act as volume scatterers to enable detection ranges in keeping with the long *Kogia* ICIs.

A similar decoupling between long inferred inspection ranges from ICI and moderate calculated biosonar detection ranges of single prey is seen in Blainville's beaked whales, which are proposed to maintain a broad auditory scene via clicking at a low rate (Johnson et al., 2006, 2008). It may thus similarly be speculated that *Kogia* use long ICIs to facilitate auditory streaming of the complex auditory scene generated by a densely packed prey layer in the deep scattering layer, so that most echoes are allowed to return before emission of the next click to avoid range ambiguity problems. Indeed, the complexity of interpreting the acoustic scene of a scattering layer is acknowledged by how difficult it is for echosounders to register individual animals when echo density is high (Madsen et al., 2005b; Benoit-Bird, 2014).

Benthic species and cephalopods that undergo diel migrations have been found in the stomachs of stranded *Kogia*, with a diet that is largely composed of prey inhabiting the epipelagic (0–200 m) and mesopelagic (~200–1000 m) zones (Plön, 2004; Beatson, 2007). The two species of *Kogia* are understood to have similar foraging ecologies and occupy similar trophic niches (Staudinger et al., 2014). It is therefore plausible that *Kogia* – contrary to their large relative the sperm whale, which has a long-range biosonar – generally forage in slope habitats where they can reliably expect to encounter prey by diving down and then use a short-range biosonar with moderate SLs to hunt once in the prey layer. This notion is reinforced by *Kogia* being a relatively small odontocete and therefore physiologically constrained to shorter duration dives, as has been observed with maximum dive durations around 18–25 min (Breese and Tershy, 1993; Willis and Baird, 1998; Scott et al., 2001). If they are hunting at depth in a narrow time frame, they must

be efficient at doing so, and a predictable prey niche would facilitate this, perhaps limiting the habitats that will support *Kogia*.

Arranz et al. (2011) suggested that as Blainville's beaked whales only start echolocating once they are in a deep scattering layer, there is probably reliability in exploiting prey in that strata. Thus, the predictability in the depth of deep scattering layers (as a function of daylight) allows for a hunting strategy involving low SL echolocation. In the same location south of Abaco Island, Bahamas, where our array was deployed, the surface and deep scattering layers have been investigated using a combination of net tows and active acoustics. Here, intense surface and diffuse deep scattering layers were identified at depths of ∼120 and ∼540 m, respectively, during the daytime, becoming more intense and migrating shallower at night (Sato and Benoit-Bird, 2017). Our sampling location has been identified as a high-quality foraging habitat for odontocetes, with high density in mesopelagic scattering layers at ∼150 and ∼700–800 m (Benoit-Bird et al., 2020). Thus, the depths of both our array and the majority of our *Kogia* localizations (Table 1) overlap with scattering layers at this location, supporting our hypothesis that they are foraging in acoustically cluttered prey layers.

Why are *Kogia* clicks so narrowband?

The NBHF click, which convergently evolved in the Phocoenidae, and in the genera *Kogia* and *Cephalorhynchus*, and some dolphins in *Lagenorhynchus* (Kyhn et al., 2009, 2010, 2013; Götz et al., 2010; Reyes Reyes et al., 2016; Bassett et al., 2009; Griffiths et al., 2020), has been hypothesized to have evolved as an adaptation both to take advantage of low ambient noise levels in the ocean at these frequencies and to reduce acoustic detectability by predators (Møhl and Andersen, 1973; Andersen and Amundin, 1976; Madsen et al., 2005a; Morisaka and Connor, 2007; Kyhn et al., 2013). While predatory killer whales (and perhaps also extinct raptorial sperm whales; Galatius et al., 2019) may still be able to hear porpoise clicks, their hearing is much less sensitive at >100 kHz (Hall and Johnson, 1972; Szymanski et al., 1999; Branstetter et al., 2017). If correct, such acoustic crypsis comes at the cost of high levels of frequency-dependent absorption and hence inherently low sonar ranges. Here, we have shown that *Kogia* address the challenge of echolocating to find prey in the deep while possibly evading acoustic detection by predators by producing clicks with a high DI, narrow frequency bandwidth, moderate SL and surprisingly long ICIs. Our observation that *Kogia* click near the surface when in deep-water environments, and that all clicks were >100 kHz (Table 1), is consistent with the acoustic crypsis hypothesis. Beaked whales, in contrast, emit lower-frequency clicks audible to killer whales, avoid clicking in depths shallower than 300 m, and surface in silence well away from where their last clicks were made (Aguilar de Soto et al., 2020). Thus, *Kogia* seem to navigate 'soundscapes of fear' differently from beaked whales, enabling them to vocalize more safely in shallower depths. The production of lower-frequency clicks by NBHF-producing Heaviside's dolphins in a conspecific communication context emphasizes the trade-off in communication range versus acoustic detection by predators (Martin et al., 2018). Predation by killer whales in the same location in which our array recordings were made (Dunphy-Daly et al., 2008; Dunn and Claridge, 2014) highlights that predation risks posed by killer whales are real and supports the notion of predation as a driver of acoustic crypsis. Even in light of updated killer whale audiograms (Branstetter et al., 2017), acoustic crypsis of *Kogia* clicks is still provided spatially via absorption, if not spectrally via overlap with a predator's auditory sensitivity.

Another notion to entertain, given their long click duration and extremely narrow bandwidth, is whether the *Kogia* biosonar system is sensitive to and makes use of Doppler shifts in the echoes of moving prey to facilitate acoustic localization, as is the case for some bats (Schnitzler, 1973). However, given the 4.5 times greater sound speed in water than in air, combined with the high frequency of *Kogia* clicks, a reasonable escape speed of a prey item of ∼1.5 m s^{-1} would yield a Doppler shift of only ∼250 Hz, which is very small given the 2–10 kHz bandwidth of their clicks (Table 1) and the 10 kHz variation in the centre frequency, leading us to conclude that echolocation using NBHF clicks is insensitive to realistic Doppler shifts (*sensu* Madsen et al., 2005a). With the long click duration comes a narrower bandwidth, and while this provides poorer range resolution than would a broadband click (Møhl and Andersen, 1973), target detection capabilities improve because the echo energy arrives in a narrower frequency band with less noise compared with the same energy distributed over a broader band (Madsen et al., 2005a). Given the highly selective foraging behaviour documented for Blainville's beaked whales (Madsen et al., 2005b; Arranz et al., 2011), it also remains an open question of how *Kogia* may perform target discrimination with a narrow-band click carrying less information about target properties than a broadband click.

Furthermore, we argue that a click of extremely narrow bandwidth would evolve in parallel with an equally narrow auditory filter matched with the high Q of their signal (mean of 56; Table 1, Figs 1 and 3). Indeed, if the auditory filter is wider in bandwidth, noise in frequencies outside the click bandwidth will contribute unnecessary masking effects. Additionally, the frequency range of the most sensitive hearing in odontocetes is generally around the average frequency of the echolocation signals (Kastelein et al., 2002), so an auditory filter matched in bandwidth to the resonant quality factor of clicks gives the best trade-off between time and frequency resolutions of the returning echoes. The hypothesis of a narrow auditory filter in *Kogia*, proposed by Madsen et al. (2005a), is consistent with anatomical inference of ganglion density in the cochlea located in the NBHF frequency region in *Phocoena* (Ketten, 2000), and by auditory brainstem evoked potential studies (Ridgway and Carder, 2001). This hypothesis could be tested by measuring the *Kogia* acoustic fovea and critical bandwidth on an animal in rehabilitation using non-invasive evoked potential techniques.

Applied implications

Here, the click parameter quantification from close-range and species-identified *Kogia* contributes to a growing body of PAM literature on this genus. Our findings on the relative stereotypy of their clicks make them a good candidate for PAM to study their presence, distribution, density and relative abundance (Hildebrand et al., 2019). Effective PAM relies on species-specific bioacoustic quantifications for classification (Zimmer, 2011; Baumann-Pickering et al., 2013) and is a critical first step for management recommendations and conservation. Confidence in acoustic ID is becoming increasingly relevant for automated processing as PAM equipment becomes cheaper and more accessible, as high-bandwidth and longer-term datasets become more common, and as acoustic monitoring methods become more autonomous (e.g. Gkikopoulou, 2018). Our quantifications are potentially useful for acoustically discriminating between *Kogia* species, which broadly overlap in distribution and are currently considered acoustically indistinguishable (Merkens et al., 2018), and for discriminating them from other, sometimes sympatric, NBHF species (see Griffiths et al., 2020). Source parameters and the beam pattern have recently

been used to estimate acoustic detection probabilities and inform density estimation in long-term datasets (Frasier et al., 2016; Hildebrand et al., 2019).

Given the high absorption (~40 dB/km) of NBHF clicks, the median ASL from the array recordings of 186 dB re. 1 μPa_{pp} at 1 m (Table 1), and assuming a typical modest detection threshold of 110 dB re. 1 μPa_{pp}, we calculate a maximum passive acoustic detection range of ~450 m. Even at the highest recorded ASL (of 197 dB re. 1 μPa_{pp} at 1 m), the maximum range at which a *Kogia* click exceeds the acoustic detection threshold is only ~750 m. Thus, while it has been noted that *Kogia* presence is underestimated in visual surveys (Barlow, 1999; Hodge et al., 2018), their presence could also be underestimated in PAM surveys if the acoustic detection probability (g0) assumes a greater SL, and as they are only detectable at ranges of less than 1 km, even under ideal conditions.

A handful of clicks with lower peak frequencies (<120 kHz) were observed here in both datasets (Fig. 3). Similar variations in *Kogia* peak frequency have been observed by others (Merkens et al., 2018; Merkens and Oleson, 2018; Hildebrand et al., 2019; Griffiths et al., 2020). Indeed, there is similar variation of ~12 kHz in the F_p of harbour porpoise clicks (Kyhn et al., 2013). Varying F_p has been found within *Kogia* click train events (Merkens et al., 2018; Griffiths et al., 2020), and is similarly shown here with F_p variation coinciding with RL variation (Fig. 6). As period B of the array recordings had no visual observation of any odontocete, it could have instead recorded the sounds of *Kogia breviceps* (Cardona-Maldonado and Mignucci-Giannoni, 1999; Dunn and Claridge, 2014), which is less commonly observed in the Bahamas. It is possible that variations in our measurements are due to undescribed acoustic differences between the two species, but similarity across acoustic parameters of on-axis clicks from both periods A and B suggests that the two recordings are from the same species, *Kogia sima* (Table S1).

Conclusion

Here, we have measured the source parameters of NBHF echolocation clicks produced by free-ranging *Kogia* recorded in deep- and shallow-water settings. While such clicks are subject to significant levels of frequency-dependent absorption losses, these whales successfully find their mesopelagic prey by producing clicks that are highly directional and extremely narrowband to hunt in the predictable layers of aggregated prey at depth. Their SLs were lower than expected, but the suggested gains in their auditory detection threshold could partially compensate for the short ranges that their low output levels beget. By comparing clicks produced by the same species in different habitats, we have demonstrated flexibility in their output levels and ICIs, and have suggested flexibility in their beamwidth to offer dynamic sensing tailored to the biosonar tasks at hand.

Acknowledgements

Many thanks to the several researchers who generously lent us their SoundTraps: Jonas Teilmann, Magnus Wahlberg, Natacha Aguilar de Soto and Jakob Tougaard. Thanks to the Zoophysiology workshop at Aarhus University (Niels Kristiansen, John Svane Jensen, Mehran Jahanara and Lasse Vestergaard Sørensen) for preparing trawl floats and designing the 3D-printed moulds used as breakouts in the vertical array. Thanks to Magnus Wahlberg for helpful comments on the initial results, Kristian Beedholm for help with the piston model, and Michael Ladegaard for assistance with click parameterization. Thanks to Jamie Macaulay for providing example on-axis harbour porpoise clicks, and to Laia Rojano-Doñate for providing click data from a dataset of 19 wild, tagged porpoises in Danish waters. Finally, many thanks to the two anonymous reviewers who found the time during a pandemic to provide helpful suggestions on an earlier version of the manuscript.

Competing interests

The authors declare no competing or financial interests.

Author contributions

Conceptualization: C.E.M., P.T.M.; Methodology: C.E.M., P.T.M.; Software: C.E.M.; Validation: C.E.M.; Formal analysis: C.E.M.; Investigation: C.E.M., P.T., C.A.D., D.E.C., T.G., S.H.E., P.T.M.; Resources: C.A.D., D.E.C., T.G., S.H.E., P.T.M.; Data curation: C.E.M.; Writing - original draft: C.E.M., P.T.M.; Writing - review & editing: C.E.M., P.T., C.A.D., D.E.C., T.G., S.H.E., P.T.M.; Visualization: C.E.M.; Supervision: P.T.M.; Project administration: C.E.M., P.T.M.; Funding acquisition: C.E.M., P.T.M.

Funding

PhD and fieldwork funding were provided by the Danmarks Grundforskningsfond (27125 to P.T.M.), the Oticon Fonden (18-0340 to C.E.M.) the Dansk Akustisk Selskab (to C.E.M.), the South Africa National Research Foundation (research career advancement fellowship to S.E.) and the Claude Leon Foundation (postdoctoral fellowship to T.G.).

Data availability

The PAMGuard data analysis software is open source and available at: https://sourceforge.net/p/pamguard/svn/HEAD/tree/PamguardJava/. The compiled software is available at: www.pamguard.org. The dataset of on-axis clicks, used for source parameter quantification, is available from Zenodo to facilitate the training of automated click classifiers: doi.org/10.5281/zenodo.4273697. This includes sound clips of all of the on- and off-axis *Kogia sima* clicks, and calculated localization ranges and off-axis angles.

Supplementary information

Supplementary information available online at
https://jeb.biologists.org/lookup/doi/10.1242/jeb.240689.supplemental

References

Aguilar de Soto, N., Johnson, M. P., Madsen, P. T., Díaz, F., Domínguez, I., Brito, A. and Tyack, P. (2008). Cheetahs of the deep sea: deep foraging sprints in short–finned pilot whales off Tenerife (Canary Islands). *J. Anim. Ecol.* **77**, 936-947. doi:10.1111/j.1365-2656.2008.01393.x

Aguilar de Soto, N., Visser, F., Tyack, P. L., Alcazar, J., Ruxton, G., Arranz, P., Madsen, P. T. and Johnson, M. (2020). Fear of killer whales drives extreme synchrony in deep diving beaked whales. *Sci. Rep.* **10**, 13. doi:10.1038/s41598-019-55911-3

Ainslie, M. A. and McColm, J. G. (1998). A simplified formula for viscous and chemical absorption in sea water. *J. Acoust. Soc. Am.* **103**, 1671-1672. doi:10.1121/1.421258

Akamatsu, T., Wang, D., Wang, K. and Naito, Y. (2005). Biosonar behaviour of free-ranging porpoises. *Proc Roy Soc B* **272**, 797-801. doi:10.1098/rspb.2004.3024

Andersen, S. and Amundin, M. (1976). Possible predator-related adaption of sound production and hearing in the harbour porpoise (Phocoena phocoena). *Aquat. Mamm.* **4**, 56-58.

Arranz, P., Aguilar de Soto, N., Madsen, P. T., Brito, A., Bordes, F. and Johnson, M. P. (2011). Following a foraging fish-finder: diel habitat use of Blainville's beaked whales revealed by echolocation. *PLoS ONE* **6**, e28353. doi:10.1371/journal.pone.0028353

Au, W. W. L. (1993). *The Sonar of Dolphins*. New York, USA: Springer-Verlag.

Au, W. W. L. and Herzing, D. L. (2003). Echolocation signals of wild Atlantic spotted dolphin (*Stenella frontalis*). *J. Acoust. Soc. Am.* **113**, 598-604. doi:10.1121/1.1518980

Au, W. W. L. and Moore, P. W. (1984). Receiving beam patterns and directivity indices of the Atlantic bottlenose dolphin *Tursiops truncatus*. *J. Acoust. Soc. Am.* **75**, 255-262. doi:10.1121/1.390403

Au, W. W. L., Floyd, R. W., Penner, R. H. and Murchison, A. E. (1974). Measurement of echolocation signals of the Atlantic bottlenose dolphin, *Tursiops truncatus* Montagu, in open waters. *J. Acoust. Soc. Am.* **56**, 1280-1290. doi:10.1121/1.1903419

Au, W. W. L., Floyd, R. W. and Haun, J. E. (1978). Propagation of Atlantic bottlenose dolphin echolocation signals. *J. Acoust. Soc. Am.* **64**, 411-422. doi:10.1121/1.382015

Au, W. W. L., Penner, R. H. and Turl, C. W. (1987). Propagation of beluga echolocation signals. *J. Acoust. Soc. Am.* **82**, 807-813. doi:10.1121/1.395278

Au, W. W. L., Moore, P. W. and Pawloski, D. A. (1988). Detection of complex echoes in noise by an echolocating dolphin. *J. Acoust. Soc. Am.* **83**, 662-668. doi:10.1121/1.396161

Au, W. W. L., Kastelein, R. A., Rippe, T. and Schooneman, N. M. (1999). Transmission beam pattern and echolocation signals of a harbor porpoise (*Phocoena phocoena*). *J. Acoust. Soc. Am.* **106**, 3699-3705. doi:10.1121/1.428221

Au, W. W. L., Lemonds, D. W., Vlachos, S., Nachtigall, P. E. and Roitblat, H. L. (2002). Atlantic bottlenose dolphin (*Tursiops truncatus*) hearing threshold for brief broadband signals. *J. Comp. Psych.* **116**, 151-157. doi:10.1037/0735-7036.116.2.151

Au, W. W. L., Kastelein, R. A., Benoit-Bird, K. J., Cranford, T. W. and McKenna, M. F. (2006). Acoustic radiation from the head of echolocating harbor porpoises (*Phocoena phocoena*). *J. Exp. Biol.* **209**, 2726-2733. doi:10.1242/jeb.02306

Au, W. W. L., Benoit-Bird, K. J. and Kastelein, R. A. (2007). Modeling the detection range of fish by echolocating bottlenose dolphins and harbor porpoises. *J. Acoust. Soc. Am.* **121**, 3954-3962. doi:10.1121/1.2734487

Barlow, J. (1999). Trackline detection probability for long-diving whales. In *Marine Mammal Survey and Assessment Methods* (ed. G. W. Garner, S. C. Ampstrup, J. L. Laake, B. F. J. Manly, L. L. McDonald and D. G. Robertson), pp. 209-221. Rotterdam, The Netherlands: Balkema Press.

Bassett, H. R., Baumann, S., Campbell, G. S., Wiggins, S. M. and Hildebrand, J. A. (2009). Dall's porpoise (*Phocoenoides dalli*) echolocation click spectral structure. *J. Acoust. Soc. Am.* **125**, 2677-2677. doi:10.1121/1.4784219

Baumann-Pickering, S., McDonald, M. A., Simonis, A. E., Solsona Berga, A., Merkens, K. P., Oleson, E. M., Roch, M. A., Wiggins, S. M., Rankin, S. and Yack, T. M. (2013). Species-specific beaked whale echolocation signals. *J. Acoust. Soc. Am.* **134**, 2293-2301. doi:10.1121/1.4817832

Baumgartner, M. F., Mullin, K. D., May, L. N. and Leming, T. D. (2001). Cetacean habitats in the northern Gulf of Mexico. *Fish. Bull.* **99**, 219-219.

Beatson, E. (2007). The diet of pygmy sperm whales, *Kogia breviceps*, stranded in New Zealand: implications for conservation. *Rev. Fish. Biol. Fisheries.* **17**, 295-303. doi:10.1007/s11160-007-9039-9

Beedholm, K. and Møhl, B. (2006). Directionality of sperm whale sonar clicks and its relation to piston radiation theory. *J. Acoust. Soc. Am.* **119**, EL14-EL19. doi:10.1121/1.2161799

Benoit-Bird, K. J. (2014). Deep-diving autonomous underwater vehicle provides insights into scattering layer dynamics. *J. Acoust. Soc. Am.* **135**, 2154-2154. doi:10.1121/1.4876983

Benoit-Bird, K. J. and Au, W. W. (2001). Target strength measurements of Hawaiian mesopelagic boundary community animals. *J. Acoust. Soc. Am.* **110**, 812-819. doi:10.1121/1.1382620

Benoit-Bird, K. J., Moline, M. A. and Southall, B. L. (2017). Prey in oceanic sound scattering layers organize to get a little help from their friends. *Limnol. Oceanog.* **62**, 2788-2798. doi:10.1002/lno.10606

Benoit-Bird, K. J., Southall, B. L., Moline, M. A., Claridge, D. E., Dunn, C., Dolan, K. A. and Moretti, D. J. (2020). Critical threshold identified in the functional relationship between beaked whales and their prey. *Mar. Ecol. Prog. Ser.* **654**, 1-16. doi:10.3354/meps13521

Bloodworth, B. E. and Odell, D. K. (2008). Kogia breviceps (Cetacea: Kogiidae). *Mamm. Species* **819**, 1-12. doi:10.1644/819.1

Branstetter, B. K., Leger, J. S., Acton, D., Stewart, J., Houser, D., Finneran, J. J. and Jenkins, K. (2017). Killer whale (*Orcinus orca*) behavioral audiograms. *J. Acoust. Soc. Am.* **141**, 2387-2398. doi:10.1121/1.4979116

Breese, D. and Tershy, B. R. (1993). Relative abundance of Cetacea in the Canal de Ballenas, Gulf of California. *Mar. Mamm. Sci.* **9**, 319-324. doi:10.1111/j.1748-7692.1993.tb00460.x

Caldwell, D. K. and Caldwell, M. C. (1989). Pygmy sperm whale *Kogia breviceps* (de Blainville, 1838): dwarf sperm whale *Kogia simus* (Owen, 1866). In *Handbook of Marine Mammals* (ed. S. Ridgway and R. Harrison), pp. 235-260. San Diego, USA: Academic Press.

Cardona-Maldonado, M. A. and Mignucci-Giannoni, A. A. (1999). Pygmy and dwarf sperm whales in Puerto Rico and the Virgin Islands, with a review of *Kogia* in the Caribbean. *Caribb. J. Sci* **35**, 29-37.

Claridge, D. E. (2006). Fine-scale distribution and habitat selection of beaked whales. *PhD thesis*, Aberdeen University, Aberdeen, UK.

Clarke, M. (2003). Production and control of sound by the small sperm whales, *Kogia breviceps* and *K. sima and their implications for other Cetacea*. *J. Mar. Biol. Assoc. UK.* **83**, 241-263. doi:10.1017/S0025315403007045h

DeRuiter, S. L., Bahr, A., Blanchet, M.-A., Hansen, S. F., Kristensen, J. H., Madsen, P. T., Tyack, P. L. and Wahlberg, M. (2009). Acoustic behaviour of echolocating porpoises during prey capture. *J. Exp. Biol.* **212**, 3100-3107. doi:10.1242/jeb.030825

Duncan, A. J. and Maggi, A. L. (2006). A consistent, user friendly interface for running a variety of underwater acoustic propagation codes. Proceedings of ACOUSTICS, pp. 471-477.

Dunn, C. and Claridge, D. (2014). Killer whale (*Orcinus orca*) occurrence and predation in the Bahamas. *J. Mar. Biol. Assoc. UK.* **94**, 1305-1309. doi:10.1017/S0025315413000908

Dunphy-Daly, M. M., Heithaus, M. R. and Claridge, D. E. (2008). Temporal variation in dwarf sperm whale (*Kogia sima*) habitat use and group size off Great Abaco Island, Bahamas. *Mar. Mamm. Sci.* **24**, 171-182. doi:10.1111/j.1748-7692.2007.00183.x

Elwen, S. H., Gridley, T., Roux, J. P., Best, P. B. and Smale, M. J. (2013). Records of kogiid whales in Namibia, including the first record of the dwarf sperm whale (*Kogia sima*). *Mar. Biodivers. Rec.* **6**, 1-9. doi:10.1017/S1755267212000942

Fais, A., Johnson, M., Wilson, M., Aguilar de Soto, N. and Madsen, P. T. (2016). Sperm whale predator-prey interactions involve chasing and buzzing, but no acoustic stunning. *Sci. Rep.* **6**, 28562. doi:10.1038/srep28562

Finneran, J. J., Mulsow, J., Branstetter, B., Moore, P. and Houser, D. S. (2016). Nearfield and farfield measurements of dolphin echolocation beam patterns: no evidence of focusing. *J. Acoust. Soc. Am.* **140**, 1346-1360. . doi:10.1121/1.4961015

Frasier, K. E., Wiggins, S. M., Harris, D., Marques, T. A., Thomas, L. and Hildebrand, J. A. (2016). Delphinid echolocation click detection probability on near-seafloor sensors. *J. Acoust. Soc. Am.* **140**, 1918-1930. doi:10.1121/1.4962279

Galatius, A., Olsen, M. T., Steeman, M. E., Racicot, R. A., Bradshaw, C. D., Kyhn, L. A. and Miller, L. A. (2019). Raising your voice: evolution of narrow-band high-frequency signals in toothed whales (*Odontoceti*). *Biol. J. Linn. Soc.* **126**, 213-224. doi:10.1093/biolinnean/bly194

Gillespie, D., Mellinger, D., Gordon, J., Mclaren, D., Redmond, P., Mchugh, R., Trinder, P., Deng, X. Y. and Thode, A. (2008). PAMGUARD: Semiautomated, open source software for real-time acoustic detection and localization of cetaceans. *J. Acoust. Soc. Am.* **30**, 54-62.

Gkikopoulou, K. C. (2018). Getting below the surface: Density estimation methods for deep diving animals using slow autonomous underwater vehicles. *PhD thesis*, University of St Andrews, St Andrews, UK.

Goold, J. C. and Clarke, M. R. (2000). Sound velocity in the head of the dwarf sperm whale, Kogia sima, with anatomical and functional discussion. *J. Mar. Biol. Assoc. UK.* **80**, 535-542. doi:10.1017/S002531540000223X

Götz, T., Antunes, R. and Heinrich, S. (2010). Echolocation clicks of free-ranging Chilean dolphins (*Cephalorhynchus eutropia*). *J. Acoust. Soc. Am.* **128**, 563-566. doi:10.1121/1.3353078

Griffiths, E. T., Archer, F., Rankin, S., Keating, J. L., Keen, E., Barlow, J. and Moore, J. E. (2020). Detection and classification of narrow-band high frequency echolocation clicks from drifting recorders. *J. Acoust. Soc. Am.* **147**, 3511-3522. doi:10.1121/10.0001229

Hall, J. D. and Johnson, C. S. (1972). Auditory thresholds of a killer whale *Orcinus orca* Linnaeus. *J. Acoust. Soc. Am.* **51**, 515-517. doi:10.1121/1.1912871

Hildebrand, J. A., Frasier, K. E., Baumann-Pickering, S., Wiggins, S. M., Merkens, K. P., Garrison, L. P., Soldevilla, M. S. and McDonald, M. A. (2019). Assessing seasonality and density from passive acoustic monitoring of signals presumed to be from pygmy and dwarf sperm whales in the Gulf of Mexico. *Front. Mar. Sci.* **6**, 66. doi:10.3389/fmars.2019.00066

Hodge, L. E. W., Baumann–Pickering, S., Hildebrand, J. A., Bell, J. T., Cummings, E. W., Foley, H. J., McAlarney, R. J., McLellan, W. A., Pabst, D. A., Swaim, Z. T. et al. (2018). Heard but not seen: Occurrence of *Kogia* spp. along the western North Atlantic shelf break. *Mar. Mamm. Sci.* **34**, 1141-1153. doi:10.1111/mms.12498

Huggenberger, S., Rauschmann, M. A., Vogl, T. J., Oelschläger, H. H. A. (2009). Functional Morphology of the Nasal Complex in the Harbor Porpoise (*Phocoena phocoena* L.). *Anatom. Rec.* **292**, 902-920. doi:10.1002/ar.20854

Jensen, F. H., Rocco, A., Mansur, R. M., Smith, B. D., Janik, V. M. and Madsen, P. T. (2013). Clicking in shallow rivers: short-range echolocation of Irrawaddy and Ganges river dolphins in a shallow, acoustically complex habitat. *PLoS ONE* **8**, e59284. doi:10.1371/journal.pone.0059284

Jensen, F. H., Wahlberg, M., Beedholm, K., Johnson, M., Aguilar de Soto, N. and Madsen, P. T. (2015). Single-click beam patterns suggest dynamic changes to the field of view of echolocating Atlantic spotted dolphins (*Stenella frontalis*) in the wild. *J. Exp. Biol.* **218**, 1314-1324. doi:10.1242/jeb.116285

Jensen, F. H., Johnson, M., Ladegaard, M., Wisniewska, D. and Madsen, P. T. (2018). Narrow acoustic field of view drives frequency scaling in toothed whale biosonar. *Curr. Biol.* **28**, 1-8. doi:10.1016/j.cub.2017.11.007

Jensen, F. H., Keller, O. A., Tyack, P. L. and Visser, F. (2020). Dynamic biosonar adjustment strategies in deep-diving Risso's dolphins driven partly by prey evasion. *J. Exp. Biol.* **223**, jeb216283. doi:10.1242/jeb.216283

Johnson, M., Madsen, P. T., Zimmer, W. M., Aguilar de Soto, N. and Tyack, P. L. (2004). Beaked whales echolocate on prey. *Proc. Roy. Soc. B.* **271**, S383-S386. doi:10.1098/rsbl.2004.0208

Johnson, M., Madsen, P. T., Zimmer, W., Aguilar de Soto, N. and Tyack, P. (2006). Foraging Blainville's beaked whales (*Mesoplodon densirostris*) produce distinct click types matched to different phases of echolocation. *J. Exp. Biol.* **209**, 5038-5050. doi:10.1242/jeb.02596

Johnson, M., Hickmott, L., Aguilar de Soto, N. and Madsen, P. T. (2008). Echolocation behaviour adapted to prey in foraging Blainville's beaked whale (*Mesoplodon densirostris*). *Proc. Roy. Soc. B.* **275**, 133-139. doi:10.1098/rspb.2007.1190

Kadane, J. and Penner, R. (1983). Range ambiguity and pulse interval jitter in the bottlenose dolphin. *J. Acoust. Soc. Am.* **74**, 1059-1061. doi:10.1121/1.389940

Kastelein, R., Au, W., Rippe, H. and Schooneman, N. (1999). Target detection by an echolocating harbor porpoise (*Phocoena phocoena*). *J. Acoust. Soc. Am.* **105**, 2493-2498. doi:10.1121/1.426951

Kastelein, R. A., Bunskoek, P., Hagedoorn, M., Au, W. W. and de Haan, D. (2002). Audiogram of a harbor porpoise (*Phocoena phocoena*) measured with narrow-band frequency-modulated signals. *J. Acoust. Soc. Am.* **112**, 334-344. doi:10.1121/1.1480835

Kastelein, R. A., Janssen, M., Verboom, W. C. and de Haan, D. (2005). Receiving beam patterns in the horizontal plane of a harbor porpoise (*Phocoena phocoena*). *J. Acoust. Soc. Am.* **118**, 1172-1179. doi:10.1121/1.1945565

Ketten, D. R. (2000). Cetacean ears. In *Hearing by Whales and Dolphins* (ed. W. W. Au and R. R. Fay), pp. 43-108. New York, USA: Springer.

Koblitz, J. C., Wahlberg, M., Stilz, P., Madsen, P. T., Beedholm, K. and Schnitzler, H.-U. (2012). Asymmetry and dynamics of a narrow sonar beam in an echolocating harbor porpoise. *J. Acoust. Soc. Am.* **131**, 2315-2324. doi:10.1121/1.3683254

Koblitz, J. C., Stilz, P., Rasmussen, M. H. and Laidre, K. L. (2016). Highly Directional Sonar Beam of Narwhals (*Monodon monoceros*) measured with a vertical 16 hydrophone array. *PLoS ONE* **11**, e0162069. doi:10.1371/journal.pone.0162069

Kyhn, L. A., Tougaard, J., Jensen, F., Wahlberg, M., Stone, G., Yoshinaga, A., Beedholm, K. and Madsen, P. T. (2009). Feeding at a high pitch: Source parameters of narrow band, high-frequency clicks from echolocating off-shore hourglass dolphins and coastal Hector's dolphins. *J. Acoust. Soc. Am.* **125**, 1783-1791. doi:10.1121/1.3075600

Kyhn, L. A., Jensen, F. H., Beedholm, K., Tougaard, J., Hansen, M. and Madsen, P. T. (2010). Echolocation in sympatric Peale's dolphins (*Lagenorhynchus australis*) and Commerson's dolphins (*Cephalorhynchus commersonii*) producing narrow-band high-frequency clicks. *J. Exp. Biol.* **213**, 1940-1949. doi:10.1242/jeb.042440

Kyhn, L. A., Tougaard, J., Beedholm, K., Jensen, F. H., Ashe, E., Williams, R. and Madsen, P. T. (2013). Clicking in a killer whale habitat: narrow-band, high-frequency biosonar clicks of harbour porpoise (*Phocoena phocoena*) and Dall's porpoise (*Phocoenoides dalli*). *PLoS ONE* **8**, e63763. doi:10.1371/journal.pone.0063763

Ladegaard, M. and Madsen, P. T. (2019). Context-dependent biosonar adjustments during active target approaches in echolocating harbour porpoises. *J. Exp. Biol.* **222**, jeb206169. doi:10.1242/jeb.206169

Ladegaard, M., Jensen, F. H., de Freitas, M., da Silva, V. M. F. and Madsen, P. T. (2015). Amazon river dolphins (*Inia geoffrensis*) use a high-frequency short-range biosonar. *J. Exp. Biol.* **218**, 3091-3101. doi:10.1242/jeb.120501

Leeney, R. H., Carslake, D. and Elwen, S. H. (2011). Using static acoustic monitoring to describe echolocation behaviour of Heaviside's dolphins (*Cephalorhynchus heavisidii*) in Namibia. *Aquat. Mamm.* **37**, 151-160. doi:10.1578/AM.37.2.2011.151

Macaulay, J. (2020). Passive acoustic monitoring of harbour porpoise behaviour, distribution and density in tidal rapid habitats. PhD thesis, University of St Andrews, St Andrews, UK.

Macaulay, J., Gordon, J., Gillespie, D., Malinka, C. and Northridge, S. (2017). Passive acoustic methods for fine-scale tracking of harbour porpoises in tidal rapids. *J. Acoust. Soc. Am.* **141**, 1120-1132. doi:10.1121/1.4976077

Macaulay, J., Malinka, C., Gillespie, D. and Madsen, P. T. (2020). High resolution three-dimensional beam radiation pattern of harbour porpoise clicks with implications for passive acoustic monitoring. *J. Acoust. Soc. Am* **147**, 4175-4188. doi:10.1121/10.0001376

MacLeod, C. D., Hauser, N. and Peckham, H. (2004). Diversity, relative density and structure of the cetacean community in summer months east of Great Abaco, Bahamas. *J. Mar. Biol. Assoc. UK.* **84**, 469-474. doi:10.1017/S0025315404009476h

Madsen, P. T. and Surlykke, A. (2013). Functional Convergence in Bat and Toothed Whale. *Physiol.* **28**, 276-283. doi:10.1152/physiol.00008.2013

Madsen, P. T. and Wahlberg, M. (2007). Recording and quantification of ultrasonic echolocation clicks from free-ranging toothed whales. *Deep Sea Res. Part I Oceanogr. Res. Pap.* **54**, 1421-1444. doi:10.1016/j.dsr.2007.04.020

Madsen, P. T., Payne, R., Kristiansen, N. U., Wahlberg, M., Kerr, I. and Møhl, B. (2002). Sperm whale sound production studied with ultrasound time/depth-recording tags. *J. Exp. Biol.* **205**, 1899-1906.

Madsen, P. T., Kerr, I. and Payne, R. (2004). Echolocation clicks of two free-ranging, oceanic delphinids with different food preferences: false killer whales *Pseudorca crassidens* and Risso's dolphins *Grampus griseus*. *J. Exp. Biol.* **207**, 1811-1823. doi:10.1242/jeb.00966

Madsen, P. T., Carder, D., Beedholm, K. and Ridgway, S. (2005a). Porpoise clicks from a sperm whale nose—Convergent evolution of 130 kHz pulses in toothed whale sonars? *Bioacoust.* **15**, 195-206. doi:10.1080/09524622.2005.9753547

Madsen, P. T., Johnson, M. P., Aguilar de Soto, N., Zimmer, W. M. X. and Tyack, P. L. (2005b). Biosonar performance of foraging beaked whales (*Mesoplodon densirostris*). *J. Exp. Biol.* **208**, 181-194. doi:10.1242/jeb.01327

Madsen, P. T., Wilson, M., Johnson, M., Hanlon, R. T., Bocconcelli, A., Aguilar de Soto, N. and Tyack, P. L. (2007). Clicking for calamari: toothed whales can echolocate squid *Loligo pealeii*. *Aquat. Biol.* **1**, 141-150. doi:10.3354/ab00014

Madsen, P. T., Aguilar de Soto, N., Arranz, P. and Johnson, M. (2013). Echolocation in Blainville's beaked whales (*Mesoplodon densirostris*). *J. Comp. Phys. A.* **199**, 451-469. doi:10.1007/s00359-013-0824-8

Malinka, C. E., Atkins, J., Johnson, M. P., Tønnesen, P., Dunn, C. A., Claridge, D. E., Aguilar de Soto, N. and Madsen, P. T. (2020). An autonomous hydrophone array to study the acoustic ecology of deep-water toothed whales. *Deep Sea Res. Part I Oceanogr. Res. Pap.* **158C**, 103233. doi:10.1016/j.dsr.2020.103233

Marten, K. (2000). Ultrasonic analysis of pygmy sperm whale (*Kogia breviceps*) and Hubbs' beaked whale (*Mesoplodon carlhubbsi*) clicks. *Aquat. Mamm.* **26**, 45-48.

Martin, M. J., Gridley, T., Elwen, S. H. and Jensen, F. H. (2018). Heaviside's dolphins (*Cephalorhynchus heavisidii*) relax acoustic crypsis to increase communication range. *Proc. Roy. Soc. B.* **285**, 20181178. doi:10.1098/rspb.2018.1178

McKenna, M. F., Cranford, T. W., Berta, A. and Pyenson, N. D. (2012). Morphology of the odontocete melon and its implications for acoustic function. *Mar. Mamm. Sci.* **28**, 690-713. doi:10.1111/j.1748-7692.2011.00526.x

Medwin, H. (1975). Speed of sound in water: A simple equation for realistic parameters. *J. Acoust. Soc. Am* **58**, 1318-1319. doi:10.1121/1.380790

Merkens, K. P. and Oleson, E. M. (2018). Comparison of High-frequency Echolocation Clicks (likely *Kogia*) in Two Simultaneously Collected Passive Acoustic Data Sets Sampled at 200 kHz and 320 kHz. NOAA Technical Memorandum NMFS-PIFSC-74.

Merkens, K., Mann, D., Janik, V. M., Claridge, D., Hill, M. and Oleson, E. (2018). Clicks of dwarf sperm whales (*Kogia sima*). *Mar. Mamm. Sci.* **34**, 963-978. doi:10.1111/mms.12488

Morisaka, T. and Connor, R. (2007). Predation by killer whales (*Orcinus orca*) and the evolution of whistle loss and narrow-band high frequency clicks in odontocetes. *J. Evol. Biol.* **20**, 1439-1458. doi:10.1111/j.1420-9101.2007.01336.x

Møhl, B. and Andersen, S. (1973). Echolocation: high–frequency component in the click of the Harbour Porpoise (*Phocoena ph*. L.). *J. Acoust. Soc. Am.* **54**, 1368-1372. doi:10.1121/1.1914435

Moss, C. F. and Surlykke, A. (2001). Auditory scene analysis by echolocation in bats. *J. Acoust. Soc. Am* **110**, 2207-2226. doi:10.1121/1.1398051

Møhl, B., Wahlberg, M., Madsen, P. T., Miller, L. A. and Surlykke, A. (2000). Sperm whale clicks: Directionality and source level revisited. *J. Acoust. Soc. Am.* **107**, 638-648. doi:10.1121/1.428329

Møhl, B., Wahlberg, M., Madsen, P. T., Heerfordt, A. and Lund, A. (2003). The monopulsed nature of sperm whale clicks. *J. Acoust. Soc. Am.* **114**, 1143-1154. doi:10.1121/1.1586258

Moore, P., Hall, R., Friedl, W. and Nachtigall, P. (1984). The critical interval in dolphin echolocation: What is it? *J. Acoust. Soc. Am.* **76**, 314-317. doi:10.1121/1.391016

Pedersen, M. B., Tønnesen, P. H., Malinka, C. E., Ladegaard, M., Johnson, M., Aguilar de Soto, N. and Madsen, P. T. (2021). Echolocation click parameters of short-finned pilot whales (*Globicephala macrorhynchus*) in the wild. *J. Acoust. Soc. Am* **149** (in press). doi:10.1121/10.0003762

Philips, J. D., Nachtigall, P. E., Au, W. W., Pawloski, J. L. and Roitblat, H. L. (2003). Echolocation in the Risso's dolphin, *Grampus griseus*. *J. Acoust. Soc. Am.* **113**, 605-616. doi:10.1121/1.1527964

Plön, S. (2004). The status and natural history of pygmy (*Kogia breviceps*) and dwarf (*K. sima) sperm whales off Southern Africa. PhD thesis*, Rhodes University Grahamstown, South Africa.

Reyes Reyes, M. V., Tossenberger, V. P., Iñiguez, M. A., Hildebrand, J. A. and Melcón, M. L. (2016). Communication sounds of Commerson's dolphins (*Cephalorhynchus commersonii*) and contextual use of vocalizations. *Mar. Mamm. Sci.* **32**, 1219-1233. doi:10.1111/mms.12321

Ridgway, S. and Carder, D. (2001). Assessing hearing and sound production in cetaceans not available for behavioral audiograms: experiences with sperm, pygmy sperm, and gray whales. *Aquat. Mamm.* **27**, 267-276.

Sato, M. and Benoit-Bird, K. J. (2017). Spatial variability of deep scattering layers shapes the Bahamian mesopelagic ecosystem. *Mar. Ecol. Prog. Ser.* **580**, 69-82. doi:10.3354/meps12295

Schnitzler, H.-U. (1973). Control of Doppler shift compensation in the greater horseshoe bat, *Rhinolophus ferrumequinum*. *J. Comp. Phys.* **82**, 79-92. doi:10.1007/BF00714171

Schnitzler, H.-U. and Kalko, E. K. (2001). Echolocation by Insect-Eating Bats We define four distinct functional groups of bats and find differences in signal structure that correlate with the typical echolocation tasks faced by each group. *Biosci.* **51**, 557-569. doi:10.1641/0006-3568(2001)051[0557:EBIEB]2.0.CO;2

Scott, M. D., Hohn, A. A., Westgate, A. J., Nicholar, J. R., Whitaker, B. R. and Campbell, W. B. (2001). A note on the release and tracking of a rehabilitated pygmy sperm whale (*Kogia breviceps*). *J. Cetacean Res. Manag.* **3**, 87-94.

Staudinger, M. D., McAlarney, R. J., McLellan, W. A. and Pabst, D. A. (2014). Foraging ecology and niche overlap in pygmy (*Kogia breviceps*) and dwarf (*Kogia sima*) sperm whales from waters of the US mid–Atlantic coast. *Mar. Mamm. Sci.* **30**, 626-655. doi:10.1111/mms.12064

Strother, G. and Mogus, M. (1970). Acoustical beam patterns for bats: some theoretical considerations *J. Acoust. Soc. Am.* **48**, 1430-1432. doi:10.1121/1.1912304

Supin, A. Y. and Popov, V. V. (1995). Temporal resolution in the dolphin's auditory system revealed by double-click evoked potential study. *J. Acoust. Soc. Am.* **97**, 2586-2593. doi:10.1121/1.411913

Surlykke, A. and Moss, C. F. (2000). Echolocation behavior of big brown bats, *Eptesicus fuscus*, in the field and the laboratory. *J. Acoust. Soc. Am.* **108**, 2419-2429. doi:10.1121/1.1315295

Szymanski, M. D., Bain, D. E., Kiehl, K., Pennington, S., Wong, S. and Henry, K. R. (1999). Killer whale (*Orcinus orca*) hearing: auditory brainstem response and behavioral audiograms. *J. Acoust. Soc. Am.* **106**, 1134-1141. doi:10.1121/1.427121

Thomas, J., Moore, P., Nachtigall, P. and Gilmartin, W. (1990). A new sound from a stranded pygmy sperm whale. *Aquat. Mamm.* **16**, 28-30.

Thornton, S. W., Mclellan, W. A., Rommel, S. A., Dillaman, R. M., Nowacek, D. P., Koopman, H. N. and Pabst, D. A. (2015). Morphology of the nasal apparatus in pygmy (*Kogia breviceps*) and dwarf (*K. sima*) sperm whales. *Anatom. Rec.* **298**, 1301-1326. doi:10.1002/ar.23168

Tønnesen, P., Oliveira, C., Johnson, M. and Madsen, P. T. (2020). The long-range echo scene of the sperm whale biosonar. *Biol. Lett.* **16**, 20200134. doi:10.1098/rsbl.2020.0134

Urick, R. J. (1983). *Principles of Underwater Sound*. Peninsula, Los Altos: McGraw-Hill.

Vel'min, V. and Dubrovsky, N. (1975). Auditory analysis of sound pulses in dolphins. *Dok. Akad. Nauk SSSR* **225**, 470-473.

Verfuß, U. K., Miller, L. A., Pilz, P. K. and Schnitzler, H.-U. (2009). Echolocation by two foraging harbour porpoises (*Phocoena phocoena*). *J. Exp. Biol.* **212**, 823-834. doi:10.1242/jeb.022137

Villadsgaard, A., Wahlberg, M. and Tougaard, J. (2007). Echolocation signals of wild harbour porpoises, *Phocoena phocoena*. *J. Exp. Biol.* **210**, 56-64. doi:10.1242/jeb.02618

Wenz, G. M. (1962). Acoustic ambient noise in the ocean: spectra and sources. *J. Acoust. Soc. Am.* **34**, 1936-1956. doi:10.1121/1.1909155

Wiebe, P. H., Greene, C. H., Stanton, T. K. and Burczynski, J. (1990). Sound scattering by live zooplankton and micronekton: empirical studies with a dual-beam acoustical system. *J. Acoust. Soc. Am.* **88**, 2346-2360. doi:10.1121/1.400077

Willis, P. M. and Baird, R. W. (1998). Status of the dwarf sperm whale, *Kogia simus*, with special reference to Canada. *Can. Field-Nat.* **112**, 114-125.

Wisniewska, D. M., Johnson, M., Beedholm, K., Wahlberg, M. and Madsen, P. T. (2012). Acoustic gaze adjustments during active target selection in echolocating porpoises. *J. Exp. Biol.* **215**, 4358-4373. doi:10.1242/jeb.074013

Wisniewska, D. M., Johnson, M., Nachtigall, P. E. and Madsen, P. T. (2014). Buzzing during biosonar-based interception of prey in the delphinids *Tursiops truncatus* and *Pseudorca crassidens*. *J. Exp. Biol.* **217**, 4279-4282. doi:10.1242/jeb.113415

Wisniewska, D. M., Ratcliffe, J. M., Beedholm, K., Christensen, C. B., Johnson, M., Koblitz, J. C., Wahlberg, M. and Madsen, P. T. (2015). Range-dependent flexibility in the acoustic field of view of echolocating porpoises (*Phocoena phocoena*). *eLife* **4**, e05651. doi:10.7554/eLife.05651

Zimmer, W. M. (2011). *Passive Acoustic Monitoring of Cetaceans*. Cambridge, UK: Cambridge University Press.

Zimmer, W. M. X., Johnson, M., Madsen, P. T. and Tyack, P. (2005). Echolocation clicks of free-ranging Cuvier's beaked whales (*Ziphius cavirostris*). *J. Acoust. Soc. Am.* **117**, 3919-3927. doi:10.1121/1.1910225

Supplementary material

Table S1. **Source parameters by recording period.** Source parameters of on-axis clicks from the array recordings in the Bahamas, separated by the two encounters (periods A and B) in which *Kogia* were acoustically detected. Both periods lasted approximately 10 minutes and were ~22 hours apart.

	Array recording, Bahamas				**Unit**
	Period A (with visually identified *K. sima*)		**Period B** (with no visual identification)		
Parameters	**Mean ± s.d.**	**Median (range)**	**Mean ± s.d.**	**Median (range)**	
SL_{pp}	184 ± 6	183 (175-193)	186 ± 6	186 (174-197)	dB re. 1 µPa at 1m
SL_{RMS}	173 ± 6	171 (164-181)	174 ± 6	174 (162-186)	dB re. 1 µPa at 1m
SL_{EFD}	135 ± 6	133 (126-143)	136 ± 6	134 (123-147)	dB re. 1 $\mu Pa^2 s$ at 1m
Duration (-10 dB)	150 ± 16	146 (127-179)	137 ± 44	135 (72-205)	µs
F_c	128 ± 1	127 (126-129)	121 ± 2	121 (118-125)	kHz
F_p	127 ± 2	128 (125-130)	120 ± 2	121 (117-127)	kHz
$BW_{-3\ dB}$	5 ± 1	5 (3-7)	4 ± 2	4 (2-9)	kHz
$BW_{-10\ dB}$	8 ± 1	8 (6-10)	8 ± 3	6 (5-16)	kHz
BW_{RMS}	2 ± 1	2 (1-3)	3 ± 1	3 (1-7)	kHz
Q_{RMS}	64 ± 15	62 (41-91)	52 ± 22	43 (19-94)	(unitless)
ICI	223 ± 64	233 (23-489)	156 ± 87	131 (26-451)	ms
Range	163 ± 17	162 (134-184)	534 ± 74	556 (401-718)	m
Depth of localization	52 ± 48	44 (5-112)	116 ± 131	47(1-392)	m
Depth of recorder	11-95	n/a	11-95	n/a	m
Depth of water at recording site	~400	n/a	~900	n/a	m
N	16		30		

Fig. S1. **Photos of the *Kogia sima* during the encounter recorded in Cape Town Harbour, South Africa.** Visual confirmation on the species identification of the animal that produced the clicks in the acoustic recordings. Photo credit: Sea Search Africa, November 2016. *Kogia* photos from the acoustically recorded encounter in the Bahamas are unavailable due to being spotted shortly before diving and while array deployment was underway.

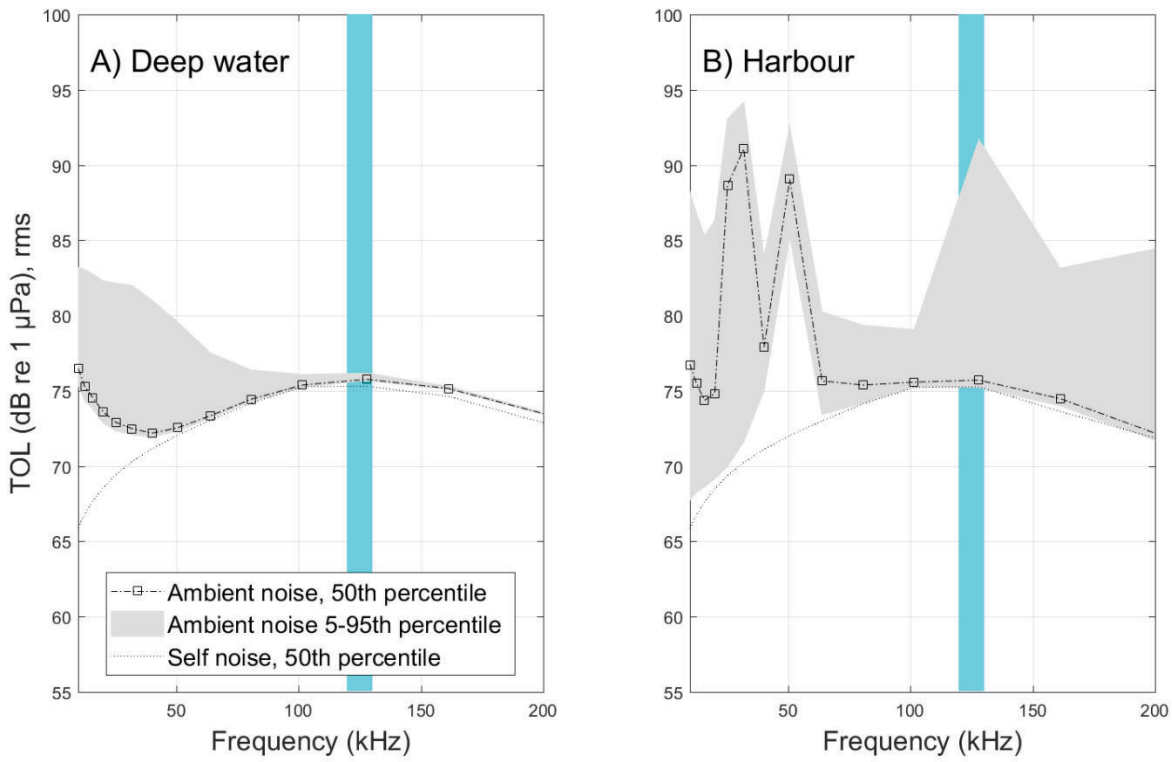

Fig. S2. **TOLs of high frequency noise in both recording environments.** Third octave levels (in the band centred at 128 kHz) of ambient noise during recordings when *Kogia* clicks were detected, at recording environments over (A) deep-water in the Bahamas (depth ~95 m), and (B) in Cape Town harbour, South Africa (depth ~7 m). The high variability in noise levels in the harbour reflects the presence of many boats and echosounders. The self noise of the SoundTrap is also shown, illustrating that lowest estimates for ambient noise measurements were limited by self noise above about ~40 kHz in these locations. The *x*-axis is shown on a linear scale to emphasize the high frequency component relevant to *Kogia* echolocation (~120-130 kHz), highlighted with cyan shading.

Chapter IV.

Full 4π porpoise beam profile

Macaulay, J. D. J., **Malinka, C. E.**, Gillespie, D., & P. T. Madsen (2020). "High resolution three-dimensional beam radiation pattern of harbour porpoise clicks with implications for passive acoustic monitoring," *The Journal of the Acoustical Society of America*, 147 (6): 4175-4188. doi: 10.1121/10.0001376

JASA ARTICLE

High resolution three-dimensional beam radiation pattern of harbour porpoise clicks with implications for passive acoustic monitoring

Jamie D. J. Macaulay,[1,a)] Chloe E. Malinka,[2,b)] Douglas Gillespie,[1,c)] and Peter T. Madsen[2,d)]
[1]*Sea Mammal Research Unit, Scottish Oceans Institute, School of Biology, University of Saint Andrews, East Sands, Saint Andrews, Fife, KY16 9LB, United Kingdom*
[2]*Zoophysiology, Department of Bioscience, Aarhus University, 8000 Aarhus C, Denmark*

ABSTRACT:
The source properties and radiation patterns of animal vocalisations define, along with propagation and noise conditions, the active space in which these vocalisations can be detected by conspecifics, predators, prey, and by passive acoustic monitoring (PAM). This study reports the 4π (360° horizontal and vertical) beam profile of a free-swimming, trained harbour porpoise measured using a 27-element hydrophone array. The forward echolocation beam is highly directional, as predicted by a piston model, and is consistent with previous measurements. However, at off-axis angles greater than $\pm 30°$, the beam attenuates more rapidly than the piston model and no side lobes are present. A diffuse back beam is also present with levels about -30 dB relative to the source level. In PAM, up to 50% of detections can be from portions of the beam profile with distorted click spectra, although this drops substantially for higher detection thresholds. Simulations of the probability of acoustically detecting a harbour porpoise show that a traditional piston model can underestimate the probability of detection compared to the actual three-dimensional radiation pattern documented here. This highlights the importance of empirical 4π measurements of beam profiles of toothed whales, both to improve understanding of toothed whale biology and to inform PAM.
 https://doi.org/10.1121/10.0001376

(Received 17 March 2020; revised 7 May 2020; accepted 13 May 2020; published online 25 June 2020)

[Editor: Klaus Lucke] Pages: 4175–4188

I. INTRODUCTION

Echolocating toothed whales ensonify their surroundings with short, powerful clicks and use weak returning echoes to navigate and find prey (Au, 1993). Broadly, these echolocation clicks can be split into four categories: sperm whales produce multi-pulsed 15–20 kHz transients (Møhl *et al.*, 2003), most dolphin and river dolphin species use short broadband clicks (Au, 1993; Ladegaard *et al.*, 2015), beaked whales produce slightly longer frequency-modulated pulses (Johnson *et al.*, 2004, 2006), whereas porpoises (Bassett *et al.*, 2009; Li *et al.*, 2007; Silber, 1991; Villadsgaard *et al.*, 2007), *Kogia* (Madsen *et al.*, 2005), *Pontoporia* (Melcón *et al.*, 2012), and six species of delphinids (Götz *et al.*, 2010; Kyhn *et al.*, 2009) have convergently evolved to produce narrow band high frequency (NBHF) clicks (~130 kHz). Despite this variation in the source properties of echolocation clicks, all toothed whales investigated thus far emit clicks in highly directional biosonar beams with similar directivity indices (Jensen *et al.*, 2018). Directing acoustic energy in this way generates higher source levels along the acoustic axis for the same power, which increases the range at which prey can be detected in a noise-limited environment while also limiting acoustic clutter (Madsen and Surlykke, 2013). A directional biosonar beam may also serve as a spatial filter of information (Madsen *et al.*, 2013), aid in the localisation of prey targets via a steep intensity gradient (Yovel *et al.*, 2010), and direct sound energy away from their acute auditory system that must detect and process weak echoes milliseconds after the emission of a powerful click (Schrøder *et al.*, 2017).

Toothed whales produce clicks by forcing pressurised air through their right pair of phonic lips in their nasal complex (Madsen *et al.*, 2013), which then is collimated using the skull and air sacs (Aroyan *et al.*, 1992) to form a directional sound beam that is radiated into the water via an impedance-matching fatty melon on the animal's rostrum (Cranford *et al.*, 1996; Cranford, 2000). The directionality of the click is seemingly defined by the size and conformation of phonic lips, skull anatomy, air sac configuration, melon structure and composition, as well as the frequency of the echolocation click. More generally, higher frequency sounds and larger physical structures will lead to a narrow beam, and lower frequencies and smaller radiating structure to a less directional beam (Au and Scheifele, 1994). Thus, as smaller species are physiologically constrained by having smaller sound producing structures, they must use higher frequency signals to maintain the same narrow acoustic field

a)Electronic mail: jdjm@st-andrews.ac.uk
b)ORCID: 0000-0003-0138-8388.
c)ORCID: 0000-0001-9628-157X.
d)ORCID: 0000-0002-5208-5259.

of view as larger toothed whales (Jensen *et al.*, 2018). However, while a narrow acoustic field of view seems to have been a significant driver in the co-evolution of nasal structures and in the scaling of spectral composition of echolocation clicks across three orders of magnitude of size in toothed whales (Jensen *et al.*, 2018), other factors, such as acoustic crypsis to reduce predation, have likely also played a role. For example, high hearing thresholds of killer whales at frequencies above 100 kHz may have led to the convergent evolution of NBHF clicks across several small toothed whales (Kyhn *et al.*, 2013; Morisaka and Connor, 2007). For such NBHF species, the consequence of using NBHF clicks for both echolocation and communication is that their active space is small and directional ahead of the communicating animal (Clausen *et al.*, 2011; Sørensen *et al.*, 2018), or that they must employ lower frequency clicks for communication (Martin *et al.*, 2018). Thus, the source parameters and beam pattern of clicks used for both echolocation and communication are inextricably linked and valuable for understanding toothed whales sensory and evolutionary biology in the context of social behaviour, predator-prey interactions, foraging ecology, and niche segregation (Madsen and Surlykke, 2013; Madsen and Wahlberg, 2007).

Quantifying toothed whale beam profiles usually involves the use of a compact array of hydrophones in a star or a linear and vertical configuration to record clicks from captive animals in controlled environments (e.g., Koblitz *et al.*, 2012; Finneran *et al.*, 2014; Smith *et al.*, 2016) or from wild animals in close proximity (e.g., Rasmussen *et al.*, 2002, 2004; Au and Herzing, 2003; Zimmer *et al.*, 2005; Kyhn *et al.*, 2013; Jensen *et al.*, 2015; Ladegaard *et al.*, 2015; Koblitz *et al.*, 2016). In most studies, only the narrow forward aspect of a beam ($\sim\pm30°$) is measured because the vast majority of the energy is contained in this small section of the beam profile, and it is that part that serves the animal in echolocation. Another attractive feature of using near on-axis apparent source levels (ASLs) (Møhl *et al.*, 2000) for beam estimation is that they can be conveniently fitted to a flat piston model to explain how most of the sound energy is radiated from the toothed whale forehead (Au, 1993). The piston model describes the beam attenuation with respect to the angle relative to the acoustic axis and depends entirely on only two parameters: the waveform of an on-axis echolocation click and the functional aperture of the emitter (Au *et al.*, 1978; Strother and Mogus, 1970). When the on-axis waveform is known for a given species, the equivalent aperture can be calculated by fitting the piston model to an empirically measured beam (e.g., Beedholm and Møhl, 2006; Jensen *et al.*, 2015; Koblitz *et al.*, 2012). For some applications, the equivalent aperture can be used to generate beam profiles of morphologically similar species for which directly measured beam data have not been collected. However, while the piston model works well for beam profile estimations $\sim\pm30°$ around the acoustic axis, it may not offer accurate measures of ASL farther off-axis. In particular, the piston model will, by definition, mathematically not work beyond 90°, and yet click energy is radiated at those extreme off-axis angles (Finneran *et al.*, 2014).

While the consequences for biosonar operation may fully be explained within angles of $\pm30°$ off-axis and thus successfully covered by the piston model, an understanding of the levels and waveforms of clicks farther off-axis is relevant for studies of other aspects of toothed whale biology and management via passive acoustic monitoring (PAM). In the correct circumstances, PAM can be used to calculate animal density—a key metric for conservation regulatory frameworks. There are multiple analytic approaches to density estimation using PAM which are usually dependent on the type of survey performed (Marques *et al.*, 2013). One possibility is to simulate the probability of detecting animals using a Monte Carlo simulation based on pre-determined auxiliary information on diving and acoustic behaviours. The efficacy of this approach is predicated on the accuracy of the model inputs, one of which is the beam profile (Frasier *et al.*, 2016; Küsel *et al.*, 2011). Another density estimation technique is the acoustic adaptation of spatially explicit capture/recapture (SECR), which is based on animals ensonifying different numbers of receivers within a widely spaced hydrophone array (Borchers *et al.*, 2015; Stevenson *et al.*, 2015); this is a relatively novel density estimation approach, but, if used with toothed whale clicks or other directional vocalisations, would require a model of an animal's beam profile (Stevenson, 2016). Knowledge of the beam profile is also a factor when designing hydrophone arrays to localises and provide acoustic quantifications for different species (e.g., Zimmer *et al.*, 2008; Malinka *et al.*, 2020).

The potential importance of beam profiles, both in understanding the sensory ecology of animals and for informing PAM, has prompted several studies on the wider radiation of sound around toothed whales. The full or near-full horizontal beam profiles of clicks ($\pm180°$), burst pulses and/or whistles have been measured for common bottlenose dolphins (*Tursiops truncatus*) (Au *et al.*, 2012a; Branstetter *et al.*, 2012; Finneran *et al.*, 2014) and for a harbour porpoise (*Phocoena phocoena*) coarsely out to 130° (Hansen *et al.*, 2008). While appropriate for their respective aims, these studies placed only a small number of hydrophones (5–8) around a stationary animal, leading to relatively poor spatial resolution (with the exception Finneran *et al.*, 2014, who used 35 hydrophones) and limited measurements to one horizontal and/or one vertical slice of the beam profile. The full 4π beam (all of the vertical and horizontal angles around a sphere) has been measured elegantly for a wild sperm whale using data from an acoustic tag deployed in tandem with a towed hydrophone array, although the nature of the equipment and sperm whale behaviour meant that on-axis beam measurements were clipped (Zimmer *et al.*, 2005).

Here we report on the full 4π beam profile of harbour porpoises. Harbour porpoises are a widespread but generally undemonstrative species with a vocal repertoire that consists entirely of stereotyped NBHF clicks. The forward beam profile of harbour porpoises has been measured multiple times

on stationary, captive harbour porpoises. Au *et al.* (1999) recorded a 16° half power (−3 dB) beamwidth, which was confirmed using suction cup hydrophones attached directly to the harbour porpoise's melon (Au, 2006). Koblitz *et al.* (2012) measured a narrower symmetric −3 dB horizontal beamwidth of 13° and a vertically compressed beamwidth of 11°. Adaptive widening of the porpoise beam was suggested by Madsen *et al.* (2010), speculated upon by Wisniewska *et al.* (2012), and later demonstrated and quantified by Wisniewska *et al.* (2015), who showed a dramatic widening of the half-power beamwidth during buzzing (clicks with a high repetition rate used in the final phase of prey capture), in some trials increasing the −3 dB beamwidth from ∼10° to 30°. The shy nature of harbour porpoises makes them difficult to study visually but they are a good candidate for PAM because, despite high attenuation in seawater (Ainslie and McColm, 1998), NBHF clicks are relatively unique in many regions, including North Atlantic shelf waters. As PAM hardware becomes more cost-effective, acoustic density estimation methods are likely to be more widely used to study harbour porpoises (e.g., Carlén *et al.*, 2018). Knowledge of the full 4π beam profile is an important aspect in both interpreting PAM data and potentially for density estimation calculations but has not been measured before. Here, we use a 27-channel hydrophone array to measure the full 4π beam pattern of a free-swimming captive harbour porpoise. The implications for the probability of detecting animals using PAM are explored by comparing the piston model measurements from previous literature with the empirically measured 4π beam pattern.

II. MATERIALS AND METHODS

A. Recording system

Data were collected in February 2018 at Fjord & Bælt in Kerteminde, Denmark, where one harbour porpoise is housed in an outdoor sea pen (3 m deep × 8 m × 13 m; Fig. 1). Twenty-seven hydrophones were arranged around the periphery of the sea pen; these consisted of eight TC-4034 hydrophones (Teledyne RESON A/S, Slangerup, Denmark), 12 high-frequency, autonomous digital sound recorders (SoundTraps, Ocean Instruments NZ, Auckland, New Zealand), and seven TC-4013 hydrophones (Teledyne RESON A/S, Slangerup, Denmark), which were arranged in a star-array (as used in Ladegaard *et al.*, 2017) and placed near one corner of the sea pen (Fig. 1).

SoundTraps were mounted above each TC-4034 hydrophone on steel poles (1 cm diameter) at depths of 1 and 1.3 m, respectively. These poles were mounted on floating pontoons. The central hydrophone in the star-array was at a depth of 1.2 m. The other six hydrophones in the star-array were located at even spaced angles (every 60°) around the centre hydrophone at alternating radial distances of 37.5 cm and 77.5 cm. The star-array was constructed from polyvinyl chloride (PVC) and the solid poles holding hydrophones in place were 2 cm diameter.

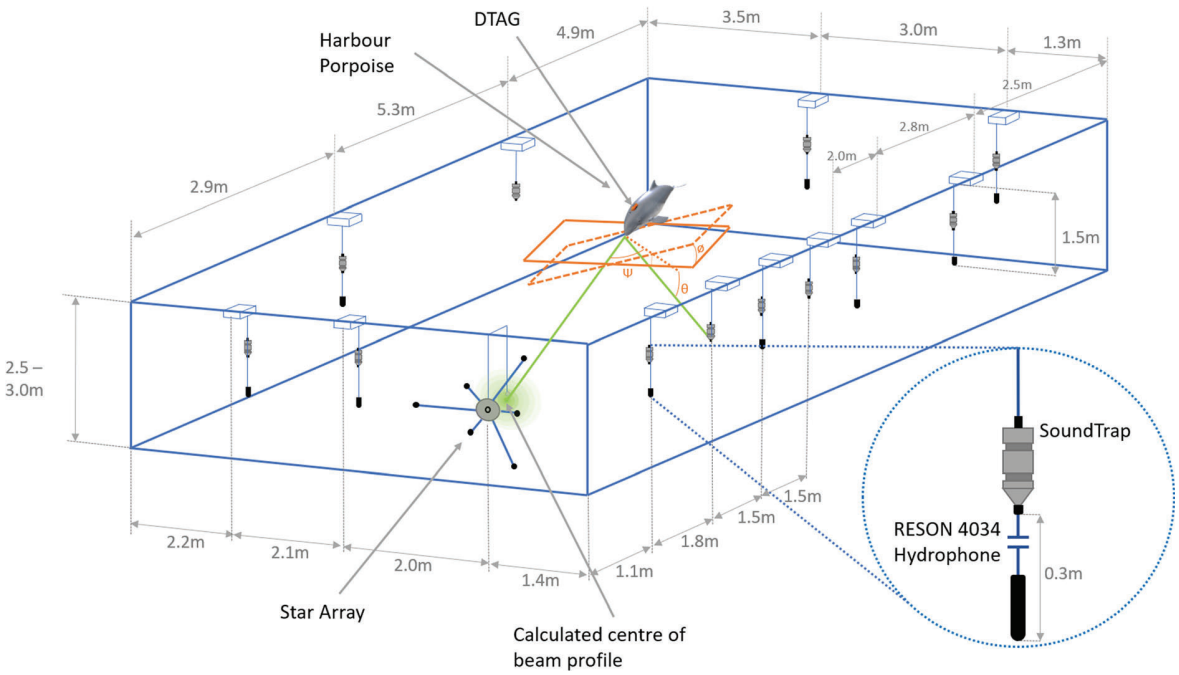

FIG. 1. (Color online) Diagram of the experimental setup (not to scale). The porpoise approached the 7-channel star-array. The RLs on the star-array were used to calculate the location of the centre of the porpoise beam. The (x, y, z) position of the porpoise was localised using the star-array. The centre of the beam and the localised porpoise position allowed for a vector to be calculated, which was the acoustic axis of the animal. DTAG data then provided the roll angle of the porpoise. This created a full set of Euler angles (heading, pitch, and roll). The RL was measured on every hydrophone (Reson and SoundTrap). A vector from each hydrophone to porpoise was calculated, and then projected onto the porpoise roll frame of reference, providing both the vertical and horizontal angle with the respect to the on-axis beam. The apparent source level for this horizontal and vertical angle was then calculated using the sonar equation, assuming spherical spreading. This process was repeated for every detected click to build up a picture of the beam profile.

Outputs from hydrophones on the star-array were amplified by 60 dB using a custom-built amplifier box with low cut (1 kHz 1-pole high pass) and anti-aliasing (200 kHz 4-pole low pass) filters (both Butterworth) before digitization at 16-bit resolution using two synchronised 8-channel analogue to digital converters (NI 6356 USB data acquisition cards, National Instruments, Austin, TX), providing 15 synchronised channels with a 4 V peak-to-peak (pp) range and a 500 kHz sample rate. This resulted in clip levels of 164 and 157 dB re 1 μPa for the TC-4034 and TC-4013 hydrophone recording chains respectively at 130 kHz. The sensitivity of the SoundTraps and TC-4013 hydrophones begins to drop off at ~150 kHz and the TC-4034 hydrophones reduce in sensitivity starting at ~200 kHz. Data from the NI cards were saved as 16 channel WAV files using PAMGuard (Gillespie *et al.*, 2008). The SoundTraps were programmed to record on high gain mode, clip level 174 dB re 1 μPa at 125 kHz. SoundTraps are autonomous single-channel units, and therefore time-synchronisation to channels on the array was completed after data collection.

The porpoise was equipped with a sound and movement tag (DTAG-4; Johnson and Tyack, 2003), mounted dorsally via suction cup behind the blowhole. Tag audio data were recorded at a sample rate of 576 kHz in 16-bit resolution (~170 dB re 1 μPa clip level). The pitch and roll data recorded by the tag allowed for the full orientation of the porpoise to be calculated and thus enabled measurement of the full 4π beam while the porpoise was free swimming.

B. Experimental procedure

The captive porpoise used in all trials, Freja, weighed 62 kg and was approximately 22 years old. Freja was trained with positive food reinforcement to swim towards a familiar target and touch it, as she has done in several previous studies (e.g., Wisniewska *et al.*, 2015; Ladegaard and Madsen, 2019). The target, a 50 mm diameter aluminium sphere (TS −39 dB), was suspended on a monofilament line and placed in front of the centre of the star-array, at ranges of ~5–30 cm. One trial comprised a target approach over 10–14 meters that concluded with the porpoise putting the tip of her rostrum on the target, at which point the porpoise was bridged with a whistle and received a fish reward. The porpoise was not explicitly asked to produce echolocation clicks while performing these tasks, but consistently did so as part of its normal behaviour. We saw a stereotypical reduction in source levels (SLs) and inter-click intervals (ICIs) during the approach, and a terminal buzz while moving up to the sphere to touch it, consistent with previous studies (Deruiter *et al.*, 2009; Ladegaard and Madsen, 2019) showing that she was echolocating to solve the task.

Target approaches were either completed with regular swimming or while rolling. Freja was given an audible and tactile signal to directly approach the target ($n = 21$), or was given a visual hand signal to actively roll while swimming in the direction of the target ($n = 18$) to provide for full 4π sampling of the acoustic radiation pattern. During rolling trials, one target approach comprised 1–3 rolls. Thirty-nine trials were run over four sessions over two consecutive days, with each session comprising up to 12 trials.

The porpoise sometimes wore opaque suction-cup eyecups during direct target-approach trials (on 7/21 target approach trials), so as to maximize the number of clicks produced, since porpoises have been observed to produce more clicks when blindfolded (Verfuß *et al.*, 2009). No eyecups were used during trials in which the porpoise was instructed to roll due to the visual cue used to request rolling.

The weather during the three days of data collection was fair, with no rain during data collection.

C. Calibrations

The three-dimensional (3D) positions of each hydrophone were calculated to centimeter accuracy using a combination of measurements from a laser range finder (Bosch GLM 50 C Professional) and an accurate tape measure. Additionally, prior to each experimental session, each hydrophone was pinged for calibration with porpoise-like clicks [130 kHz, ten cycles, generated by a waveform generator (model 33220A, Agilent Technologies, La Jolla, CA)] from the same reference distance using a B&K 8105 hydrophone (Brüel & Kjær Sound & Vibration Measurement A/S, Nærum, Denmark) as a transducer.

The pinging trials were used to calculate the sensitivity of all hydrophones. A manual analyst marked out all clicks detected from the output hydrophone in PAMGuard (Gillespie *et al.*, 2008), which were then imported into MATLAB (The Mathworks Inc., Natick, MA) and a 60 kHz 4-pole high-pass filter was applied. The relative pp amplitudes of the received clicks on each hydrophone were measured and individual hydrophone sensitivities were calculated by comparing these levels to the levels on the central hydrophone on the star-array, assuming spherical spreading and a 0.04 dB/m transmission loss (at 130 kHz). This ensured that the relative sensitivities of each receiver were accurately calculated (standard deviation of ~1 dB in measurements), allowing for precise estimation of the beam profile while also permitting the absolute levels to be determined.

SoundTrap and DTAG clocks can drift at a rate of up to 20 ppm, i.e., up to 72 ms per hour. The typical ICIs of a harbour porpoise are <100 ms, and so clock drift on SoundTraps over several hours could potentially result in errors when matching clicks between different devices. Both DTAG and SoundTrap clocks were therefore aligned with the synchronised hydrophone array at the beginning of each session. Time alignment was performed in MATLAB by cross correlating the first 2 s of a detected click train. Each session was around 10 min, which equates to a maximum of 12 ms of clock drift and thus this provided sufficient time alignment for matching clicks, but did not allow for the SoundTraps to be used for acoustic localisation purposes.

D. Method validation

To verify that we could estimate beam directionalities reliably, trials were also run with a known directional transducer, a TC-2130 transducer (Teledyne RESON A/S, Slangerup, Denmark), with a directivity index (DI) very similar to that of a porpoise (see Jensen *et al.*, 2015). This transducer emitted a series of simulated NBHF clicks at 130 kHz generated by a waveform generator (model 33220A, Agilent Technologies, La Jolla, CA). The TC-2130, mounted on a broomstick, was manually moved towards the star-array along the approximate swim path of the real porpoise while emitting clicks. The porpoise was not in the research pen while these trials were conducted. The data from this were analysed in the same manner as clicks from the real porpoise. Additionally, the beam profile of the TC-2130 was accurately measured in a calibration tank. Details of the method validation can be found in the Supplemental Materials.[1]

E. Data analysis

Given the 3D approach tracks of a porpoise, detected porpoise clicks and properly time-aligned and calibrated hydrophones, it was possible to measure the beam profile of a free-swimming porpoise. Data analysis involved a five-stage process. First, 3D approach tracks were determined by detecting and localising received clicks on the star-array. Second, clicks received between the different hydrophones were matched. Third, received levels (RLs) were measured. Fourth, the absolute orientation at each point on the track was calculated using the RLs on the star-array and roll measurements on the DTAG. Finally, the RLs and range to the porpoise at each hydrophone were used to calculate the ASLs with respect to horizontal and vertical angles of the porpoise's own reference frame. This process was performed for all detected clicks over multiple trials to build up a large number of measurements of the beam profile at different horizontal and vertical angles.

1. Click detection and localisation

In all trials, clicks received on each hydrophone were automatically extracted from raw sound files using PAMGuard (as in Sec. II C). Porpoise positions were then calculated using the known spatial hydrophone configuration and the time of arrival differences of the same click between the receivers. To minimise errors arising from echoes, only the star-array was used for localisation calculations. For every click detected on the central channel of the star-array, all possible combinations of porpoise clicks detected on other channels were determined. Time of arrival differences for each combination were calculated and a Simplex minimisation algorithm (Nelder and Mead, 1965) was used to calculate the range and direction to the porpoise. The time delay combination with the best fit to the localisation algorithm (i.e., the set of time delays which made most physical sense) was selected as the correct position of the porpoise. If this position was outside of the bounds of the pen it was discarded. A Savitzky-Golay finite impulse response (FIR) smoothing filter (Press and Teukolsky, 1990) (polynomial order, 3; window length, 9) was then applied to all localised positions within a specified trial to construct a 3D interpolated track of the harbour porpoise approach, as shown in Fig. 2.

2. Matching clicks

All detected clicks were imported into MATLAB. For every click received on the central channel of the star-array, the same click was located on all other hydrophones around the sea pen. For each hydrophone, a time window was calculated. The centre of the time window was based on the time for a click to travel from the track position of the porpoise to the hydrophone, assuming a sound speed of 1500 ms^{-1}. For synchronised hydrophones, the time window was ± 1 ms from this time; for SoundTraps, which were not synchronised as accurately, the time window was ± 10 ms. If multiple clicks were detected within the time window, then the first click was selected, as any secondary click was likely an echo.

3. RL calculation

For all matched clicks, the pp RLs were calculated using the absolute sensitivity of each receiving hydrophone. RLs were measured by first filtering click waveforms with a 60 kHz 4-pole high-pass filter to reduce any ambient noise at lower frequencies.

4. Calculating orientation

For each detected click, the acoustic axis vector of the porpoise was calculated using the star-array. An interpolated surface (2nd order polynomial in both x and y) was constructed based on the RLs of the click and positions of the hydrophones within the star-array using MATLAB curve fitting toolbox. The maximum peak of the surface was considered the received location of the central axis of the acoustic beam, and the height of the peak was the relative on-axis apparent source level from which all beam loss measurements were calculated. A vector from the on-axis beam location to the position of the harbour porpoise on the approach track was then calculated and roll from the DTAG was extracted. The roll, combined with the acoustic axis vector, created a full set of Euler angles for the porpoise (heading, pitch, and roll).

5. Calculating the ASL ($\theta, \emptyset$)

A vector to the position of the porpoise on the approach track was then calculated for every hydrophone within the array, which detected the click. The vector was projected onto the rotational frame of reference of the porpoise using the Rodrigues rotation formula (Rodrigues, 1840). The horizontal angle of the projected vector with respect to the acoustic axis vector was the horizontal beam angle, θ. The

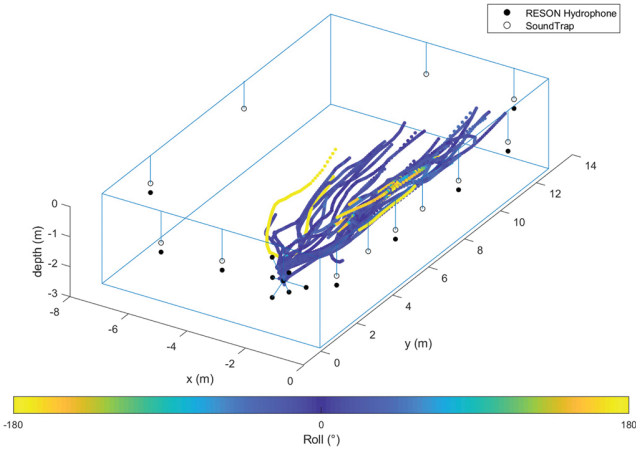

FIG. 2. (Color online) Plot of localised swim paths of the harbour porpoise in 40 trials to scale. The porpoise was tasked with swimming towards a target just in front of the star-array. The colour of the track shows the roll of the porpoise. Most roll values are near 0° because a single roll is a relatively brief event.

vertical angle from the plane of the acoustic axis to the hydrophone was the vertical beam angle, $\emptyset$.

The beam apparent source level for this horizontal and vertical angle was calculated using the sonar equation [Eq. (1)],

$$ASL_{pp}(\theta, \emptyset) = RL_{pp} + 20\log_{10}R + \propto R, \quad (1)$$

where $ASL_{pp}(\theta, \emptyset)$ is the apparent source level (see Møhl *et al.*, 2000) with respect to horizontal (θ) and vertical angles ($\emptyset$). R is the range (in meters) from the hydrophone to the porpoise track at the time of the received click, RL_{pp} is the relative pp RL, α is the absorption coefficient (0.04 dB/m for porpoise frequency; Ainslie and McColm, 1998), and spreading loss is assumed to be spherical. The on-axis apparent source level was calculated in the same manner by considering RL_{pp} to be the maxima of the interpolated RL surface on the star-array. All ASL measurements were then normalised by subtracting the on-axis source level.

Every manually annotated click detected on the central star-array hydrophone over all trials was analysed in this way. Data were then filtered to attempt to remove spurious results; specifically, all clicks which were detected when the acoustic axis was calculated to occur outside of the 40 cm radius from the central hydrophone on the star-array were removed, as these often lead to inaccurate on-axis source level calculations. Measurements where the porpoise was within 0.5 m of a respective hydrophone were also removed as the log scale in Eq. (1) means that small changes in the range at close ranges result in very large errors in ASL. Finally, the curve fitting algorithm occasionally registered a peak in the RL surface of the star-array when the true peak of the beam was in fact outside of the star-array. These spurious results could be removed by setting a lower amplitude limit of 156 dB re 1 μPa pp to calculated on-axis source levels.

F. Piston model

The beam profile was compared to a piston model. The piston model was generated by calculating the first order Bessel function that makes up the spatial transfer function of a circular surface with a diameter of 6.5 cm for horizontal angles and 8.3 cm for vertical angles (Koblitz *et al.*, 2012). The fast Fourier transform (FFT) of a porpoise click was multiplied by the complex conjugate of the Bessel function for a given angle and the pp amplitude of the inverse Fourier transform of the result is the value of the piston model at that angle (Beedholm and Møhl, 2006). The position of side lobes on the piston model can be sensitive to the exact input waveform. To account for variation within on-axis clicks, a piston model was generated for every porpoise click detected on the central hydrophone array and within the filter parameters described in Sec. II E 5. The linear power outputs of the piston models for all these clicks were averaged and then converted to dB amplitude to give a final piston model.

G. Probability of detection simulations

Monte Carlo simulations can be used to calculate the probability of detecting animals on PAM instruments (Frasier *et al.*, 2016; Küsel *et al.*, 2011). There are multiple input parameters to such simulations one of which is the beam profile of animals. To test the implications of using an empirically measured beam profile, as opposed to a piston model, a Monte Carlo simulation for a harbour porpoise was developed which placed an animal at a random x, y location with a total range from a hydrophone between 0 and 750 m and maximum depth of 30 m. The simulated porpoises' source level, horizontal and vertical orientation, and depth at each location were parametrised from empirical measures of swim behaviour, source level, and the beam pattern measurements. A RL was then calculated for a simulated hydrophone placed at the centre of the simulation $x, y = (0,0)$ and thirty meters depth. A simulated click was considered detected if the RL was above a specified minimum detection threshold, otherwise it was considered not detected. If detected, then the location was recorded as successful (coded 1), otherwise the location was recorded as being unsuccessful (coded 0). 250 000 random locations were considered and a probability of detection then calculated by dividing the total number of successful detections by the total number of attempts. Each simulation was bootstrapped 20 times and averaged to increase precision.

Detection probability simulations were run for a range of detection thresholds (110–133 dB re 1 μPa pp) and several different beam profiles. Three beam profiles were tested for these detection thresholds; the empirically measured beam, a full −90° to 90° piston model with the back beam set to −40 dB (the lowest value of the piston model), and the −30° to 30° piston model, with all other values set to −200 dB beam attenuation (i.e., no side energy). The measured beam profile contained some holes at angles where no clicks were detected (see Fig. 3); however, the Monte Carlo

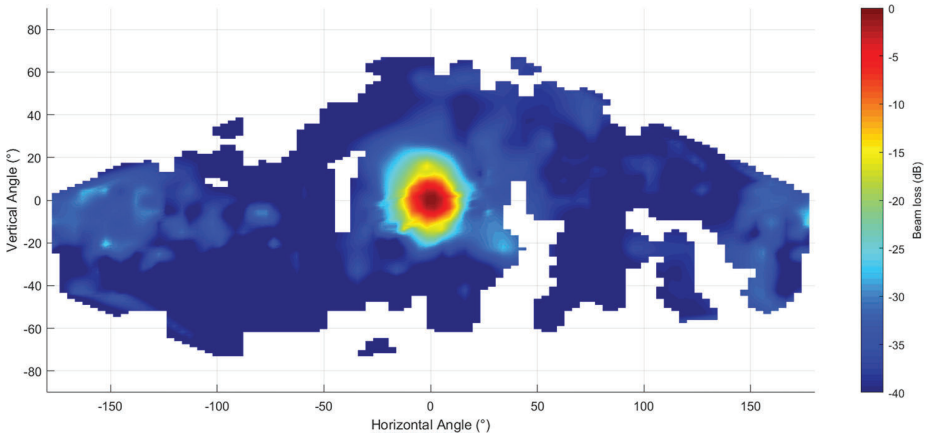

FIG. 3. (Color online) Porpoise beam profile showing full aspect coverage the beam. 2 × 2° grid bins used between ±30°, and 5 × 5° grids were used to take the median of the beam profile at all other angles. The intense forward beam is evident on-axis (0°, 0°). This attenuates rapidly towards ±90°. Behind the porpoise there is evidence of a diffuse acoustic energy, which is ∼25–30 dB less than the on-axis source level. Blank spaces indicate area where there were no measurements.

simulation requires these to have some value to function properly. Therefore, any holes at the edge of the beam profile surface (near ±180° horizontal and ±90° vertical) were assumed to be −45 dB (the lowest value of the measured beam profile) and any remaining holes were filled by interpolating the surrounding surface using Sibson interpolation (Park *et al.*, 2006).

Other parameters remained constant across all simulations. The porpoise was assumed to have a normal distribution of vertical orientation angles [mean = 0°, standard deviation (STD) = 25°] a log normal depth distribution (shape = 2, scale = 3, max depth 30 m) and mean source level of 191 dB re 1 μPa pp (Villadsgaard *et al.*, 2007) and STD in source level of 5 dB.

The detection probability simulations assumed that clicks were always correctly classified; however, it is a consequence of narrow beam profiles that off-axis angles clicks become highly distorted (Au *et al.*, 2012b). Automated PAM detectors may perform less efficiently in detecting these clicks and so the assumption that all clicks are equally as detectible if above threshold does not necessarily hold. A "beam volume" for the measured beam profile was constructed to test the number of distorted clicks that might be detected by a PAM device. The beam volume is the 3D space inside which a recorder with a specified detection threshold would detect a porpoise click assuming a particular on-axis source level, spherical spreading loss, and accounting for absorption. The proportion of the total volume in which distorted clicks would be detected can then be estimated and used as a rough proxy for the percentage of distorted clicks a PAM device might detect.

III. RESULTS

In total, there were 40 successful trials in which 100 264 clicks were detected over all hydrophones in the array. Of these, 15 154 were collected when the harbour porpoise was on-axis to the star-array, i.e., the center of the beam falls within a 40 cm radius of the central star-array hydrophone. During trials in which the porpoise was instructed to roll (no eyecups) only 699 clicks were detected; however, all trials contained some on-axis clicks.

The maximum variation in source levels of on-axis clicks used in beam profile measurements was 16 dB (minimum 156 dB re 1 μPa pp and maximum 172 dB re 1 μPa pp) with a mean of 161 dB re 1 μPa pp and confidence interval (CI) of ± 7 dB. This is slightly higher than other studies (e.g., Ladegaard and Madsen, 2019); however, this is likely due to the exclusion of lower source level clicks from beam profile calculations as detailed in Sec. II E 5.

Beam profile measurements consisted of many overlapping measurements at different horizontal and vertical angles. An average beam profile surface was calculated by taking the median of all results within 2° (horizontal) by 2°(vertical) bins. Larger bins (5° × 5°) were used for horizontal angles >±30° off the acoustic axis because there were fewer results at increasing off-axis angles (due to much lower signal to noise ratio). The median levels were plotted as a surface (Fig. 3), demonstrating an intense forward beam and weaker diffuse energy behind the animal. Note that clicks were not detected for all possible angles, and as such are represented as blank spaces in the surface.

The spectra of clicks between ±3° vertical angle were plotted on a waterfall spectrogram with respect to absolute horizontal angle (i.e., $\pm\theta$ are plotted as $+\theta$). All clicks within the vertical angle bounds were grouped into 5° horizontal angle bins. The power spectra of all clicks were calculated and plotted on a surface in angle order for each 5° bin. The 5° bin surfaces were then stretched or compressed to a uniform width and plotted together to create a concatenated click angular spectrogram. Figures 4(A) and 4(B) show that the narrowband click spectrum breaks down at around 20° off the peak of the beam and is replaced by spectra with less predictable and more broadband components. It should be noted that the sensitivity of some of the hydrophones begins to drop off at around 150 kHz and that it is likely that many of the broader band components outside 100–150 kHz in Fig. 4(B) are due to the much lower signal to noise ratio of clicks at larger off-axis angles. At off-axis angles (>20°) some of the angle bins also contain very few clicks, which likely causes some of the variation in standard deviation and mean measurements. However, in Fig. 4(B), there is clearly structure to the peak frequency of sequential clicks in the 100–150 kHz band and thus

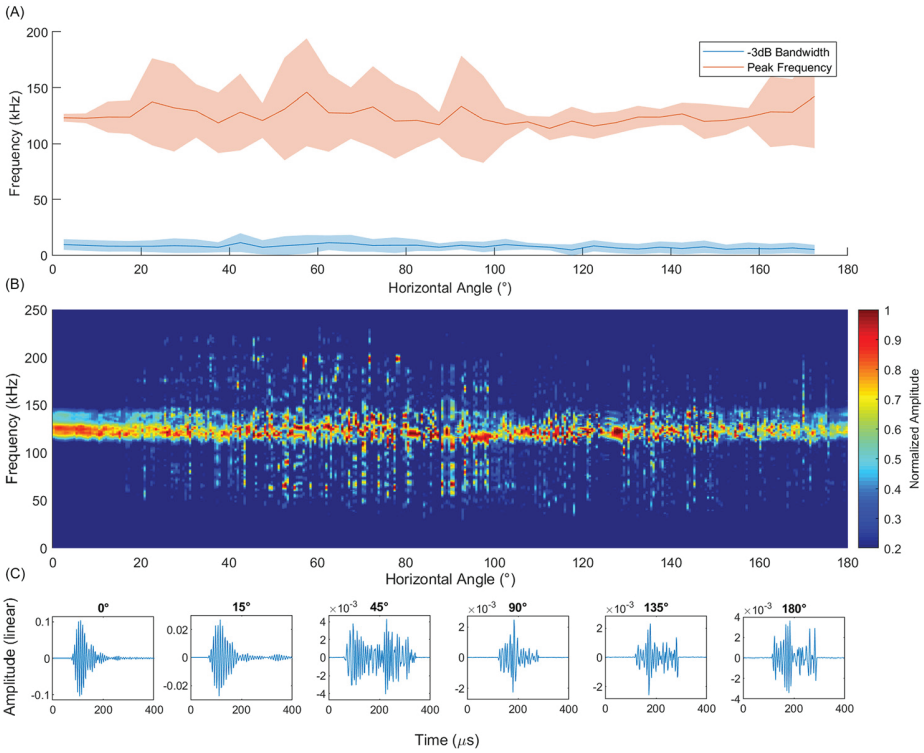

FIG. 4. (Color online) Frequency metrics, a waterfall spectrogram of clicks and examples of click waveforms with respect to horizontal axis. Clicks are split into 5° horizontal bins which contain all detected clicks within ±3° vertical angle sorted in order of horizontal angle. (A) Shows the mean peak frequency and −3 dB bandwidth, with standard deviation for each bin (note that data points are plotted as the centre of each bin), and (B) is a waterfall spectrogram of all clicks within each bin. The graphs show the break down in spectra beyond ∼20° with peak frequency significantly more variable and with additional energy in higher and lower frequency components. It is likely that a portion of this distortion comes from the much lower signal to noise ratio of off-axis clicks; however, at off-axis angles and within the 100 to 150 kHz frequency band, there is clear structure to the spectra of sequential clicks that are not explained simply by lower SNR. Note that the frequency axis limits on the waterfall spectrogram are between 50 and 200 kHz. (C) Shows an example of the waveforms of clicks extracted by PAMGuard at different horizontal angles. Note that some of these are zero padded to show a consistent time scale.

stochastic noise introduced by lower signal-to-noise ratio (SNR) likely does not solely explain distortion of the click spectra.

A. Comparison to the piston model

To assess how closely the piston model predicts off-axis beam attenuation, the empirically measured beam and a piston model were compared in two and three dimensions in Figs. 5 and 6. Figure 5 shows the raw beam for ±3° slices of the horizontal and vertical raw beam measurements plotted against a piston model with horizontal and vertical effective aperture diameters of 6.5 and 8.3 cm, respectively (Koblitz *et al.*, 2012). The piston model was constructed of multiple received on-axis clicks and then averaged as described in Sec. II F. The standard deviation in directivity index was 0.15 dB and thus click waveform variation had little effect on the piston model other than suppressing side lobes.

Figure 6 shows the measured beam and two piston models plotted as surface plots of expected RL assuming spherical spreading laws with an absorption coefficient of 0.04 dB m^{-1} (Ainslie and McColm, 1998) and an on-axis source level of 191 dB re 1 μPa pp (an average recorded in a study of wild porpoises; Villadsgaard *et al.*, 2007). For angles greater than 90°, the first piston model assumed beam attenuation was constant and equal to the lowest value predicted at ±90°, in this case − 40 dB. The second piston model assumed beam attenuation was −200 dB (i.e., no energy) beyond ±30° (i.e., has energy only in the forward part of the beam). The plot shows the expected RL if a device were placed at (x, y) assuming a porpoise is facing in the $+y$ direction at (0,0). This shows the typical acoustic space a wild animal might occupy in PAM studies.

B. Implications for PAM

There are clear differences between the measured and piston model beam in Figs. 5 and 6. In the context of PAM, it is important to understand whether the assumption of a piston model will make any appreciable difference to density estimation. Figure 7 shows the results of three Monte Carlo simulations of detection probability using the beam profiles in Fig. 6. The probability here ($\hat{P}$) is the probability of detection multiplied by a triangular step function and hence shows the probability of encountering a click, usually used when analysing data from a stationary or drifting PAM devices. The area under the graph therefore directly divides the density estimation equation (Marques *et al.*, 2013). The results

https://doi.org/10.1121/10.0001376

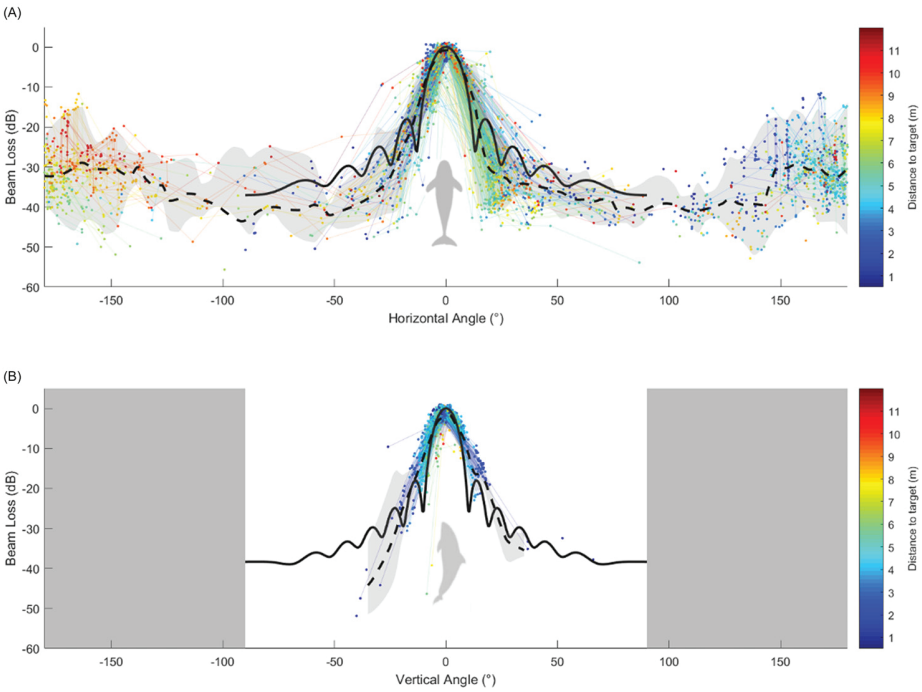

FIG. 5. (Color online) Raw beam data compared to the −90° to 90° piston model of an on-axis porpoise click for horizontal and vertical slices of the beam profile. (A) Shows all horizontal angles which have vertical angles between −3° and 3° and (B) shows vertical angle measurements which have horizontal angles between −3° and 3°. Scatter points are back-calculated beam source levels with respect to angle. The solid black line is the average piston model results discussed in Sec. II F. The dashed black line shows the average beam measurement with grey area indicating the 95% confidence interval. The thin coloured lines group single clicks detected on multiple hydrophones together. Scatter points and lines are coloured by the distance to the target.

in Fig. 7 show that, for a detection threshold of 110 dB (a typical value for an automated click detector) and source level of 191 dB re 1 μPa pp, the full −90° to 90° piston model makes little different to $\hat{P}$ and the −30° to 30° piston model with no side energy underestimates $\hat{P}$ by around half.

Figure 8 shows how $\hat{P}$ scales with different minimum detection threshold levels (i.e., the minimum click level required to register a detection on the PAM device) assuming a source level of 191 dB re 1 μPa pp. The ratio of $\hat{P}$ is not constant between beam profiles for different detection thresholds, with the piston model with side energy

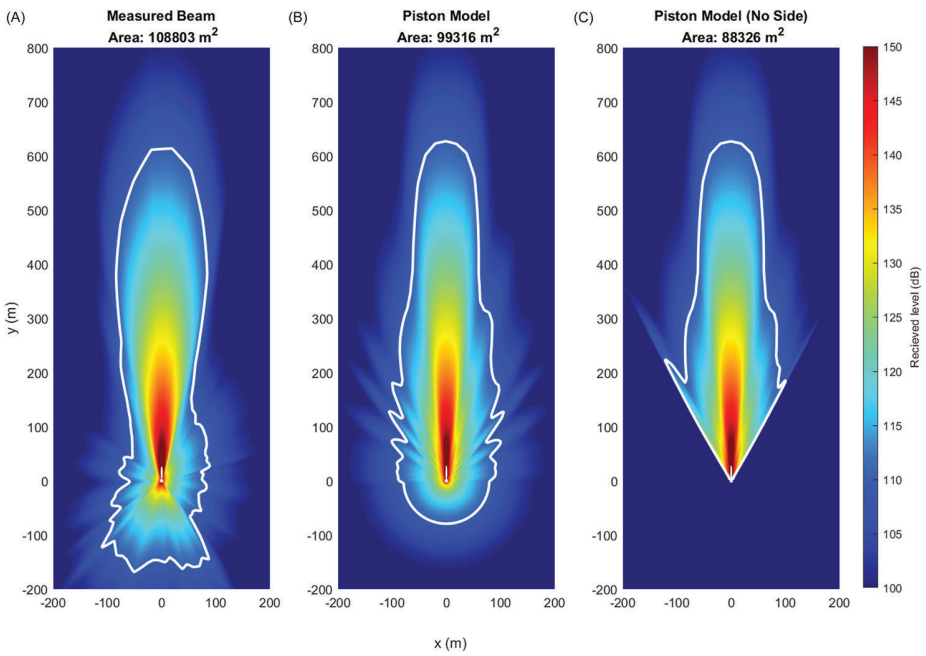

FIG. 6. (Color online) Beam profile detectability for an echolocation click with a SL of 191 dB re 1 μPa pp. Each point on the plot is coloured by the expected RL if a porpoise were facing in the y direction and located at (0,0). (A) Shows the measured beam profile for a harbour porpoise and (B) shows piston model results assuming a −40 dB uniform back beam (the lowest value of the piston model) using effective aperture diameter measurements. (C) Is the same piston as (B) but with all energy removed past ±30° (i.e., only contains energy in the forward part of the beam). The lower colour limit of 100 dB re 1 μPa pp was applied as this is below the usual limit (e.g., ∼110 dB) for automated detection of clicks in PAM studies; thus, in darker blue areas in which a PAM device is less likely to detect a click, the white line in both plots indicates what the detectable area would be for a PAM study using an automated detection algorithm with a pp threshold of 110 dB re 1 μPa pp. Titles show the area within the white lines.

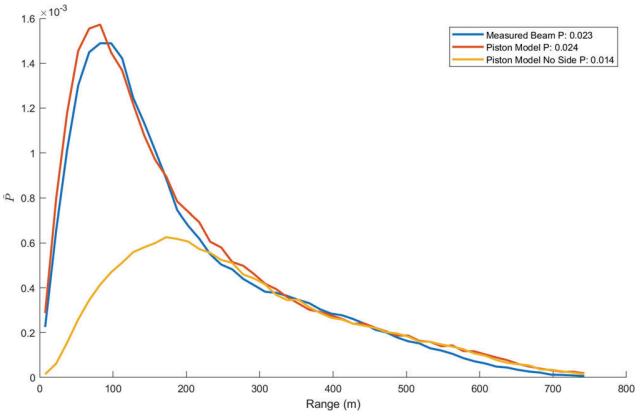

FIG. 7. (Color online) An example of the simulated probability of encounter ($\hat{P}$) with respect to range for different beam profiles assuming a mean source level of 191 dB re 1 μPa pp, a standard deviation of 5 dB, and detection threshold of 110 dB re 1 μPa pp. This is the probability that an animal will be detected at a specified range assuming a homogenous distribution of animals around the sensor. The integral of these curves is a divisor of density estimation equation for fixed sensors.

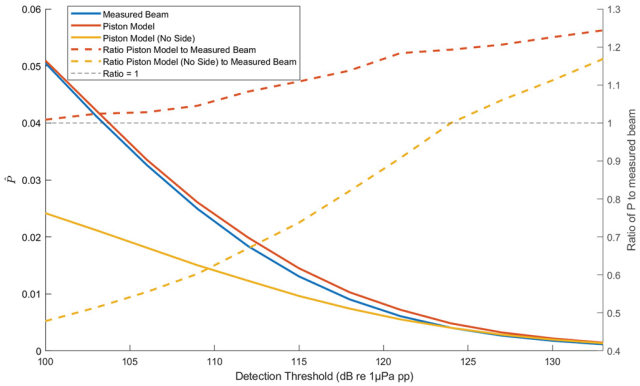

FIG. 8. (Color online) Probability of encounter ($\hat{P}$) modelled for different beam profiles as a function of detection threshold levels assuming a source level of 191 dB re 1 μPa pp. As expected, the probability of detection decreases with increasing detection thresholds for all beam profiles (left axis). The dotted lines show the ratio of the probability of detection of the piston model beam compared to the measured beam (right axis) and the grey horizontal line shows a ratio of 1.0, i.e., when detectability is equal to measured beam. This shows that the ratio of the beam profiles does not remain constant and changes depending whether side energy is assumed. This shows that the ratio of the probability of detection of the measured beam to each of the piston models does not remain constant. For example, at lower detection thresholds, the piston model with side energy has a probability of detection closer to the measured beam profile. However, if no side energy is assumed, then the piston model is closer to the measured beam at higher detection thresholds.

underestimating $\hat{P}$ by almost 30% at high detection thresholds, but only by around 5% at the lowest detection threshold source levels. The piston model with no side energy consistently underestimates $\hat{P}$.

In the above simulations it assumed that, as long as a click is above a certain amplitude threshold, it is detected. Figure 4 indicates a breakdown in the stereotypical spectra of NBHF clicks after around 20°. To test the potential consequence of this for PAM, beam volumes assuming a source level of 191 dB re 1 μPa pp and detection thresholds between 100 and 130 dB re 1 μPa pp were constructed and the percentage volume of >20° section of the beam calculated. Figure 9 shows that, at high detection thresholds, the percentage of distorted clicks which would be detected by a PAM receiver is very low <5%; however, at lower detection thresholds the number of distorted clicks is much larger, reaching ~50% for a threshold of 100 dB re 1 μPa pp. Thus, depending on detection threshold (and/or source level), between 5% and 50% of click detections on PAM instruments would likely contain significant spectral distortion compared to on-axis clicks.

IV. DISCUSSION

In this study we confirm that the tightly focused forward beam with a DI around 24 dB (Figs. 3, 5, and 6) of a harbour porpoise can be successfully modelled with a flat piston for angles between ±30° (Au, 2006; Koblitz *et al.*, 2012; Wisniewska *et al.*, 2015). However, at larger off-axis angles, the piston model underestimates the beam attenuation and

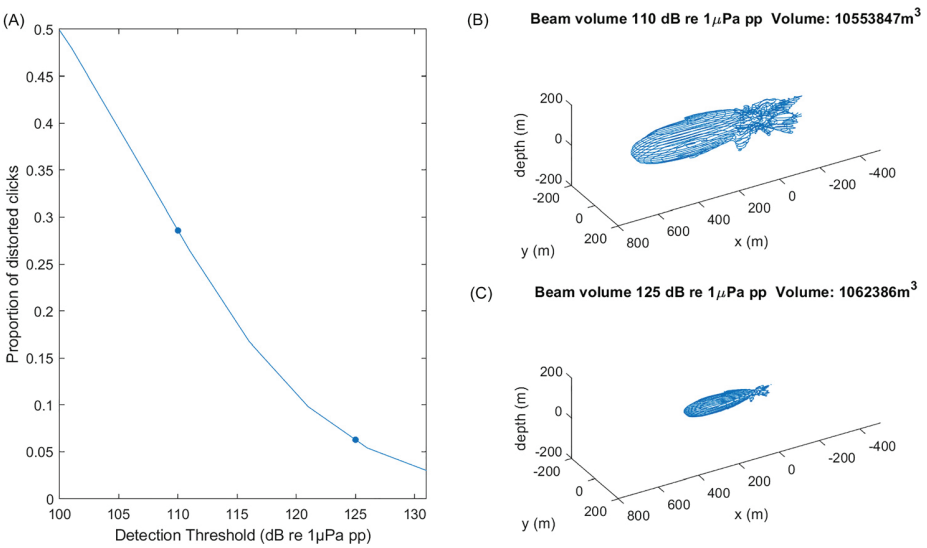

FIG. 9. (Color online) Plots showing the proportion of distorted clicks likely to be received by a PAM device and examples of beam volumes at differing detection thresholds. Plot (A) shows the proportion of distorted clicks as a function of detection threshold, i.e., the number of clicks beyond ±20° off-axis. The two points indicate the detection thresholds of the example beam volumes shown in plots (B) and (C) (110 and 125 dB re 1 μPa pp, respectively).

creates a series of side lobes [Figs. 5 and 6(B)], which were not evident in the measured beam profile. This side lobe suppression is likely formed through natural selection of harbour porpoise biosonars to (i) increase SL for the same power, (ii) reduce the amount of unwanted echoes in the form of clutter, (iii) provide a spatial filter to aide localisation, discrimination, and tracking of targets of interest, and (iv) to direct sound of the outgoing click away from the ears to minimise forward masking of faint echoes returning milliseconds after click emission (Schrøder *et al.*, 2017). Thus, from an evolutionary perspective, it is perhaps not surprising that harbour porpoise biosonar has evolved both to minimise side lobes and to outperform a flat piston model in beam attenuation with angle. Side lobes are created from edge effects of the modelled piston aperture. However, there is no morphological structure which exactly mirrors the theoretical piston aperture in a porpoise. Thus, a more realistic equivalent aperture may be something which is not entirely radially symmetric and does not have a hard edge, minimising side lobes. We also tested the hypothesis that porpoises might use their melon to change the effective piston aperture, which, when averaged over many clicks, will reduce side lobes. However, averaging out a piston model using the horizontal 5.5–7.4 cm (mean 6.5 cm) apertures, as reported by Koblitz *et al.* (2012), still leaves two small side lobes at $\pm 17°$. Even if clicks are filtered to almost pure tones (between 125 and 130 kHz), which should increase the size of any side lobes, no side lobes are evident in the data (see Supplemental Data 2).[1] This suggests that the piston model, at anything other than on-axis angles, does not fully account for the morphological complexity of toothed whales. Madsen *et al.* (2010) noted that clicks produced by the phonic lips in the porpoise are initially quite broadband before they are filtered by waveguide coupling with the melon to form the NBHF click. This notion is supported here, where we see that the typical narrowband spectra of a NBHF click breaks down at about 20° (Fig. 4), after which clicks are characterised by less predictable spectra.

When measuring the ASL farther off-axis, it appears that porpoises produce a diffuse back beam at 180° off-axis, some 30 dB down from the ASL. Madsen *et al.* (2010) have shown that harbour porpoises use their right pair phonic lips, which, in concert with air sacs and skull, collimate most of the produced sound energy through the melon to form a narrow forward beam. It is likely that some acoustic energy, especially when directed backwards, escapes this process, producing the back-end beam. Any baffled dipole source sound production system leads intrinsically to some diffuse waste acoustic energy as also observed for our Reson transducer calibrations (see Supplemental Material[1]). Thus, the diffuse and weak back-end beam of a harbour porpoise may simply be the remnants of a natural selection process towards a directional dipole source to work efficiently in a biosonar system for navigation or feeding. Whether it also serves a purpose of, for example, facilitating eavesdropping by calves to better trail their mothers during biosonar-based foraging dives may be plausible (Hansen *et al.*, 2008), but at this stage is entirely a speculative function for toothed whales at large. A similar weak back-end beam has also been reported in sperm whales (Zimmer *et al.*, 2005) with a very different bauplan of their hypertrophied sound producing nose.

While the deviations between predictions from the piston model and the measured beam profile are interesting from physiological and biological perspectives, they also have consequences for PAM and density estimation. The distortion in click spectra at larger off-axis angles in Fig. 4 will likely affect the performance of automated porpoise click classifiers, many of which are set up or trained for on-axis clicks (e.g., Cosentino *et al.*, 2019; Gillespie and Chappell, 2002). Such click classifiers may perform poorly with distorted off-axis clicks, which make up between ~5% and 50% of the detectible beam volume, depending on detection threshold as demonstrated in Fig. 9. Thus, whereas signal to noise ratio is generally considered the primary driver of relative classifier performance, for harbour porpoises and most likely other toothed whales, the proportion of correctly *classified* clicks may also be dependent on the orientation of the animal and the detection threshold/on-axis source level.

The difference between modelled and empirically measured beam profiles can also significantly influence the probability of encountering clicks if side energy (>30°) is not taken into account. In Fig. 7, the measured and full −90° to 90° piston beam models both have a higher probability of encountering a click at shorter ranges compared to the piston model without side energy. There are two interacting factors occurring here. First, the probability of *detecting* a click is increased slightly at shorter ranges because of the diffuse energy at the back of the measured and full piston beam profile. Second, as the range increases, the number of animals within each range bin also increases, and thus small increases in the probability of *detecting* a click result in a disproportionally larger increase in *encountering* a click ($\hat{P}$). However, as range continues to increase, eventually any side and back beam energy becomes undetectable—at this stage, the detectible energy is very similar for all beam profiles and thus at larger ranges $\hat{P}$ is almost identical. The point at which the back energy is no longer detected is therefore important in determining how different the overall value of $\hat{P}$ is. Thus, at the high detection thresholds shown in Fig. 8, any beam back energy will quickly fall below threshold and so the measured beam and piston model (no side) result in a similar $\hat{P}$. However, if the detection threshold decreases, the range at which back energy is detectible becomes larger, and thus the piston model without side or back energy increasingly underestimates $\hat{P}$ compared to the measured beam profile and piston model with side energy. At very high detection thresholds, both piston models have a slightly higher $\hat{P}$ likely due to the side lobes, which are not present in the measured beam, continuing to make a small contribution to detectability.

The probability of encountering a click is a direct divisor of the density estimation equation for static PAM

devices (Marques *et al.*, 2013) and so any differences in $\hat{P}$ propagate to estimates of animal density. Compared to the measured beam profile, the piston model with side energy over-estimated $\hat{P}$ by between ~5% and 25%, depending on the source level distribution of the animals in question. Assuming the piston model with no side energy and only a forward-facing beam resulted in an estimate of $\hat{P}$, which was between +20% and −50% compared to the measured beam profile. Thus, assuming a situation in which harbour porpoises are clicking at a source level of 191 dB re 1 μPa pp and a typical detection threshold of 110 dB re 1 μPa pp, the piston model with no side energy would have almost doubled the density estimate but a piston model assuming both side and back energy would be roughly correct. Although the exact error in the modelling of the probability detection will be dependent on the survey type and combination of the many possible input model parameters used in a Monte Carlo detection probability simulation, this indicates that beam profiles are potentially a significant source of error in these models.

Empirical measures of the probability of detection are always preferred because they account for variation in beam pattern, propagation, source level, etc. However, empirical measurements are often difficult to obtain and simulation provides an alternative methodology to obtain measures of $\hat{P}$. Here we have shown that, if using simulation methods for density estimation is indeed required, direct measurements of the full 4π radiation pattern is preferential wherever possible; if these are not available then an accurate piston model assuming both side and back energy should be used. Alternatively, a forward piston model with a no side energy but combined with a higher detection threshold may also be accurate.

V. CONCLUSION

Harbour porpoises produce an intense forward beam and much lower level diffuse acoustic energy to their rear. The beam profile of a porpoise, relevant for assessing echolocation performance, can be modelled successfully with a piston model at ±30° around the beam axis, but at off-axis angles of more than ±30°, the measured beam shows greater attenuation than the piston model predicts, and no distinct side lobes can be observed. Thus, porpoises have a slightly narrower acoustic field of view than predicted by the piston model. We also document a weak and diffuse back beam with ASLs some 30 dB below the SL. We show with modelling that there can be a substantially higher probability of detection when using the empirically measured beam profile with a weak back-end beam, as opposed to the standard piston model, but this is dependent on detection threshold and whether side and back energy in the piston model is assumed. As such, this study highlights the need for synergy between sensory physiology, functional morphology and the continued development of PAM methodologies and their subsequent interpretations, especially in the application of density estimation.

ACKNOWLEDGMENTS

Thanks to the animal trainers J. Kristensen and F. Johansson for helping run the trials at Fjord & Bælt. Thanks to M. Wahlberg and J. Tougaard for lending hydrophones and SoundTraps, and to M. Johnson for access to a DTAG-4. Thanks to K. Beedholm, M. Wahlberg, J. Tougaard, M. Ladegaard, V. Janik, P. White and S. Northridge for helpful discussions and comments. Equipment and training time were funded by a Danish Research Council FNU grant to PTM. Thanks to our reviewers who were both very helpful and made this a better manuscript. The animals used in this study are maintained by Fjord&Bælt, Kerteminde, Denmark, under Permit Nos. SN 343/FY-0014 and 1996-3446-0021 from the Danish Forest and Nature Agency, Danish Ministry of Environment. All authors conceived the idea; J.D.J.M., C.E.M., and P.T.M. designed methodology; J.D.J.M. and C.E.M. collected the data; J.D.J.M. and C.E.M. analysed the data; J.D.J.M. lead the writing of the manuscript; D.G. advised on density estimation and PAM aspects. All authors contributed critically to the drafts and gave final approval for publication.

[1]See supplemental material at https://doi.org/10.1121/10.0001376 for a description of the validation experiment of the beam measurement methodology and for a brief analysis of the beam profile applying a narrow filter to all measurement in order to search for side lobes.

Ainslie, M. A., and McColm, J. G. (**1998**). "A simplified formula for viscous and chemical absorption in sea water," J. Acoust. Soc. Am. **103**, 1671–1672.

Aroyan, J. L., Cranford, T. W., Kent, J., and Norris, K. S. (**1992**). "Computer modeling of acoustic beam formation in Delphinusdelphis," J. Acoust. Soc. Am. **92**, 2539–2545.

Au, W. W. L. (**1993**). *The Sonar of Dolphins, Acoustics Australia* (Springer, New York).

Au, W. W. L. (**2006**). "Acoustic radiation from the head of echolocating harbor porpoises (Phocoena phocoena)," J. Exp. Biol. **209**, 2726–2733.

Au, W. W. L., Branstetter, B., Moore, P. W., and Finneran, J. J. (**2012a**). "The biosonar field around an Atlantic bottlenose dolphin (Tursiops truncatus)," J. Acoust. Soc. Am. **131**, 569–576.

Au, W. W. L., Branstetter, B., Moore, P. W., and Finneran, J. J. (**2012b**). "Dolphin biosonar signals measured at extreme off-axis angles: Insights to sound propagation in the head," J. Acoust. Soc. Am. **132**, 1199–1206.

Au, W. W. L., Floyd, R. W., and Haun, J. E. (**1978**). "Propagation of Atlantic bottlenose dolphin echolocation signals," J. Acoust. Soc. Am. **64**, 411–422.

Au, W. W., and Herzing, D. L. (**2003**). "Echolocation signals of wild Atlantic spotted dolphin (*Stenella frontalis*)," J. Acoust. Soc. Am. **113**, 598–604.

Au, W. W. L., Kastelein, R. A., Rippe, T., and Schooneman, N. M. (**1999**). "Transmission beam pattern and echolocation signals of a harbor porpoise (Phocoena phocoena)," J. Acoust. Soc. Am. **106**, 3699–3705.

Au, W. W., and Scheifele, P. M. (**1994**). "The sonar of dolphins," J. Acoust. Soc. Am. **95**, 585–586.

Bassett, H. R., Baumann, S., Campbell, G. S., Wiggins, S. M., and Hildebrand, J. A. (**2009**). "Dall's porpoise (Phocoenoides dalli) echolocation click spectral structure," J. Acoust. Soc. Am. **125**, 2677–2677.

Beedholm, K., and Møhl, B. (**2006**). "Directionality of sperm whale sonar clicks and its relation to piston radiation theory," J. Acoust. Soc. Am. **119**, EL14–EL19.

Borchers, D. L., Stevenson, B. C., Kidney, D., Thomas, L., and Marques, T. A. (**2015**). "A unifying model for capture–recapture and distance sampling surveys of wildlife populations," J. Am. Stat. Assoc. **110**, 195–204.

Branstetter, B. K., Moore, P. W., Finneran, J. J., Tormey, M. N., and Aihara, H. (**2012**). "Directional properties of bottlenose dolphin (Tursiops

truncatus) clicks, burst-pulse, and whistle sounds," J. Acoust. Soc. Am. **131**, 1613–1621.

Carlén, I., Thomas, L., Carlström, J., Amundin, M., Teilmann, J., Tregenza, N., Tougaard, J., Koblitz, J. C., Sveegaard, S., Wennerberg, D., Loisa, O., Dähne, M., Brundiers, K., Kosecka, M., Kyhn, L. A., Ljungqvist, C. T., Pawliczka, I., Koza, R., Arciszewski, B., Galatius, A., Jabbusch, M., Laaksonlaita, J., Niemi, J., Lyytinen, S., Gallus, A., Benke, H., Blankett, P., Skóra, K. E., and Acevedo-Gutiérrez, A. (**2018**). "Basin-scale distribution of harbour porpoises in the Baltic Sea provides basis for effective conservation actions," Biol. Conserv. **226**, 42–53.

Clausen, K. T., Wahlberg, M., Beedholm, K., Deruiter, S., and Madsen, P. T. (**2011**). "Click communication in harbour porpoises Phocoena phocoena," Bioacoustics **20**, 1–28.

Cosentino, M., Guarato, F., Tougaard, J., Nairn, D., Jackson, J. C., and Windmill, J. F. C. (**2019**). "Porpoise click classifier (PorCC): A high-accuracy classifier to study harbour porpoises (Phocoena phocoena) in the wild," J. Acoust. Soc. Am. **145**, 3427–3434.

Cranford, T. W. (**2000**). In *Search of Impulse Sound Sources in Odontocetes* (Springer, New York), pp. 109–155.

Cranford, T. W., Amundin, M., and Norris, K. S. (**1996**). "Functional morphology and homology in the odontocete nasal complex: Implications for sound generation," J. Morphol. **228**, 223–285.

Deruiter, S. L., Bahr, A., Blanchet, M.-A., Hansen, S. F., Kristensen, J. H., Madsen, P. T., Tyack, P. L., and Wahlberg, M. (**2009**). "Acoustic behaviour of echolocating porpoises during prey capture," J. Exp. Biol. **212**, 3100–3107.

Finneran, J. J., Branstetter, B. K., Houser, D. S., Moore, P. W., Mulsow, J., Martin, C., and Perisho, S. (**2014**). "High-resolution measurement of a bottlenose dolphin's (Tursiops truncatus) biosonar transmission beam pattern in the horizontal plane," J. Acoust. Soc. Am. **136**, 2025–2038.

Frasier, K. E., Wiggins, S. M., Harris, D., Marques, T. A., Thomas, L., and Hildebrand, J. A. (**2016**). "Delphinid echolocation click detection probability on near-seafloor sensors," J. Acoust. Soc. Am. **140**, 1918–1930.

Gillespie, D., and Chappell, O. (**2002**). "An automatic system for detecting and classifying the vocalisations of harbour porpoises," Bioacoustics **13**, 37–61.

Gillespie, D., Gordon, J., Mchugh, R., Mclaren, D., Mellinger, D., Redmond, P., Thode, A., Trinder, P., and Deng, X. Y. (**2008**). "PAMGUARD: Semiautomated, open source software for real-time acoustic detection and localisation of cetaceans," Proc. Inst. Acoust. **30**, 54–62.

Götz, T., Antunes, R., and Heinrich, S. (**2010**). "Echolocation clicks of free-ranging Chilean dolphins (Cephalorhynchus eutropia)," J. Acoust. Soc. Am. **128**, 563–566.

Hansen, M., Wahlberg, M., and Madsen, P. T. (**2008**). "Low-frequency components in harbor porpoise (Phocoena phocoena) clicks: Communication signal, by-products, or artifacts?," J. Acoust. Soc. Am. **124**, 4059–4068.

Jensen, F. H., Johnson, M., Ladegaard, M., Wisniewska, D. M., and Madsen, P. T. (**2018**). "Narrow acoustic field of view drives frequency scaling in toothed whale," Biosonar. Curr. Biol. **28**, 3878–3885.

Jensen, F. H., Wahlberg, M., Beedholm, K., Johnson, M., de Soto, N. A., and Madsen, P. T. (**2015**). "Single-click beam patterns suggest dynamic changes to the field of view of echolocating Atlantic spotted dolphins (Stenella frontalis) in the wild," J. Exp. Biol. **218**, 1314–1324.

Johnson, M., Madsen, P. T., Zimmer, W. M. X., de Soto, N. A., and Tyack, P. L. (**2004**). "Beaked whales echolocate on prey," Proc. R. Soc. Lond. Ser. B Biol. Sci. **271**, S383–S386.

Johnson, M., Madsen, P. T., Zimmer, W. M. X., de Soto, N. A., and Tyack, P. L. (**2006**). "Foraging Blainville's beaked whales (Mesoplodon densirostris) produce distinct click types matched to different phases of echolocation," J. Exp. Biol. **209**, 5038–5050.

Johnson, M. P., and Tyack, P. L. (**2003**). "A digital acoustic recording tag for measuring the response of wild marine mammals to sound," IEEE J. Ocean. Eng. **28**, 3–12.

Koblitz, J. C., Stilz, P., Rasmussen, M. H., and Laidre, K. L. (**2016**). "Highly directional sonar beam of narwhals (Monodon monoceros) measured with a vertical 16 hydrophone array," PLoS One **11**, e0162069.

Koblitz, J. C., Wahlberg, M., Stilz, P., Madsen, P. T., Beedholm, K., and Schnitzler, H.-U. (**2012**). "Asymmetry and dynamics of a narrow sonar beam in an echolocating harbor porpoise," J. Acoust. Soc. Am. **131**, 2315–2324.

Küsel, E. T., Mellinger, D. K., Thomas, L., Marques, T. A., Moretti, D., and Ward, J. (**2011**). "Cetacean population density estimation from single fixed sensors using passive acoustics," J. Acoust. Soc. Am. **129**, 3610–3622.

Kyhn, L. A., Tougaard, J., Beedholm, K., Jensen, F. H., Ashe, E., Williams, R., and Madsen, P. T. (**2013**). "Clicking in a killer whale habitat: Narrow-band, high-frequency biosonar clicks of harbour porpoise (Phocoena phocoena) and Dall's porpoise (Phocoenoides dalli)," PLoS One **8**, e63763.

Kyhn, L. A., Tougaard, J., Jensen, F., Wahlberg, M., Stone, G., Yoshinaga, A., Beedholm, K., and Madsen, P. T. (**2009**). "Feeding at a high pitch: Source parameters of narrow band, high-frequency clicks from echolocating off-shore hourglass dolphins and coastal Hector's dolphins," J. Acoust. Soc. Am. **125**, 1783–1791.

Ladegaard, M., Jensen, F. H., Beedholm, K., Da Silva, V. M. F., and Madsen, P. T. (**2017**). "Amazon river dolphins (Inia geoffrensis) modify biosonar output level and directivity during prey interception in the wild," J. Exp. Biol. **220**, 2654–2665.

Ladegaard, M., Jensen, F. H., de Freitas, M., Ferreira da Silva, V. M., and Madsen, P. T. (**2015**). "Amazon river dolphins (Inia geoffrensis) use a high-frequency short-range biosonar," J. Exp. Biol. **218**, 3091–3101.

Ladegaard, M., and Madsen, P. T. (**2019**). "Context-dependent biosonar adjustments during active target approaches in echolocating harbour porpoises," J. Exp. Biol. **222**, 206169.

Li, S., Wang, D., Wang, K., Akamatsu, T., Ma, Z., and Han, J. (**2007**). "Echolocation click sounds from wild inshore finless porpoise (Neophocaena phocaenoides sunameri) with comparisons to the sonar of riverine N. P. asiaeorientalis," J. Acoust. Soc. Am. **121**, 3938–3946.

Madsen, P. T., Carder, D. A., Bedholm, K., and Ridgway, S. H. (**2005**). "Porpoise clicks from a sperm whale nose—Convergent evolution of 130 kHz pulses in toothed whale sonars?," Bioacoustics **15**, 195–206.

Madsen, P. T., de Soto, N. A., Arranz, P., and Johnson, M. (**2013**). "Echolocation in Blainville's beaked whales (Mesoplodon densirostris)," J. Comp. Physiol. A Neuroethol. Sens. Neural Behav. Physiol. **199**, 451–469.

Madsen, P. T., Lammers, M., Wisniewska, D., and Beedholm, K. (**2013**). "Nasal sound production in echolocating delphinids (Tursiops truncatus and Pseudorca crassidens) is dynamic, but unilateral: Clicking on the right side and whistling on the left side," J. Exp. Biol. **216**, 4091–4102.

Madsen, P. T., and Surlykke, A. (**2013**). "Functional convergence in bat and toothed whale biosonars," Physiology **28**, 276–283.

Madsen, P. T., and Wahlberg, M. (**2007**). "Recording and quantification of ultrasonic echolocation clicks from free-ranging toothed whales," Deep Sea Res. Part I Oceanogr. Res. Papers **54**, 1421–1444.

Madsen, P. T., Wisniewska, D., and Beedholm, K. (**2010**). "Single source sound production and dynamic beam formation in echolocating harbour porpoises (Phocoena phocoena)," J. Exp. Biol. **213**, 3105–3110.

Malinka, C. E., Atkins, J., Johnson, M. P., Tønnesen, P., Dunn, C. A., Claridge, D. E., de Soto, A. N., and Madsen, P. T. (**2020**). "An autonomous hydrophone array to study the acoustic ecology of deep-water toothed whales," Deep Sea Res. Part I Oceanogr. Res. Papers **158**, 103233.

Marques, T. A., Thomas, L., Martin, S. W., Mellinger, D. K., Ward, J. A., Moretti, D. J., Harris, D., and Tyack, P. L. (**2013**). "Estimating animal population density using passive acoustics," Biol. Rev. Camb. Philos. Soc. **88**, 287–309.

Martin, M. J., Gridley, T., Elwen, S. H., and Jensen, F. H. (**2018**). "Heaviside's dolphins (Cephalorhynchus heavisidii) relax acoustic crypsis to increase communication range," Proc. R. Soc. B Biol. Sci. **285**, 20181178.

Melcón, M. L., Failla, M., Iñíguez, M. A., Melcón, M. L., Failla, M., and Iñíguez, M. A. (**2012**). "Echolocation behavior of franciscana dolphins (Pontoporia blainvillei) in the wild," J. Acoust. Soc. Am. **131**, EL448–EL453.

Møhl, B., Wahlberg, M., Madsen, P. T., Heerfordt, A., and Lund, A. (**2003**). "The monopulsed nature of sperm whale clicks," J. Acoust. Soc. Am. **114**, 1143–1154.

Møhl, B., Wahlberg, M., Madsen, P. T., Miller, L. A., and Surlykke, A. (**2000**). "Sperm whale clicks: Directionality and source level revisited," J. Acoust. Soc. Am. **107**, 638–648.

Morisaka, T., and Connor, R. C. (**2007**). "Predation by killer whales (Orcinus orca) and the evolution of whistle loss and narrow-band high frequency clicks in odontocetes," J. Evol. Biol. **20**, 1439–1458.

Nelder, J. A., and Mead, R. (**1965**). "A simplex method for function minimization," Comput. J. **7**, 308–313.

Park, S. W., Linsen, L., Kreylos, O., Owens, J. D., and Hamann, B. (**2006**). "Discrete Sibson interpolation," IEEE Trans. Vis. Comput. Graph. **12**, 243–253.

Press, W. H., and Teukolsky, S. A. (**1990**). "Savitzky-Golay smoothing filters," Comput. Phys. **4**, 669–672.

Rasmussen, M. H., Miller, L. A., and Au, W. W. (**2002**). "Source levels of clicks from free-ranging white-beaked dolphins (*Lagenorhynchus albirostris* Gray 1846) recorded in Icelandic waters," J. Acoust. Soc. Am. **111**, 1122–1125.

Rasmussen, M. H., Wahlberg, M., and Miller, L. A. (**2004**). "Estimated transmission beam pattern of clicks recorded from free-ranging white-beaked dolphins (*Lagenorhynchus albirostris*)," J. Acoust. Soc. Am. **116**, 1826–1831.

Rodrigues, O. (**1840**). "Es lois géometriques qui regissent les déplacements d' un systéme solide dans l' espace, et de la variation des coordonnées provenant de ces déplacement considérées indépendant des causes qui peuvent les produire" ("Geometric laws which govern the displacements of a solid system in space, and the variation of the coordinates coming from these displacements considered independent of the causes which can produce them"), J. Math. Pures Appl. **5**, 380–440.

Schrøder, A. E. M., Beedholm, K., and Madsen, P. T. (**2017**). "Time-varying auditory gain control in response to double-pulse stimuli in harbour porpoises is not mediated by a stapedial reflex," Biol. Open **6**, 525–529.

Silber, G. K. (**1991**). "Acoustic signals of the vaquita (Phocoena sinus)," Aquat. Mamm. **17**, 130–133.

Smith, A. B., Kloepper, L. N., Yang, W.-C., Huang, W.-H., Jen, I.-F., Rideout, B. P., and Nachtigall, P. E. (**2016**). "Transmission beam characteristics of a Risso's dolphin (Grampus griseus)," J. Acoust. Soc. Am. **139**, 53–62.

Sørensen, P. M., Wisniewska, D. M., Jensen, F. H., Johnson, M., Teilmann, J., and Madsen, P. T. (**2018**). "Click communication in wild harbour porpoises (Phocoena phocoena)," Sci. Rep. **8**, 9702.

Stevenson, B. C. (**2016**). "Methods in spatially explicit capture-recapture," Ph.D. thesis, University of St. Andrews, St. Andrews, UK.

Stevenson, B. C., Borchers, D. L., Altwegg, R., Swift, R. J., Gillespie, D. M., and Measey, G. J. (**2015**). "A general framework for animal density estimation from acoustic detections across a fixed microphone array," Methods Ecol. Evol. **6**, 38–48.

Strother, G. K., and Mogus, M. (**1970**). "Acoustical beam patterns for bats: Some theoretical considerations," J. Acoust. Soc. Am. **48**, 1430–1432.

Verfuß, U. K., Miller, L. A., Pilz, P. K. D., and Schnitzler, H. U. (**2009**). "Echolocation by two foraging harbour porpoises (Phocoena phocoena)," J. Exp. Biol. **212**, 823–834.

Villadsgaard, A., Wahlberg, M., and Tougaard, J. (**2007**). "Echolocation signals of wild harbour porpoises, Phocoena phocoena," J. Exp. Biol. **210**, 56–64.

Wisniewska, D. M., Johnson, M., Beedholm, K., Wahlberg, M., and Madsen, P. T. (**2012**). "Acoustic gaze adjustments during active target selection in echolocating porpoises," J. Exp. Biol. **215**, 4358–4373.

Wisniewska, D. M., Ratcliffe, J. M., Beedholm, K., Christensen, C. B., Johnson, M., Koblitz, J. C., Wahlberg, M., and Madsen, P. T. (**2015**). "Range-dependent flexibility in the acoustic field of view of echolocating porpoises (Phocoena phocoena)," Elife **4**, 1–16.

Yovel, Y., Falk, B., Moss, C. F., and Ulanovsky, N. (**2010**). "Optimal localization by pointing off axisl," Science **327**, 701–704.

Zimmer, W. M. X., Harwood, J., Tyack, P. L., Johnson, M. P., and Madsen, P. T. (**2008**). "Passive acoustic detection of deep-diving beaked whales," J. Acoust. Soc. Am. **124**, 2823–2832.

Zimmer, W. M. X., Tyack, P. L., Johnson, M. P., and Madsen, P. T. (**2005**). "Three-dimensional beam pattern of regular sperm whale clicks confirms bent-horn hypothesis," J. Acoust. Soc. Am. **117**, 1473–1485.

Chapter V.

Spatial Filtering

Malinka, C. E., Rojano-Donate, L., & P. T. Madsen. (2021). "Directional biosonar beams allow echolocating harbour porpoises to actively discriminate and intercept closely-spaced targets," (*Submitted manuscript*).

Directional biosonar beams allow echolocating harbour porpoises to actively discriminate and intercept closely-spaced targets

Authors (ORCHID ID)

Chloe E Malinka[1*] (0000-0003-0138-8388),
Laia Rojano-Doñate[1] (0000-0002-1438-0281),
Peter T Madsen[1] (0000-0002-5208-5259)

[1] Zoophysiology, Dept. Biology, Aarhus University, Aarhus, Denmark.

* Author email for correspondence: chloe.e.malinka@bio.au.dk

Keywords

Echolocation · biosonar · acoustic gaze · acoustic field of view · auditory scene analysis · echo stream

Abstract

Echolocating toothed whales face the problem that high sound speeds in water mean that echoes from closely-spaced targets will arrive at time delays within their reported auditory integration time of some 264 µsec. Here we test the hypothesis that echolocating harbour porpoises cannot resolve and discriminate targets within a clutter interference zone given by their integration time. To do this, we trained two harbour porpoises (*Phocoena phocoena*) to actively approach and choose between two spherical targets at four varying inter-target distances (13.5, 27, 56 and 108 cm) in a two-alternative forced-choice task. The free-swimming, blindfolded porpoises were tagged with a sound and movement tag (DTAG4) to record their echoic scene and acoustic outputs. The known ranges between targets and the porpoise, combined with the sound levels received on target-mounted hydrophones revealed how they controlled their acoustic gaze. When targets were close together and the discrimination task was more difficult due to smaller echo time delays and lower echo level ratios between the targets, buzzes were longer and started from farther away, source levels were reduced at short ranges, and the porpoises clicked faster, scanned across the targets more, and delayed making their discrimination decision until closer to the target. We conclude that harbour porpoises can resolve and discriminate closely-spaced targets, suggesting a clutter rejection zone much shorter than their auditory integration time below which toothed whales are reportedly unable to parse independent echo streams, and that such clutter rejection is greatly aided by spatial filtering with their directional biosonar beam.

Introduction

Echolocating animals estimate range to a target via the two-way travel time (TWTT) between emission of a biosonar pulse and return of the target echo (Hartridge, 1945; Cahlander et al., 1964; Simmons, 1973), calling for acute auditory time resolution and short integration times (Moore et al., 1984). Within this framework of converting TWTT to spatial target representation along a range axis are the processes of ranging (*e.g*. Penner, 1988; Thomas and Turl, 1990), jitter detection (*e.g*. Simmons, 1979; Moss and Schnitzler, 1989;

Finneran et al., 2020), and resolving the target echo of interest from a possible multitude of clutter echoes (*e.g*. Sümer et al., 2009; Brinkløv et al., 2010; Warnecke et al., 2014). Owing to the high sound speeds in air and water, echolocating animals must resolve closely timed echoes to effectively forage with echolocation near acoustic clutter (Madsen and Surlykke, 2013). Ultimately, there is a lower echo delay limit, where echolocators face difficulty in resolving target echoes from clutter echoes, and this forms the clutter interference zone (Simmons et al., 1988, 1989).

A recent psychophysical study on a species of leaf-nosed bat (*Phyllostomus discolour*) showed that echoes of similar levels from closely-spaced targets cannot be resolved when the time delays are on par with, or are shorter than, the likely auditory integration time of some 2 ms reported for active bat biosonar (in big brown bats, *Eptesicus fuscus*; Surlykke and Bojesen, 1996), forming a clutter interference zone of some 34 cm on the same range axis as the target of interest (Wagenhäuser et al., 2020). This problem is exacerbated for toothed whales that echolocate in a medium with a sound speed of around 1500 m/s – about 4.5 times faster than for echolocators in air. Perhaps to remedy that problem, or to employ an integration time in keeping with their much shorter echolocation signals, the auditory integration time of some 264 µs of the toothed whale biosonar system is about an order of magnitude shorter than for FM bats (Vel'min and Dubrovskiy, 1975; Vel'min, 1976; Moore et al., 1984; Au et al., 1988). If this integration time, as implied in the bat studies, is a measure of the clutter interference zone (the region where prey echoes overlap with clutter echoes; Schnitzler and Kalko, 2001), it would follow that toothed whales cannot resolve targets with echo delays shorter than 264 µs, corresponding to a target-clutter spacing of about 20 cm on the same range axis. The logic behind that prediction is that the integration time is estimated by testing the detection thresholds for click pairs with varying delays. When the delays get short enough, the detection threshold is lowered compared to single clicks of the same amplitude, and the delay at which the threshold starts to decrease defines the integration time (Au et al., 1988). Another interpretation is that it is the time window beyond which gap detection or pulse-pair experiments indicate separate signals; here, two echoes within the integration time become part of the same auditory percept, precluding the resolution and discrimination of two targets (Branstetter et al., 2020). Accordingly, we hypothesize that the odontocete auditory integration time marks a point of reference below which echolocation performance would deteriorate.

The ability to discriminate between ensonified targets is dependent not just on temporal resolution, but also spatial and spectral resolutions in their biosonar system (Schmidt, 1992; Au, 1993; Au et al., 2009; Branstetter et al., 2020). In the aforementioned psychophysical study on leaf-nosed bats (Wagenhäuser et al., 2020), it was observed that when echo level differences between different auditory streams were very high (> 50 dB), the bats could cope with time delays shorter than the apparent auditory integration time and still resolve the targets. The flight paths of free-flying bats in cluttered environments suggest that the echoic interpretation of a target is enhanced by echo level variations that would arise from a variable azimuth and/or elevation of the targets relative to beam center (Moss et al., 2011; Falk et al., 2014; Taub and Yovel, 2020), therefore hinting at the use of their directional beam as part of a spatial filter in an echolocation task (Moss and Surlykke, 2010; Linnenschmidt and Wiegrebe, 2016). The highly directional biosonar beam of toothed whales (with DIs of ~24-32 dB) is much narrower than that of bats (with DIs of ~10-16 dB) (Madsen and Surlykke, 2013; Jakobsen et al., 2013; Jensen et al., 2018), and thus would yield greater differences in the returning echo levels for the same target spacing and ranges.

Here, we conducted a clutter interference experiment to psychoacoustically investigate temporal and spatial masking arising from a distracting object. Specifically, we tested the hypothesis that echolocating harbour porpoises cannot resolve and discriminate two targets when they are closer than a clutter interference zone defined by their auditory integration time. To do that, we presented free-swimming, tagged

porpoises with a two-alternative forced-choice target discrimination task using targets at four different inter-target spacings, offering discrimination tasks of varying difficulty, owing to the increased clutter from the distracting target at close range. We predicted that when targets are more closely-spaced, the auditory stream segregation task will be more difficult as reflected in the porpoises' echolocation performance or effort to complete the task. We further predicted that, despite the presumed advantage of a highly directional beam, that successful discrimination between targets will break down as the difference in echo time delays nears the auditory integration time.

Materials and Methods

Experimental procedure

The study was carried out on captive harbour porpoises (*Phocoena phocoena*, Linnaeus 1758) at Fjord & Bælt, Kerteminde, Denmark. Two porpoises participated in the experiments: Freja and Sif, both female, and at the facility since both were ~1-2 years old in April 1997 and July 2004, respectively (Lockyer, 2003; Wisniewska et al., 2015). The porpoises were housed in a ~30 x 10 m outdoor netted enclosure in Kerteminde harbour.

Echolocation clicks were recorded as the porpoises closed in on targets while performing a two-alternative forced-choice task (Schustermann, 1980). The recording setup included hydrophones on the targets and high-resolution movement and sound recording tags on the porpoises. The task involved a discrimination between two simultaneously presented spherical targets (5.08 cm diameter; Fig. 1) of different material (aluminium or stainless steel), with similar target strengths of -39 and -37 dB, respectively (Wisniewska et al., 2012). A spherical target was chosen (instead of a cylindrical target, for example), because the target strength of a sphere is independent of aspect. The porpoises were trained to always target the aluminium sphere, indicating their selection by touching it with the tip of its rostrum, and wore a blindfold (opaque, silicone eyecups) to exclude visual cues from informing their biosonar-informed decisions. Both animals had extensive experience with wearing a tag and eyecups in previous psychoacoustic experiments (*e.g*. Verfuß et al., 2005; DeRuiter et al., 2009; Linnenschmidt et al., 2012; Wisniewska et al., 2012). Note that target discrimination abilities of the study porpoises have been previously shown (*e.g*. Wisniewska et al., 2012); the purpose of including a secondary target in this experiment was to make it so that multiple targets would be within the beam swath, thereby introducing an acoustic distractor or clutter by means of an additional, simultaneous echo stream.

The porpoises were free-swimming during the echolocation task to avoid obscuring any variability and/or richness in biosonar behaviours, as is likely the case for artificiality-imposing experimental designs involving stationary animals (Moore et al., 2008). Additionally, the free-swimming set-up provides information on how the animal uses echolocation in tasks that are both dynamic and more closely resemble those encountered in the wild (Houser et al., 2005). No rolling behaviour was observed during approaches, and so all quantifications concern the horizontal beam pattern, of which no asymmetry was accounted for.

For each trial, targets were presented at one of four different inter-target distances (target centers could be spaced 108, 54, 27, or 13.5 cm apart; Fig. 1A). Targets were suspended from microfilament lines suspended from an out-of-water metal frame, and lowered into the water to a depth of 1 m at the start of each trial (as in both Wisniewska et al., 2012, and Hermannsen, 2019; Figs. 1 A, B). During one trial, an individual porpoise was instructed to perform the discrimination task (Fig. 1D), whereby the trainer sent the porpoise to the other side of the ~8 x ~13 m experimental pool to the targets. Upon targeting the aluminium

sphere, the behaviour was bridged with a whistle to indicate a correct response, and the porpoise then returned to the starting station for fish reinforcement. No bridge or fish reward was given for the incorrect response of targeting the steel sphere. The frame suspending the targets was lifted out of the water after each trial. The distances between the targets varied from trial to trial. For each session, a Gellerman pseudo-random schedule (Gellerman, 1933) randomised both the distance between targets, as well as the order in which targets were presented (left/right) to avoid "focal expectancy" (*sensu* Vandenberghe et al., 2001). A total of 120 trials occurred over three days in July 2017. Trials for each porpoise were run in sessions with a maximum of 12 trials per session, and 2 sessions per porpoise, per day.

The porpoises were free to modify their swim paths to alter both the spatial and temporal separation of the targets, but the extent to which this could be achieved was limited by the inter-target distance (Fig. 1B). To maximize differences in the time delays of the returning echoes, the porpoise must approach from the side, and to maximize the angular offset to the distracting target, the porpoise must conduct a direct approach perpendicular to the axis defined by the line connecting both targets (Fig. 1B). The bearing offset between the on-axis target and the distracting target is shown for all on-axis clicks (Figs. 1C), demonstrating the maximal angular separation of targets that could be achieved with each inter-target spacing. Porpoises must be closer to the targets in order to obtain greater angular separation of the two targets, and this pattern is for physical reasons emphasized for smaller inter-target distances (Fig. 1C). Additionally, at close inter-target distances, the porpoise needs to be closer to the targets to obtain greater differences in both echo time delays (ΔT) and echo levels (ΔEL) reflecting off of the two targets; at large ranges, range to each target will be more similar and the angular offset between targets will be small. Note that for the smallest inter-target distance value of 13.5 cm, differences in echo time delays between the targets are never greater than the estimated auditory integration time of ~264 µsec (Vel'min and Dubrovskiy, 1975; Vel'min, 1976; Moore et al., 1984; Au et al., 1988), no matter how close the porpoise gets to the target of interest.

Echolocation clicks received at the targets were recorded by custom-built cylindrical hydrophones (flat frequency response ±2 dB between 100 and 160 kHz) mounted 3 cm above the centre of each sphere (Figs. 1 A, D). These hydrophones were calibrated against a TC-4034 hydrophone (Teledyne Reson, Slangerup, Denmark) by using simulated porpoise clicks, and were found to have a sensitivity of -211 dB re 1 V/µPa. Both hydrophones were connected to a custom-built amplifier box with +40 dB of gain, where an anti-aliasing filter (180 kHz, 4-pole, low-pass) and a pre-whitening high-pass filter (1 kHz, 1-pole) were applied. In the recording hut (Fig. 1A) signals on each target were digitized with a multifunction acquisition device (National Instruments USB-6251, Austin, TX, USA), sampling at 500 kHz per channel, 16 bit resolution and saved as files with a custom-built LabView program (National Instruments, TX, USA).

Echolocation clicks and returning echoes were also recorded by an on-animal sound and movement tag (DTAG-4; Johnson and Tyack, 2003; Johnson et al*.,* 2009; www.soundtags.org) non-invasively attached via suction cups behind the sound generating nasal complex and immediately posterior to the blow hole. The multi-sensor digital recording tag continuously sampled audio data on a single hydrophone at 576 kHz (flat frequency response $\pm$2 dB from 0.4 to 150 kHz). The combined recording of echolocation - both on the animal and on the targets - allowed for insights into sensory focus (Fig. 2). The time delays between click emission and echo reception allowed for the tag to both provide range-to-target information and to record the echoic scene as experienced by the porpoise (Fig. 2E). Thus, the complete acoustic circuit could be observed via recording the acoustic information available to the porpoise. While the tag also recorded data from its pressure sensor, tri-axial accelerometers, and tri-axial gyroscopes, its placement behind the blowhole prohibited the measuring any movement signatures arising from head-scanning.

At the start of each trial, a short high-frequency sweep signal (from 180 to 210 kHz), above the effective hearing range of harbour porpoises (Kastelein et al., 2002), was projected into the water to time-synchronise the tag data with the target-hydrophone data. The sweeps were generated by the sound-recording multifunction device, tightly synchronized to the onset of recording of the on-target hydrophone signals, which were driven off of the same timer. Trials were additionally monitored underwater with a GoPro Hero 2 video camera (GoPro Inc, San Mateo, CA) mounted 2.5 m behind the target frame.

Data analysis

Data processing and acoustic analysis were conducted in MATLAB (version 8.5, The Mathworks, Natick, MA, USA). The hydrophone and tag recordings were time-aligned for each trial, using the synchronization sweeps, followed by manual confirmation using the inter-click intervals (ICIs, defined as the time between each click and the previous one) unique to each trial.

Each porpoise echolocation click was identified using a supervised click detector run on both the filtered acoustic data on the tag and on the target-hydrophone recordings (90-180 kHz 4-pole Butterworth band-pass filter). Received levels (RLs) on the targets were quantified as the clip level of the recording system (171 dB re 1 µPa) + $20 \cdot \log_{10}$(peak-to-peak amplitude). Relative peaks in the RLs of consecutive clicks, as recorded by the target-mounted hydrophones, were manually identified as candidate on-axis clicks as the porpoise scanned across a given target (*n*=2,688; Figs. 2A, B, C; Madsen *et al.* 2004; Madsen and Wahlberg 2007; Jensen et al., 2009).

The distance between the porpoise and the on-axis target was measured using the time delays between on-axis click emission and echo reception. “Echograms”, akin to echosounder images from an echolocator’s perspective, were created from the tag data (Johnson *et al*. 2004, 2009; Johnson 2014), and the echo streams corresponding to the two targets were used to confirm the range of the porpoise to the target that was being scanned (Fig. 2E). For all candidate on-axis clicks on either target, the time delay ($\Delta T_{\text{at targets}}$) of the click as received on both target-mounted hydrophones was measured via cross-correlation of triple up-sampled waveforms, with the duration of the search window constrained by the maximum inter-target distance (whereby the search window was click time on on-axis target $\pm$ inter-target distance/c·fs). The range of the porpoise to the off-axis target was calculated from the time delay measurement at the targets (whereby range to off-axis target = $c \cdot \Delta T_{\text{at targets}}$ + range to on-axis target). Due to low SNR clicks, and/or the multi-pulsed nature of porpoise clicks, spatial aliasing errors arose from incorrect cross-correlations (Gillespie and Macaulay, 2019), manifesting themselves as ranges to off-axis targets that resulted in impossible triangles. Therefore, clicks were removed if the $\Delta T_{\text{at targets}}$ measurement yielded an impossible triangle, or when low SNRs of the cross-correlated clicks made it so the signal was not obvious, reducing the dataset (*n*=2,000). $\Delta T_{\text{at targets}}$ was multiplied by 2 to give the $\Delta T_{\text{at porpoise}}$, and from hereon out, “ΔT” refers to the time delay at the porpoise location.

Given the known distance between the targets, the measured range to the on-axis target, and the calculated range to the off-axis target, the bearing to the off-axis target could be calculated for all on-axis clicks (Fig. 1B). In this way, non-straight swim-paths could be accounted for, and porpoise approach tracks could be extracted. If the signature of the click as received on the off-axis target was unclear, no time delay (and therefore no localisation point) could be reliably calculated. On-axis click candidates were excluded from further analyses if the time delay arising from the cross-correlation resulted in a manually identified erroneous porpoise localisation (reducing the dataset from 2,000 on-axis click candidates to 1,810 on-axis click candidates). 2D approach tracks for each trial were created via cubic interpolation between the remaining on-axis click candidates (Fig. 4).

The RL of the same click recorded on both target-mounted hydrophones, along with the known target strengths (TS) of the two targets and the ranges to them from the porpoise location, were used to calculate the difference in echo level (ΔEL) for returning target echoes as received at the porpoise location. Source levels (SLs) of on-axis click candidates, defined as the sound level of this click referenced to 1 meter ahead of the animal and along its beam axis, were calculated. Additionally, apparent source levels (ASLs) of the same clicks as received on the off-axis target, defined as the sound pressure back-calculated to 1 m ahead of the animal with an aspect angle that is not 0°, were back-calculated. EL, SL and ASL measurements all assumed spherical spreading ($20 \cdot \log_{10}(R)$) and frequency-dependent transmission loss (TL) due to absorption (of 0.04 dB/m at 130 kHz) that can be ignored for the short ranges considered here.

To confirm whether on-axis click candidates were truly part of scans across a target – as opposed to being from a scan where the beam was pointed near to, but did not scan *across* the target – increasing and decreasing patterns in the ASL (back-calculated from each target) of the three clicks preceding and three clicks following each on-axis click candidate were examined (noting that as ranges could only be measured for on-axis clicks, interpolated ranges for the porpoise to each target was used for the preceding and following clicks). So, for example, a click was considered truly on-axis if the ASL signature on the left target increased prior to and decreased after the on-axis click, *and* if the ASL signature increased both prior to and after the on-axis click. 906 clicks passed this *true-scan* criteria and were deemed as being recorded truly on-axis.

Several variables were measured as proxies to assess porpoise biosonar performance in scenes of varying acoustic complexity. For each manually identified on-axis click (n=1,810), we measured: i) the time delay of target echoes at the porpoise location (ΔT, µs), ii) the difference in echo levels from each target (ΔEL, dB), and iii) inter-click interval (ICI, ms). For each truly on-axis click, whereby scans across the target were confirmed (n=906), we also measured the SL (dB re 1 μPa_{pp}) and the bearing to the off-axis target (°). Note that the larger dataset (n=1,810) could be used for ΔT and ΔEL because these values are unaffected by the true-scan criterion. However, to be conservative, only the smaller dataset (n=906) was used for reporting of SL and bearing, as measurements of both are only reliable if they pass the true-scan criterion.

For each trial, several variables were measured to assess task difficulty (*sensu* Kastelein et al., 2008) and acoustic gaze adjustments, (here defined as the spatial extent of echoic information as controlled by the beam pattern, sampling rate, and output energy, as in Wisniewska et al., 2012). These variables were: i) trial duration (s; from the start of a trial to target interception), ii) total buzz duration (s; with buzzing defined by inter-click intervals (ICI) <13 ms (Wisniewska et al., 2012)), iii) range to the on-axis target at buzz onset (m), iv) the number of scans across each target, indicating the number of times the porpoise switched focus between targets (*sensu* Wisniewska et al., 2012), and v) the range to the targets at the discrimination decision (m). When and at what range the porpoise last focused its biosonar beam on the non-chosen target was taken as a proxy for the target discrimination decision. Additionally, we noted whether this "last glance" occurred before or after the initial buzz onset, and whether it occurred during a buzz.

Statistical analysis

The statistical analysis was implemented in R software (version 3.6.1; R Core Team, 2019). To quantify how porpoises modified their echolocation behaviour according to the complexity of the acoustic scene, we used inter-target distance (a proxy for acoustic clutter) as the main explanatory variable, and nine response variables (trial duration, number of scans, buzz duration, range from targets at buzz onset, range-to-targets at the discrimination decision, ICI, the time delay of target echoes, difference in echo levels from each target, and the SL of true on-axis clicks). To estimate these associations, we used Generalized Linear Mixed-Models (*glmer* in the *lme4* package, version 1.1-21, Bates et al., 2015) to account for the dependent nature of data

coming from the same animal, as well as the data coming from the same day and session: all models included animal ID, date of the trial, and session as random intercepts. Additionally, all models included a random slope for inter-target distance related to animal ID. Inter-target distance was included as a categorical variable with four categories (13.5, 27, 54, and 108 cm), and hence we additionally performed a Cuzick's test (Cuzick, 1985) to assess whether there was an increasing or decreasing trend for each outcome following the ordered distance categories. When investigating the association between the SL of true on-axis clicks and inter-target distance, we adjusted the relationship by the effect of range-to-target using an asymptotic function, and included an interaction term to account for potentially different relationships between inter-target distance and SL depending on range-to-target (Fig. S1). While ICI is known to decrease as porpoises get closer to a given target, there was no difference in the distributions of ranges to target with different inter-target distances (Fig. S2), and hence, it was not necessary to adjust for the potential confounding effect of range-to-target. A Gaussian family function was used for most response variables, where the assumptions of normality and homoscedasticity of residuals were checked. A Poisson (link = log) family function was fitted when the response variable represented counts, such as number of scans. Results are reported by an estimate (alpha, in the unit of each parameter, [95% confidence intervals (CI)]), and a p-value (p) or p-trend when using Cuzick's test.

Results

Both porpoises had high success rates (95.0% for Freja, and 93.3% for Sif) in correctly identifying the aluminium target irrespective of spacing to the alternative target (Fig. 3A). While errors by Freja only occurred in trials where inter-target distance was 108 cm, errors by Sif were not related to inter-target distance. Most of the other target discrimination performance-related variables were associated with inter-target distance, after adjusting for the random effects of porpoise ID, session, and date (Figs. 3, 4, 7).

While trial duration did not change significantly in relation to inter-target distance (ptrend =0.510; Fig. 3B), the total number of scans on both targets per trial increased with decreasing inter-target distance ($alpha_{13.5cm}$ =18 scans [16.6, 20.4], $alpha_{27cm}$ =15 [13.4, 17.8], $alpha_{54cm}$ =15 [13.7, 16.8], $alpha_{108cm}$ =14 [12.8, 15.9], ptrend < 0.001; Fig. 3C). Each scan comprised about 5-10 clicks across a target (Figs. 2B, 2C). Similarly, we observed that both buzz duration and range to the on-axis target at the onset of the buzz were associated with inter-target distance ($ptrend_{duration}$ <0.001; $ptrend_{range}$ <0.001, Figs. 4B, 4C). Shorter inter-target distances were associated with longer total buzz durations that started farther away from the target (<u>buzz duration</u>: $alpha_{13.5cm}$ =2.4 seconds [2.05, 2.83], $alpha_{27cm}$ =2.2 [1.48, 2.89], $alpha_{54cm}$ =2.0 [1.23, 2.77], $alpha_{108cm}$ =1.7 [1.22, 2.21]; <u>range at buzz start</u>: $alpha_{13.5cm}$ =0.7 meters [0.64, 0.75], $alpha_{27cm}$ =0.6 [0.55, 0.66], $alpha_{54cm}$ =0.5 [0.42, 0.53], $alpha_{108cm}$ =0.5 [0.45, 0.55]; Figs. 4B, 4C). Additionally, the porpoises made their discrimination decision closer to the targets when the targets were more closely-spaced ($alpha_{13.5cm}$ =0.5 meters [0.34, 0.59], $alpha_{27cm}$ =0.6 [0.29, 0.83], $alpha_{54cm}$ =0.8 [0.32, 1.33], $alpha_{108cm}$ =1.2 [0.92, 1.53], ptrend <0.001; Figs. 7A). Porpoises more often made their discrimination decision before to the onset of the buzz when targets were far apart, and after buzz initiation when targets were closely-spaced. When targets were closely-spaced, discrimination decisions were often made during the buzz (Fig. 10), and there was evidence of maintaining the buzz phase while scanning across and between the two targets (as seen in Fig. 2E).

The challenge of separating echoes from closely-spaced targets is demonstrated (Figs. 2, 6). Visual analogues of the received echo streams from targets show that they are more distinct from one another when targets are spaced farther apart (Fig. 2E). When the targets are closely-spaced, the challenge of segregating overlapping auditory streams is also demonstrated with clicks of overlapping amplitudes on the two target-

mounted hydrophones (Figs. 2A,B,C), smaller time delays (ΔT; Fig. 2F), smaller comparative echo strengths (ΔEL; Fig. 2G), and smaller bearing offsets between the targets (Fig. 2H). Fairly direct and comparable swim path approaches to the targets across inter-target distance treatments are observed (Fig. 5).

Modelling results showed that the differences in both the echo levels (ΔEL) and time delays (ΔT) of the returning echoes decreased as inter-target distance decreased (ΔEL: $alpha_{13.5cm}$ =7.3 dB [4.54, 10.12], $alpha_{27cm}$ =12.4 [7.96, 16.86], $alpha_{54cm}$ =18.6 [13.67, 23.59], $alpha_{108cm}$ =26.7 [25.19, 28.24], ptrend <0.001; ΔT: $alpha_{13.5cm}$ =44.4 µseconds [3.01, 85.72], $alpha_{27cm}$ =130.1 [86.78, 173.42], $alpha_{54cm}$ =265.8 [219.67, 309.91], $alpha_{108cm}$ =398.4 [210.35, 586.43], ptrend <0.001; Figs. 7B, 7C). While both the maximal ΔT and the bearing to the distracting target relative to the beam axis (Fig. 1C) have an upper bound that is constrained by inter-target distance, these values depend on the porpoise's position relative to the two targets (Fig. 1B). Figure 6 shows the variability in ΔT for all on-axis clicks (*n*=1,810) and across all inter-target distances. ΔT could theoretically reduce to 0 s in any inter-target distances treatment if the porpoise positioned itself so that the range to both targets was identical. As the separation between targets decreased, the porpoise was constrained in making its discrimination decision with information of reduced contrast, specifically, when the ΔEL was lower (Figs. 2G), when ΔT was smaller (Figs. 2F, 6) and when the bearing to the distracting target relative to the biosonar beam axis was smaller (Figs. 2H, 9).

Closely-spaced targets gave rise to echoes from both targets that returned at temporal delays that were within the nominal auditory integration time of 264 µsec (Figs. 6, 10). In the smallest inter-target distance treatment, the set-up geometry constrained the ΔT of returning echoes so that they could never exceed the estimated odontocete auditory integration time of 264 µs (Fig. 6). Despite this, target discrimination decisions were made when time delays of the echoes were below the auditory integration time (Fig. 10). For the inter-target distances of 13.5, 27, 54, and 108 cm, respectively, target discrimination decisions were made at a median ΔT of 52, 158, 233, and 238 µs (10th percentiles of 6.9, 33.7, 52.1, 38.3 µs; 90th percentiles of 104, 234, 479, and 802 µs) and at a median ΔEL of 6, 11, 20 and 27 dB (10th percentiles of 0.9, 2.2, 3.8, 11.7 dB ; 90th percentiles of 15, 24, 33, and 40 dB). The comparison of ΔT and ΔEL differences at the discrimination decision reveals that as long as there was ~2 dB of difference in the echo levels returning from the targets at the moment of discrimination, the porpoises were successfully able to discriminate between the targets (Fig. 10). There was no pattern in either the time delays or the echo levels at which any of the 7 incorrect target discriminations occurred (Fig. 10).

Inter-click intervals (ICI) of non-buzz on-axis clicks were associated with inter-target distance: ICI decreased when targets were closer together, though no difference were observed between the two closest inter-target distances ($alpha_{13.5cm}$ =32.8 ms [30.66, 34.92], $alpha_{27cm}$ =32.3 [28.50, 36.02], $alpha_{54cm}$ =33.2 [28.63, 37.78], $alpha_{108cm}$ =37.4 [33.51, 41.29]; ptrend <0.001; Figs. 4A). After adjusting by the asymptotic function of range-to-target, the SLs of true on-axis clicks were also associated with inter-target distance (Fig. 8). Although, the porpoises presented different average SLs (Sif produced clicks 5 dB higher on average), SLs were lower when targets were closer together ($alpha_{13.5cm}$ =142 dB re 1 μPa_{pp}, $alpha_{27cm}$ =149, $alpha_{54cm}$ =155, $alpha_{108cm}$ =161; ptrend <0.001; Fig. 8). However, the interaction term was also statistically significant (p <0.001), and while the asymptote lies, in all four treatments, at around 166 dB re 1 μPa_{pp} (Figs. 8A, 8B), the SL at the closest ranges to the target depended on inter-target distance (Fig. 8C): Specifically, at closer target ranges, porpoise clicks were weaker when targets were closer together, but the SL was the same between different inter-target distances when porpoises at ranges >2-3 meters from the target (Fig. 8C).

The differences between SL and ASL as a function of bearing of the biosonar beam to the off-axis target mostly clustered along previously measured harbour porpoise beam profiles (Macaulay et al., 2020) (Fig. 9). A

pattern consistent with production of clicks with wider beamwidths at closer ranges to the target is observed, across all inter-target distance treatments, and these broader beamwidths corresponded with buzz clicks (Fig. 9). A pattern of broader beamwidth clicks accompanying small inter-target distances is apparent, but there were more on-axis clicks recorded at close range when inter-target distances were small (Fig. 9), linked to more scans across the targets when inter-target distances were small (Fig. 3C). Outliers (*e.g.* in Fig. 9D) where the bearing offset to the off-axis target is large and the difference between SL and ASL are low are thought to arise from errors in range estimates (as highlighted in Fig. 1C).

Discussion

In this study, we investigated the echolocation abilities of porpoises as they completed an active target discrimination task with varying target spacing. We hypothesized that the auditory streams of simultaneously presented targets could not be resolved and discriminated from one another when the echoes arrived within the reported auditory integration time of 264 µsec and were therefore within the clutter interference zone (Simmons et al., 1988, 1989). We reject our hypothesis by showing that echolocating porpoises can resolve a target from a distractor when echoes arrive well below this critical interval. We propose that, for toothed whales, the clutter interference zone is shorter than this, and below we discuss both the implications of such time resolution and how the directional biosonar beam helps resolve closely-spaced auditory streams via spatial filtering.

Performance and acoustic behaviour

The close proximity of auditory streams generated by closely-spaced targets was predicted to present the porpoises with a challenging echolocation task, and this was anticipated to be reflected in their echolocation performance. However, the high success rate (Fig. 3A) of correctly targeting the aluminium sphere was in alignment with previously reported success rates of target discrimination carried out by Freja and Sif (of 94% and 89% respectively; Wisniewska et al., 2012). Thus, rather than discrimination performance deteriorating with more intense distractors or more closely-spaced distractors, as is the case for bats (Wagenhäuser et al., 2020), we find discrimination performance to be acute in echolocating porpoises subjected to distractors placed at minimal spatial and temporal separation from the target of interest (Fig. 10).

Previous echolocation performance studies have reported trial duration to increase with increasing acoustic complexity and therefore harder discrimination tasks (*e.g*. Wisniewska et al., 2012; Hermannsen, 2019), but no significant trend was observed in the present study (Fig. 3B). The porpoises scanned more across each target when targets were closely-spaced together (Figs. 3C), and while it would be predicted that this would lead to a longer trial duration, this was likely offset by the porpoise having to spend more time moving its head back and forth more to scan across widely-spaced targets when at close target range.

When confronted with a more acoustically challenging discrimination task (*i.e*. targets closely-spaced), the buzz onset occurred at a farther range (Figs. 4C) and the porpoises buzzed for longer (Figs. 4B). This pattern has been observed in previous experiments on the same porpoises, whereby buzz duration increased when confronted with more acoustic clutter (Ladegaard and Madsen, 2019). Similarly, Daubenton's bat (*Myotis daubentonii*) and the big brown bat (*Eptesicus fuscus*) (Moss et al., 2006; Hulgard and Ratcliffe, 2016), as well as beaked whales (Johnson et al., 2008), produce longer terminal buzzes in cluttered scenarios. Thus, longer buzz duration appears to coincide with greater task complexity across different guilds of echolocators.

Increasing the rate of sensory feedback to accommodate a more difficult discrimination task can also be achieved by clicking faster in non-buzz clicks. We show here that the porpoises had lower mean ICIs (Fig. 4A) when the targets were more closely-spaced. Dolphins have similarly been observed to increase the

number of clicks produced when a target is near a clutter screen (Au and Turl, 1983). Similarly, some bats can increase information update rates via higher call rates as the echolocation task increased in difficulty (Lewanzik and Goerlitz, 2021).

Approach angles

Modifying the approach angle offers a means of managing complex echo streams. Modifying the approach angle could also give rise to spectral cues that vary as a function of off-axis angle (see the polargrams in Au et al., 2009). While high aspect approaches have been observed in echolocating bats and toothed whales, reported to be a means of reducing clutter (Turl et al., 1991; Geipel et al., 2019; Moss et al., 2006; Moss and Surlykke, 2001; Greiter and Firzlaff, 2017), bats have behaviourally demonstrated the difficulty of finding and capturing prey using echolocation near clutter screens (Schmeider et al., 2012). In our experiment, although the temporal and spatial cues in the returning echoes were constrained by the proximity between the targets, the porpoises swam freely so they could adjust their approach angles, and thus their orientation relative to the two targets during target approaches. This means they could modify both ΔTs and ΔELs (Figs. 1C). While the maximal angular bearing of the distractor to the porpoise's beam axis was constrained by the inter-target distance (Fig. 1C), approaching the two targets from the side (Fig. 1B) would maximize difference in the echo delay (ΔT), whereas a head-on approach and sequential scanning across the targets would maximize differences in level (ΔEL) of the returning echoes. Resolutions in both spatial and temporal separation (Fig. 2C) increased as range to the targets decreased.

The fairly direct and comparable approach paths across inter-target distance treatments (Fig. 5), along with the absence of side-on approaches that would maximize echo time delays (Figs. 1B, 6), show that the porpoise did not seek to maximize echo delays from the two targets. The porpoise could have positioned itself to maximize temporal resolution, but this was not observed (Figs. 5, 6). Rather, we show that the porpoises could successfully discriminate the targets despite echoes from both targets arriving well within the suggested auditory integration time of 264 µsec for many of the trials (Fig. 10).

Auditory integration time and target resolution

The auditory integration time, or "critical interval", for odontocete audition of 200-300 µs was first reported from pulse-pair discrimination experiments with *Tursiops* (Vel'min and Dubrovskiy, 1975; Vel'min, 1976), as determined with a 75% correct discrimination occurring at pulse intervals of 230 ±40 µs. A similar value of 264 µs was found in *Tursiops* using simulated echoes (Au et al., 1988). In a backwards masking experiment with *Tursiops*, Moore et al. (1984) found a essentially the same interval of 265 µs, as this was the minimum time delay between target echo and noise masker in a target detection task at which a success rate of 70% was achieved. These studies on the bottlenose dolphin auditory system of ~260 µs can be interpreted as the time window below which acoustic events merge (Vel'min and Dubrovskiy, 1976) or appear as an acoustic whole (Dubrovskiy, 1990), or as the integration time of the dolphin's auditory system when acting as an energy detector (Au et al., 1988; Supin and Popov, 1995; de Boer 1985). Recent studies using auditory brainstem responses (ABR) in dolphins reported peak amplitudes occurring at latencies of ~260 µs (Jones et al., 2019; Finneran et al., 2020) and presented this as further support for the previously published estimates of a critical interval of the same duration. However, the interpretation of both ABR findings and modulation rate transfer functions (*e.g*. Linnenschmidt et al., 2013) to estimate time resolution capabilities is contested (Beedholm and Miller, 2008). In contrast, much shorter integration times for odontocetes have been proposed (Beedholm and Miller, 2008; Zaslavski, 2012). Specifically, time resolution constants as low as 20 µs have been suggested for *Tursiops* and 50 µs for harbour porpoises in behavioural experiments involving the discrimination of targets placed near a clutter screen (Zaslavskiy 2003; Zaslavski, 2008, 2012). However, owing

to different methodological approaches, these results are difficult to reconcile or compare to the ones converging on ~260 µsec.

In the present study, the majority of on-axis clicks in all treatments had ΔT values below the 264 µs auditory integration time (Fig. 6), with ΔT never able to exceed 180 µs at the smaller inter-target distance of 13.5 cm. Similarly, many of the discrimination decision clicks occurred below the 264 µs auditory integration time, as well as below the much lower and later proposed auditory integration time of 50 µs for porpoises (Fig. 10; Zaslavski, 2012). The latter value of 50 µs is shorter than a porpoise click, and therefore also shorter than an echo. While the auditory integration time has not been psychophysically measured in porpoises, it may be surmised that is expected to be equal to or longer than the dolphin auditory integration time, given that porpoise click duration (~80 µs; Wisniewska et al., 2015) is longer than dolphin click duration (~20 µs). Our results call into question the use of the auditory integration time as a hard delay limit for the clutter interference zone for toothed whales, below which echoes supposedly cannot be independently processed. Acoustic clutter rejection is conventionally described in the temporal domain, with bats and toothed whales placing echoes of interest between inner and outer windows, as demonstrated in the lab (*e.g.* Wilson and Moss, 2004) and field (*e.g.* Kalko and Schnitzler, 1993; Madsen et al., 2005; Stidsholt et al., 2021). However, here we see that the porpoises must be effectively rejecting the clutter of the distracting echo stream given their successful discrimination of closely-spaced targets, and in the case of shortest inter-target distance, they are doing so in a very short to non-existent overlap-free window (the time after one click and before the next click). How then can an echolocating toothed whale achieve such clutter rejection? Part of the answer may be due to the fact that toothed whales likely can resolve two auditory streams well shorter than the 265 µsec integration time and that critical interval is more on par with the 50 µsec values suggested by Zaslavski (2012). However, for very short echo delays, another explanation may pertain to differences in spectral interference depending on whether the porpoises ensonify one target more than the other (de Boer, 1985). Because of the different sound speeds in aluminium and steel, the interference patterns of same-sized targets of the two materials will be different, allowing for discrimination based on spectral cues (Au et al., 2009; Wisniewska et al., 2012), and when one target is ensonified more than the other, the relative contributions of these interference patterns may offer spectral cues useful for solving the task (Moore et al., 1984; Schmidt, 1992; Branstetter et al., 2020). Finally, this discrimination process may be greatly aided by the weighting of each of the target echo by level differences in the two echo streams due to sequential scanning of a directional beam across them as we will discuss in detail below.

Biosonar beam as a spatial filter

As only the targets within the narrow swath of a directional beam will render strong echoes, the echoes from off-axis targets will be weaker (Kalko and Schnitzler, 1993; Schnitzler and Kalko, 2001; Surlykke et al., 2009a; Schmieder et al., 2010, 2012). In this way, a highly directional biosonar beam could act as a spatial filter for clutter rejection by having one echo stream significantly louder than the other. The ΔEL ratios observed between on- and off-axis targets (Fig. 10), even when the targets were closely-spaced and therefore ΔT was smaller than the auditory integration time, likely facilitated clutter rejection. Here, ΔEL values could be as small as ~2 dB for the porpoises to successfully discriminate between the targets (Fig. 10). In a phantom target experiment, *Eptesicus fuscus* bats were confronted with delays between echoes (of 5-50 µs) much lower than their auditory integration time (of ~2 ms; Surlykke and Bojesen, 1996), and the authors suggested that the echo level returning from the two targets informed the discrimination decision (Simmons et al., 1989). As such, we suggest that ΔELs of closely-spaced objects within different parts of the acoustic field of view substantially aid clutter rejection via spatial filtering.

Similar to our study, an experiment on the biosonar behaviour of *Phyllostomus discolor* bats confronted with clutter showed that bats could spatially resolve distractors/maskers at temporal delays smaller than the bat auditory integration time when the spatial release from masking increased (Wagenhäuser et al., 2020). Indeed, shifting the clutter/distractor farther off-axis has been shown to facilitate target detection in *Eptesicus fuscus* bats (Sümer et al., 2009; Warnecke et al., 2014). To do this in the present study, the porpoises here would have had to be closer to the closely-spaced targets to resolve and perceive a gap in the spatial perception of the two targets, and we indeed observe this (Fig. 7A). Discrimination performance in bats has been shown to deteriorate with both decreasing ΔELs and inter-masker delays (Wagenhäuser et al., 2020), and while this was not observed here, perhaps our minimal ΔEL values (Figs. 7C, 10) were not small enough to deteriorate performance.

The smallest inter-target distance used here was a biologically reasonable distance between neighbouring prey items in a school (see Benoit-Bird et al., 2017), and this gave rise to ΔTs well below the auditory integration time. Additionally, echolocating odontocetes also face arguably the most intense acoustic clutter when sonar recognition of buried targets is required. Our finding that echo streams can be independently resolved when received at temporal intervals below the critical interval lends credence to the mechanisms facilitating biosonar-mediated foraging when the targets/prey are buried in sediment (Roitblat et al., 1995; Houser et al., 2005) - a topic that warrants further studies.

Acoustic clutter rejection thus appears to occur in the spatial and spectral domains when it cannot be resolved fully in the temporal domain. The example auditory scenes (Figs. 2E) and the performance results taken as a whole (Figs. 3-10) show that echolocation behaviours vary according to the acoustic complexity of the scene, and demonstrates the usefulness of a directional sound beam that reduces ensonification of off-axis clutter. Jensen et al. (2018) proposed a narrow acoustic field of view as the primary evolutionary driver for the highly directional biosonar beams in toothed whales. We posit that a strong driver for this convergence is the clutter rejection demonstrated here via spatial filtering, though we recognize that directional hearing in porpoises (Kastelien et al., 2005) also contributes to this advantage.

Within the convergence on similar beamwidths of toothed whales, there is increasing evidence for active control of the acoustic field of view around that mean. Active biosonar adjustments, including those to beamwidth, can act to pre-filter the auditory streams (Lewanzik and Goerlitz, 2021). Dynamic adjustments of biosonar beamwidths have been demonstrated, whereby echolocators can have adjust the size of the area and volume ensonified. Studies on bats (Jakobsen and Surlykke, 2010; Jakobsen *et al.,* 2013; Linnenschmidt and Wiegrebe, 2016), delphinids (Moore *et al.,* 2008; Finneran *et al.,* 2014), and porpoises (Wisniewska *et al.,* 2015) have shown such dynamic widening of the beam, even in the wild (Jensen *et al.,* 2015; Ladegaard *et al.,* 2017). The adaptive widening of the beam during the final phases of prey capture, which evolved convergently, is likely crucial to hunting since it allows for keeping fast-moving, evasive prey items within the field of view at close range (Jakobsen and Surlykke, 2010).

We would therefore hypothesize, given the demonstrated flexibility in beamwidth, that a narrow beam would be used at close range when echolocating on closely-spaced targets. Recent findings on wild mouse-eared bats (*Myotis myotis*) and captive *Phyllostomus discolor* bats showed that just prior to prey capture, the acoustic field of view was narrowed to focus on the echo stream generated from a target of interest (Linnenschmidt and Wiegrebe, 2016; Stidsholt et al., 2021). Narrowing the beamwidth during the final phase of target interception runs counter to the observed beamwidth widening in the buzz phase of porpoises as they intercept a single-target (Wisniewska et al., 2015). In the present study, if the beamwidth was constant and static throughout the echolocation sequence, the difference in SL and ASL as a function of bearing to the

distracting target would have been expected to be constant across inter-target spacings (*i.e.* points in Fig. 9 would cluster along the beam profile). If, as previously demonstrated, the porpoises used a broader beamwidth, akin to a "floodlight" (Wisniewska et al., 2015), we would expect to observe points clustering at great bearings (Fig. 9). That we do observe this (Fig. 9) suggests that the porpoises adjusted the degree of beamwidth steering according to the complexity of acoustic scene, but in the opposite way from that which was hypothesized. Specifically, a broader functional beamwidth (from ~±20° to ±40°) was observed in on-axis clicks when targets were more closely-spaced (Fig. 9). Therefore, while porpoises can adjust their beamwidth, they were not observed to actively narrow their beam to exclude distracting acoustic clutter from non-target objects.

The porpoises buzzed from farther away (Fig. 4C) and buzzed for longer (Fig. 4B) when acoustic complexity was greater and the auditory streams were spatially and temporally closer to one another. When the click beamwidth was broader (during buzz clicks; Fig. 9), the spatial filter offered by the beam would be less steep and of lower order (*i.e.* ΔEL contrasts would be lower). Of course, this assumes that the wide beamwidth is hardwired with the buzz, but the observation of broader beamwidth clicks having ICIs <13 ms supports this (Fig. 9). Thus, the higher contrasts in the auditory streams of on- and off-axis targets, as provided by using a narrow beamwidth, were not available when using broader beamwidth buzz clicks. This is the case for echolocating bats, whose much broader beamwidth does not offer the stark contrast in the level of returning echoes from on- and off-axis targets (Ghose and Moss, 2003; Nelson and MacIver, 2006). Indeed, the bat's broader beam means that almost equal sound energy arrives at objects within the wide swath of its beam (Surlykke et al., 2009a). While bats are thought to have more directional hearing, this poorer spatial resolution has been behaviourally demonstrated in bats presented with multiple and simultaneous acoustic reflectors (Geberl et al., 2019). Instead, spectral cues and beam aim are thought to be more important for guiding auditory stream segregation in bats (Surlykke et al., 2009b).

Sequential scanning

The porpoises in this study, along with bats and other toothed whales, exhibit sequential scanning behaviour with their echolocation beams (*e.g*. Evans, 1973; Ghose and Moss, 2003; Martin et al., 2005; Surlykke et al., 2009b; Wisniewska et al., 2012, 2015; Zimmer et al., 2005), and some bats also have conspicuous ear movements accompanying their echolocation (*e.g.* Kugler and Wiegrebe, 2017). Scanning behaviours may aid in the detection or localization of targets by providing cues for binaural reception (Aytekin et al., 2004), as well as spectral cues of the returning echoes if the clicks are broadband (Arditi et al., 2015). The presence of distractors has been shown to influence head-scanning movements in bats (Mao et al., 2016). While the placement of the biologging tag in our study prevented accurate measurements on the degree of head-scanning movement in the porpoises, the number of scans across each target could be quantified: the porpoises scanned across the targets more in the scenarios with close inter-target distance (Figs. 3C, S1). As each scan comprised about 5-10 clicks across a target, and the porpoises made more scans across the targets when closely-spaced (Fig. 3C), a larger amount of echoic information was needed to resolve more acoustically complex scenes. This is similar to a study on *Eptesicus fuscus* bats which showed that biosonar adjustment magnitude depended on the angular offset to the distractor (Aytekin et al., 2011). Head movement also increases the effective swath of the beam if integrating information over several sequential clicks. Therefore, it worth noting that the functional beamwidth considered on a click-by-click basis is a conservative estimate of the acoustic field of view: spatial memory likely updates an auditory scene spanning several beamwidths (Madsen et al., 2013), and there is spatial redundancy between the ensonified sensory volumes generated by each click (Stidsholt et al., 2021).

A target discrimination study in harbour porpoises by Wisniewska et al. (2012) purposefully placed targets at a 1 m range from one another so that through much of the approach, the porpoise would not be able to ensonify both targets simultaneously, but rather have to scan the acoustic scene to solve the target discrimination task. In that study, it was often observed that when the porpoises homed in on a target, and then changed its decision in the discrimination task, they would often re-enter the regular echolocation click phase before buzzing on the other target. While this was also observed in the present study, we also observed inter-target buzzing (Fig. 2E), and that target discrimination can take place in the buzz phase (Fig. 10). This contrasts reported bat echolocation behaviour, whereby their approach phase calls lock onto a target several hundred milliseconds prior to prey capture, and thus can be interpreted as an intention to complete the echolocation task (Ghose and Moss, 2003; Surlykke et al., 2009b; Koblitz et al., 2011).

Ecological relevance

Porpoises continue to entangle and drown in nets that their biosonar is capable of detecting (Read et al., 2006). The acute time resolution demonstrated by porpoises in this study supports the idea that the biosonar of wild toothed whales would be capable of detecting and resolving both fishing nets and nearby prey in keeping with net detection experiments (Au and Jones, 1991; Au, 1994; Kastelein et al., 2000). Therefore, the acoustic complexity of an auditory scene comprised of prey next to a net (and therefore rendering echoes with short time delays), is likely not the culprit of bycatch. Instead, perhaps net detection is more challenging if the porpoise's attention is focused on prey items within the net, or by external factors such as anthropogenic stressors. When a task is difficult and attention-demanding, foraging performance can be constrained and the detection of threats may be hindered (Dukas and Kamil, 2000). Noise has also been suggested to act as a distractor and narrow the attention in bats, whereby it reduces hunting performance in biosonar-mediated prey capture and drinking (Allen et al., 2021; Domer et al., 2021). For porpoises, it is plausible that attention on biosonar-mediated prey capture could similarly reduce vigilance to predators or fishing nets. Alternatively, acoustic clutter arising from net presence may act as an as an echo-acoustic flow (Kugler et al., 2016; Warenecke et al., 2016) to serve as a spatial anchor for orientation (Stidsholt et al., 2021).

List of Abbreviations

ASL	apparent source level (back-calculated from RL on the off-axis target)
ΔEL	echo level (dB)
FOV	field of view
ICI	inter-click interval
ITD	inter-target distance
pp	peak to peak
RL	received level
SL	source level (back-calculated from RL on the on-axis target)
$\Delta T_{\text{at target}}$	The time delay between a single click as it arrives on 2 targets
ΔT	The time delay between echoes arriving at the porpoise. Equivalent to $2 \cdot \Delta T_{\text{at target.}}$
TL	transmission loss (dB)
TS	target strength
TWTT	two-way travel time

Acknowledgements

We are grateful to Josefin Larsson, Fredrik Johansson, Mathilde Kjølby and Jakob Højer Kristensen at Fjord & Bælt, Kerteminde, Denmark for assistance in conducting the experiment. Thanks to Kristian Beedholm for building the LabView program with which the target-mounted hydrophone data was collected and time-marking sweeps generated. We thank John Svane Jensen for creating the targets and the metal target frame. Thanks to Mark Johnson for providing the DTAG4, and to Magnus Wahlberg for providing both office space in Kerteminde and the example target discrimination video. We thank Danuta Wisniewska and Mark Johnson for thoughtful discussions on experimental design, and Lasse Jakobsen, whose helpful criticism at the Odense echolocation symposium steered the analysis in a different and improved direction. We also thank Peter Tyack, John Buck, and K Alex Shorter for helpful comments on early results, and Laura Stidsholt, Kristian Beedholm, and Jakob Tougaard for thoughtful feedback on an earlier version of the manuscript. Thanks in advance to the reviewers who found the time during a pandemic to critique and improve this manuscript.

Ethics Statement

The porpoises are maintained by Fjord & Bælt, Kerteminde, Denmark, under permits no. SN 343/FY-0014 and 19963446-0021 from the Danish Nature Agency under the Ministry of Environment and Food of Denmark.

Competing Interests

The authors declare no competing or financial interests.

Author Contributions

Roles	**Contributors**
Conceptualization	CEM, PTM
Methodology	CEM, PTM, LRD
Software	CEM
Validation	CEM
Formal Analysis	CEM, LRD
Investigation	CEM
Resources	PTM
Data Curation	CEM
Writing: original draft preparation	CEM, PTM
Writing: review & editing	CEM, PTM, LRD
Visualization	CEM, LRD
Supervision	PTM
Project Administration	PTM, CEM
Funding Acquisition	PTM

Funding

PhD funding was provided by Danish National Research Council grants to PTM (grant 27125). This, along with ONR awards N00014-18-1-2062 and N00014-20-1-2709, covered research time at Fjord & Bælt.

Data Availability

The data supporting this paper are available on Zenodo [doi will be pasted here once accepted]. Custom software is available upon request.

References

Allen, L. C., Hristov, N. I., Rubin, J. J., Lightsey, J. T., and Barber, J. R. (2021). Noise distracts foraging bats. **Proc Roy Soc B** 288 (1944), 20202689.

Arditi, G., Weiss, A.J., and Yovel, Y. (2015). Object localization using a biosonar beam: how opening your mouth improves localization. **Roy Soc Open Sci** 2 (8).

Au, W. W. (1993). The Sonar of Dolphins. Springer-Verlag, New York.

Au, W. W. (1994). Sonar detection of gillnets by dolphins: theoretical predictions. **Rep Int Whal Comm Spec** (15), 565-571.

Au, W. W., Moore, P. W., and Pawloski, D. A. (1988). Detection of complex echoes in noise by an echolocating dolphin. **J Acoust Soc Am** 83 (2), 662-668.

Au, W. L., and Jones, L. (1991). Acoustic reflectivity of nets: implications concerning incidental take of dolphins. **Mar Mamm Sci**, 7(3), 258-273.

Au, W. W., and Benoit-Bird, K. J. (2003). Automatic gain control in the echolocation system of dolphins. **Nature** 423 (6942), 861-863.

Au, W. W., Branstetter, B. K., Benoit-Bird, K. J., and Kastelein, R. A. (2009). Acoustic basis for fish prey discrimination by echolocating dolphins and porpoises. **J Acoust Soc Am** 126(1), 460-467.

Aytekin, M., Grassi, E., Sahota, M., and Moss, C. F. (2004). The bat head-related transfer function reveals binaural cues for sound localization in azimuth and elevation. **J Acoust Soc Am** 116 (6), 3594-3605.

Aytekin, M., Mao, B., and Moss, C. F. (2010). Spatial perception and adaptive sonar behavior. **J Acoust Soc Am** 128 (6), 3788-3798.

Bates, D., Mächler, M., Bolker, B., and Walker, S. (2015) Fitting linear mixed-effects models using lme4. **J. Stat. Software** 67, 34.

Beedholm, K., and Miller, L. A. (2008). Temporal resolution in the hearing system and auditory evoked potentials. **J Acoust Soc Am**, Paris, France, pp. 3445-3445.

Benoit-Bird, K. J., Moline, M. A., and Southall, B. L. (2017). Prey in oceanic sound scattering layers organize to get a little help from their friends. **Limnol Oceanog** 62 (6), 2788-2798.

Branstetter, B. K., Alstyne, K. R. V., Strahan, M. G., Tormey, M. N., Wu, T., Breitenstein, R. A., Houser, D. S., Finneran, J. J., and Xitco, M. J. (2020). Spectral cues and temporal integration during cylinder echo discrimination by bottlenose dolphins (*Tursiops truncatus*). **J Acoust Soc Am** 148 (2), 614-626.

Brinkløv, S., Kalko, E. K., and Surlykke, A. (2010). Dynamic adjustment of biosonar intensity to habitat clutter in the bat Macrophyllum macrophyllum (*Phyllostomidae*). **Behavioral Ecology and Sociobiology** 64 (11), 1867-1874.

Cahlander, D., McCue, J., and Webster, F. (1964). The determination of distance by echolocating bats. **Nature** 201 (4919), 544-546.

Cuzick, J. (1985). A Wilcoxon-type test for trend. **Stat Med** 4 (1), 87-90.

de Boer, E. (1985). Auditory time constants: a paradox? In: Time resolution in auditory systems (pp. 141-158). Berlin, Heidelberg: Springer.

DeRuiter, S. L., Bahr, A., Blanchet, M.-A., Hansen, S. F., Kristensen, J. H., Madsen, P. T., Tyack, P. L., and Wahlberg, M. (2009). Acoustic behaviour of echolocating porpoises during prey capture. **J Exp Biol** 212 (19), 3100-3107.

Domer, A., Korine, C., Slack, M., Rojas, I., Mathieu, D., Mayo, A., and Russo, D. (2021). Adverse effects of noise pollution on foraging and drinking behaviour of insectivorous desert bats. **Mamm Biol**, 1-5.

Dubrovskiy, N. A. (1990). On the two auditory subsystems in dolphins. Sensory abilities of cetaceans. Springer, pp. 233-254.

Dukas, R., and Kamil, A. C. (2000). The cost of limited attention in blue jays. **Behav Ecol** 11 (5), 502-506.

Evans, W. (1973). Echolocation by marine delphinids and one species of fresh-water dolphin. **J Acoust Soc Am** 54 (1), 191-199.

Falk, B., Jakobsen, L., Surlykke, A., and Moss, C. F. (2014). Bats coordinate sonar and flight behavior as they forage in open and cluttered environments. **J Exp Biol** 217 (24), 4356-4364.

Finneran, J. J., Branstetter, B. K., Houser, D. S., Moore, P. W., Mulsow, J., Martin, C., and Perisho, S. (2014). High-resolution measurement of a bottlenose dolphin's (*Tursiops truncatus*) biosonar transmission beam pattern in the horizontal plane. **J Acoust Soc Am** 136:2025-2038.

Finneran, J. J., Mulsow, J., Strahan, M. G., Houser, D. S., and Burkard, R. F. (2020). Role of the temporal window in dolphin auditory brainstem response onset. **J Acoust Soc Am** 148, 3360-3371.

Geberl, C., Kugler, K., and Wiegrebe, L. (2019). The spatial resolution of bat biosonar quantified with a visual-resolution paradigm. **Curr Biol**. 29 (11): 1842-1846.

Geipel, I., Steckel, J., Tschapka, M., Vanderelst, D., Schnitzler, H.-U., Kalko, E. K. V., Peremans, H., and Simon, R. (2019). Bats Actively Use Leaves as Specular Reflectors to Detect Acoustically Camouflaged Prey. **Curr Biol** 29 (16), 2731-2736.e2733.

Gellermann, L. W. (1933). Chance orders of alternating stimuli in visual discrimination experiments. **Pedagog Sem J Genet Psych** 42 (1), 206-208.

Ghose, K., and Moss, C. F. (2003). The sonar beam pattern of a flying bat as it tracks tethered insects. **J Acoust Soc Am** 114 (2), 1120-1131.

Gillespie, D., and Macaulay, J. (2019). Time of arrival difference estimation for narrow band high frequency echolocation clicks. **J Acoust Soc Am** 146 (4), EL387-EL392.

Greiter, W., and Firzlaff, U. (2017). Echo-acoustic flow shapes object representation in spatially complex acoustic scenes. **J Neurophys** 117 (6), 2113-2124.

Hartridge, H. (1945). Acoustic Control in the Flight of Bats. **Nature**, 156 (3965), 490-494.

Hermannsen, L. (2019). Anthropogenic underwater noise pollution and its impacts on marine mammals, Aarhus University.

Houser, D., Martin, S. W., Bauer, E. J., Phillips, M., Herrin, T., Cross, M., Vidal, A., and Moore, P. W. (2005). Echolocation characteristics of free-swimming bottlenose dolphins during object detection and identification. **J Acoust Soc Am** 117 (4), 2308-2317.

Hulgard, K., and Ratcliffe, J. M. (2016). Sonar sound groups and increased terminal buzz duration reflect task complexity in hunting bats. **Sci Rep** 6, 21500.

Jakobsen, L., and Surlykke, A. (2010). Vespertilionid bats control the width of their biosonar sound beam dynamically during prey pursuit. **Proc Nat Acad Sci** 107:13930-13935.

Jakobsen, L., Ratcliffe, J. M., and Surlykke, A. (2013). Convergent acoustic field of view in echolocating bats. **Nature** 493:93-96.

Jensen, F. H., Bejder, L., Wahlberg, M., and Madsen, P. T. (2009). Biosonar adjustments to target range of echolocating bottlenose dolphins (*Tursiops sp*.) in the wild. **J Exp Biol** 212, 1078-1086.

Jensen, F. H., Wahlberg, M., Beedholm, K., Johnson, M., Aguilar de Soto, N., and Madsen, P. T. (2015). Single-click beam patterns suggest dynamic changes to the field of view of echolocating Atlantic spotted dolphins (*Stenella frontalis*) in the wild. **J Exp Biol** 218:1314-1324.

Jensen, F. H., Johnson, M., Ladegaard, M., Wisniewska, D., Madsen, P. T. (2018). Narrow acoustic field of view drives frequency scaling in toothed whale biosonar. **Curr Biol** 28, 1-8.

Johnson, M. P., and Tyack, P. L. (2003) A digital acoustic recording tag for measuring the response of wild marine mammals to sound. IEEE **J Ocean Eng** 28:3-12.

Johnson, M., Madsen, P. T., Zimmer, W. M., Aguilar de Soto, N., and Tyack, P. L. (2004). Beaked whales echolocate on prey. **Proc Roy Soc B** 271:S383-S386.

Johnson, M., Hickmott, L., Aguilar de Soto, N., and Madsen, P. T. (2008). Echolocation behaviour adapted to prey in foraging Blainville's beaked whale (*Mesoplodon densirostris*). **Proc Roy Soc B** 275 (1631), 133-139.

Johnson, M., Aguilar de Soto, N., and Madsen, P. T. (2009). Studying the behaviour and sensory ecology of marine mammals using acoustic recording tags: a review. **Mar Ecol Prog Ser** 395:55-73.

Johnson, M. (2014). On-animal methods for studying echolocation in free-ranging animals. *In*: Surlykke, A., Nachtigall, P. E., Fay, R. R., Popper, A. N. (Eds.), Biosonar. Springer, pp. 195-229.

Jones, R., Finneran, J. J., Mulsow, J., and Burkard, R. F. (2019). Effects of stimulus cosine onset properties on bottlenose dolphin (Tursiops truncatus) auditory brainstem responses. **J Acoust Soc Am** 145 (5), 2994-3002.

Kalko, E. K., and Schnitzler, H.-U. (1993). Plasticity in echolocation signals of European pipistrelle bats in search flight: implications for habitat use and prey detection. **Behav Ecol Sociobiol** 33 (6), 415-428

Kastelein, R., Au, W., and de Haan, D. (2000). Detection distances of bottom-set gillnets by harbour porpoises (*Phocoena phocoena*) and bottlenose dolphins (*Tursiops truncatus*). **Mar Environ Res** 49 (4), 359-375.

Kastelein, R., Bunskoek, P., Hagedoorn, M., Au, W. W., and de Haan, D. (2002). Audiogram of a harbor porpoise (*Phocoena phocoena*) measured with narrow-band frequency-modulated signals. **J Acoust Soc Am** 112(1), 334-344.

Kastelein, R. A., Janssen, M., Verboom, W. C., and de Haan, D. (2005). Receiving beam patterns in the horizontal plane of a harbor porpoise (*Phocoena phocoena*). **J Acoust Soc Am**, 118(2), 1172-1179.

Kastelein, R. A., Verlaan, M., and Jennings, N. (2008). Number and duration of echolocation click trains produced by a harbor porpoise (*Phocoena phocoena*) in relation to target and performance. **J Acoust Soc Am** 124(1), 40-43.

Koblitz, J. C., Stilz, P., Pflästerer, W., Melcón, M. L., Schnitzler, H.-U. (2011). Source level reduction and sonar beam aiming in landing big brown bats (*Eptesicus fuscus*). **J Acoust Soc Am** 130 (5), 3090-3099.

Kugler, K., Greiter, W., Luksch, H., Firzlaff, U., and Wiegrebe, L. (2016). Echo-acoustic flow affects flight in bats. **J Exp Biol** 219 (12), 1793-1797.

Kugler, K., and Wiegrebe, L. (2017). Echo-acoustic scanning with noseleaf and ears in phyllostomid bats. **J Exp Biol** 220 (15), 2816-2824.

Ladegaard, M., Jensen, F. H., Beedholm, K., da Silva, V. M. F., and Madsen, P. T. (2017). Amazon river dolphins *Inia geoffrensis* modify biosonar output level and directivity during prey interception in the wild. **J Exp Biol** 220, 2654-2665.

Ladegaard, M., and Madsen, P. T. (2019). Context-dependent biosonar adjustments during active target approaches in echolocating harbour porpoises. **J Exp Biol** 222, jeb. 206169.

Lewanzik, D., and Goerlitz, H. R. (2021). Task-dependent vocal adjustments to optimize biosonar-based information acquisition. **J Exp Biol** 224 (1), jeb234815.

Linnenschmidt, M., Beedholm, K., Wahlberg, M., Højer-Kristensen, J., and Nachtigall, P. E. (2012). Keeping returns optimal: gain control exerted through sensitivity adjustments in the harbour porpoise auditory system. **Proc Roy Soc B**, rspb20112465.

Linnenschmidt, M., Wahlberg, M., and Hansen, J. D. (2013). The modulation rate transfer function of a harbour porpoise (*Phocoena phocoena*). **J Comp Phys A**, 199(2), 115-126.

Linnenschmidt, M., and Wiegrebe, L. (2016). Sonar beam dynamics in leaf-nosed bats. **Sci Rep**, 6(1), 29222.

Lockyer, C., Desportes, G., Hansen, K., Labberté, S., and Siebert, U. (2003). Monitoring growth and energy utilisation of the harbour porpoise (*Phocoena phocoena*) in human care. **NAMMCO Scientific Publications** 5, 107-120.

Macaulay, J., Malinka, C., Gillespie, D., and Madsen, P. T. (2020). High resolution three-dimensional beam radiation pattern of harbour porpoise clicks with implications for passive acoustic monitoring. **J Acoust Soc Am** 147 (6), 4175-4188.

Madsen, P. T., and Wahlberg, M. (2007). Recording and quantification of ultrasonic echolocation clicks from free-ranging toothed whales. **Deep Sea Res I**, 54(8), 1421-1444.

Madsen, P., Johnson, M., de Soto, N. A., Zimmer, W., and Tyack, P. L. (2005). Biosonar performance of foraging beaked whales (*Mesoplodon densirostris*). **J Exp Biol**, 208(2), 181-194.

Madsen, P. T., and Surlykke, A. (2013). Functional Convergence in Bat and Toothed Whale. **Physiology** 28, 276-283.

Madsen, P. T., Aguilar de Soto, N., Arranz, P., and Johnson, M. (2013). Echolocation in Blainville's beaked whales (*Mesoplodon densirostris*). **J Comp Phys A** 199:451-469.

Mao, B., Aytekin, M., Wilkinson, G.S., and Moss, C. (2016). Big brown bats (*Eptesicus fuscus*) reveal diverse strategies for sonar target tracking in clutter. **J Acoust Soc Am** 140 (3), 1839-1849.

Martin, S. W., Phillips, M., Bauer, E. J., Moore, P. W., and Houser, D. S. (2005). Instrumenting free-swimming dolphins echolocating in open water. **J Acoust Soc Am** 117 (4), 2301-2307.

Moore, P., Hall, R., Friedl, W., and Nachtigall, P. (1984). The critical interval in dolphin echolocation: What is it? **J Acoust Soc Am** 76 (1), 314-317.

Moore, P. W. B., Dankiewicz, L. A., and Houser, D. S. (2008). Beamwidth control and angular target detection in an echolocating bottlenose dolphin (*Tursiops truncatus*). **J Acoust Soc Am** 124:3324-3332.

Moss, C. F., and Schnitzler, H.-U. (1989). Accuracy of target ranging in echolocating bats: acoustic information processing. **J Comp Phys A**, 165(3), 383-393.

Moss, C. F., and Surlykke, A. (2001). Auditory scene analysis by echolocation in bats. **J Acoust Soc Am** 110 (4), 2207-2226.

Moss, C. F., and Surlykke, A. (2010). Probing the natural scene by echolocation in bats. **Front Behav Neurosci**, 4, 33.

Moss, C. F., Bohn, K., Gilkenson, H., and Surlykke, A. (2006). Active listening for spatial orientation in a complex auditory scene. **PLoS Biol** 4 (4), e79.

Moss, C. F., Chiu, C., and Surlykke, A. (2011). Adaptive vocal behavior drives perception by echolocation in bats. **Curr Opinion Neurobiol** 21 (4), 645-652.

Nelson, M. E., and MacIver, M. A. (2006). Sensory acquisition in active sensing systems. **J Comp Phys A** 192 (6), 573-586.

Read, A. J., Drinker, P., and Northridge, S. (2006). Bycatch of marine mammals in US and global fisheries. **Conservation Biology** 20 (1), 163-169.

Roitblat, H. L., Au, W. W. L., Nachtigall, P. E., Shizumura, R., and Moons, G. (1995). Sonar recognition of targets embedded in sediment. **Neural Networks** 8 (7), 1263-1273.

Schmieder, D. A., Kingston, T., Hashim, R., and Siemers, B. M. (2010). Breaking the trade-off: rainforest bats maximize bandwidth and repetition rate of echolocation calls as they approach prey. **Biol Lett** 6 (5), 604-609.

Schmieder, D.A., Kingston, T., Hashim, R., and Siemers, B.M. (2012). Sensory constraints on prey detection performance in an ensemble of vespertilionid understorey rain forest bats. **Fun Ecol** 26 (5), 1043-1053.

Schnitzler, H.-U., and Kalko, E. K. (2001). Echolocation by Insect-Eating Bats We define four distinct functional groups of bats and find differences in signal structure that correlate with the typical echolocation tasks faced by each group. **Bioscience** 51 (7), 557-569.

Schusterman, R. J. (1980). Behavioral methodology in echolocation by marine mammals. Animal sonar systems. Springer.

Simmons, J. A. (1973). The resolution of target range by echolocating bats. **J Acoust Soc Am**, 54(1), 157-173.

Simmons, J. A. (1979). Perception of echo phase information in bat sonar. **Science**, 204(4399), 1336-1338.

Simmons, J. A., Kick, S. A., Moffat, A. J., Masters, W. M., and Kon, D. (1988). Clutter interference along the target range axis in the echolocating bat, *Eptesicus fuscus*. **J Acoust Soc Am** 84:551-559.

Simmons, J.A., Freedman, E.G., Stevenson, S.B., Chen, L., and Wohlgenant, T.J. (1989). Clutter interference and the integration time of echoes in the echolocating bat, *Eptesicus fuscus*. **J Acoust Soc Am** 86 (4), 1318-1332.

Stidsholt, L., Greif, S., Goerlitz, H. R., Beedholm, K., Macaulay, J., Johnson, M., and Madsen, P.T. (2021). Hunting bats adjust their echolocation to receive weak prey echoes for clutter reduction. **Science Advances** 7 (10), eabf1367.

Sümer, S., Denzinger, A., and Schnitzler, H.-U. (2009). Spatial unmasking in the echolocating Big Brown Bat, Eptesicus fuscus. **J Comp Phys A** 195 (5), 463-472.

Supin, A. Y., and Popov, V. V. (1995) Temporal resolution in the dolphin's auditory system revealed by double-click evoked potential study. **J Acoust Soc Am**, 97:2586-2593.

Surlykke, A., and Bojesen, O. (1996). Integration time for short broad band clicks in echolocating FM-bats *(Eptesicus fuscus*). **J CompPhys A**, 178(2), 235-241.

Surlykke, A., Boel Pedersen, S., and Jakobsen, L. (2009a). Echolocating bats emit a highly directional sonar sound beam in the field. **Proc Roy Soc B** 276 (1658), 853-860.

Surlykke, A., Ghose, K., and Moss, C.F. (2009b). Acoustic scanning of natural scenes by echolocation in the big brown bat, *Eptesicus fuscus*. **J Exp Biol** 212 (7), 1011-1020.

Taub, M., and Yovel, Y. (2020). Segregating signal from noise through movement in echolocating bats. **Sci Rep** 10, 382.

Turl, C. W., Skaar, D. J., Au, W. W. (1991). The echolocation ability of the beluga (*Delphinapterus leucas*) to detect targets in clutter. **J Acoust Soc Am** 89 (2), 896-901

Vandenberghe, R., Gitelman, D., Parrish, T., and Mesulam, M. (2001). Location-or feature-based targeting of peripheral attention. **NeuroImage** 14:37-47.

Vel'min, V., and Dubrovsky, N. (1975). Auditory analysis of sound pulses in dolphins. **Doklady Akademii Nauk SSSR** 225, 470-473.

Vel'min, V. (1976). The critical interval of active hearing in dolphins. **Soviet Physics and Acoustics** 2, 351-352.

Verfuß, U. K., Miller, L. A., Pilz, P. K., and Schnitzler, H.-U. (2009). Echolocation by two foraging harbour porpoises (*Phocoena phocoena*). **J Exp Biol** 212:823-834.

Wagenhäuser, P.A., Wiegrebe, L., and Baier, A.L. (2020). Biosonar spatial resolution along the distance axis: revisiting the clutter interference zone. J **Exp Biol** 223 (20).

Warnecke, M., Bates, M. E., Flores, V., and Simmons, J. A. (2014). Spatial release from simultaneous echo masking in bat sonar. The **J Acoust Soc Am** 135 (5), 3077-3085

Wisniewska, D. M., Johnson, M., Beedholm, K., Wahlberg, M., and Madsen, P. T. (2012). Acoustic gaze adjustments during active target selection in echolocating porpoises**. J Exp Biol**. 215:4358-4373.

Wisniewska, D. M., Ratcliffe, J. M., Beedholm, K., Christensen, C. B., Johnson, M., Koblitz, J. C., Wahlberg, M., and Madsen, P. T. (2015). Range-dependent flexibility in the acoustic field of view of echolocating porpoises (*Phocoena phocoena*). **eLife**:e05651.

Zaslavskiy, G. (2003). Target echo processing in the dolphin's auditory system. Oceans 2003. Celebrating the Past... Teaming Toward the Future IEEE, San Diego, CA, USA, pp. 620-628.

Zaslavski, G. L. (2008). The auditory time resolution in bottlenose dolphins: Behavioral experiments versus auditory evoked potential methods. **J Acoust Soc Am**, Paris, France, pp. 3618-3618.

Zaslavski, G. (2012). High auditory time resolution in bottlenose dolphins is effective protection against reverberation. The effects of noise on aquatic life. Springer, pp. 37-40.s

Figures

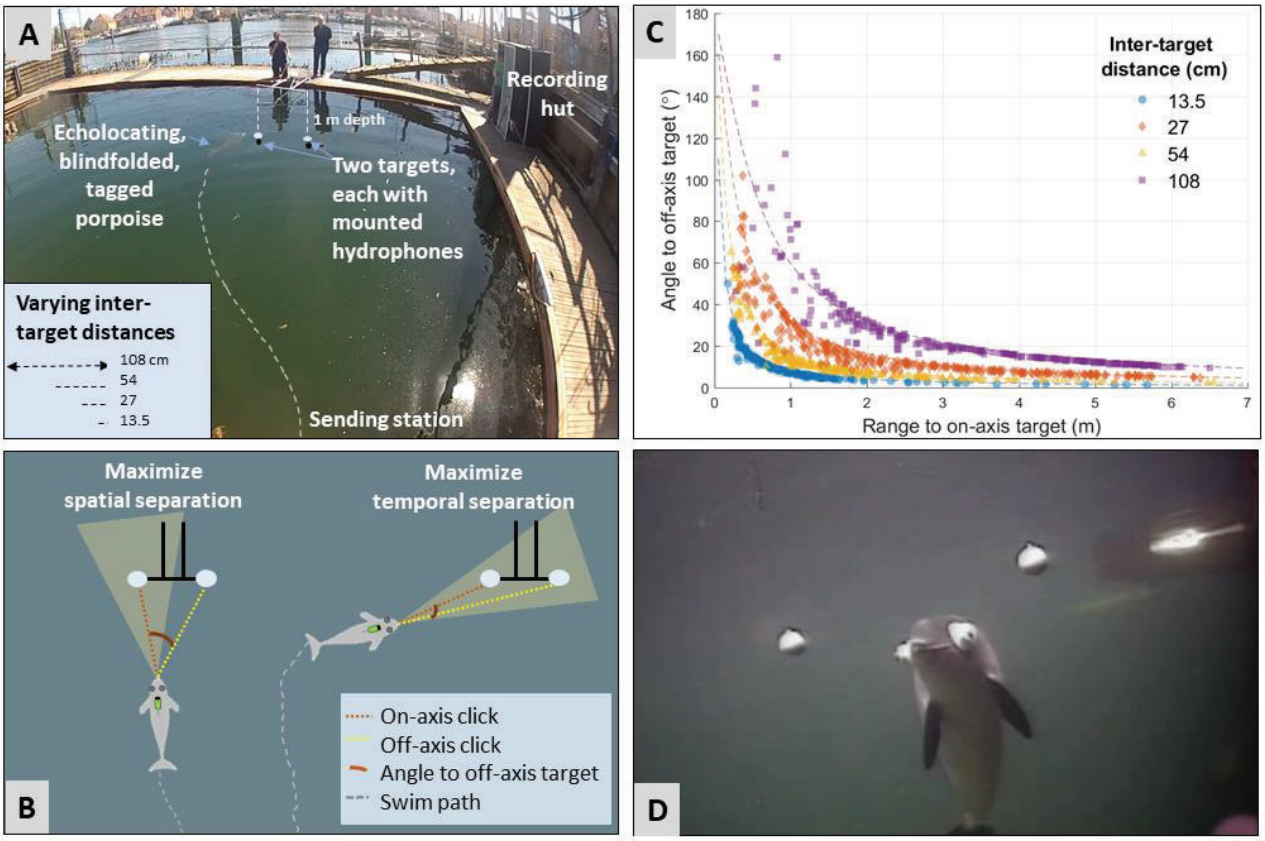

Fig. 1. **Experimental set-up. A)** Photo of a representative trial, where blindfolded, tagged porpoises used echolocation to discriminate between aluminium and steel targets suspended at varying inter-target distances in randomly varying orientation orders. Target-mounted hydrophones recorded clicks that were digitized in the recording hut. **B)** Schematic demonstrating an echolocation strategy that would maximize the angular offset between targets (thus maximizing ΔEL and the spatial separation at the echolocator) versus one which maximizes the time delays (ΔT) of returning echoes. For all on-axis clicks, the angle to the off-axis target was calculated. The time delay between each on-axis click being received on each target was used to obtain the relative position of the porpoise to the targets (thus accounting for non-straight swim paths) was used to calculate the ΔT of the echoes as received at the porpoise. **C)** The angle to the distracting target is shown for all on-axis clicks (n = 906) across all trials (n = 120) as a function of range to the on-axis target for all four inter-target distances, demonstrating the diminishing upper limit of angular resolution that existed as inter-target distance decreased. Dotted lines show theoretical maximum angles for each range, and points to the right of this line signify errors in range measurement. **D)** Demonstration of a porpoise repeatedly scanning its biosonar across two targets in a discrimination task (video courtesy of Magnus Wahlberg).

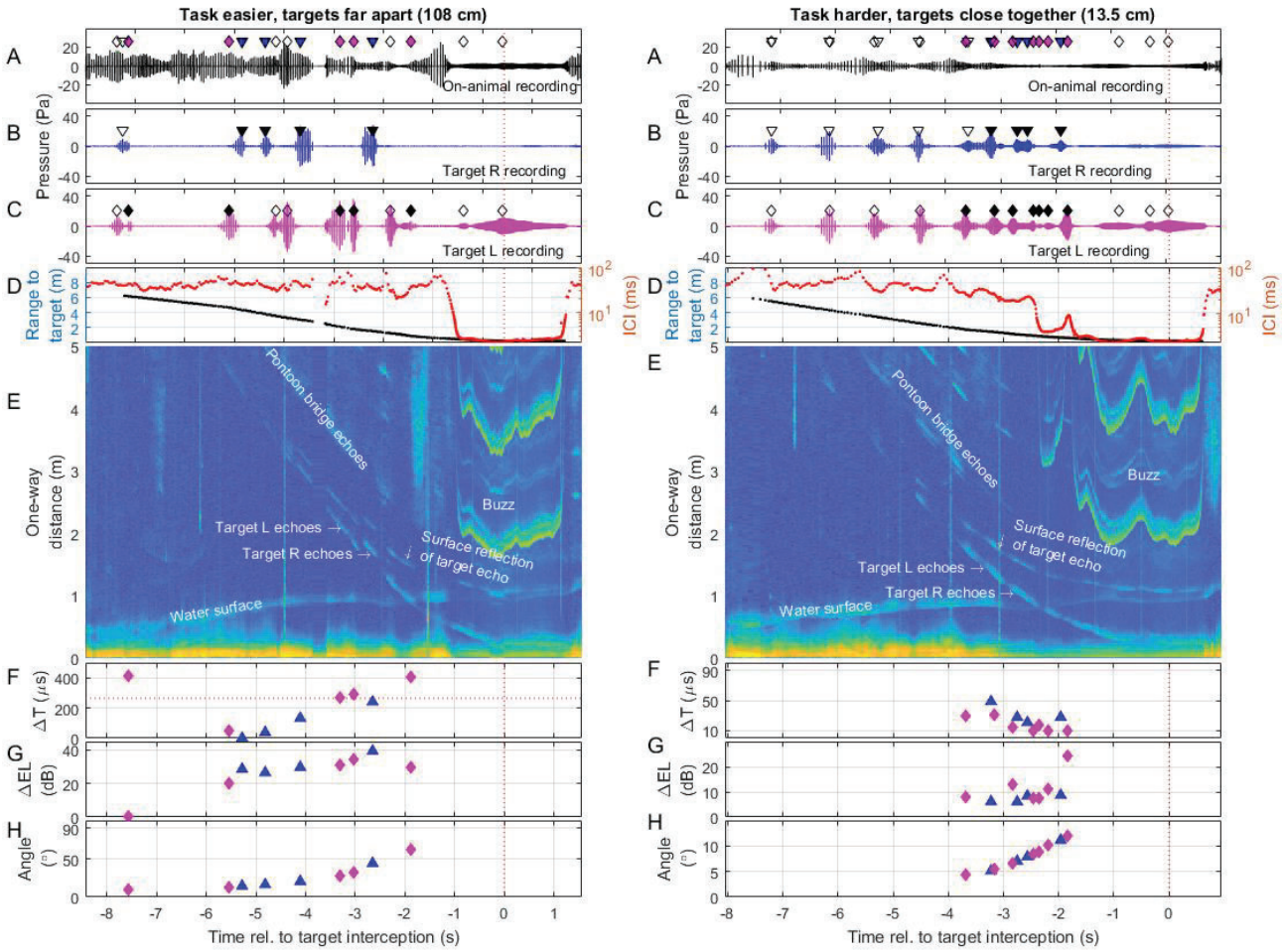

Fig. 2. **Example target approaches for easier and more difficult discrimination tasks.** The easier example refers to a trial with targets farthest apart (1.08 m, left), and the difficult example to a trial with the targets closest together (0.135 m, right). A-E show time series relative to target interception, with on-axis clicks on either target highlighted with triangles (right-target) and diamonds (left-target). Shapes are filled if they passed all on-axis criteria (see text). **A)** On-animal recording. **B)** Right-target audio recording. **C)** Left-target audio recording. **D)** Range to chosen target (m) and inter-click interval (ICI, s). **E)** Echogram created from the on-animal recording, offering a visualization of the challenge of separating the echo streams. **F)** Time delays (ΔT) and **G)** differences in echo level (ΔEL) of the echoes from both targets as received at the porpoise's location. **H)** Angle to the off-axis target for all on-axis clicks. Note that the y-axis scales vary for **F**, **G**, and **H** between the two examples.

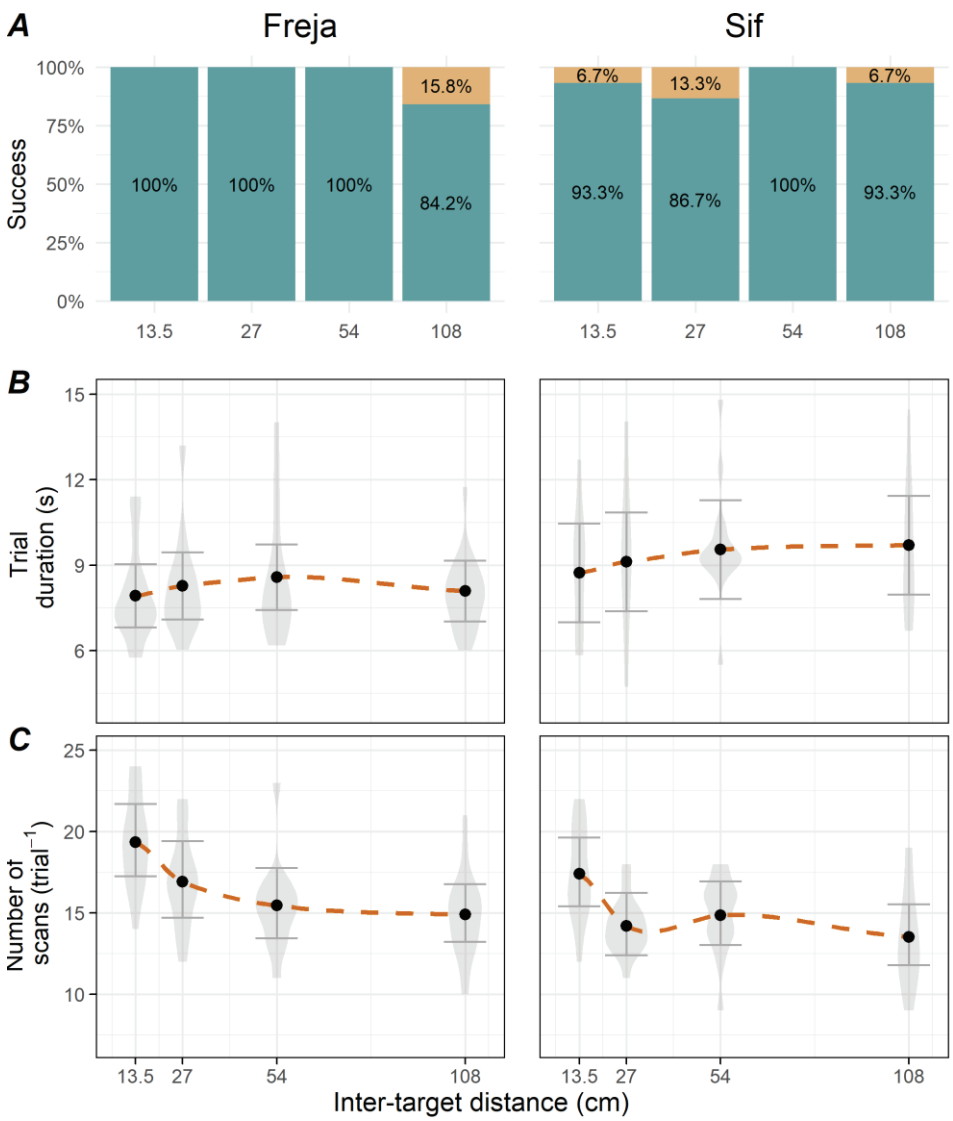

Fig. 3. Experiment-wide target discrimination performance for the two porpoises as a function of inter-target distance. Columns are separated by porpoise (left, Freja, *n* = 60; right, Sif, *n* = 60), for a total of *n* = 120. **A)** Success rates of correctly targeting the aluminium sphere, indicating correct (green) and incorrect (orange) selection, with success rate overlaid. **B)** There was no significant trend in trial duration (s) as a function of inter-target distance. **C)** Total number of scans across both targets per trial increased with decreasing inter-target distance. Distributions of the raw data are shown as violin plots, while the black dot and whiskers represent the model estimates and 95% confidence intervals, respectively.

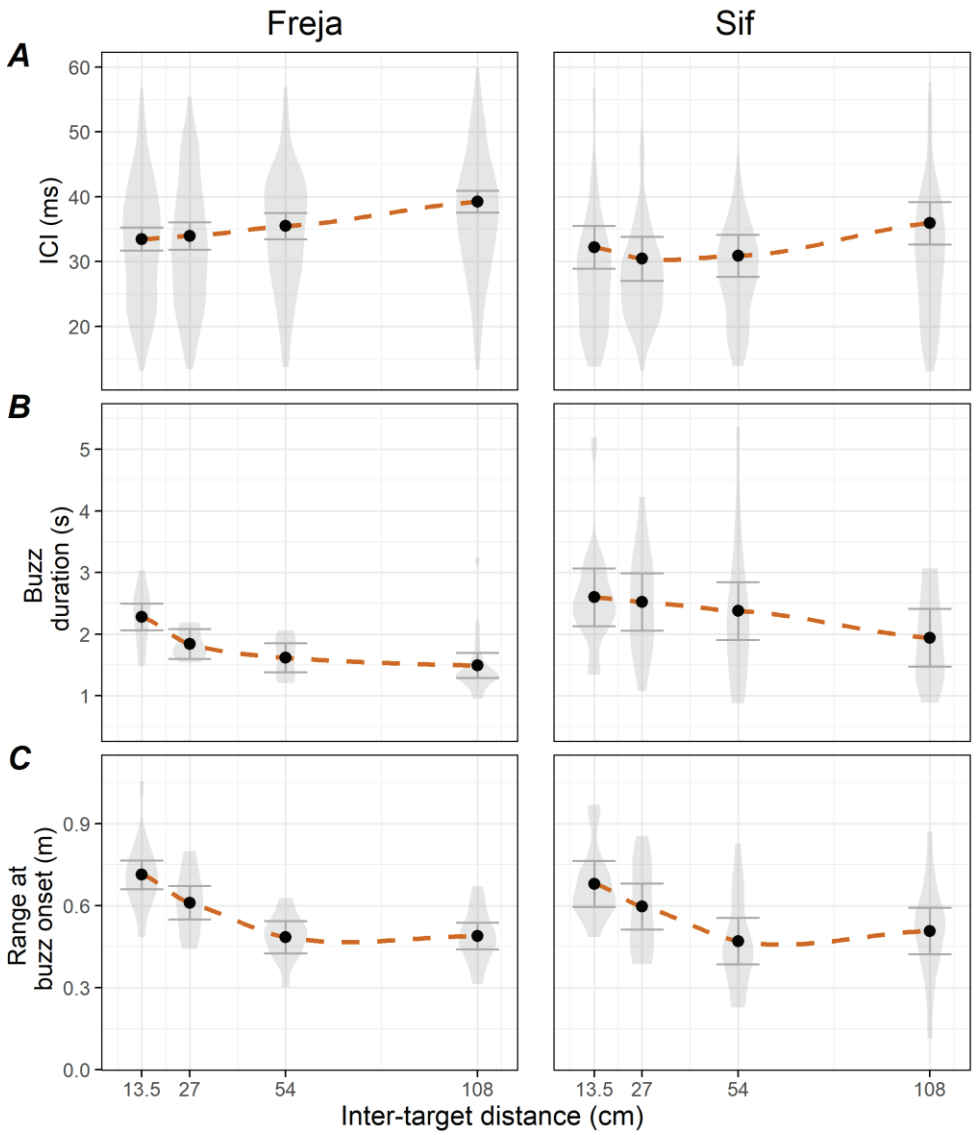

Fig. 4. Experiment-wide target discrimination performance for the two porpoises as a function of inter-target distance concerning their echolocation click rate. A) Inter-click interval (ICI) for non-buzz clicks (ICI ≥ 13 ms) decreased with decreasing inter-target distance. **B)** Total buzz duration (s) increased with decreasing inter-target distance. **C)** Range to on-axis target at the onset of the buzz (ICI < 13 ms) was greater when the targets were more closely spaced. Distributions of the raw data (*n* =60 for Freja, and *n* = 60 for Sif) are shown as violin plots, while the black dot and whiskers represent the model estimates and 95% confidence intervals, respectively.

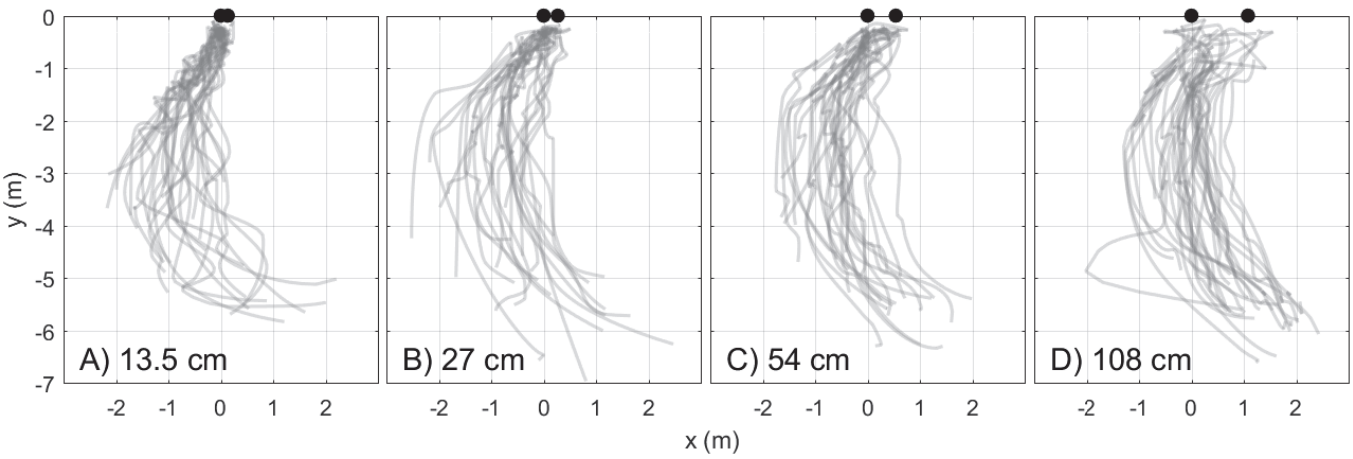

Fig. 5. Bird's-eye view of porpoise approach tracks for all 4 inter-target distances. Black dots show the locations of the left target (0,0) and right target (inter-target distance, 0). **A)** Inter-target distance of 13.5 cm (*n* = 31), **B)** 27 cm (*n* = 27), **C)** 54 cm (*n* = 28), and **D)** 108 cm (*n* = 34). Tracks were created by connecting localized points of on-axis clicks. The sending station was at (1,-8).

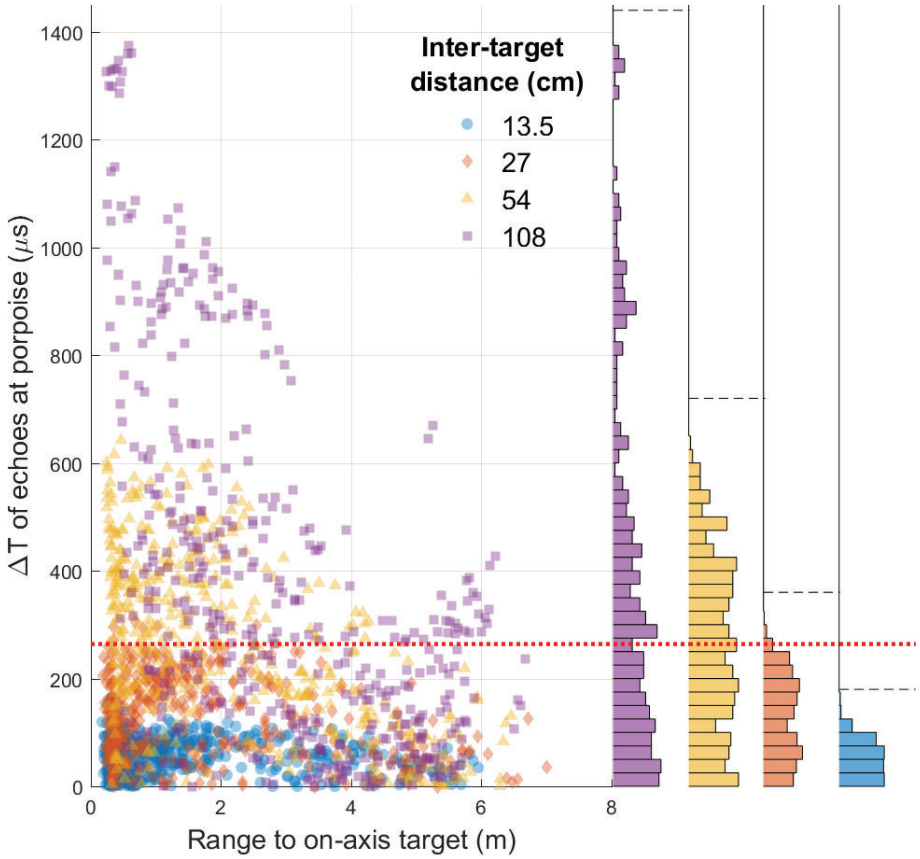

Fig. 6. Temporal delay differences between echoes returning at the porpoise's position as a function of range to the on-axis target for all on-axis clicks (*n* = 1,810). Shapes and colours denote inter-target distance treatments. The red dotted line shows the nominal auditory integration time of 264 µs. Histograms of the echo time delays (ΔT) for each inter-target distance distribution are shown on the right (25 µs bins). Maximal possible time delays based on target spacing geometry are shown with dashed black lines. Note that clicks did not have to fulfil true-scan criteria in order to be included here, as time delay information is insensitive to exclusions brought about by the true-scan criterion.

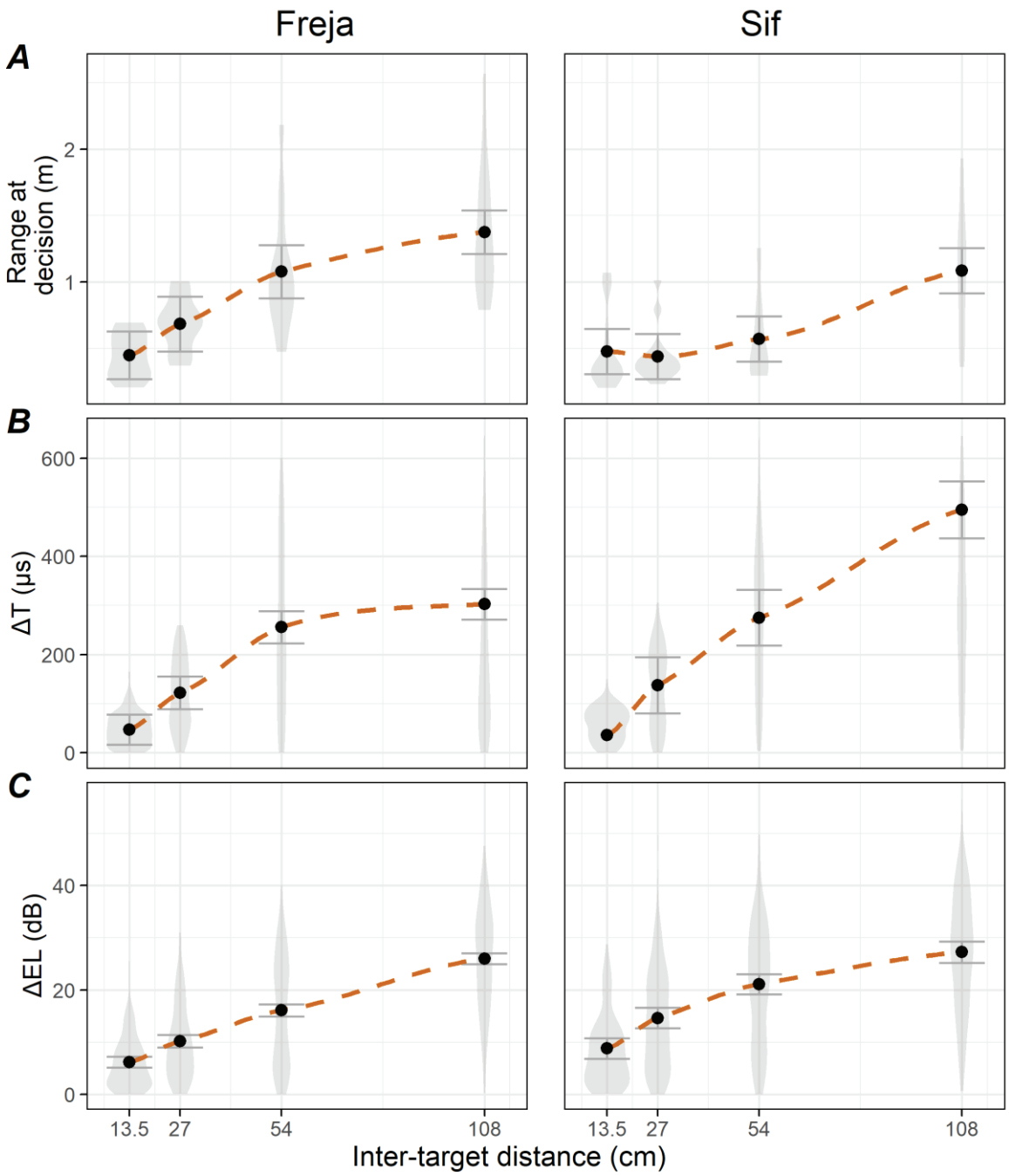

Fig. 7. Cues at the discrimination decision for the two porpoises as a function of inter-target distance. A) Range at the discrimination decision (m) for each trial (*n* = 120) decreased with decreasing inter-target distance. **B)** The time delay between echoes (ΔT, µs) and **C)** the echo level ratio (ΔEL, dB) both increased with increasing inter-target distance for all on-axis clicks (*n* = 1,810). Distributions of the raw data are shown as violin plots, while the black dot and whiskers represent the model estimates and 95% confidence intervals, respectively.

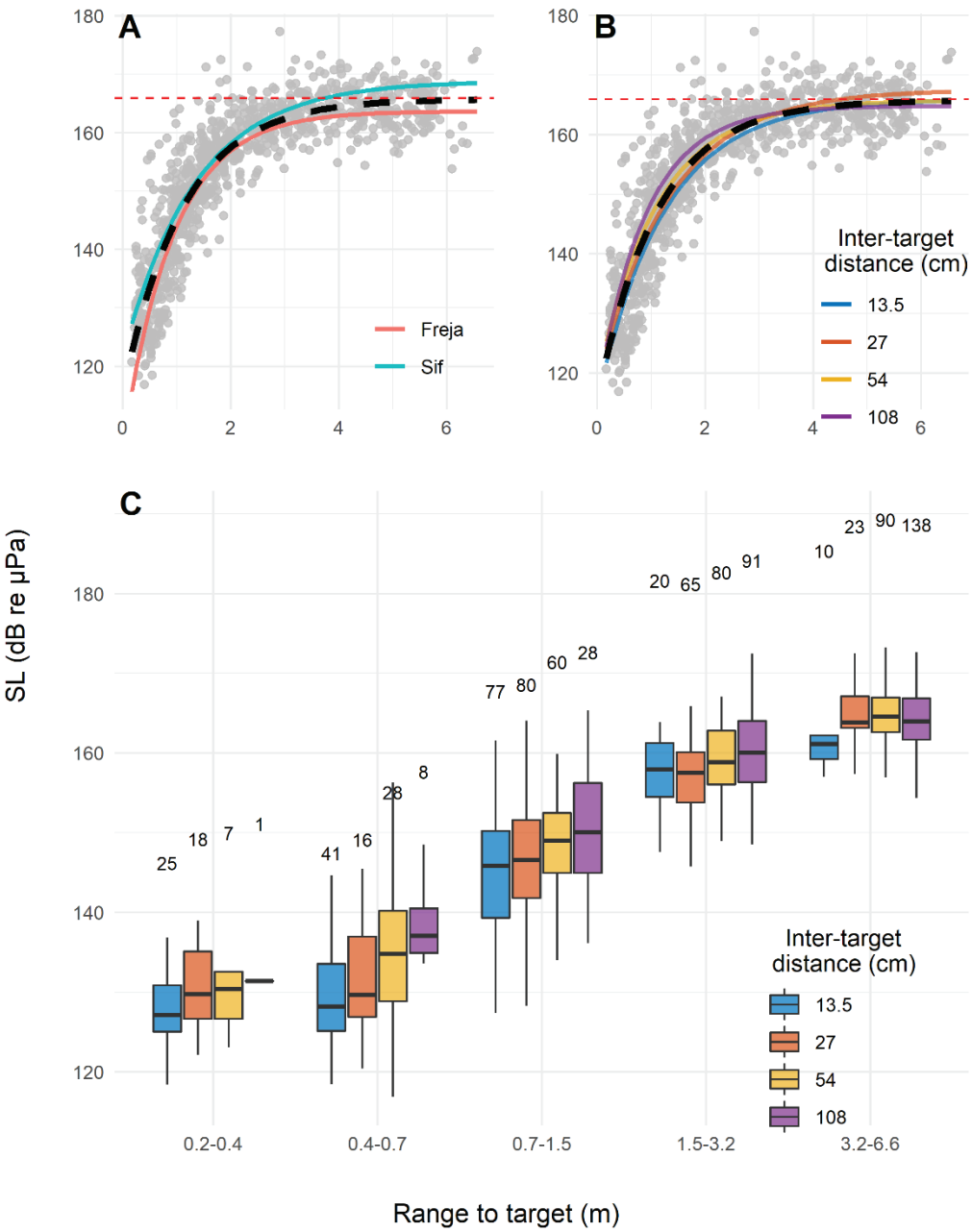

Fig. 8. Source level (SL) as a function of range to target for A) Freja and Sif, B) four inter-target distances, and C) in logarithmically-spaced bins for four inter-target distances. SLs are shown as peak-to-peak values (dB re 1 µPa$_{pp}$) for all true on-axis (n = 906), and adjusted for range-to-target (m). **A, B)** The relationship between SL and range to target is approximated by an asymptotic function in **A** and **B**, where the red dashed line represents the asymptote at 166 dB re 1 µPa. The black dashed line represents the overall function estimate. The number of points contributing to each box in **C** are shown.

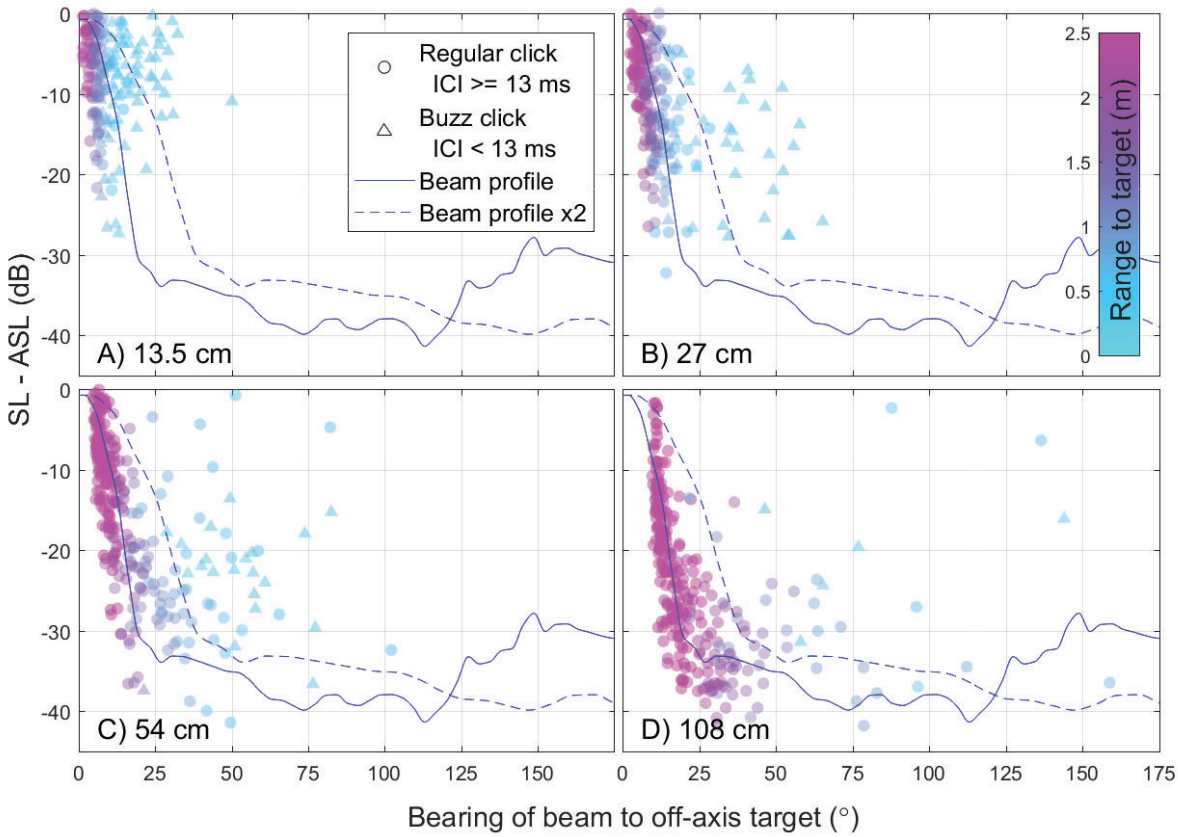

Fig. 9. Bearing from the biosonar beam to the off-axis target for all on-axis clicks (*n* = 906) in relation to porpoise biosonar beam pattern. The difference in back calculated source levels for on-axis (SL) and off-axis (ASL) targets (dB rel. to level at 0°), as calculated from the RLs on both target-mounted hydrophones, the known target strengths (TS), and the measured range to each target. This is shown as a function of horizontal angle to the distracting target (*n* = 120). Subplots show varying inter-target distances: **A)** 13.5 cm, **B)** 27 cm, **C)** 54 cm, and **D)** 108 cm. The average horizontal beam pattern of the same porpoises (from Macaulay *et al.*, 2020) is overlaid, as is double of this beam pattern. Point shape denotes whether or not the discrimination decision was made during a buzz click (triangle, ICI < 13 ms) or during a regular echolocation click (circle, ICI ≥13 ms).

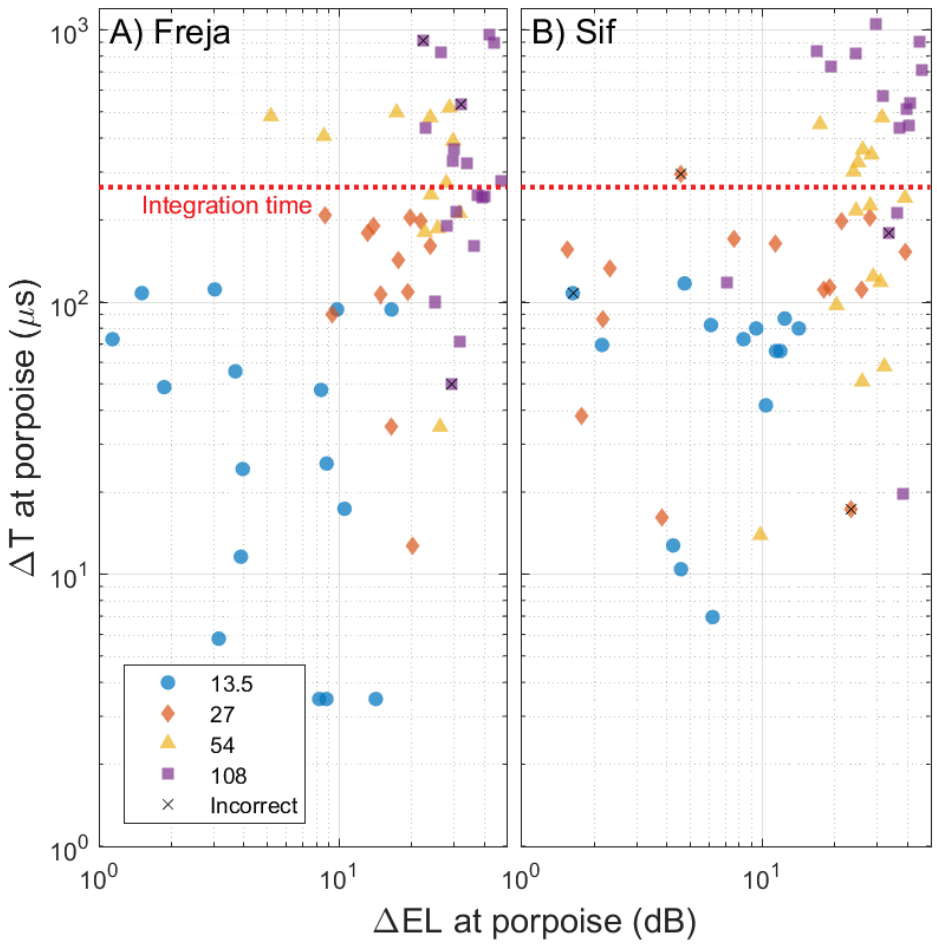

Fig. 10. Timing and relative level of target echoes as received at the porpoise during all discrimination decision clicks. A) Freja (*n* = 60), and **B)** Sif (*n* = 60). Both ΔEL and ΔT are plotted on a log-scale. Shapes and colours denote inter-target distance treatments. The red dotted line shows the reported auditory integration time of 264 µs, and highlights that many discrimination decision clicks occurred at temporal resolutions beneath this threshold. Incorrect target discriminations are denoted with an overlaid black 'x'.

Supplementary Materials

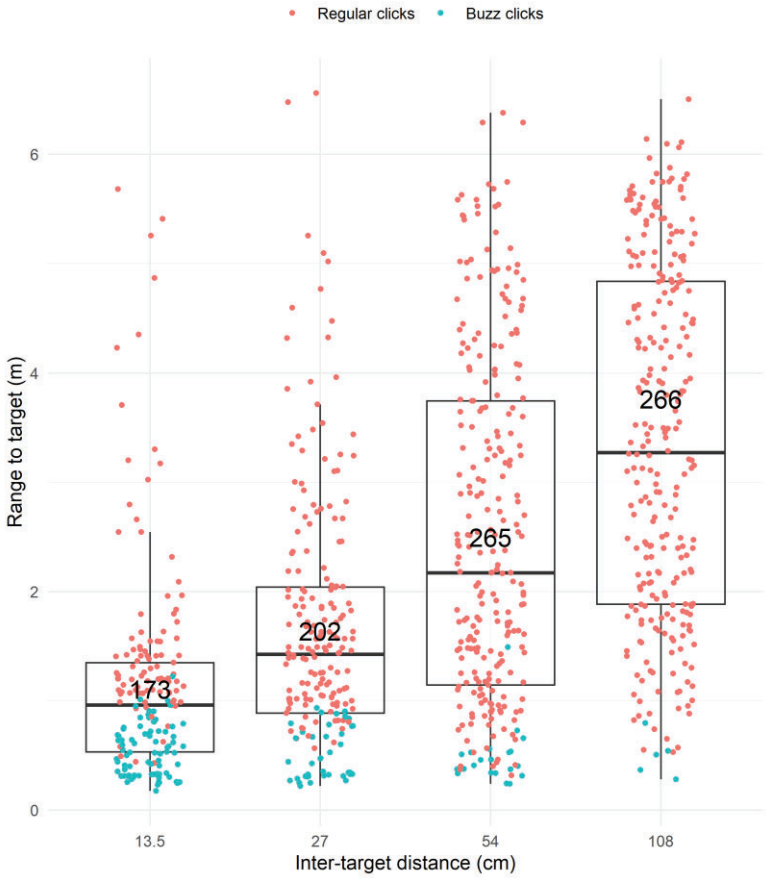

Fig. S1. Range distribution of true on-axis clicks (*n* = 906) used for source level measurement. The non-uniformity of distributions across inter-target distance lead us to adjust for range-to-target in the model. Colour of the clicks denotes whether it was beneath the buzz threshold of 13 ms (turquoise) or not (red). The total number of points comprising each inter-target distance bin is shown atop the boxplot.

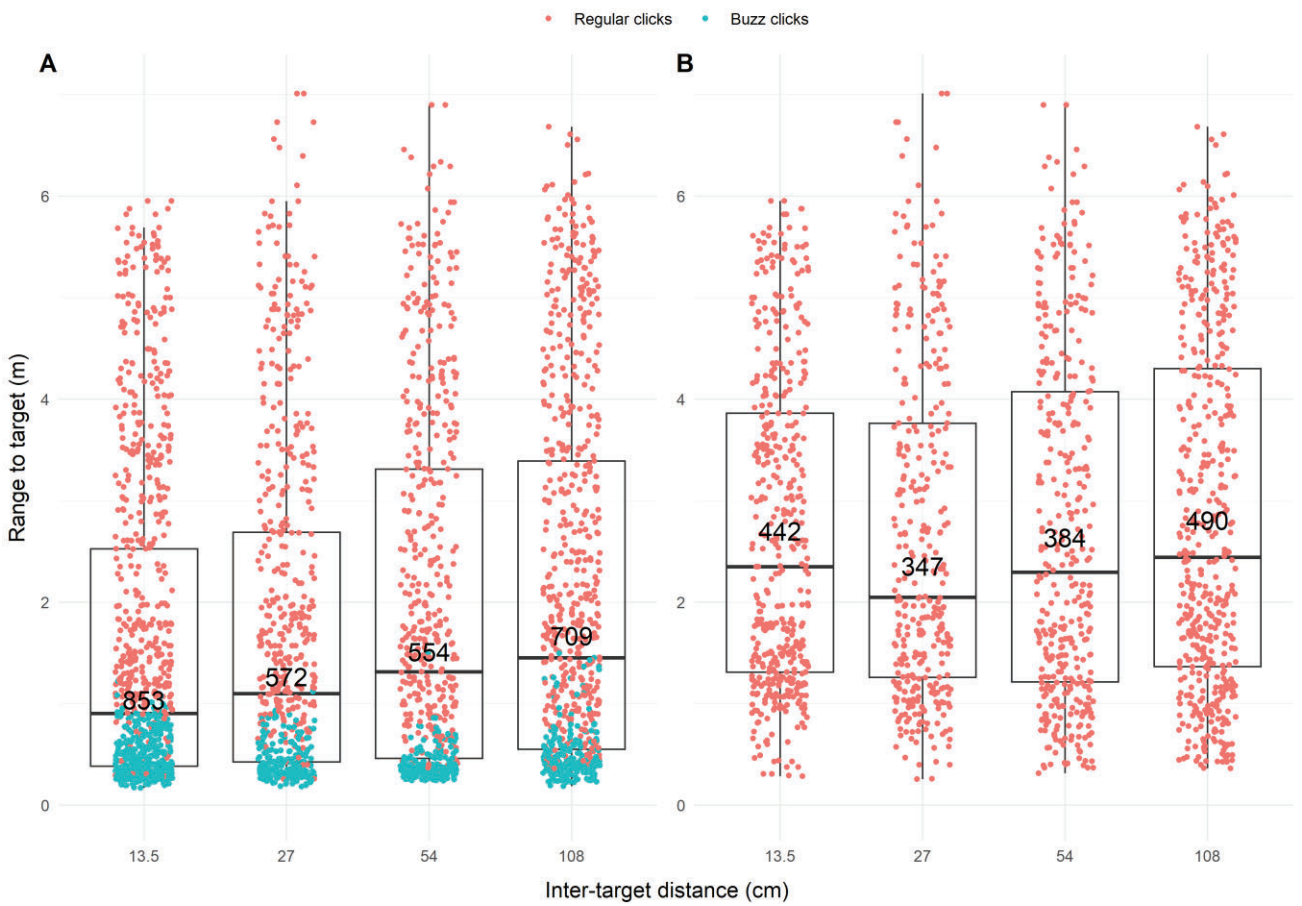

Fig. S2. Comparable range distributions of manually identified on-axis click candidates used for inter-click interval measurement (*n* = 2,688). Colour of the clicks denotes whether it was beneath the buzz threshold of 13 ms (turquoise) or not (red). Distributions are shown for: **A)** buzz and regular clicks, and **B)** just regular echolocation clicks. The total number of points comprising each inter-target distance bin is shown atop the boxplot.

Chapter VI.

Phantom Targets

Malinka, C. E., Beedholm, K., & P. T. Madsen. "Auditory stream segregation in echolocating porpoises during active target approaches," (*Progress Report*).

Auditory stream segregation in echolocating porpoises during active target approaches

Progress report of an ongoing study

Authors (ORCHID ID)

Chloe E Malinka[1*] (0000-0003-0138-8388), Kristian Beedholm[1] (0000-0001-5699-0849), and Peter T Madsen[1] (0000-0002-5208-5259)

[1] Zoophysiology, Dept. Bioscience, Aarhus University, Aarhus, Denmark.

* Author email for correspondence: chloe.e.malinka@bio.au.dk

(To potentially be populated with more co-authors upon publication)

Keywords

Echolocation · biosonar · acoustic gaze · auditory scene analysis · echo stream · phantom echo generation

Abstract

Echolocating toothed whales are often within complex auditory scenes arising from cluttered and/or reverberant environments. It is not understood how they routinely negotiate simultaneously presented echo streams when using their biosonar, for example, to mediate prey capture. Here, we investigated this using set-up novel for odontocete echolocation research: a phantom echo generation in with an actively swimming harbour porpoise (*Phocoena phocoena*) during a target interception task. We chose phantom echo delays of long (3 ms) and short (0.1 ms) durations and different strengths relative to the real target (focusing on +0, 6, 12, 18 dB), to allow for examining both whether the porpoise placed the phantom echo stream within or outside the outer window, and how the porpoise acoustically behaved when the phantom echo stream was within their clutter interference zone. This study builds upon previous investigations into temporal and spatial separation of simultaneously presented echo streams by exploring auditory stream segregation in harbour porpoises in a scenario in which they cannot capitalize on any spatial filtering benefits provided by their directional beam. Our preliminary results show that Freja does not seem to buzz with longer ICIs to accommodate a clutter echo stream at the 3 ms phantom delay that is much louder than the echo stream from the target of interest, and thus hints towards the existence of acute and high resolution auditory stream segregation. For phantom delays of 0.1 ms, well with the 265 µsec auditory integration time for toothed whales, we find that they buzz for longer, perhaps due to compromised ranging arising from clutter interference.

Introduction

Echolocators must retrieve, process, and organize information obtained in complex acoustic environments and use this information to guide subsequent vocal and motor behaviour. However, it is poorly understood how they negotiate acoustic scenes filled with unwanted echoes, as would routinely be the case for echolocators in reverberant or cluttered habitats. To effectively manage the sensory load from an acoustically cluttered environment, echolocating toothed whales must be able to segregate incoming

auditory streams, made all the more difficult when these echo streams are close in space and/or time. This difficulty has recently been explored in both the temporal and spatial domains for porpoises (**Chapter V**, Malinka et al., *submitted*), whereby it was found that they could successfully discriminate targets when echo streams from both a target and a distractor arrived within the reported toothed whale auditory integration time of ~264 µs (Vel'min and Dubrovskiy, 1975; Vel'min, 1976; Moore et al., 1984; Au et al., 1988). The same holds true even if instead accepting the much smaller proposed auditory integration time of 50 µs for harbour porpoises (Zaslavski, 2012). Since the porpoises (in **Chapter V**, Malinka et al., *submitted*) could resolve multiple different auditory streams when echoes arrived within a temporal window in which acoustic events are thought to merge or appear as an acoustic whole (Dubrovskiy, 1990), it was proposed that their highly directional biosonar beams (Jensen et al., 2018; Macaulay et al., 2020) offered spatial filtering benefits that would allow for successful completion of the task via high contrast in returning echo levels (EL).

It remains to be understood how multiple, simultaneous auditory streams are perceptually segregated or handled by adjustments in an echolocator's active sampling when the benefits of spatial filtering provided by a directional beam cannot be taken advantage of. In other words, can a porpoise still successfully intercept a target using echolocation when exposed to a distracting echo stream with a short echo delay that is consistently along the same axis as the target of interest? Secondly, will a porpoise accommodate a more delayed clutter echo so that it is between its inner and outer windows by waiting longer before its next click is emitted, or can it segregate the two echo streams to only worry about range ambiguity for the echoes coming from the target of interest?

The degree to which an acoustic scene is cluttered can be manipulated in experimental contexts. Clutter can been introduced via the presence of physical distractors (*e.g.* Aytekin et al., 2010; Kothari et al., 2014) or by the injection of phantom echoes. By projecting simulated echoes, the acoustic scene available to an echolocating animal is modified so that the animal receives both real echoes from a real target, and 'phantom echoes' from a phantom target. The phantom target is called as such because it does not physically exist, but instead exists perceptually for the porpoise via an echo. A phantom echo generation system can give the experimenter full control over both the echo-generating process and the phantom echo itself, allowing for great potential in investigating biosonar feedback loops (*e.g.* Schmidt, 1992; Aubauer et al., 2000; Finneran et al., 2013, 2019).

Phantom echoes have been used in a variety of detection and discrimination experiments in bats and toothed whales. These have included the investigation of target detection ability in a noisy environment (Au et al., 1988; Møhl, 1986), determining the time difference discrimination threshold (Schmidt 1988, 1992), investigating matched filter processing (Simmons, 1973; Finneran et al., 2013), as well as quantifying the auditory integration times of echoes (Au et al., 1988; Surlykke and Bojeson, 1996). Acoustic parameters of simulated echoes can be controlled in the time or frequency domain. These include manipulations of echo amplitudes, durations, delays, distances between echo wavefronts, frequency bandwidths, and the number of returned echoes per outgoing click (Aubauer et al., 2000; Surlykke, 1992). Changes to the echo level will make the phantom target appear bigger or smaller relative to the real target. In previous experiments, the outgoing phantom target playback signal has been a reversed signal (*e.g.* Masters and Jacobs, 1989; Au and Pawlowski, 1989; Finneran et al., 2013), a signal from a conspecific (*e.g.* Miller, 1991; Surlykke, 1992), and the signal received but projected back after a delay (*e.g.* Aubauer and Au, 1998; Muller et al., 2007). A common thread across all these phantom target experiment for both bats and toothed whales is the use of stationed animals echolocating on either fully phantom generated echoes or

a mix of real and phantom echoes; to our knowledge, only one study on bats (Goerlitz et al., 2012) has ever introduced phantom targets to freely moving echolocators under conditions closer to those they face in the wild, but under acute experimental control.

In an attempt to do that for toothed whales, we here investigate the biosonar dynamics of a free-swimming harbour porpoise as she actively completes a physical target interception task with and without phantom targets of different target strength and delay behind it. We use a phantom echo generator to vary the magnitude of introduced acoustic clutter in the form of an extra echo stream, and thus vary the difficulty in the auditory stream segregation task. We test whether porpoises adjust their biosonar to the target of interest, or to the phantom target 'appearing' behind the actual target, by measuring changes in the rate and intensity of echolocation clicks, indicating switched target ensonification (Atem et al., 2009; Wisniewska et al., 2012). This will uncover whether and when porpoises can time-gate to manage their echoic scene by effectively ignoring irrelevant echoes to reduce range ambiguity (Surlykke, 1992). The co-location of the real target with the projection of the phantom echo meant that the phantom target would always be perceived to be positioned behind the real target, no matter the relative position of the porpoise. We chose to use two different echo delays: a longer delay of 3 ms so that that the phantom echo stream is just outside of the outer window of typical buzzing, and a shorter delay of 0.1 ms so that the phantom echo stream is between the inner and outer windows. In the latter case, the phantom echo stream would be within the clutter interference zone, as estimated by the reported ~264 µsec auditory integration time (Vel'min and Dubrovskiy, 1975; Vel'min, 1976; Moore et al., 1984; Au et al., 1988)

We hypothesize that the overlap of real and louder phantom target echoes with the 0.1 ms delay will make the task harder for the porpoise due to poorer ranging from clutter interference within the integration time of ~260 µsec. As the distractor, in the form of a phantom target, increases in perceived size and decreases in perceived proximity to the real target, biosonar adjustments are hypothesized to be manifested by decreases in source level (SL) (as in Ladegaard and Madsen, 2019, and Malinka et al., *submitted*) in an attempt to reduce the ELs of the phantom stream. For the 3 ms delay between the real and phantom targets, we predict porpoise ICI to increase (and be greater than the two-way travel time to both the real and phantom targets) to accommodate the presence of the phantom target when the target strength (TS) of the phantom target is greater. Specifically, this accommodation would entail placing the echo streams of both the target and the phantom target in an overlap-free time-window between the emitted click and before the next click, the so-called outer window. Placing echo streams of interest between the inner and outer windows has recently been shown in wild echolocating bats (Stidsholt et al., 2021). This prediction is in line with recent reports of the same porpoises: they click faster when intercepting a target near a reflective wall (Ladegaard and Madsen, 2019), and they click faster when a secondary echo stream was temporally and spatially closer to the echo stream of interest (**Chapter V**, Malinka et al., *submitted*). We also predict porpoise approach swim speed to be slower when the phantom echo delay is smaller and represents an acoustically complex scene with spatially overlapping phantom and real targets.

Materials and Methods

Experimental Procedure

The study was conducted on one captive harbour porpoise (*Phocoena phocoena*, Linneaus 1758) at the Fjord & Bælt, Kerteminde, Denmark in December 2017 and March 2018. The participating porpoise,

Freja, is housed in a ~30 x 10 m outdoor netted enclosure in Kerteminde Harbour, and she has been at the facility since she was ~1-2 years old in April 1997 (Lockyer, 2003).

Echolocation clicks were recorded on both the target and by a tag on the free-swimming porpoise as she closed in on a target in a detection and interception task. The porpoise was trained to place the tip of its rostrum on a single, spherical, solid aluminium target (diameter of 7.62 cm or 3 inches), with a measured target strength of -34 dB. The porpoise wore a blindfold (opaque, silicone eyecups) to exclude visual cues from informing biosonar-informed behaviour. Freja has previously worn both a tag and eyecups in other psychoacoustic experiments (*e.g.* Verfuß et al., 2005, 2009; DeRuiter et al., 2009; Linnenschmidt et al., 2012; Wisniewska et al., 2012; **Chapter V**, Malinka et al., *submitted*).

The target was suspended from an out-of-water horizontal pole by a monofilament line near the centre of the sea pen, so that echoes from peripheral pontoons did not interfere. It was lowered into the water to a depth of 1 m at the start of a trial, and removed from the water at the end of a trial (as in Wisniewska et al., 2012, Hermannsen et al., *in prep.*, and **Chapter V**, Malinka et al., *submitted*). At the start of each trial, a trainer cued the porpoise to swim over and touch the target, at a range of ~10 m from the starting position (**Figure 1**). If targeting was successful, the behaviour was bridged with a whistle to indicate a correct response, and the porpoise returned to the sending station for fish reinforcement. No bridge or fish reward was given for the incorrect response of not targeting. Trials were run in blocks over eight days, with no more than 11 trials comprising a session, and no more than 3 sessions per porpoise per day. A total of 186 trials were performed.

Trials varied according to the presence of, or the properties of, the phantom echo. In the control scenario, no phantom target was projected. In non-control trials, phantom echo presentations varied in intensity (phantom target strength level) and delay (distance between the real and phantom targets) relative to the real target. Phantom echoes were presented at temporal delays of either 0.1 ms or 3 ms, relative to the reception of the echolocation click on the target, corresponding to the phantom target being perceived as being 0.075 m or 2.25 m behind the real target. Note that other phantom delays were also briefly used (at 1, 2 and 4 ms), as the dataset (of n = 186) includes some pilot trials before focus was put on the set phantom delays. Phantom target were projected at varied levels relative the target strength (TS) of the real target, at either: 0 +6, +12, or +18 dB, so that the highest TS of the phantom target was -16 dB (-34+18). Note that other phantom strengths were also briefly used (of -12 dB and -6 dB), as the dataset includes some pilot trials collected prior to data collection efforts focusing on +0, +12 and +18 dB. Each trial consisted of a combination of a given phantom target strength with a given phantom echo delay, with combinations presented using a pseudo-random schedule (Gellerman, 1933) for a given session. Neither delays nor intensities of the phantom echoes varied within a given trial.

Acoustic recordings on the target were made with a small, custom-built cylindrical hydrophone (flat frequency response ±2 dB between 100 and 160 kHz) mounted 2 cm above the top of the sphere. The target-mounted hydrophone was connected to a custom-built amplifier box with +40 dB of gain, where an anti-aliasing filter (180 kHz, 4-pole, low-pass) and a pre-whitening high-pass filter (1 kHz, 1-pole) were applied. Received signals were digitized with a multifunction acquisition device, comprising three PXI3e-6358 data acquisition cards each slotted into a PXIe-1078 chassis (National Instruments, Austin, TX, USA), sampling at 500 kHz per channel, 16 bit resolution. The crossing of a threshold prompted the field-programmable gate array (FPGA) of the LabView program (National Instruments, TX, USA) – hereon out collectively referred to as the 'phantom echo generator' (PEG)– to send out the digitized waveform at the desired delay, which was transmitted on the same kind of aforementioned

cylindrical hydrophone, here mounted 2 cm below the bottom of the sphere and acting as an emitting transducer (**Figure 1**). During phantom echo transmission, whatever the recording hydrophone picked up was replaced with silence, so as not to become a phantom echo, and thereby eliminating the possibility of a runaway feedback loop in the PEG.

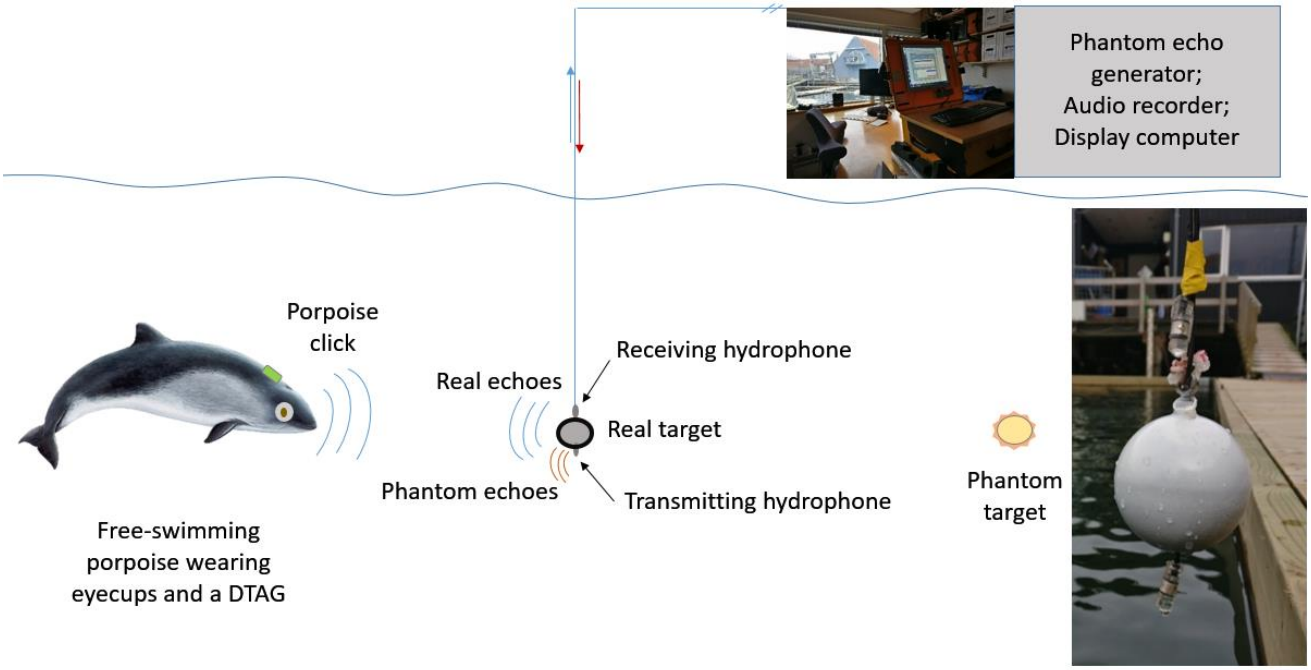

***Figure 1**. Schematic of a given trial. As the blindfolded, tagged porpoise approaches a target while echolocating, she receives both real echoes from the physical target, as well as simulated echoes representing a phantom target. The phantom echo delay determines the distance along the range axis between the real and phantom targets, and the level of the phantom echo relative to the real target sets the size of the phantom target. The phantom echo generator was placed inside with a window looking out onto where the experiment was taking place.*

Note that clicks needed to be above a threshold in order to gate the transmission of a phantom echo, which effectively meant that it was only present when the real target was within a narrow swath near the axis of its biosonar beam. This also means that the porpoise was only subject to receiving phantom echoes when its beam was pointing close to the target. As the separation of the phantom and real targets was only set by a time delay, the phantom target would always be perceived as being directly behind the real target. While the porpoise was freely swimming and able to adjust its incoming direction relative to the suspended target, it would never be able to spatially separate the real and phantom target streams on the left-right plane.

These receiving and transmitting transducers mounted on the real target were calibrated against a TC-4034 hydrophone (Teledyne Reson, Slangerup, Denmark) using simulated porpoise clicks (projected from a TC-2130; also Teledyne Reson) generated by a waveform generator (model 33220A, Agilent Technologies, Santa Clara, CA, USA), and were found to have a sensitivity of -211 dB re 1 V/μPa. The PEG saved a two-channel acoustic recording for each trial, with channels recording the receiving and transmitting streams, respectively. The PEG was housed inside during experiments for protection from the elements, but was immediately adjacent to and visible from the data collection site (**Figure 1**). Indoor lights were turned off to reduce electrical noise contamination.

Echolocation clicks and returning echoes were also recorded by a multi-sensor, on-animal sound and movement digital recording tag (DTAG-4; Johnson and Tyack, 2003; www.soundtags.org) attached non-invasively via suction cups behind the sound generator and immediately anterior to the blow hole. The tag continuously sampled audio data on a single hydrophone at 576 kHz (flat frequency response +2 dB from 0.4 to 150 kHz). The time delays between click emission and echo reception, as recorded on the tag, provided range-to-target information. Additionally, the tag recorded the echoic scene available to the porpoise, enabling the creation of echograms (Johnson, 2014).

The phantom echo generator was calibrated in Aarhus harbour using simulated porpoise clicks projected at known ranges from a transducer (TC-2130). The receiving hydrophone was mounted immediately atop the target, and the transmitting hydrophone was mounted immediately above the target. Whenever an echolocation click was received on the top-mounted hydrophone on the target, it gated the phantom echo generation at a set delay and at a set gain. Calibration of the phantom echo generator involved ensuring that only echolocation clicks originating from the porpoise gated the transmission of phantom echoes, so that the phantom echoes did not themselves trigger the gating and further production of phantom targets. Avoiding such positive feedback was also aided by the shading provided by the large size of the spherical target (7.62 cm, or 3 inches in diameter).

The co-location of the target with the playback transducer meant that the phantom target was always in line with the real target, even if the porpoise changed its relative location. Therefore our experimental set-up does not have the flexibility of distractor position as in Aytekin et al. (2010), as we can only introduce phantom echoes that are along the same range axis as the real target: the phantom target distractors can only be perceived as being behind the real target; we cannot present distractors that are above/below or left/right of the real target. Warnecke et al. (2014) studied bat biosonar performance with varied locations and directions of phantom echoes, and found spatial release from masking of clutter echoes. In this set-up, however, there is no opportunity for the spatial release of masking.

Trials were additionally monitored with a GoPro Hero-2 video camera (GoPro Inc, San Mateo, CA) mounted above water on the horizontal beam that suspended the target. The target was painted white to facilitate visualization of the underwater target by both the camera and researchers on the pontoon.

Data Analysis

Acoustic Analysis

Acoustic analysis and data processing were conducted in MATLAB (version 8.5, The Mathworks, Natick, MA, USA). The unique inter-click intervals (ICIs) of echolocation clicks produced by the porpoise during target approaches were used to time-synchronize the audio recorded on the tag and on the target for each trial.

Acoustic recordings from the target-mounted receiving hydrophone were filtered (90-180 kHz, 4-pole Butterworth band-pass filter). Porpoise clicks were then detected using a supervised click detector. Received levels (RLs) on the targets were quantified as the clip level of the system (171 dB re 1 μPa) + 20·log10(peak-to-peak amplitude). On-axis clicks were manually identified in the relative RLs of consecutive clicks, indicating when the porpoise likely scanned across the target (Madsen and Wahlberg, 2007). The distance between the porpoise and the target was measured using the time delays between on-axis click emission and echo reception on the tag, and the range to target was interpolated between these points. Echograms (Johnson, 2014) were created for each trial, and enabled the visual confirmation of echo streams from both the real target and the phantom target (**Figure 2**). The example in **Figure 2**

demonstrates that phantom echoes were only produced by the phantom echo generator and subsequently recorded on the acoustic tag on the porpoise when the porpoise scanned across the real target.

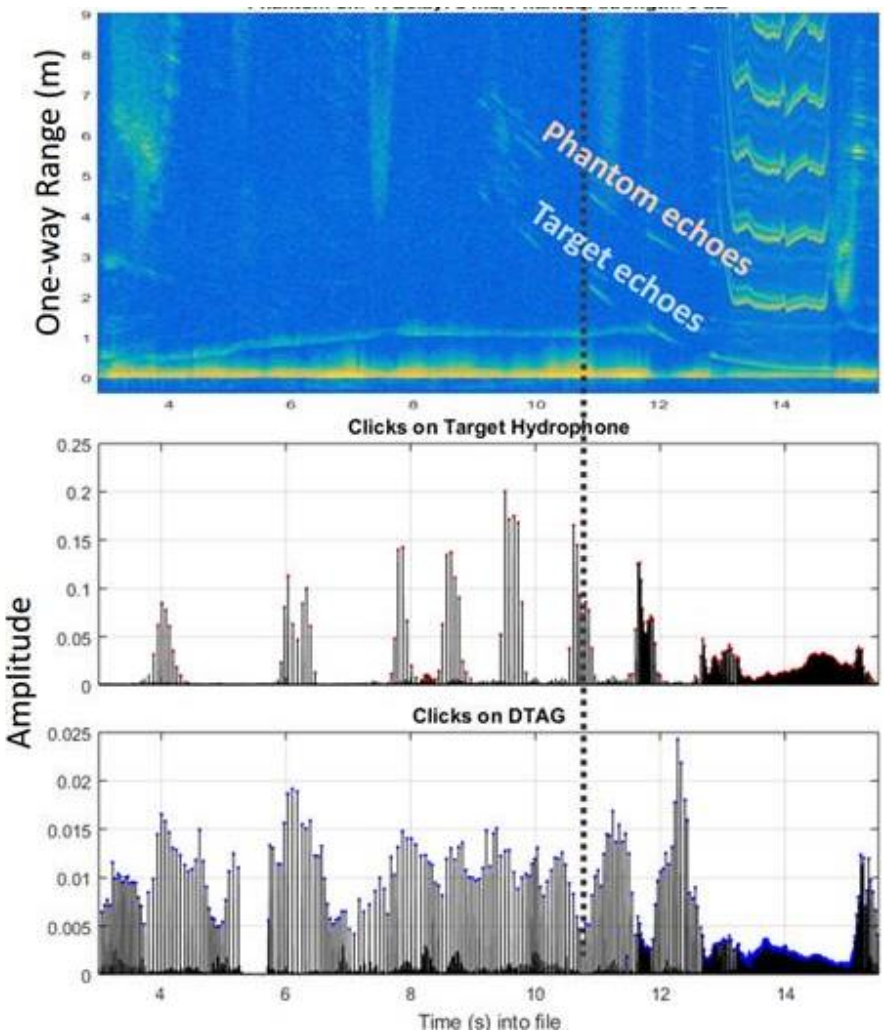

Figure 2*. Example of the echo streams from the real target and the phantom target for an example trial, demonstrating viability of phantom echo generator. Here, the phantom target was presented with a delay of 3 ms and a relative level of +0 dB. The top panel shows clearly that phantom echoes were only recorded on the acoustic tag on the porpoise when the porpoise scanned across the real target (middle panel), despite near continuous clicking of the porpoise during the target approach (bottom panel).*

Using: (i) the measured range of the porpoise to the target (R), (ii) the set range between the phantom target and the real target, and (iii) the set target level of the phantom target relative to the real target, all allowed for the calculation of the received echo levels (EL) of both the real and phantom target streams. ELs for the real-target stream were calculated as: $RL_{on\ target} + TS - 20\log_{10}(R)$. Source levels (SL) of the porpoise clicks were calculated for all on-axis clicks, referenced to 1 m ahead of the animal and along its beam axis. Absorption losses (~0.04 dB/m at 130 kHz) were ignored due to the short-ranges (<10 m) considered here.

To assess task difficulty and monitor biosonar behaviour, several echolocation metrics will be measured. These will include: i) trial duration (s; from the start of a trial to target interception), (ii) total buzz duration (s; with buzzing defined as clicks with ICIs < 13 ms (Wisniewska et al., 2012)), (iii) the range to the real target at buzz onset, or the so-called 'hand-off distance' (m), (iv) the number of scans across

the real target, (v) the SL of on-axis clicks, (vi) the ICIs during the target approach, and (vii) the median buzz ICI to see if the porpoise clicks slower to accommodate the 3 ms phantom delay by making their outer window larger. Furthermore, the range to which the ICI pattern suggests the porpoise is adjusting her biosonar to / attending to will be calculated. This will be compared to the measured ranges between the porpoise and the real and phantom targets. Should these suggest that the porpoise was adjusting her echolocation to the range of the phantom target, the duration of the 'recovery time' of locking onto the phantom target to locking onto the real target will be measured. Finally, the 'wobbliness' of the buzz will be calculated since previous research suggested that small changes in ICIs, termed 'jittering', could aid in reducing range ambiguity (Kadane and Penner, 1983).

Statistical Analysis

The statistical analyses will be completed using R software (version 3.6.1; R Core Team, 2019). To quantify how the porpoise modified her echolocation behaviour according to the complexity of the acoustic scene, phantom target level and delay (together determining the prominence of the phantom echo stream) will be the main explanatory variables, tested against eight response variables (trial duration, number of scans, buzz duration, range from targets at buzz onset, buzz wobbliness, median buzz ICI, recovery time, ICI, and the SL of true on-axis clicks). Generalized linear mixed-models will be used to evaluate these associations.

Results and Discussion

Analysis is on-going, and so while conclusions on the study as a whole are yet to be available, several figures of example trials are shown below. An overview of the number of trials and the combinations of phantom delay and phantom strength are presented in **Table 1**.

Table 1*. Overview of data collection (n = 186), with the number of trials collected with each combination of phantom target strength (dB) relative to the real target and phantom echo delay (ms) shown. Trials with "no phantom" are control trials. Combinations of phantom target strengths and delays that are shown as examples within this progress report are highlighted yellow.*

		Phantom target strength (dB)						
		-12	-6	0	+6	+12	+18	No phantom
Phantom delay (ms)	0.1	0	0	22	0	16	23	n/a
	1	0	0	4				n/a
	2	0	0	2	3			n/a
	3	0	1	26	3	17	21	n/a
	4	3	11	9	1			n/a
	No phantom	n/a	n/a	n/a	n/a	n/a	n/a	24 controls

Preliminary results are here presented as examples of echo streams during target approaches during control trials and trials where the PEG was active. A control trial (**Figure 3**) shows a typical trial in which no phantom echo streams were projected. The echogram shows the reducing range between the porpoise and the target as time progresses. Echoes present in the echogram arose from the sea surface and the wall ~3.5-4 m from the target location. **Figure 4** shows the combination of the longer phantom delay (3 ms) with a phantom target strength equivalent to the target strength of the real target (+0 dB). Here, and as in

the other combination of a longer delay (3 ms) and a stronger phantom target strength (+18 dB) (**Figure 5**), note that the buzz ICIs are not made longer to accommodate the phantom echo stream. In other words, the phantom echo stream is positioned outside and beyond the outer window.

Figure 6 shows the combination of the shorter phantom delay (0.1 ms) with a phantom target strength equivalent to that of the real target (+0 dB), and a slightly longer buzz is observed. **Figure 7** and **Figure 8** both show the most challenging combination of a short delay (0.1 ms) and a strong phantom target (+18 dB), with the difference being that the first time this combination is ever presented to the porpoise is shown in **Figure 7**. This is the only example in which the porpoise did not buzz despite being at a range to the target typical for doing so, and it is also the only example in which the porpoise did not touch the target and in which she abandoned the task altogether. Interestingly, on subsequent occasions of being presented with the close and strong phantom echo stream (**Figure 8**), Freja successfully touched the target.

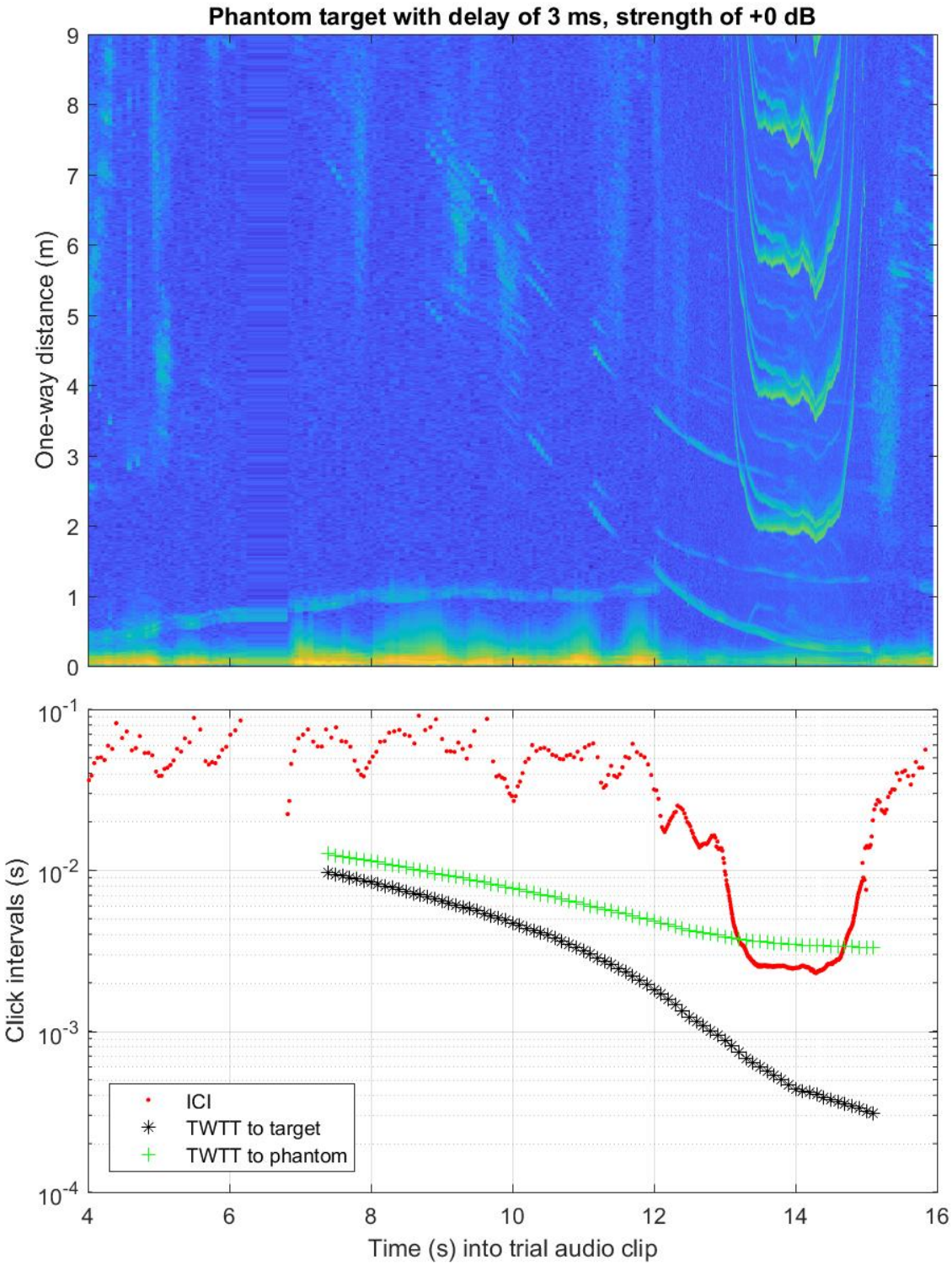

Figure 4 Note here that the buzz is also longer than in control trials. In the short delay trials (**Figures 6, 7, 8**), the click rate during the buzz is not fast enough to place the phantom echo stream in the outer window. This is not surprising as the porpoise would have to buzz at a click rate that is an order of magnitude faster than the smallest recorded buzz ICI of ~2 ms (Wisniewska et al., 2016).

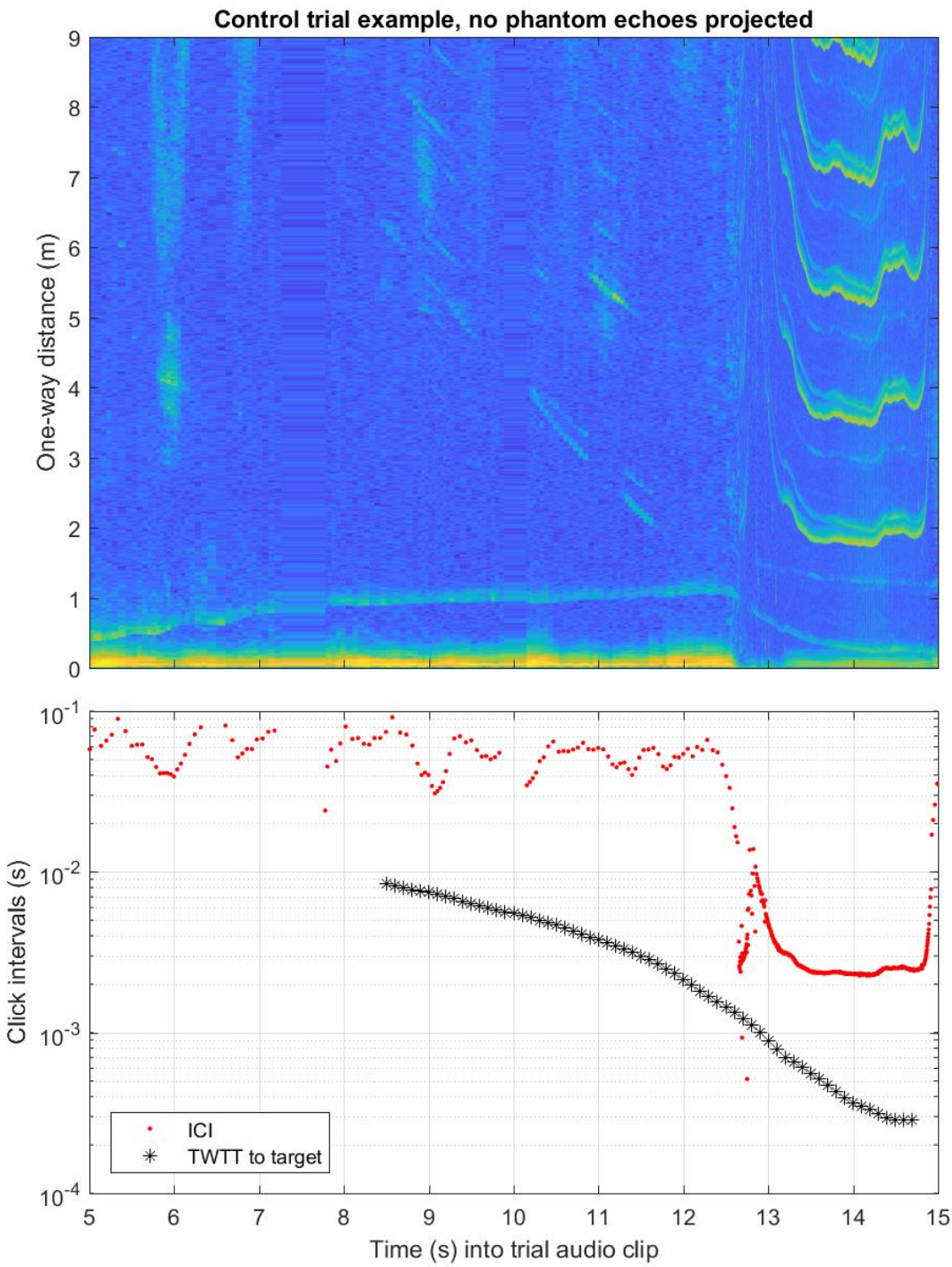

Figure 3. *Example trial data during a control trial in which no phantom echoes were projected, meaning that the only echo stream arises from the real target. A) shows the echogram, and B) shows the inter-click interval (ICI) and two-way travel time (TWTT) of the porpoise to the real target.*

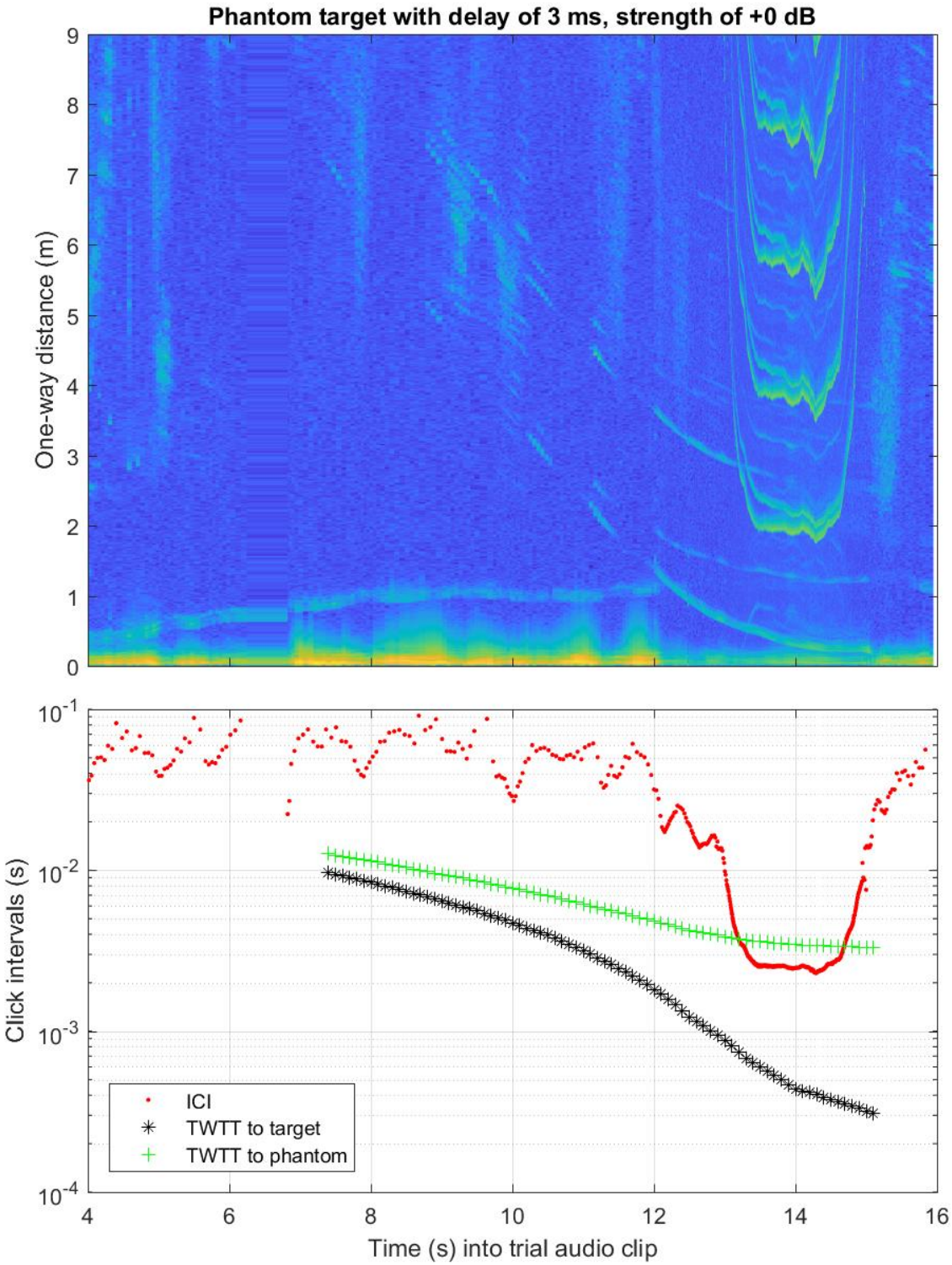

Figure 4. *Example trial data where the phantom delay was large (3 ms) and the phantom target strength was the same as the real target strength (+0 dB). A) shows the echogram, and B) shows the inter-click interval (ICI) and two-way travel time (TWTT) of the porpoise to the real and phantom targets. Note that the buzz ICIs are not made longer to accommodate the phantom echo stream so that it is within the outer window.*

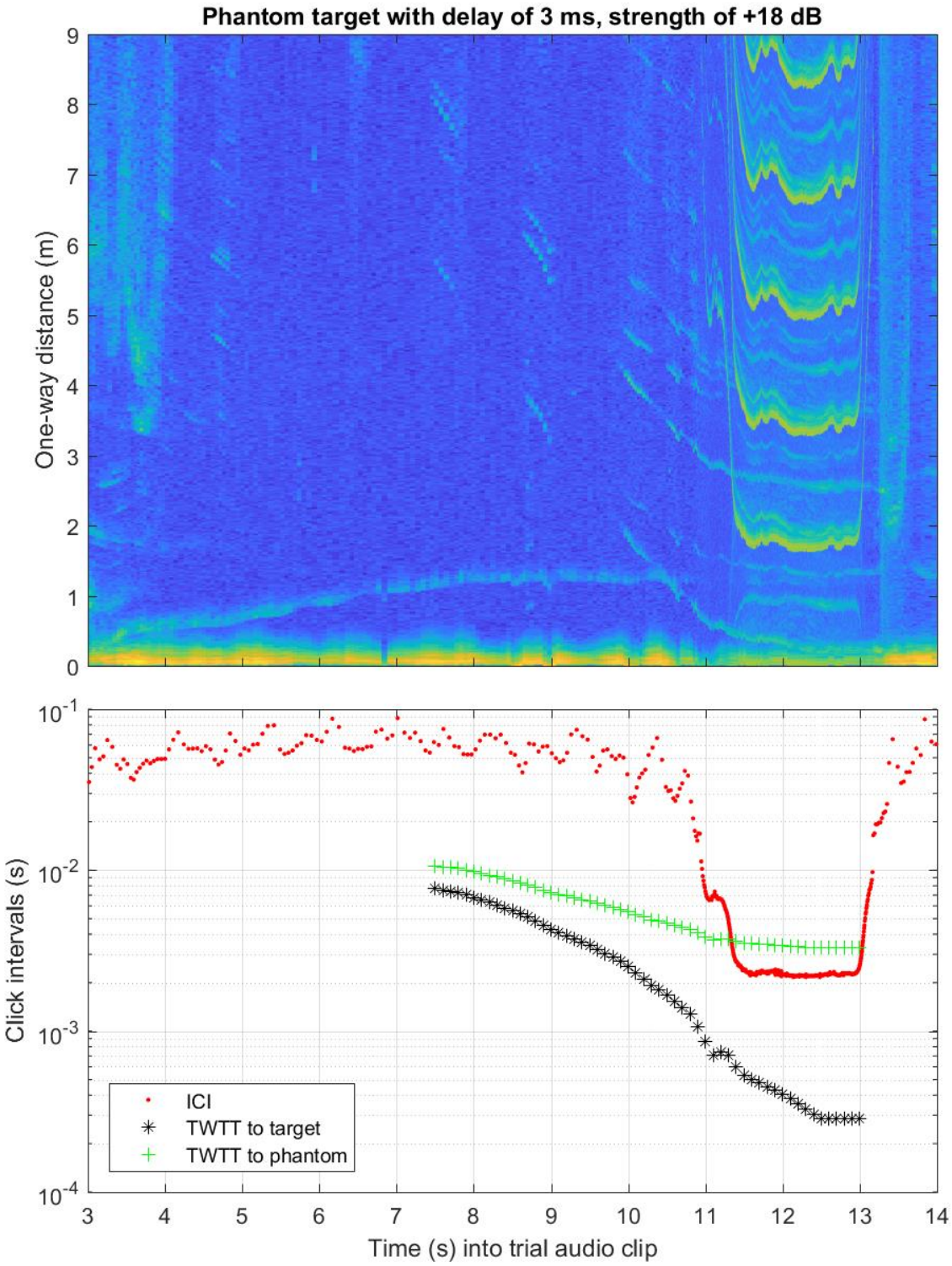

Figure 5. *Example trial data where the phantom delay was large (3 ms) and the phantom target strength was much larger than the real target strength (+18 dB). A) shows the echogram, and B) shows the inter-click interval (ICI) and two-way travel time (TWTT) of the porpoise to the real and phantom targets. Note that the buzz ICIs are not made longer to accommodate the phantom echo stream so that it is within the outer window.*

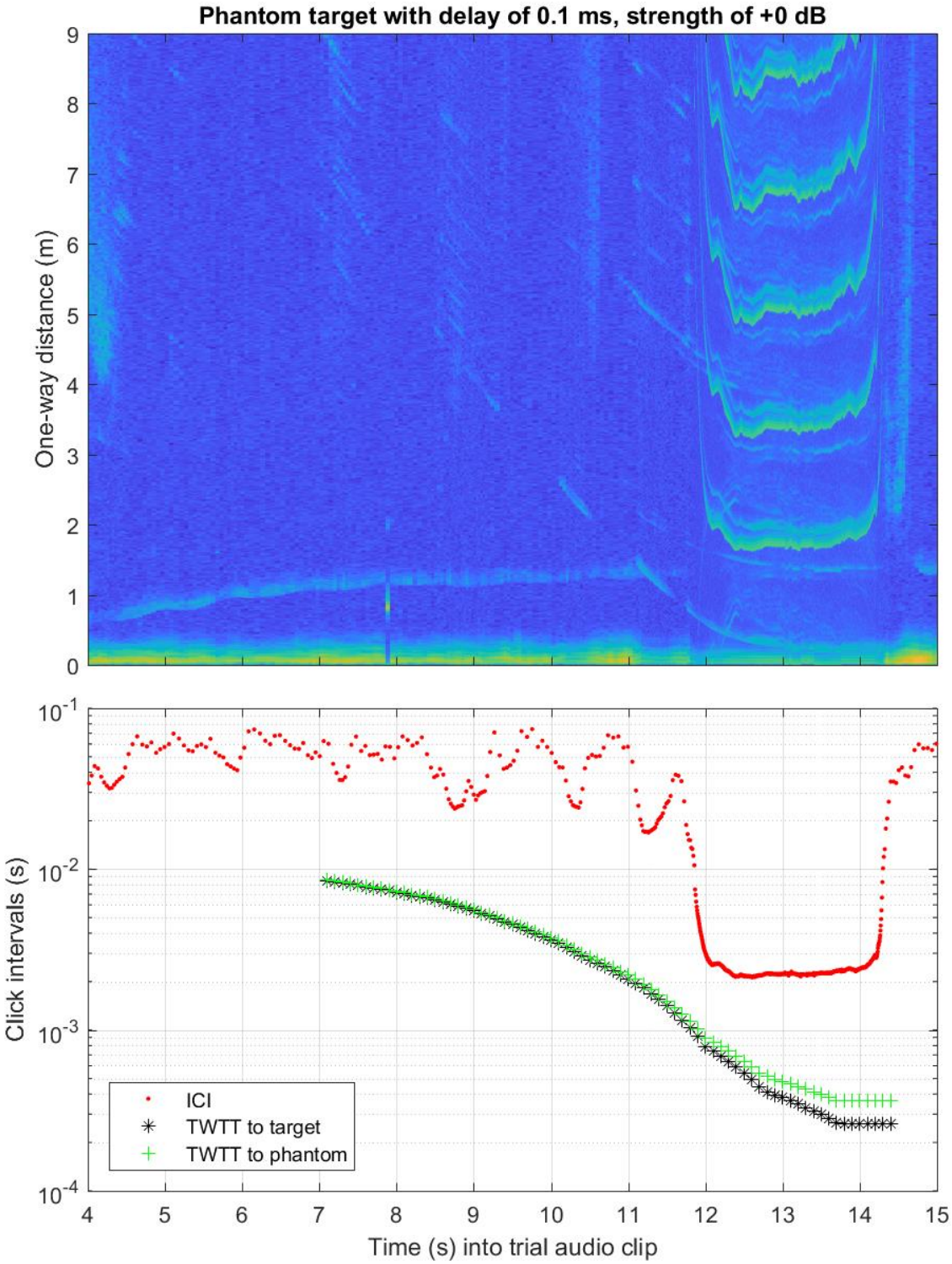

Figure 6. *Example trial data where the phantom delay was small (0.1 ms) and the phantom target strength was the same as the real target strength (+0 dB). A) shows the echogram, and B) shows the inter-click interval (ICI) and two-way travel time (TWTT) of the porpoise to the real and phantom targets. Note that the buzz is perhaps slightly longer than normal in this treatment.*

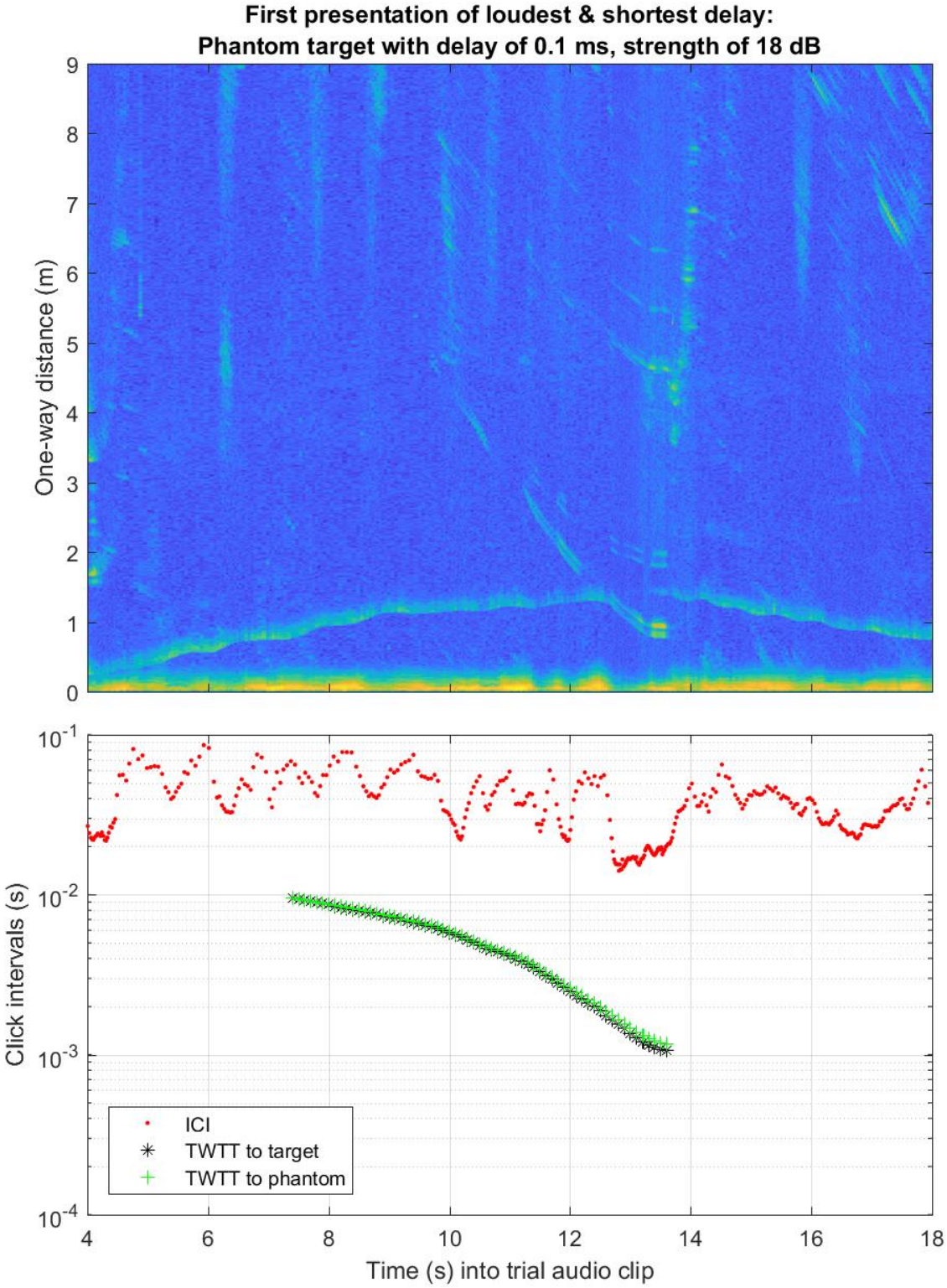

Figure 7. *Example trial data where the phantom delay was small (0.1 ms) and the phantom target strength was larger than the real target strength (+18 dB). This was the first time the porpoise was subjected to the combination of largest phantom target strength with shortest phantom echo delay, in which the porpoise did not buzz or touch the target despite it being at the normal hand-off distance at which a buzz usually occurs. A) shows the echogram, and B) shows the inter-click interval (ICI) and two-way travel time (TWTT) of the porpoise to the real and phantom targets.*

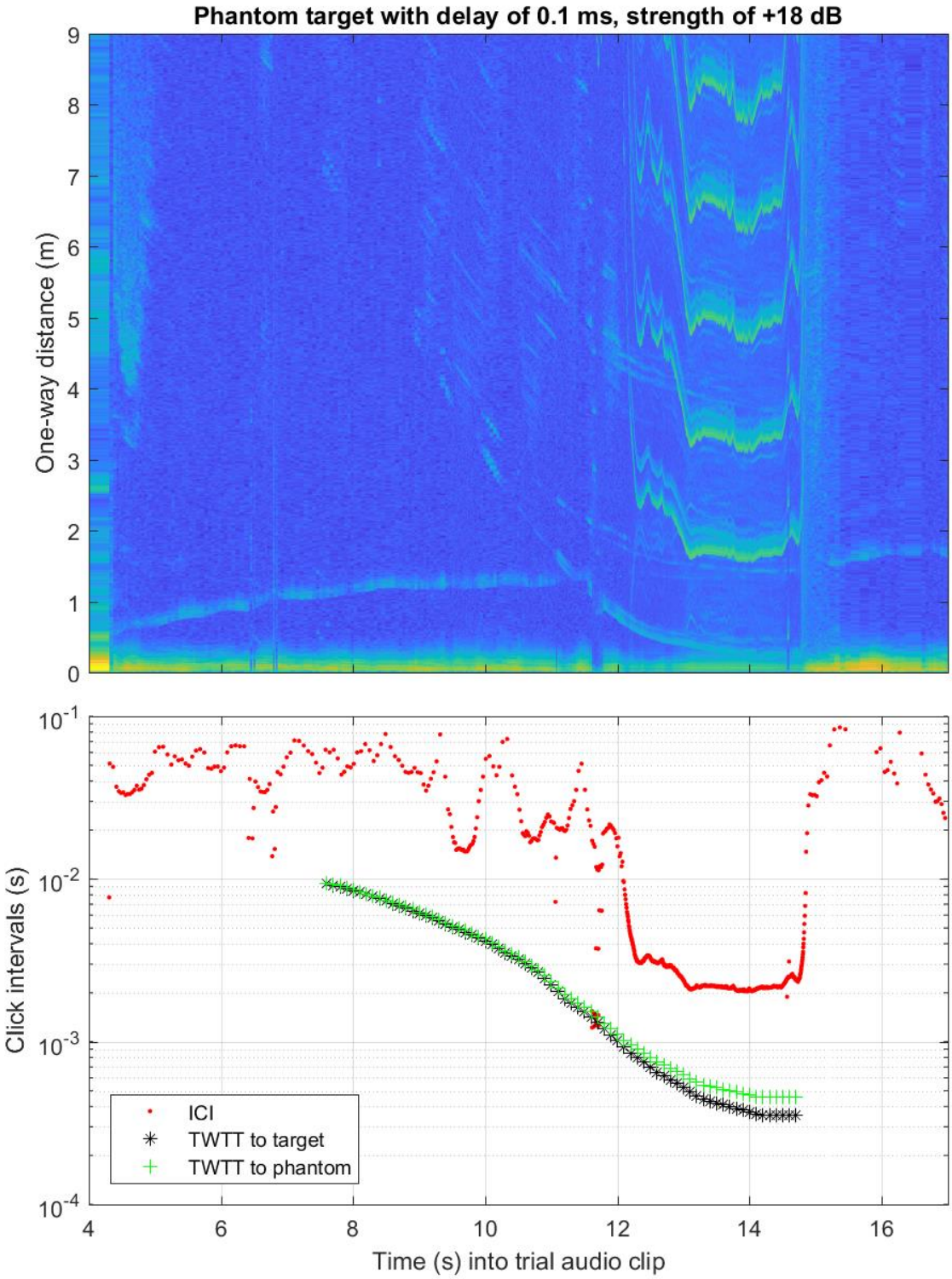

Figure 8. *Example trial data where the phantom delay was small (0.1 ms) and the phantom target strength was much larger than the real target strength (+18 dB). A) shows the echogram, and B) shows the inter-click interval (ICI) and two-way travel time (TWTT) of the porpoise to the real and phantom targets. Note that the buzz is perhaps slightly longer than during controls.*

Preliminary Conclusion

Freja does not seem to buzz using longer ICIs to accommodate a clutter echo stream at the 3 ms phantom delay that is much louder than the echo stream from the target of interest (**Figure 8**) providing strong evidence for acute and high resolution auditory stream segregation. For phantom delays of 0.1 ms, well with the 265 µsec integration time, it is perhaps the case that the task is more difficult as reflected in longer buzzes, due perhaps to compromised ranging due to clutter interference.

To do list:

In order to complete the manuscript, the following analyses are needed:

- Complete supervised click detection on the DTAG and the target-mounted acoustic recordings.
- Measure the range to the target throughout all target approaches using the tag acoustic data.
- For each trial, quantify the trial duration, number of scans across the target, the buzz duration, the range from targets at buzz onset, the buzz wobbliness (and decide how this is quantified), the ICI throughout the approach, the median buzz ICI, and the recovery time (if applicable).
- Calculate of the RLs on the target, and the received echo levels (ELs) of both the real and phantom target streams during target approaches. Use the measured RLs and the measured ranges to calculate the SLs of on-axis clicks.
- Feed variables into a GLMM to model results of biosonar adjustments.

Acknowledgements

We are grateful to Josefin Larsson, Fredrik Johansson, Mathilde Kjølby and Jakob Højer Kristensen at the Fjord & Bælt center, Kerteminde, Denmark for assistance in conducting the experiment. We thank John Svane Jensen for manufacturing the target and constructing the metal calibration frame. Thanks to Captain Torben Vang for allowing calibration off of Aarhus University's research ship, Aurora. Thanks to Mark Johnson for providing the DTAG4 and useful analytical tools, and to Magnus Wahlberg for providing office space. Thanks to Cynthia Moss, John R. Buck, and Peter Tyack for helpful comments on the initial results.

Ethics Statement

The porpoise at Fjord & Bælt, Kerteminde, Denmark, is maintained under permits no. SN 343/FY-0014 and 19963446-0021 from the Danish Nature Agency under the Ministry of Environment and Food of Denmark.

Competing Interests

The authors declare no competing or financial interests.

Author Contributions

Roles	**Contributors**
Conceptualization	CEM, PTM, KB
Methodology	CEM, PTM, KB
Software	CEM, KB
Validation	CEM

Formal Analysis	CEM
Investigation	CEM
Resources	PTM, KB
Data Curation	CEM
Writing: original draft preparation	CEM
Writing: review & editing	CEM, [PTM, KB]
Visualization	CEM
Supervision	PTM
Project Administration	PTM, CEM
Funding Acquisition	PTM

Funding

PhD funding was provided by Danish National Research Council to PTM (grant 27125). This, along with ONR awards N00014-18-1-2062 and N00014-20-1-2709, covered research time at Fjord & Bælt.

References

Atem, A. C. G., Rasmussen, M. H., Wahlberg, M., Petersen, H. C. and L. A. Miller. (2009). Changes in click source levels with distance to targets: Studies of free-ranging white-beaked Dolphins *Lagenorhynchus albirostris* and captive Harbour Porpoises *Phocoena Phocoena*. **Bioacoustics**, 19(1-2): 49-65.

Au, W. W., Moore, P. W. B., and D. A. Pawloski (1988). Detection of complex echoes in noise by an echolocating dolphin. **J Acoust Soc Am**, 83 (2): 662-668.

Au, W. W. and D. A. Pawloski (1989). A comparison of signal detection between an echolocating dolphin and an optimal receiver. **J Comp Phys A**, 164 (4): 451-458.

Aubauer, R. and W. W. Au (1998). Phantom echo generation: A new technique for investigating dolphin echolocation. **J Acoust Soc Am**, 104 (3): 1165-1170.

Aubauer, R., Au, W. W. L., Nachtigall, P. E. Pawloski, D. A. and C. M. DeLong. (2000). Classification of electronically generated phantom targets by an Atlantic bottlenose dolphin (*Tursiops truncatus*). **J Acoust Soc Am**, 107 (5): 2750-2754.

Aytekin, M., Mao, B. and C. F. Moss (2010). Spatial perception and adaptive sonar behavior. **J Acoust Soc Am**, 128 (6): 3788-3798.

DeRuiter, S. L., Bahr, A., Blanchet, M.-A., Hansen, S. F., Kristensen, J. H., Madsen, P. T., Tyack, P. T. and M. Wahlberg. (2009). Acoustic behaviour of echolocating porpoises during prey capture. **J Exp Biol**, 212 (19): 3100-3107.

Dubrovskiy, N. A. (1990). On the two auditory subsystems in dolphins. *In:* Sensory Abilities of Cetaceans. Springer, pp. 233-254.

Finneran, J. J., Wu, T., Borror, N., Tormey, M., Brewer, A., Black, A. and K. Bakhtiari (2013). Bottlenose dolphin (*Tursiops truncatus*) detection of simulated echoes from normal and time-reversed clicks. **J Acoust Soc Am**, 134 (6): 4548-4555.

Finneran, J. J., Jones, R., Mulsow, J., Houser, D. S., and Moore, P. W. (2019). Jittered echo-delay resolution in bottlenose dolphins (*Tursiops truncatus*). **J Comp Phys A**, 205(1), 125-137.

Goerlitz, H. R., Genzel, D., and Wiegrebe, L. (2012). Bats' avoidance of real and virtual objects: Implications for the sonar coding of object size. **Behav**, 89(1), 61-67.

Jensen, F. H., Johnson, M., Ladegaard, M., Wisniewska, D., and P. T. Madsen. (2018). Narrow acoustic field of view drives frequency scaling in toothed whale biosonar. **Curr Biol**, 28, 1-8.

Johnson, M. (2014). On-animal methods for studying echolocation in free-ranging animals. *In*: Surlykke, A., Nachtigall, P. E., Fay, R. R., and Popper, A. N. (Eds.), *Biosonar*. Springer, pp. 195-229.

Johnson, M. P. and P. L. Tyack. (2003). A digital acoustic recording tag for measuring the response of wild marine mammals to sound. **IEEE J Ocean Eng**, 28(1), 3-12.

Kadane, J. and R. Penner. (1983). Range ambiguity and pulse interval jitter in the bottlenose dolphin. **J Acoust Soc Am**, 74 (3), 1059-1061.

Kothari, N. B., Wohlgemuth, M. J., Hulgard, K., Surlykke, A. and C. F. Moss (2014). Timing matters: sonar call groups facilitate target localization in bats. **Front Physiol**, 5: 168.

Ladegaard, M., Beedholm, K., Malinka C. E., Johnson, M. and P. T. Madsen. (*In prep.*) Sensory-motor control of output levels as a function of range and target strength in echolocating porpoises.

Linnenschmidt, M., Beedholm, K., Wahlberg, M., Højer-Kristensen, J. and P. E. Nachtigall (2012). Keeping returns optimal: gain control exerted through sensitivity adjustments in the harbour porpoise auditory system. **Proc Roy Soc B**, rspb20112465.

Lockyer, C., Desportes, G., Hansen, K., Labberté, S. and U. Siebert. (2003). Monitoring growth and energy utilisation of harbour porpoise (*Phocoena phocoena*) in human care. **Nammco Sci Pub** 5, 107-120.

Macaulay, J. D. J., Malinka, C. E., Gillespie, D., and P. T. Madsen. (2020). High resolution three-dimensional beam radiation pattern of harbour porpoise clicks with implications for passive acoustic monitoring. **J Acoust Soc Am**, 147 (6): 4175-4188.

Madsen, P. T. and M. Wahlberg. (2007). Recording and quantification of ultrasonic echolocation clicks from free-ranging toothed whales. **Deep Sea Res I**, 54(8), 1421-1444.

Malinka C. E., Rojano-Donate, L. and P. T. Madsen. (*Submitted*). Directional biosonar beams allow echolocating harbour porpoises to actively discriminate and intercept closely-spaced targets.

Masters, W. M. and S. C. Jacobs (1989). Target detection and range resolution by the big brown bat (*Eptesicus fuscus*) using normal and time-reversed model echoes. **J Comp Phys A**, 166 (1): 65-73.

Miller, L. A. (1991). Arctiid moth clicks can degrade the accuracy of range difference discrimination in echolocating big brown bats, *Eptesicus fuscus*. **J Comp Phys A**, 168 (5): 571-579.

Møhl, B. (1986). Detection by a pipistrelle bat of normal and reversed replica of its sonar pulses. **Acustica**, 61 (1): 75-82.

Moore, P., Hall, R., Friedl, W. and P. Nachtigall. (1984). The critical interval in dolphin echolocation: What is it? **J Acoust Soc Am**, 76 (1), 314-317.

Schmidt, S. (1988). Evidence for a spectral basis of texture perception in bat sonar. **Nature**, 331: 617-619.

Schmidt, S. (1992). Perception of structured phantom targets in the echolocating bat, *Megadermalyra*. **J Acoust Soc Am**, 91 (4): 2203-2223.

Simmons, J. A. (1973). The resolution of target range by echolocating bats. **J Acoust Soc Am**, 54(1), 157-173.

Stidsholt, L., Greif, S., Goerlitz, H. R., Beedholm, K., Macaulay, J., Johnson, M., and Madsen, P. T. (2021). Hunting bats adjust their echolocation to receive weak prey echoes for clutter reduction. **Sci Adv**, 7(10), eabf1367.

Surlykke, A. (1992). Target ranging and the role of time-frequency structure of synthetic echoes in big brown bats, *Eptesicus fuscus*. **J Comp Phys A**, 170 (1): 83-92.

Surlykke, A. and O. Bojesen (1996). Integration time for short broad band clicks in echolocating FM-bats (*Eptesicus fuscus*). **J Comp Phys A**, 178 (2): 235-241.

Vel'min, V. and N. Dubrovsky. (1975). Auditory analysis of sound pulses in dolphins. **Doklady Akademii Nauk SSSR**, 225, 470-473.

Vel'min, V. (1976). The critical interval of active hearing in dolphins. **Soviet Phys Acoust,** 2, 351-352.

Verfuß, U. K., Miller, L. A. and H. Schnitzler (2005). Spatial orientation in echolocating harbour porpoises (*Phocoena phocoena*). **J Exp Biol**, 208 (17): 3385-3394.

Verfuß, U. K., Miller, L. A., Pilz, P. K. D. and H. Schnitzler (2009). Echolocation by two foraging harbour porpoises (*Phocoena phocoena*). **J Exp Biol**, 212 (6): 823-834.

Warnecke, M., Bates, M. E., Flores, V. and J. A. Simmons (2014). Spatial release from simultaneous echo masking in bat sonar. **J Acoust Soc Am**, 135 (5): 3077-3085.

Wisniewska, D. M., Johnson, M., Beedholm, K., Wahlberg, M., and P. T. Madsen (2012). Acoustic gaze adjustments during active target selection in echolocating porpoises. **J Exp Biol**, 215 (24): 4358-4373.

Wisniewska, D. M., Johnson, M., Teilmann, J., Rojano-Doñate, L., Shearer, J., Sveegaard, S., Miller, L. A., Siebert, U., and P. T. Madsen (2016). Ultra-high foraging rates of harbor porpoises make them vulnerable to anthropogenic disturbance. **Curr Biol**, 26, 1441–1446.

Zaslavski, G. (2012). High auditory time resolution in bottlenose dolphins is effective protection against reverberation. *In*: A. N. Popper and A. Hawkins (Eds.), *The Effects of Noise on Aquatic Life*, Springer, pp. 37-40.

Chapter VII.

Revisiting Optimal Localization Hypothesis

Beedholm, K., **Malinka, C. E.**, Ladegaard, M., & P. T. Madsen (2020). "The right aim: Do echolocating toothed whales direct their acoustic gaze on or off target in a static detection task?" *The Journal of the Acoustical Society of America*, 149 (1): 581-590. doi: 10.1121/10.0003357

JASA ARTICLE

Do echolocating toothed whales direct their acoustic gaze on- or off-target in a static detection task?

Kristian Beedholm,[a)] Chloe Malinka,[b)] Michael Ladegaard,[c)] and Peter Teglberg Madsen[d)]
Zoophysiology, Department of Biology, Aarhus University, 8000 Aarhus C, Denmark

ABSTRACT:
Echolocating mammals produce directional sound beams with high source levels to improve echo-to-noise ratios and reduce clutter. Recent studies have suggested that the differential spectral gradients of such narrow beams are exploited to facilitate target localization by pointing the beam slightly off targets to maximize the precision of angular position estimates [maximizing bearing Fisher information (FI)]. Here, we test the hypothesis that echolocating toothed whales focus their acoustic gaze askew during target detection to maximize spectral cues by investigating the acoustic gaze direction of two trained delphinids (*Tursiops truncatus* and *Pseudorca crassidens*) echolocating to detect an aluminum cylinder behind a hydrophone array in a go/no-go paradigm. The animals rarely placed their beam axis directly on the target, nor within the narrow range around the off-axis angle that maximizes FI. However, the target was, for each trial, ensonified within the swath of the half-power beam width, and hence we conclude that the animals solved the detection task using a strategy that seeks to render high echo-to-noise ratios rather than maximizing bearing FI. We posit that biosonar beam adjustment and acoustic gaze strategies are likely task-dependent and that maximizing bearing FI by pointing off-axis does not improve target detection performance.
 https://doi.org/10.1121/10.0003357

(Received 2 October 2020; revised 14 December 2020; accepted 28 December 2020; published online 25 January 2021)
[Editor: Brian Branstetter] Pages: 581–590

I. INTRODUCTION

Echolocating toothed whales use high-power, directional ultrasonic clicks to find and intercept prey and to navigate (Au, 1993). By placing the axis of their directional beam (0°) directly on targets of interest, biosonar systems can maximize echo-to-noise (ENR) or echo-to-clutter (ECR) ratios to facilitate target detection and auditory analysis of target properties. When modeling biosonar performance, it is therefore usually assumed that echolocating animals seek to keep the targets of interest in the center of their sound beams (Au, 1993; Ghose and Moss, 2003; Madsen *et al.*, 2007). However, the directionality of broadband echolocation clicks varies with frequency, with higher frequencies being transmitted more directionally (e.g., Madsen and Surlykke, 2013). For a broadband sonar pulse, a target at different angles off the beam axis will therefore receive and reflect a particular spectrum of frequencies, which inherently means that the spectrum of the echo carries potential information on the bearing to the target if that frequency range can be processed (Arditi *et al.*, 2015).

In keeping with this information potential, studies involving the biosonar strategies of Egyptian fruit bats (*Rousettus aegyptiacus*; Yovel *et al.*, 2010) and bottlenose dolphins (*Tursiops truncatus*; Kloepper *et al.*, 2018) have reported that these broadband echolocators consistently direct their acoustic gaze slightly off-axis of the target of interest. So, rather than aligning the central axis of its beam with the target, as assumed by the sonar equation for maximizing the ENR or ECR, they are instead reported to deliver most of the energy at a modest off-target angle. By locking the maximum of the slope of the beam amplitude (Yovel *et al.*, 2010) or via applying angle-dependent spectral changes (Kloepper *et al.*, 2018) of their beam on the target, small changes in the angle are potentially more readily inferred by the changes in amplitude and/or spectrum. Under certain assumptions about the receiver, this proposed strategy maximizes the precision of the angular position estimate, the so-called Fisher information (FI) (Yovel *et al.*, 2010; Kloepper *et al.*, 2018).

Kloepper *et al.* (2018) reported that one bottlenose dolphin (*T. truncatus*), on average, pointed its beam 7.2° off the target, as precisely predicted if the animal was seeking to maximize the bearing FI. Bearing FI, in this case, is the information about the angular position of an object in the beam that is available from the spectral changes that are imposed on a broadband signal, when it is projected from a directional source. Assuming that the signal source can be modeled as a piston transducer (e.g., Beedholm and Møhl, 2006), bearing FI can be calculated from the spectrum of the signal and the size of the equivalent radiating aperture.

In Kloepper *et al.* (2018), the data were collected with a stationed bottlenose dolphin ("BJ"; *T. truncatus*) trained to report on the presence/absence of a large cylindrical target always presented a few meters directly in front of the

[a)]ORCID: 0000-0001-5699-0849.
[b)]Electronic mail: Chloe.e.malinka@bio.au.dk, ORCID: 0000-0003-0138-8388.
[c)]ORCID: 0000-0001-7559-9271.
[d)]Also at: Aarhus Institute of Advanced Studies, Aarhus University, 8000 Aarhus C, Denmark, ORCID: 0000-0002-5208-5259.

animal. This raises the question of why the dolphin would use a strategy of aiming its acoustic gaze away from the target as if solving a different task, namely one of accurate target localization, for which it was not rewarded. What would the benefit be of accurately aiming the sonar beam off-axis in relation to the expected target location when solving a task where the target might be absent? Aiming the sonar beam off-target reduces both the ENR and ECR; these are the key factors for correctly determining target presence/absence and hence for maximizing the food pay-off during training and experiments in the Kloepper *et al.* (2018) setup. Using the aim angle that optimizes the returning bearing FI by aiming away from the target concomitantly reduces the returning echo level as compared to aiming the beam directly at a target. Why would the dolphin choose the former strategy for solving a target presence/absence task, and how can it point so accurately 7.2° off the direction of the target? If the animal can place its beam so accurately off-axis, it must already know or expect (Kloepper *et al.*, 2014) where the target is and thus no longer need to determine the bearing to it.

Here, we seek to address these questions by first considering the expected results of the experiment by Kloepper *et al.* (2018) under the assumption of the two hypothetical scenarios (on-target versus off-target gaze direction). In scenario 1, an on-axis strategy would represent a situation where, in one dimension, the distribution of aim angles around 0° is a normal distribution, with a standard deviation (SD) of σ. If the aiming accuracy is the same in both x and y dimensions, then the distribution of absolute angles conforms to the Rayleigh distribution, with a mean angle of $\sigma\sqrt{\pi/2}$ and angle mode equal to σ (Mertikas, 1985, and see Fig. 1). So, perhaps surprisingly, if the animals were in fact trying to echolocate directly on the target, the expected mean absolute pointing angle would not be zero. This situation is akin to a dart player aiming for bullseye; regardless of the skill level of the player, the distribution will not have a mean absolute angle of 0°, but rather also be described by a Rayleigh distribution with σ being lower for better players. In scenario 2, where the animal seeks to maximize bearing FI by placing its beam where spectral information gain about the bearing is maximal, it is expected that the angle distribution would exhibit a large peak with low variance at the predicted optimal FI angle.

Accordingly, to test the hypothesis that echolocating animals utilize an optimal FI angle, we must study the distribution of aim angles in more detail and compare it to the predictions derived from the two mutually exclusive scenarios about the beam aiming strategy employed by the animal.

Kloepper *et al.* (2018) made the prediction that their study dolphin, BJ, would aim its beam at 7.2° with respect to the target and proceeded to find exactly an average absolute angle of 7.2°. Given the relationship between the mean and the mode of a Rayleigh distribution, as explained in Fig. 1, this result would also have been obtained were the dolphin aiming for 0° with an accuracy resulting in a

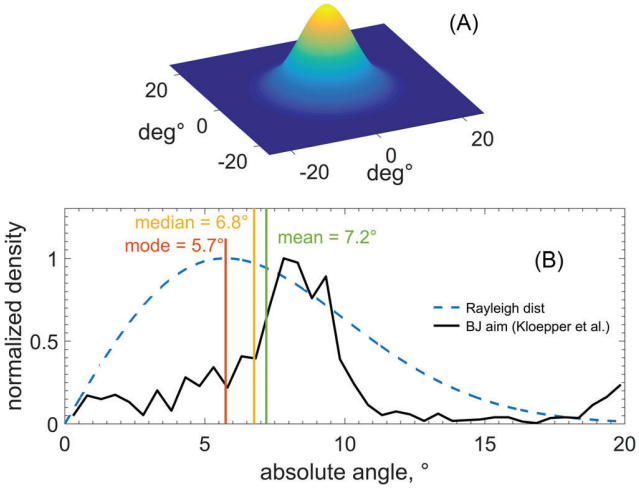

FIG. 1. (Color online) (A) Relationships between parameters of a two-dimensional Gaussian distribution with mean = 0° and SD = 9.0° for a transect through (0,0); (B) the corresponding Rayleigh distribution, describing the absolute angles (in a blue dashed line). Under this distribution, the mean absolute angle is 7.2°, the median is 6.8°, and the mode is 5.7°. The shape of the distribution of absolute angles in (B) will, in this case, resemble a curve describing the way bearing FI depends on angle. The solid black line depicts the absolute angle distribution from the heat plots of aims from the bottlenose dolphin, BJ, in Fig. 2 of Kloepper *et al.* (2018).

Rayleigh distribution with a mode of 5.7°. We estimated the distribution of aim angles off-target from the heat plots in Figs. 2(A)–2(D) of Kloepper *et al.* (2018) and plotted them here (Fig. 1) together with a Rayleigh distribution with a mean of 7.2°. This distribution estimate has a mode of 8.4° and a mean of 7.5° [if excluding aim angles on the edge of the array (>18°) as was done in the analysis by Kloepper *et al.*, 2018], which differs slightly from the reported mean of 7.2° (Kloepper *et al.*, 2018). Prompted by that discrepancy and the fact that angle distributions with non-zero means and modes can be explained by both scenario 1 and 2, we here seek to reinvestigate the question of whether toothed whales deliberately point their beam off-axis to maximize bearing FI: the optimal bearing FI hypothesis.

Specifically, we test the optimal localization hypothesis for toothed whales engaged in a static target detection task. We use data collected from the same bottlenose dolphin (BJ), at the same facility in Hawai'i, using a similar cylindrical target as in Kloepper *et al.* (2014) and Kloepper *et al.* (2018), and complement the data with identical measurements from the false killer whale, "Kina" (*Pseudorca crassidens*), at the same facility, in the same setup, performing the same task. Additionally, we present a reanalysis of the data presented in Kloepper *et al.* (2018), as well as on our own data, to test if different analytical approaches render different conclusions on the optimal bearing FI hypothesis. We show that the target is predominantly ensonified within the half-power (–3 dB) beam width, but based on the variation in biosonar aim angles and the different aim strategies between animals, we do not find support for the hypothesis that delphinids aim to maximize bearing FI.

https://doi.org/10.1121/10.0003357

II. MATERIALS AND METHODS

A. Animals and setup

Data collection took place within the floating pen complex at the University of Hawai'i Marine Mammal Facility on Coconut Island in Kaneohe Bay, Oahu, Hawai'i, in January 2012. Experiments involved two animals: a false killer whale, *P. crassidens*, Kina (female, >28 yrs old), and an Atlantic bottlenose dolphin, *T. truncatus*, BJ (female, 30 yrs old). Both animals had high frequency hearing loss; Kina's hearing thresholds ranged from 80 to 90 dB re 1 μPa in the range of ~8–~35 kHz, and she was reported to hear poorly $\gtrsim$ 40 kHz (Yuen *et al.*, 2005; Kloepper *et al.*, 2010), and BJ's hearing thresholds ranged from 80 to 90 dB re 1 μPa in the range of 16–38 kHz, with a high frequency cutoff at ~45 kHz (Nachtigall and Supin, 2014; Nachtigall and Supin, 2015; Nachtigall *et al.*, 2016).

Both animals participated in a go/no-go paradigm in which they used echolocation through an acoustically transparent PVC screen to determine whether a standard aluminum target was present or absent. The target, a 6.9 cm long aluminum cylinder (outer diameter = 38 mm, inner diameter = 25 mm) with a target strength of −36 dB, was presented 2.65 m ahead of the hoop station at 1 m depth via a vertical pulley system. The animals either left the hoop to press a response paddle to indicate target presence or remained on station to indicate target absence (for details, see Kloepper *et al.*, 2010). Target presence/absence alternated according to a pseudo-random schedule (Gellermann, 1933).

Five hydrophones were suspended from monofilament lines in a small array at 0° and ±15° in the horizontal plane and ±10° in the vertical plane [Figs. 2(C) and 2(E)]. These hydrophones were custom made and individually calibrated (sensitivity of −211 dB re 1 V μPa^{-1}) using a TC-4013 hydrophone (Teledyne RESON A/S, Slangerup, Denmark) as a reference. The hydrophones were connected to custom-built conditioning boxes with 40 dB gain and a 1–200 kHz bandpass filter (Butterworth, one pole high-pass, four pole low-pass). Recordings were made with an eight-channel National Instruments multi-purpose USB device (NI USB 6356; National Instruments, Austin, TX, USA), simultaneously sampling at 500 kHz per channel with 16-bit resolution (see Madsen *et al.*, 2013 for details).

B. Analysis

Data were analyzed using MATLAB (2016a, Mathworks Inc., Natick, MA, USA). The click data were evaluated as peak-to-peak (pp) received level (RL, dB re 1 μPa, pp) and were corrected for the slight differences in range between the specific hydrophones and the head of the animal assuming spherical spreading loss, to render apparent source levels (ASLs). Source levels were estimated for clicks where the highest ASL was measured from the center hydrophone in the horizontal plane (for comparison with Madsen *et al.*, 2013b). To arrive at the beam angle relative to the line that connects the center of the hoop with the center of the aluminum target, we treated the ASL data for each angle as two orthogonally oriented linear arrays. The center of the beam aim in X and Y within the array was found as the peak of the second-degree polynomial (Lagrange polynomial) matching the amplitude data, separately in the two dimensions. The angle off-axis was then derived as $\mathrm{atan}((X^2+Y^2)^{0.5}/\mathrm{range})$. We generated two-dimensional histograms (heat plots) of the resulting distributions of beam aims and displayed these as heat plots, similar to the displays presented in Kloepper *et al.* (2018).

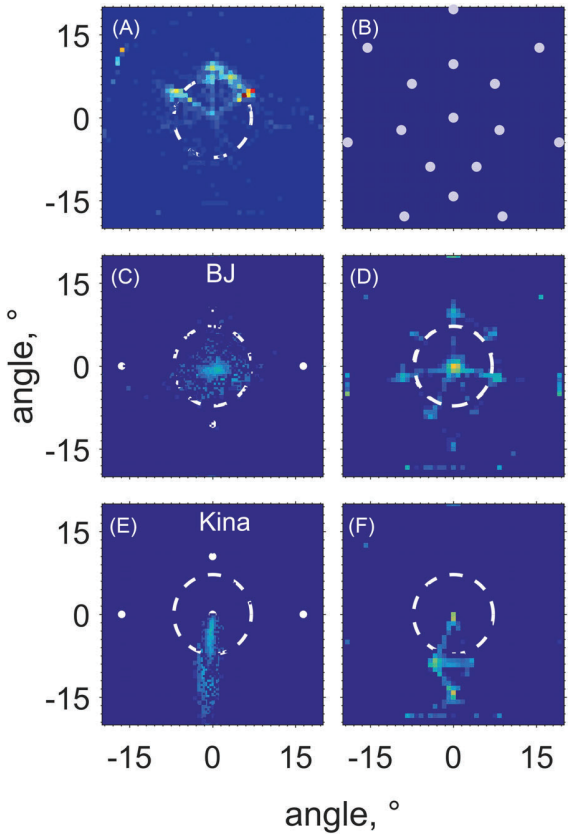

FIG. 2. (Color online) Heat plots of real and simulated aim distributions. (A) Data presented by Kloepper *et al.* (2018) show the distribution of BJ's aims in target-absent trials—the scenario where BJ produced the most clicks. The white dashed circle in all subplots denotes a 7.2° off-target aim. (B) The hydrophone array of Kloepper *et al.* (2012a), Kloepper *et al.* (2012b), Kloepper *et al.* (2014), and Kloepper *et al.* (2018). (C) Beam aim distribution of the bottlenose dolphin, BJ, from our data. The white dots represent the positions of our hydrophones (the white dots are plotted behind the aim data; therefore, some are hidden). (D) Simulated beam aim distribution of BJ. Specifically, this is the result of re-interpolating the data of (C), under the assumption of a piston radiation pattern as it would have been recorded on the array in (B) and then interpolated into a grid with cubic interpolation in MATLAB. (E) Beam aim distribution of the false killer whale, Kina; explanation as in (C). (F) Simulated beam aim distribution of Kina; explanation as in (D).

The FI component, which is proportional to the rate of power spectral change with angle, was calculated for the mean click spectrum of the signals that were recorded <2° off-axis for both species. In computing the FI, as described in the legend of Fig. 1 in Kloepper *et al.* (2018), we took the derivative of the sum of the power spectral components of

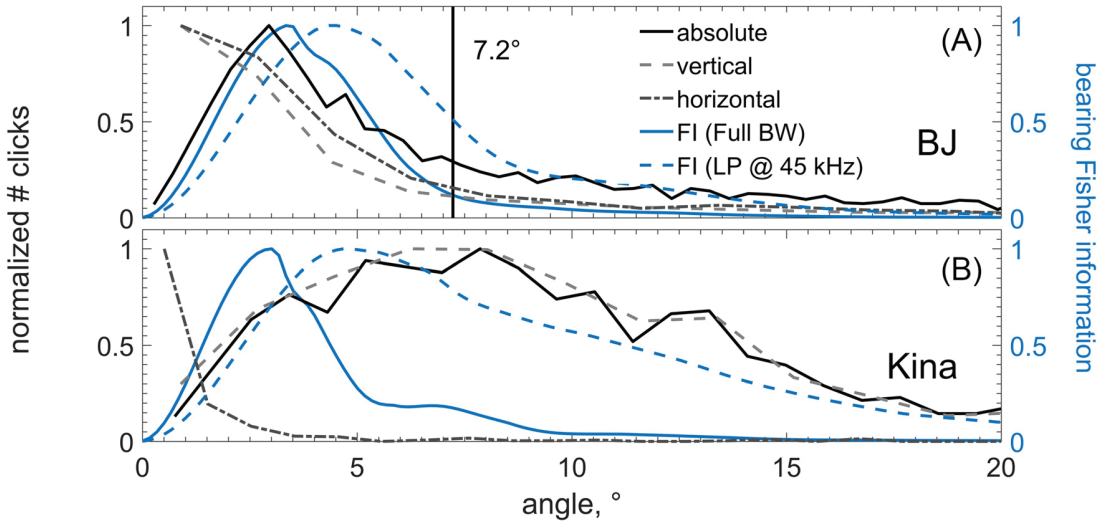

FIG. 3. (Color online) Absolute aim distributions and Fisher information for BJ (A) and Kina (B). The green lines show the normalized bearing Fisher information as calculated for the average spectrum of the clicks recorded within 2° of the center hydrophone. Gray dashed lines are aim distributions in the vertical plane, and gray dotted-dashed lines are distributions in the horizontal plane. The vertical line in the top panel at 7.2° is the average beam angle found by Kloepper *et al.* (2018). The dashed green lines show the Fisher information of the same clicks as the solid green lines but simulating the influence of high frequency hearing losses by low-pass filtering the click with a first order filter with –3 dB cutoff at 45 kHz.

the Fourier spectrum as would have been radiated by a circular piston as a function of angle off-axis. For calculating FI under the influence of the reported presbycusis for both animals (Yuen *et al.*, 2005; Kloepper *et al.*, 2010; Nachtigall and Supin, 2014; Nachtigall *et al.*, 2016; Nachtigall and Supin, 2015), we low-pass filtered the mean on-axis signal with a first order low-pass filter at 45 kHz (Fig. 3).

III. RESULTS

All trials could be separated into three stages, easily identifiable in the recorded traces as belonging to (1) a positioning stage, where the animal came into the hoop station; (2) a scanning stage, where the animal echolocated toward the target while stationed in the hoop; and (3) a navigation stage, where the animal backed out of the hoop to touch a "go" target and/or returned to the trainer to get the fish reward. Clicks during the scanning stage were recorded at much higher amplitudes (as they were directed in the general direction of the target). Here, we only consider clicks belonging to the scanning stage as only these are of relevance to the posed hypotheses. Both animals participated in three sessions, each comprising ≥20 trials, each with the configuration we report on here (Table I).

Mm. 1. An animated video displays echolocation performance visualized by the click aim angles of both BJ and Kina during the static detection task. This is a file of type "mp4" (14.6 MB).

A heat plot of two-dimensional beam aim densities of BJ from data presented in Kloepper *et al.* (2018) is shown in Fig. 2(A). Similar heat plots for our data are shown in Fig. 2(C) (BJ) and Fig. 2(E) (Kina).

A. BJ

The bottlenose dolphin, BJ, echolocated using an arithmetic mean of the absolute gaze aim angles of 6.4° [Fig. 3(A)], a mode of 2.6°, and a median of 3.5°. A long thin tail of aim angles was observed up to 90°, which carries

TABLE I. Basic statistics concerning the six sessions analyzed in the present study. The number of clicks reported is all clicks from the scanning phase of the trials. The estimated SLs are the range-corrected received levels at the central hydrophone for the clicks that were registered with the highest received level at the center hydrophone in the horizontal plane only (for comparison with Madsen *et al.*, 2013b). Mean minimum aim angle is the mean within each session of the minimum absolute angle recorded in each trial.

Session	Animal	No. of trials	No. of clicks	Mean SL ± SD (dB re 1 μPa pp)	Mean [minimum aim angle (degrees)] per trial ± SD	% correct responses
1	BJ	20	880	196.7 ± 5.7	1.3 ± 1.2	95
2		20	1445	199.9 ± 5.5	1.3 ± 0.7	100
3		20	1109	198.9 ± 5.0	1.4 ± 0.8	100
1	Kina	20	611	193.7 ± 7.5	5.5 ± 4.2	100
2		20	606	195.6 ± 9.4	3.3 ± 1.9	100
3		21	637	198.8 ± 8.3	2.9 ± 1.7	95

considerable leverage, which drags the mean up to higher values than the median. In the two-dimensional aim distribution, there is no peak at positions corresponding to angles near 7°, and the angle corresponding to the two-dimensional aim mode is 1.5°. The target was ensonified within the –3 dB beam width for 77% of the clicks and within the −10 dB beam width for 92% of the clicks [Fig. 2(C)]. In all trials, the target was within the –3 dB beam width (6.3°) of at least one click during the scanning stage in all trials. The aim angle maximizing bearing FI for BJ was estimated to be 3.0° [Fig. 3(A)]. Incorporating the effect on the Fisher information resulting from high frequency (>45 kHz) hearing loss, we found that factoring this into the effective spectrum available to the animal results in an optimal aim angle of 4.5°.

B. Kina

The false killer whale, Kina, used a different echolocation strategy than BJ. Kina mostly varied the beam aim in the vertical plane, and while the absolute angle that corresponds to the mode of the two-dimensional aim distribution is 2.6°, a large proportion of her clicks were aimed below the target [Fig. 2(E)]. The resulting angle distribution is very broad, with an arithmetic mean of 10.0°, median of 8.4°, and mode of 7.2° [Fig. 3(B)]. The target was within the –3 dB beam width for 29% of the total clicks, while 64% of the clicks covered the target within the −10 dB beam width. The fraction of trials in which the minimum aim angle was within the angle defining the –3 dB beam width was 85%, while the trial fraction with minimum aim angle inside the −10 dB beam width was 98.3%. The aim angle maximizing bearing FI for Kina was estimated to 3.1° [Fig. 3(B)]. For Kina, the effect of high frequency hearing loss on the estimated FI curve resulted in an optimum aim angle of 4.7°.

IV. DISCUSSION

Toothed whales in captivity have most often been studied in a context where the animals are stationed and echolocating on a single target at a fixed range and tasked with reporting presence or absence (e.g., Au and Penner, 1981 and Au, 1988). In more recent experiments, animals have been blindfolded and free-swimming toward a target so that the task consists of initially detecting the target, prior to more accurate localization throughout the subsequent approach, with the localization accuracy being most important immediately prior to target interception (e.g., Wisniewska *et al.*, 2015 and Ladegaard *et al.*, 2019). Both of the experimental settings in this paper represent situations that differ from one of the main tasks that wild animals utilize echolocation for, namely the capture of agile nektonic prey that further may have target strengths lower than those of targets used in typical lab experiments (Fruozova *et al.*, 2005). Toothed whales have directional hearing systems (Au and Moore, 1984; Kastelein *et al.*, 2005) and echolocate using a highly directional biosonar beam, with a directionality index of typically 26 ± 3 dB (Jensen *et al.*, 2018). The returning echo information available to the animal is therefore highly dependent on where in the sonar beam the targets are located. For the simple detection part of these tasks, the optimal biosonar behavior would be to center the beam as precisely on the target as possible, to maximize both the ENR and the ECR. In contrast, for non-static target approaches, other echolocation strategies may come into play, for instance one that would optimize positional information, tracking, or classification. Since target detection, tracking, and interception all present different challenges, it might well be that the animals change their biosonar behavior to optimize the information return corresponding to the different phases of the hunt.

If indeed the animals do adjust their beam aiming strategy according to the specific task that they are facing, we would expect to find the highest density of clicks aimed near the center of the target according to a Rayleigh distribution in a detection task. This strategy (scenario 1) maximizes returning echo levels for a given sonar output, which is optimal in a detection experiment, such as the present one and that of Kloepper *et al.* (2018). Alternatively, precise tracking and classification of moving targets may have been such a strong evolutionary driver that toothed whales always employ an echolocation strategy that involves precise target localization (scenario 2) by means of maximizing bearing FI, as reported by Kloepper *et al.* (2018), despite the fact that this strategy decreases ENR and ECR, appearing suboptimal when detecting a static target. In that case, the mode, not the mean, is predicted to conform to the angle that maximizes bearing FI. Here, we address these two competing hypotheses about the biosonar aim of delphinids.

A. Target detection is not solved by optimizing Fisher information

In our experiment, and in the highly comparable experiment of Kloepper *et al.* (2018), performed ∼1.5 yrs after our experiments, the animals were rewarded for correctly indicating whether a large target was present or absent in a go/no-go procedure. We can only speculate on the consequences of this interlude between data collections, but we find it hard to explain why BJ would switch to a different aim strategy during the data collection of Kloepper *et al.* (2018) when she performed with very high success rates during our data collection with her (Table I). Kloepper *et al.* (2018) calculated the angle of maximal bearing FI to be 7.2° off-axis relative to the target, based on average spectral energy distributions in dolphin clicks and predictions from the piston model (diameter = 11.75 cm), and BJ was subsequently reported to aim at that exact angle on average. In our study, we estimated bearing FI based on the average spectra of on-axis clicks and found the optimal angle for maximizing bearing FI for BJ to be 3.0° [Fig. 3(A)]. Whether this indeed is the maximum FI angle from a perceptual viewpoint can be debated as BJ suffers from a high frequency hearing loss (Nachtigall and Supin, 2014; Nachtigall and Supin, 2015; Nachtigall *et al.*, 2016), suggesting that the maximum FI angle should be at a higher angle

if the high frequencies that contribute to the maximum spectral slope are not available to her. When simulating this effect numerically (see Fig. 3), we find the maximum FI occurs instead at 4.5° when using a first order low-pass filter at 45 kHz to simulate the presbycusis. Using higher order low-pass filters, the FI curves can become very broad with peak FI at angles that exceed 10°.

For calculating FI, we used the mean spectrum of clicks recorded within 2° off-axis for each of the species, and for BJ, we assumed the same circular 11.75 cm diameter piston as Kloepper *et al.* (2018), who, on the other hand, used an average click spectrum where we do not know the exact details of the selection criteria. This could explain some of the substantial discrepancies between our findings, since a mean spectrum for a liberal click distribution is likely to have less high frequency content compared to the near on-axis spectrum used here. For the same transmitter size, the emission of clicks with a lower frequency emphasis will result in a broader beam width, and the maximal FI gain will occur at correspondingly higher off-axis angles. However, for this to account for the observed differences, the average click spectrum would have to have included a relatively large proportion of clicks recorded rather far off-axis.

Our result that BJ's absolute modal aim angle was 2.9° disagrees with the 7.2° prediction by Kloepper *et al.* (2018) but resembles our estimate of 3.0° for the angle that maximizes bearing FI [Fig. 3(A)] using only the clicks closest to on-axis (<2° off-axis). However, when considering the aim distributions in a narrow (±5°) transect passing through 0.0° (also Fig. 3), the mode can be seen to be quite close to 0°. Also, visually evaluating the distribution of aim positions in a heat plot [Fig. 2(C)], it appears that BJ did not use a strategy of consistently aiming off-axis relative to the target. Rather, it supports the hypothesis of scenario 1, namely that BJ, in this detection task, sought to optimize the ENR and/or ECR for rapid assessment of target presence or absence.

The false killer whale, Kina, used a rather different biosonar behavior for detecting the target compared to BJ, who seemed to center the beam on the target. Kina mainly scanned her beam in the vertical plane below the center of the target [Fig. 2(E)], resulting in mean and median angles of 10.0° and 8.4° off the target [Fig. 3(B)], respectively, and a mode close to 7.2°. The mode is therefore similar to the optimal aim angle predicted and reported by Kloepper *et al.* (2018) for BJ. However, the beam pattern, and hence optimal off-axis angle for maximizing FI, depends on the size of the transmitting aperture as well as on the spectral characteristics of the outgoing clicks. Using the mean piston diameter (mean of the length of the axes) from Au *et al.* (1995) and the average on-axis spectrum (<2° off-axis) from our recordings, we found the peak in bearing FI to lie close to 3.3° for Kina [Fig. 3(B)]. This value is quite far from the mode of the distribution of absolute angles of 7.1°, but—in contrast to BJ (Mm. 1)—it appears that Kina often pointed her beam farther off-axis than the FI optimum. From the video of animated click aims (Mm. 1), it appears that Kina rarely aimed her beam directly on-target. However, it also appears that Kina did not aim her beam on a narrow ring 3.3° off the target (Mm. 1), which is what is predicted [Fig. 3(B)] if Kina used an optimal bearing FI aiming strategy. Again, a higher modal off-axis angle may be explained by high frequency hearing loss in Kina (Yuen *et al.*, 2005; Kloepper *et al.*, 2010). Considering this hearing loss effect numerically results in an expected aim angle of 4.5°. Neither of these estimates nor the broad distribution of actual aim angles are consistent with a strategy of maximizing FI.

Thus, we find that BJ generally pointed her beam close to the target [Fig. 2(C)], whereas Kina was more relaxed about accurately pointing the beam on-target during the target present situation and opted for a vertical scanning strategy aimed below the target center [Fig. 2(E)]. However, in the vast majority of trials, the target was at some point within the half-power beam (BJ: 100%, Kina: 85%), and the minimum off-axis angle was nearly always within the −10 dB beam (BJ: 100%, Kina 98.3%). This behavioral difference shows that the estimated aim distribution patterns are not the result of a systematic bias in our setup or analysis. Had there been substantial errors in hydrophone calibrations or in the methods of interpolation, we would have expected similar aim distribution patterns between the two animals, which is not the case. Despite the differences in echolocation strategies between the two dolphins, the results from both BJ and Kina show that for a target detection task, neither animal directed the gaze of their biosonar beam in a narrow range of angles off the target (Fig. 2). Therefore, they did not seek to optimize the bearing FI of returning echoes as predicted by our scenario 2.

B. Acoustic gaze interpolation

Since the results and conclusions from our experiment deviate markedly from those obtained by Kloepper *et al.* (2018) using the same setup and animal, we have sought explanations for the discrepancy. We have explored the major experimental differences between the two setups, which included the geometry of the recording arrays, and the method used for interpolating the data. In Kloepper *et al.* (2018), the array [Fig. 2(B)] was star-shaped with 16 hydrophones (as in Ibsen *et al.*, 2012), whereas in our study, it consisted of five hydrophones arranged in a cross. We used simple quadratic interpolation to estimate the peak position in two independent dimensions, whereas Kloepper *et al.* (2018) used the MATLAB implementation of cubic interpolation to find the peak position in a 50×50 grid spanning 140 cm.

The heat plots of Figs. 2(D) and 2(F) depict the results of a simulation that consisted of interpolating and resampling our beam aim data with a piston radiation model. Using the piston model, the data were evaluated for received amplitude at the points corresponding to the hydrophone positions in Kloepper *et al.* (2018) (citing Ibsen *et al.*, 2012) and then interpolated using MATLAB's cubic interpolation.

Plots show that the peaks appear very close to the virtual hydrophones [Fig. 2 in Kloepper *et al.*, 2018, shown here as Fig. 2(A)]. The innermost circle of hydrophones in the star-shaped array of Kloepper *et al.* (2018) seems to attract a large number of peak positions [Fig. 2(A)].

The expected result of the simulation [Figs. 2(D) and 2(F)] was to end up with a heat plot closely resembling the distribution of the original data [Figs. 2(C) and 2(E)] on which the simulation was based. The phenomenon that interpolated aim angle estimates are biased toward hydrophone locations or paths between hydrophones [Figs. 2(D) and 2(F)] is therefore likely to be an error that arises from the cubic interpolation. The innermost ring of hydrophones in Kloepper *et al.* (2018) are placed at ∼35 cm from the center, which, at an array distance of 2.0 m (Kloepper *et al.*, 2014), translates into an angle of 9.9°. Their reported average bearing FI value of 7.2° then appears to stem from the clusters of curiously high density at the aim positions near the inner ring in the array arising from interpolation errors [as our simulations show in Figs. 2(D) and 2(F)]. There are also a number of clicks that land at the position of the outer hydrophones, but these were reportedly not included in the analysis of Kloepper *et al.* (2018). We therefore posit that the average beam angle in the experiment by Kloepper *et al.* (2018) happens to match the prediction from a FI optimization strategy as a curious coincidence owing to the hydrophone spacing and the artefacts arising from cubic spline interpolation. The average value stems from a relatively broad distribution of aim angles, whereas a confirmation of the bearing FI optimization hypothesis would require that the beam aim directions fall within a narrow range close to the optimal angle that Kloepper *et al.* (2018) estimate to 7.2° for BJ and we estimate to 3° [Fig. 3(A)]. The data in Kloepper *et al.* (2018) are clustered rather closely on or on lines connecting the hydrophones with a mode at about 8.4° [Fig. 2(A)]. Apparently, peaks in the interpolated data show up predominantly at angles that are slightly central relative to the sensor positions in the inner hydrophone ring of the array, resulting in a mode value of about 8.4° [Fig. 2(A)]. None of these observations are in agreement with the predictions of maximizing FI in scenario 2.

Our simulation of the interpolation does not explain all of the differences between the two sets of results. For example, there seem to be relatively few clicks at the center hydrophone in Fig. 2(A), whereas most of the clicks in our simulation [Fig. 2(D)] are actually close to the center hydrophone in the simulation. Therefore, there do seem to be differences in the hydrophone calibration, the animal-target-hydrophone alignment, and/or the behavior of BJ between the two experiments.

To further investigate differences in results reported in Fig. 2(A) of Kloepper *et al.* (2018) with simulated results [Fig. 2(D)], we considered array geometry and interpolation method. In Fig. 4, we use alternative array geometries and artificial data to show the phenomenon of peak aim positions clustering close to (or on lines connecting) actual array elements when interpolating onto a grid in MATLAB. Figure 4 demonstrates one means of the bias toward peak beam angles that are equal to the angles of the receivers off the target arising from cubic interpolation. We further investigated this conundrum using LABVIEW (2015; National Instruments) and found that the same phenomenon occurs with that software package and also with cubic spline interpolation and many different simulated array geometries. In the supplementary materials,[1] we supply a LABVIEW program for the reader to explore this further.

1. Implications of looking off- or on-axis

In the easy detection task presented to the animals in the present experiment, the ENR is likely generous, and the animal can solve the task without directing the center of their beam directly at the target, but merely by glancing at it, as Kina seemed to do [Fig. 2(E)]. Additionally, the extensive history of both animals in controlled biosonar experiments likely contributes to the easiness of the target detection task (Table I). However, for longer target ranges and smaller targets, such as when searching for smaller fish in a hunting situation, directing the acoustic gaze off-target will have consequences for the probability of consistent target tracking. By keeping the target at an off-axis angle that would maximize bearing FI, the target will receive roughly 4 dB less sound energy than if ensonified on-axis [using the ∼7° optimal angle of Kloepper *et al.* (2018) and a piston with 11.75 cm diameter radiating our most on-axis click from BJ]. Thus, under these circumstances, the ENR would be more than halved relative to echolocating on-target, or the echolocator will have to produce 2.5 times more sound energy (the 4 dB) to compensate. Clicking louder to hear a weaker echo from a target off the center of the beam means there will be more forward masking for a given echo delay (Nachtigall and Supin, 2014), obfuscating echo detection and processing. Why the animals should complicate their echolocation tasks in these ways to achieve knowledge about the absolute angle to their target via angle-dependent spectral features appears puzzling.

Certainly, during a target approach, but also during a static detection task such as the ones reported on here, the source levels of odontocete clicks vary. Given that there is a relatively tight coupling between source level and click frequency content for delphinids making broad clicks (Au *et al.*, 1995, and see Fig. 6 in Madsen *et al.*, 2013b), the FI optimum for target angle will vary with SL and any dynamic changes in the effecting radiating aperture from muscle deformations of airsacs and the melon, which reduce, or at least complicate, this measure's potential usefulness to the animal. This problem is further compounded by the fact that both BJ and Kina have high frequency hearing losses (Yuen *et al.*, 2005; Kloepper *et al.*, 2010; Nachtigall and Supin, 2014; Nachtigall *et al.*, 2016; Nachtigall and Supin, 2015), meaning that the perceived FI maximum will be at higher off-axis angles than the calculated FI maximum (Fig. 3).

Dynamic gaze strategies of biosonars are likely task-dependent. For example, in the experiments considered

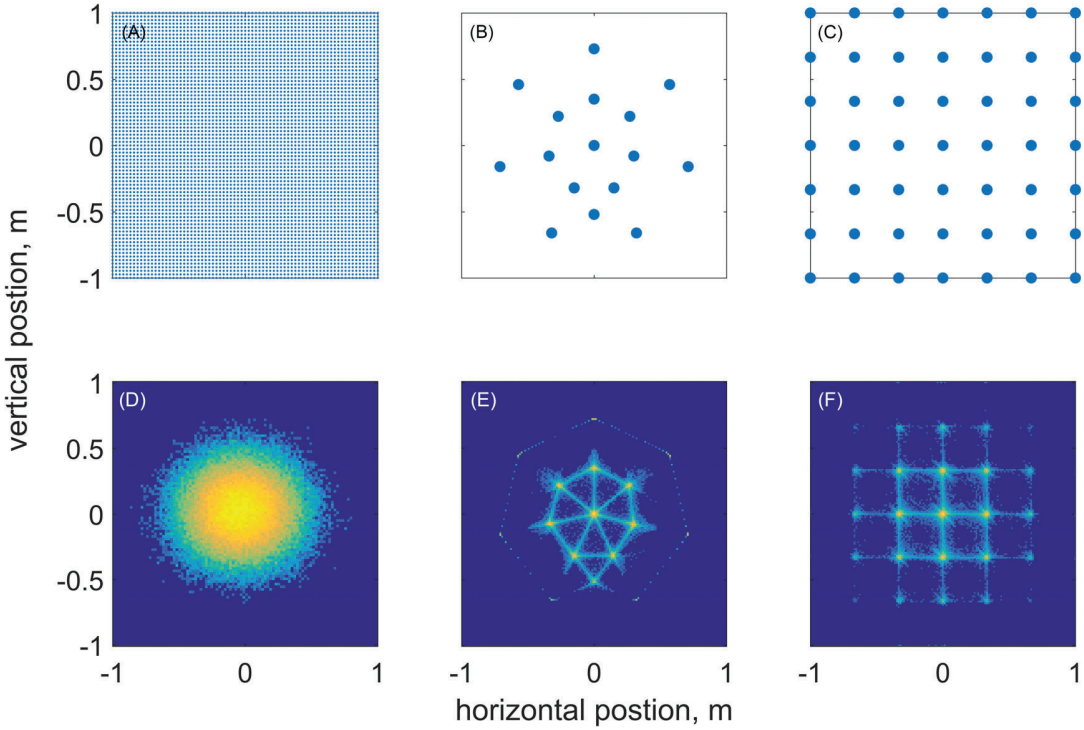

FIG. 4. (Color online) Cubic interpolation of simulated beam data on two different sensor array geometries. (A) illustrates a very dense (and expensive) array that would always correctly determine the correct position of peak amplitude position, since no interpolation would be necessary. (B) and (C) show two sparser array layouts, and (D) illustrates the distribution of peak amplitude positions ensonified with a bimodally normal aim distribution with mean at 0.0° and SD of 0.25 m, as seen on the 150 × 150 pixel wide grid shown in (A). (E) shows the simulated peak amplitude data as recorded on the array in (B) (similar to Kloepper *et al.*, 2018) using cubic interpolation to fill the same grid as (D). (F) shows the same as (E) but as recorded on the uniform sensor array configuration shown in (C). The simulated data used an 11.75 cm diameter flat, circular piston at 2 m distance, projecting an echolocation click (from BJ) at the 100 000 positions indicated by the distribution in (D).

here, the stationed animals performed a detection task involving a stationary target, and they were found to keep the target within the −10 dB beam for most of the clicks. An experimental setup consisting of a freely moving echolocator intercepting a stationary target would constitute not only a detection task, but also localization and tracking tasks. In this case, we may expect a different echolocation strategy that perhaps is more similar to that proposed by Kloepper *et al.* (2018) or Yovel *et al.* (2010), in which the beam is moved back and forth across the target out to the maximum slope of the beam. In nature, however, both the echolocator and the target of interest (i.e., prey) are in motion during interception. Echogram displays showing the acoustic scenes ahead of both *Tursiops* (BJ) and *Pseudorca* (Kina) as they caught dead (but sinking) fish (see Fig. 1 in Wisniewska *et al.*, 2014) feature clearly discernible prey echoes throughout the approach. This phenomenon, which is an unequivocal example of toothed whales keeping the target within the swath of its beam, is also evident in echogram displays of wild porpoises and beaked whales during approach to live, escaping prey (Madsen *et al.*, 2013a; Wisniewska *et al.*, 2016).

For intercepting a static target, accurate localization may in turn be facilitated by actively placing or moving the biosonar beam at various angles with respect to the target, which will then return information about the echo intensity and spectral content from the different angles ensonified (Arditi *et al.*, 2015). For chasing and capturing live prey, toothed whales might also scan across the targets for localizing purposes. Angular position in the plane of the scan is then simply given by the angle where the animal receives the highest echo level. However, given that the prey is moving, then even if the whale attempts to lock on to the target, the arrival angle of the echo and therefore its intensity and spectral information are bound to change as the prey makes excursions within the swath of the biosonar beam. In fact, moving the beam away from the (suspected) direct aim so that the target stays closer to the edge could jeopardize successful biosonar-mediated prey capture; since echo levels drop off rapidly with angle off the center of the target, an echolocation strategy that maximizes bearing FI elevates the risk of the target/prey item escaping. Especially toward the end of a prey capture attempt, where close ranges mean that small prey movements correspond to large angular changes, such a strategy of aiming off-axis would be highly risky. Therefore, it makes sense that echolocating toothed whales broaden their biosonar beam at close range and seek to direct the beam directly at the target (Moore *et al.*, 2008; Kloepper *et al.*, 2012a; Jensen *et al.*, 2015; Wisniewska *et al.*, 2015; Ladegaard *et al.*, 2017). During target approaches, the variation in spectral characteristics (Wisniewska *et al.*, 2014) and any flexibility in the radiation patterns of the beam (Wisniewska *et al.*, 2015) would tend to make the use of an

optimal off-target aim impractical, because the optimal aim angle varies with both source level and phase of the hunt.

V. CONCLUSION

We conclude that the two studied echolocating delphinids did not direct their acoustic gaze at a specific narrow range off of the target to maximize Fisher information, but rather—at least in the easy detection tasks given here—they kept the target within their −10 dB or even –3 dB (half-power) beam width. For echolocators, we posit that echolocation beam direction with respect to a target is unlikely to be one-size-fits-all, and future research on biosonars may therefore benefit from addressing the use of their directional sound beams during different active echolocation tasks, including some of ecological and evolutionary relevance.

ACKNOWLEDGMENTS

We are indebted to Stephanie Vlachos, Christopher Quintos, Marlee Breese, and Paul Nachtigall for their hospitality, dedicated collaboration, and highly skilled training of the animals. We also thank Danuta Wisniewska, Aude Pacini, Nina K. Iversen, Jessica Chen, Laura Kloepper, Aliza Milette, Sanami Nakayma, and Adam Smith for their assistance during data collection. We thank Paul Nachtigall and John R. Buck for constructive discussions and two anonymous reviewers for helpful comments on an earlier version of this manuscript. Experiments were conducted under University of Hawai'i Institutional Animal Care and Use Committee Protocol 09-712 and United States Marine Mammal Permit No. 978-1567 issued to Paul Nachtigall. This work was supported by Frame grants from the National Danish Research foundation (FNU) to P.T.M. (6108-00355B) and by funding from ONR to P. L. Tyack. We dedicate this paper to the late Professor Whitlow Au, the founding father of quantitative studies of toothed whale echolocation.

[1]See supplementary material at https://www.scitation.org/doi/suppl/10.1121/10.0003357 for a LABVIEW program allowing exploration of the phenomenon of peaks in cubic and spline interpolations with several different simulated array geometries.

Au, W. W. L. (**1988**). "Sonar target detection and recognition by odontocetes," in *Animal Sonar: Processes and Performance*, edited by P. E. Nachtigall and P. W. B. Moore (Plenum, New York), pp. 451–465.

Au, W. W. L. (**1993**). *The Sonar of Dolphins* (Springer-Verlag, New York).

Au, W. W. L., and Moore, P. W. B. (**1984**). "Receiving beam patterns and directivity indices of the Atlantic bottlenose dolphin *Tursiops truncatus*," J. Acoust. Soc. Am. **75**, 255–262.

Au, W. W. L., Pawloski, D., Nachtigall, P. E., Blonz, M., and Gisner, R. (**1995**). "Echolocation signals and transmission beam pattern of a false killer whale (*Pseudorca crassidens*)," J. Acoust. Soc. Am. **98**, 51–59.

Au, W. W. L., and Penner, R. H. (**1981**). "Target detection in noise by echolocating Atlantic bottlenose dolphins," J. Acoust. Soc. Am. **70**, 687–693.

Arditi, G., Weiss, A. J., and Yovel, Y. (**2015**). "Object localization using a biosonar beam: How opening your mouth improves localization," R. Soc. Open Sci. **2**, 150225.

Beedholm, K., and Møhl, B. (**2006**). "Directionality of sperm whale sonar clicks and its relation to piston radiation theory," J. Acoust. Soc. Am. **119**, EL14–EL19.

Frouzova, J., Kubecka, J., Balk, H., and Frouz, J. (**2005**). "Target strength of some European fish species and its dependence on fish body parameters," Fish Res. **75**, 86–96.

Gellermann, L. W. (**1933**). "Chance orders of alternating stimuli in visual discrimination experiments," Pedagog. Semin. J. Gen. Psych. **42**, 206–208.

Ghose, K., and Moss, C. F. (**2003**). "The sonar beam pattern of a flying bat as it tracks tethered insects," J. Acoust. Soc. Am. **114**, 1120–1131.

Ibsen, S. D., Nachtigall, P. E., Krause-Nehring, J., Kloepper, L., Breese, M., Li, S., and Vlachos, S. (**2012**). "Spatial orientation of different frequencies within the echolocation beam of a *Tursiops truncatus* and *Pseudorca crassidens*," J. Acoust. Soc. Am. **132**, 1213–1221.

Jensen, F. H., Johnson, M., Ladegaard, M., Wisniewska, D., and Madsen, P. T. (**2018**). "Narrow acoustic field of view drives frequency scaling in toothed whale biosonar," Curr. Biol. **28**, 1–8.

Jensen, F. H., Wahlberg, M., Beedholm, K., Johnson, M., Aguilar de Soto, N., and Madsen, P. T. (**2015**). "Single-click beam patterns suggest dynamic changes to the field of view of echolocating Atlantic spotted dolphins (*Stenella frontalis*) in the wild," J. Exp. Biol. **218**, 1314–1324.

Kastelein, R. A., Janssen, M. H. M., Verboom, W., and de Haan, D. (**2005**). "Receiving beam patterns in the horizontal plane of a harbor porpoise (*Phocoena phocoena*)," J. Acoust. Soc. Am. **118**, 1172–1179.

Kloepper, L. N., Nachtigall, P. E., Donahue, M. J., and Breese, M. (**2012a**). "Active echolocation beam focusing in the false killer whale, *Pseudorca crassidens*," J. Exp. Biol. **215**, 1306–1312.

Kloepper, L., Nachtigall, P. E., Gisiner, R., and Breese, M. (**2010**). "Decreased echolocation performance following high-frequency hearing loss in the false killer whale (*Pseudorca crassidens*)," J. Exp. Biol. **213**, 3717–3722.

Kloepper, L. N., Nachtigall, P. E., Quintos, C., and Vlachos, S. A. (**2012b**). "Single-lobed frequency-dependent beam shape in an echolocating false killer whale (*Pseudorca crassidens*)," J. Acoust. Soc. Am. **131**, 577–581.

Kloepper, L. N., Smith, A. B., Nachtigall, P. E., Buck, J. R., Simmons, J. A., and Pacini, A. F. (**2014**). "Cognitive adaptation of sonar gain control in the bottlenose dolphin," PLoS One **9**, e105938.

Kloepper, L. N., Buck, J. R., Liu, Y., and Nachtigall, P. E. (**2018**). "Off-axis targets maximize bearing Fisher Information in broadband active sonar," J. Acoust. Soc. Am. **143**, EL43–EL48.

Ladegaard, M., Jensen, F. H., Beedholm, K., da Silva, V. M. F., and Madsen, P. T. (**2017**). "Amazon river dolphins (*Inia geoffrensis*) modify biosonar output level and directivity during prey interception in the wild," J. Exp. Biol. **220**, 2654–2665.

Ladegaard, M., Mulsow, J., Houser, D. S., Jensen, F. H., Johnson, M., Madsen, P. T., and Finneran, J. J. (**2019**). "Dolphin echolocation behaviour during active long-range target approaches," J. Exp. Biol. **222**, 1–12.

Madsen, P. T., Aguilar de Soto, N., Arranz, P., and Johnson, M. (**2013a**). "Echolocation in Blainville's beaked whales (*Mesoplodon densirostris*)," J. Comp. Physiol. A **199**, 451–469.

Madsen, P. T., Lammers, M., Wisniewska, D., and Beedholm, K. (**2013b**). "Nasal sound production in echolocating delphinids (*Tursiops truncatus* and *Pseudorca crassidens*) is dynamic, but unilateral: Clicking on the right side and whistling on the left side," J. Exp Biol. **216**, 4091–4102.

Madsen, P. T., and Surlykke, A. (**2013**). "Functional convergence in bat and toothed whale," Physiol. **28**, 276–283.

Madsen, P. T., Wilson, M., Johnson, M., Hanlon, R. T., Bocconcelli, A., Aguilar de Soto, N., and Tyack, P. L. (**2007**). "Clicking for calamari: Toothed whales can echolocate squid *Loligo pealeii*," Aquat. Biol. **1**, 141–150.

Mertikas, S. P. (**1985**). "Error Distributions and Accuracy Measures in Navigation: An Overview," Technical Report No. 113 (University of New Brunswick, Fredericton, New Brunswick, Canada).

Moore, P. W. B., Dankiewicz, L. A., and Houser, D. S. (**2008**). "Beamwidth control and angular target detection in an echolocating bottlenose dolphin (*Tursiops truncatus*)," J. Acoust. Soc. Am. **124**, 3324–3332.

Nachtigall, P. E., and Supin, A. Y. (**2014**). "Conditioned hearing sensitivity reduction in a bottlenose dolphin (*Tursiops truncatus*)," J. Exp. Biol. **217**, 2806–2813.

Nachtigall, P. E., and Supin, A. Y. (**2015**). "Conditioned frequency-dependent hearing sensitivity reduction in the bottlenose dolphin (*Tursiops truncatus*)," J. Exp. Biol. **218**, 999–1005.

Nachtigall, P. E., Supin, A. Y., Smith, A. B., and Pacini, A. F. (**2016**). "Expectancy and conditioned hearing levels in the bottlenose dolphin (*Tursiops truncatus*)," J. Exp. Biol. **219**, 844–850.

Wisniewska, D. M., Johnson, M., Nachtigall, P. E., and Madsen, P. T. (**2014**). "Buzzing during biosonar-based interception of prey in the delphinids *Tursiops truncatus* and *Pseudorca crassidens*," J. Exp. Biol. **217**, 4279–4282.

Wisniewska, M. D., Ratcliffe, J. M., Beedholm, K., Christensen, C. B., Johnson, M., Koblitz, J. C., Wahlberg, M., and Madsen, P. T. (**2015**). "Range-dependent flexibility in the acoustic field of view of echolocating porpoises (*Phocoena phocoena*)," eLife **4**, e05651.

Wisniewska, D. M., Johnson, M., Teilmann, J., Rojano-Doñate, L., Shearer, J., Sveegaard, S., Miller, L. A., Siebert, U., and Madsen, P. T. (**2016**). "Ultra-high foraging rates of harbor porpoises make them vulnerable to anthropogenic disturbance," Curr. Biol. **26**, 1441–1446.

Yovel, Y., Falk, B., Moss, C. F., and Ulanovsky, N. (**2010**). "Optimal localization by pointing off axis," Sci. **327**, 701–704.

Yuen, M. M., Nachtigall, P. E., Breese, M., and Supin, A. Y. (**2005**). "Behavioral and auditory evoked potential audiograms of a false killer whale (*Pseudorca crassidens*)," J. Acoust. Soc. Am. **118**, 2688–2695.

Chapter VIII.

High-frequency Masking

Hermannsen, L., Tønnesen, P., Ladegaard, M., **Malinka, C. E.**, Beedholm, K., Tougaard, J., & P. T. Madsen (2021). "Porpoise echolocation can be masked by weak high-frequency vessel noise," (*Manuscript draft*).

Porpoise echolocation can be masked by weak high-frequency vessel noise

L. Hermannsen[1,2a], P. Tønnesen[1], M. Ladegaard[1], C. Malinka[1],
K. Beedholm[1], J. Tougaard[2] and P.T. Madsen[1]
[1] Zoophysiology, Department of Biology, Aarhus University, Denmark
[2]Marine Mammal Research, Department of Bioscience, Aarhus University, Denmark
[a] Corresponding author. Email: lihe@bios.au.dk

ABSTRACT

Noise from fast moving vessels can extend into frequency ranges that overlap with echolocation signals of toothed whales with a potential to mask their echolocation. To address that potential problem, we tested the hypothesis that high frequency noise at realistic vessel noise levels can mask the echolocation performance of harbour porpoises (*Phocoena phocoena)*. Two trained and free-swimming porpoises wearing a multi-sensor tag (DTAG) were tasked with discriminating between two targets by echolocation, mimicking the ecologically relevant scenario of a foraging toothed whale. At the same time they were exposed to third-octave band limited noise at 2 kHz (Low frequency band, 122-128 dB re 1µPa RMS) or 125 kHz (echolocation band, 105-111 dB re 1 µPa RMS). C We conducted 392 trials of which half were no-noise controls and show that porpoises increase median click source levels by 4-17 dB when exposed to 125 kHz noise with a Lombard response of 0.5 dB/dB. Despite this, both animals were still significantly poorer at discriminating the targets during these trials, demonstrating their inability to compensate sufficiently to alleviate masking impacts. When the porpoises were offered spatial release from masking, they regained their echolocation performance. In comparison, the porpoises maintained their click source levels and performance when exposed to low frequency noise. . We conclude that relatively low levels of high-frequency noise, such as from cavitating vessel propellers, can cause masking of porpoise echolocation and that compensatory mechanisms evoked by the animals are insufficient to maintain echolocation performance during target discrimination. As a consequence, high frequency components of vessel noise may have negative fitness impacts on porpoises and other small toothed whales, and we therefore recommend that high frequency vessel noise effects are considered in marine management.

INTRODUCTION

Echolocating toothed whales hunt and navigate by emission of ultrasonic clicks and subsequent acute auditory processing of echoes returning from the ensonified environment (Au, 1993). The detection of weak echoes from prey items is facilitated by very sensitive and directional hearing at ultrasonic frequencies (Kastelein et al., 2005), which along with a directional outgoing sound beam (Jensen et al., 2018) suppress interference from echo generators that are not of interest (clutter) and in-band noise above the hearing threshold (masking). The virtues of such spatial filtering of interference phenomena is likely one of the primary drivers of the high transmission and receiving directionalities in toothed whale biosonar systems (Jensen et al., 2018). While directionality is the only way to suppress clutter, masking effects may also be alleviated through increased source levels (SL) to improve resulting echo to noise ratios as seen from the noise limited sonar equation:

$$ENR = SL_{RMS} - 2*TL + TS - (NL - DI)$$

The echo-to-noise ratio (ENR) is given by the sonar source level (SL) minus the two-way transmission loss (TL) plus the target strength of the target of interest (TS) minus the masking noise given by the isotropic noise level in the frequency band of the click (NL, TOL of 125 kHz band), corrected for the receiving directivity index (DI) of the animal's auditory system. Consequently, if the noise level (NL) increases while target and range are kept constant, the echolocating toothed whale will face a reduced ENR resulting in a potentially poorer ability to detect, localize and classify a target (Au et al., 1988). However, when facing increased masking noise, echolocating toothed whales can maintain the ENR by increasing the source level (SL) of the clicks (Au et al., 1985; **Chapter IX,** Ladegaard *in prep*.), and by employing spatial release from masking by approaching the target so that it is not on line with the source of masking noise source.

While the consequences of such masking effects in principle are readily quantifiable from the sonar equation, surprisingly little is known about how masking impedes toothed whale biosonar operation and the degree to which compensatory mechanisms are employed by toothed whales to cope with natural fluctuations in ambient noise levels. The relevance of this pertinent data gap is further compounded by the significant increases in noise levels in the worlds oceans over the last century from increased shipping (Hildebrand, 2009). While vessel noise generally is dominated by energy at low frequencies, recent studies have documented high-frequency components of vessel noise from cavitating propellers all the way up to 150 kHz that is the upper hearing range of even the smallest toothed whales (Hermannsen et al., 2019). Because of the often low ambient noise levels in the high frequency bands used by toothed whales for echolocation, such relatively weak high frequency components in vessel noise have the potential to reduce the ENR of echolocating whales by many hundreds of meters from a moving vessel (Hermannsen et al., 2014). Unless compensated for by the exposed animals, such masking of echolocation by vessel noise may result in reduced acoustic detection ranges and a reduced ability to identify and discriminate prey items. Accordingly, vessel noise-induced masking effects on biosonar operation may have direct consequences on survival and fitness via a reduced capability to detect gill nets, or by a reduced food intake per time (Wisniewska et al., 2018).

A few controlled exposure studies have demonstrated masking effects in toothed whales (*e.g.* Au et al., 1988; Au and Moore, 1990; Branstetter et al., 2013). However, these studies have invariably used stationary animals in single target detection tasks, which has limited the transferability to the actual masking impacts and compensatory behaviour of wild free-swimming toothed whales that echolocates to hunt food. In turn, ddemonstration of masking of echolocation in wild toothed whales is very difficult, however, because of a large number of confounding behavioural variables and environmental unknowns such as the directions to the noise source and targets of interest. Studies of wild toothed whales have shown decreased echolocation or foraging activity in association with vessel noise exposure (Aguilar Soto et al., 2006; Williams et al., 2006; Wisniewska et al., 2018), but whether these effects are due to masking or behavioral disruption remains unresolved.

In an attempt to bridge the gap between having enough control to quantify masking effects and compensatory mechanisms, and yet offer a setting of ecological validity to make the results informative in the context of mitigation noise effects at sea, we trained two free-swimming harbor porpoises (*Phocoena phocoena*) to actively discriminate between two targets in varying, but controlled noise fields. Specifically, we sought to test the hypotheses that i) a drop in sonar performance is due to masking by only being affected by noise within the same frequency range as the sonar signals, ii) masking effects on performance are smaller, if the target echo and masking noise

are not aligned, providing spatial release from masking, and iii) that the porpoises would increase the intensity of sonar signals to compensate for the masking. To do that we employed levels of masking and non-masking noise selected to match received levels of noise measured on wild porpoises with onboard tags. We show that porpoise echolocation performance deteriorated when exposed to weak high-frequency noise, resembling noise from high-speed vessels at 100-360 m, implying that negative fitness effects of masked echolocation in small toothed whales must be considered part of the potential suite of impacts of vessel noise.

METHODS

Experimental setup

Experiments were conducted in an 8x12 m semi-natural research pool at the Fjord & Belt Centre, Kerteminde, Denmark (Fig. 1) with two trained female harbor porpoises "Freja" (female, ~20 years old) and "Sif" (female, ~14 years old) from November 2016 to March 2017. The animals were presented with a two-alternatives forced-choice task (Schusterman, 1980), following the protocol of Wisniewska et al. (2012). The animals were rewarded for selecting a standard target (aluminium sphere, target strength -38 dB) against an alternative target, placed 1 m from the standard. The non-rewarded, alternative target was either made of PVC (target strength -42 dB), considered an easy task for the animal, or stainless steel (target strength -37 dB), considered more difficult (Wisniewska et al., 2012). All three targets were 50.8 mm (diameter) solid spheres attached via lines and hooks to a two-armed metal frame to allow for easy target repositioning. Two calibrated custom-built cylindrical hydrophones (sensitivity -212 dB re 1µPa/1V) placed 7 cm above the targets continuously recorded sound during trials (sampling rate of 500 kHz, 16 bit, flat frequency response of ± 2 dB between 100 and 160 kHz). During the experimental trials, porpoises were blindfolded (using opaque silicone eyecups) to ensure that they could not solve the task visually.

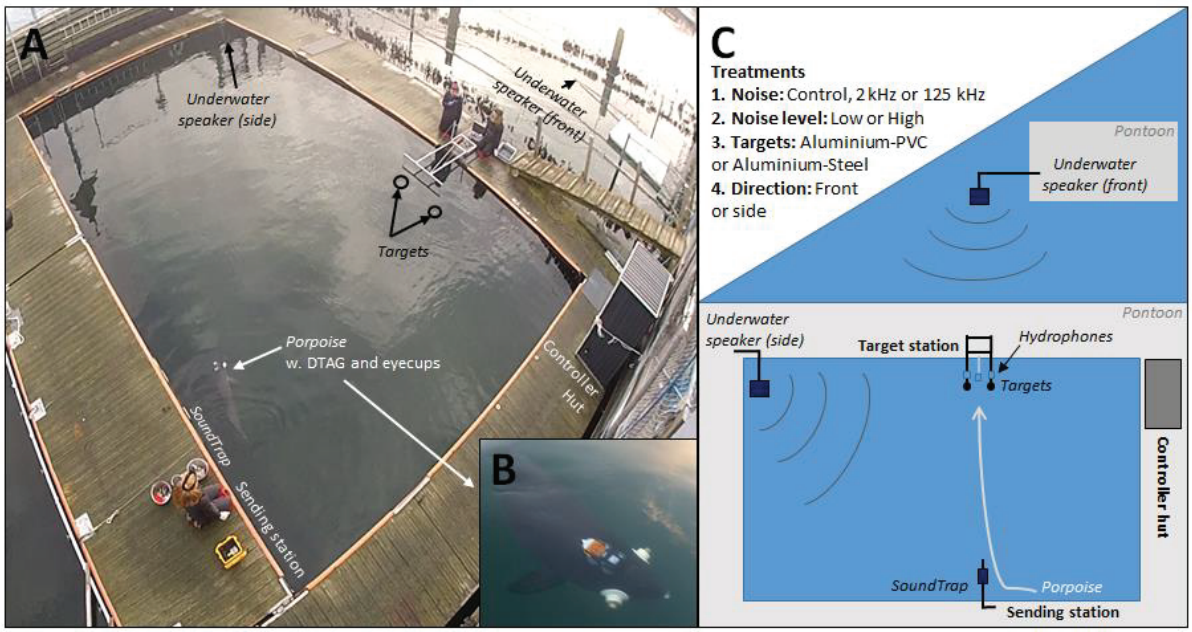

Figure 1. Experimental setup: **A)** balcony view and **C)** schematic view. **B)** Porpoise with DTAG and eyecups.

Porpoises were free-swimming and also carried a sound-recording tag (DTAG3 [500 kHz sampling rate, 16 bit, 170 dB re 1 µPa clip level] or DTAG4 [576 kHz sampling rate, 16 bit, 170 dB re 1 µPa clip level]; Johnson and Tyack 2003) with a flat (±3 dB) frequency response from 0.5 to 150 kHz. The DTAG was attached dorsally behind the blowhole with suction cups (Fig. 1B), in order to monitor noise levels and echolocation behaviour.

During each trial of the discrimination task, the animal was exposed to either ambient noise only (control, *i.e.* no exposure given) or one of four noise signals. The noise was third-octave band filtered noise centred at either 2 kHz or 125 kHz, and presented at either a low or a high level (Figs 2-3, and supplementary Table S1). The 125 kHz noise band was chosen as the most likely signal to cause masking, as it overlaps with the frequencies of the porpoise biosonar clicks (Møhl and Andersen, 1973; Kyhn et al., 2013). The 2 kHz noise band was chosen to represent a realistic distractor noise, well outside of the frequency band used for echolocation, but still within the range where porpoises have good hearing (Kastelein et al., 2002, 2010; supplementary Fig. S1). We chose noise levels to mimic realistic noise exposure levels from vessels. These levels were informed by tag recordings on wild porpoises by Wisniewska et al. (2018), and were either the maximum noise level across all recordings, or the 10%-exceedance level (L_{10}, the noise level exceeded 10% of the time) also across all recordings. Since Wisniewska et al. (2018) quantified vessel noise in a third-octave band at 16 kHz, we used the spectral characteristics of a high-speed vessel (from Hermannsen et al., 2014) to estimate the offsets from the measurements at 16 kHz to the bands at 2 kHz and 125 kHz, used in the experiment. The maximum level at 16 kHz in the recordings of Wisniewska et al. (2018) was 10 dB above the level at 16 kHz from Hermannsen et al. 2014 and L_{10} at 16 kHz was 25 dB below the level from Hermannsen et al. (2014). These factors were then used to define the exposure levels 'high' (+10 dB re. Hermannsen et al., 2014) and 'low' (-25 dB re. Hermannsen et al., 2014) at 2 kHz and 125 kHz, used in the experiment. See supplementary Fig. S1 for additional details. For the low and high noise exposure treatments, we therefore aimed to produce a received third octave level (TOL) at the target that was either at 75 or 110 dB re µPa (RMS), respectively, in the 125 kHz third octave band, or at 95 and 130 dB re µPa (RMS) in the 2 kHz third octave band.

Noise was generated in Matlab (version 2016a, MathWorks Inc., Ma, USA) by applying third octave band filters centred at 2 and 125 kHz to white Gaussian noise. It was presented via a data acquisition port on a multi-purpose instrument (NI USB-6356, National Instruments, TX, USA), using custom written software (LabVIEW, version 2015) to reach the desired noise playback levels (supplementary Fig. S1). The speakers were either 10 m behind and in line with the targets or 8 m to the left of the left target, perpendicular to the swimming path of the animals (Fig. 1). On-axis noise exposures at 2 kHz were played at source levels (SLs) of 115 and 150 dB re µPa (RMS) at 1 m from an underwater speaker (LL916 Lubell Labs Inc., OH, USA), while 125 kHz noise was transmitted at SLs of 95 and 130 dB re µPa (RMS) from a hydrophone (type 8105, Brüel & Kjær Sound & Vibration Measurement A/S, Nærum, Denmark transmitting response of ~144 dB re 1 µPa/V at 1 m;). An HS150 hydrophone (resonance frequency ~150 kHz, transmitting response 130 dB re 1 µPa/V; SRD Ltd, U.K.) was used for the playbacks of 125 kHz noise from the side of the pool. The playback levels of all transducers were calibrated prior to the experiments using a calibrated acoustic logger (SoundTrap, version ST202HF, oceaninstruments.co.nz; sampling rate of 576 kHz) located at the sending station (Fig. 1). A hydrophone placed between the targets (custom build, as hydrophones mounted above targets) was used to transmit sweeps between 180 kHz and 210 kHz at the beginning and end of each trial, to allow for post-processing time synchronization of all three acoustic recorders (the target hydrophones, the SoundTrap, and the DTAG).

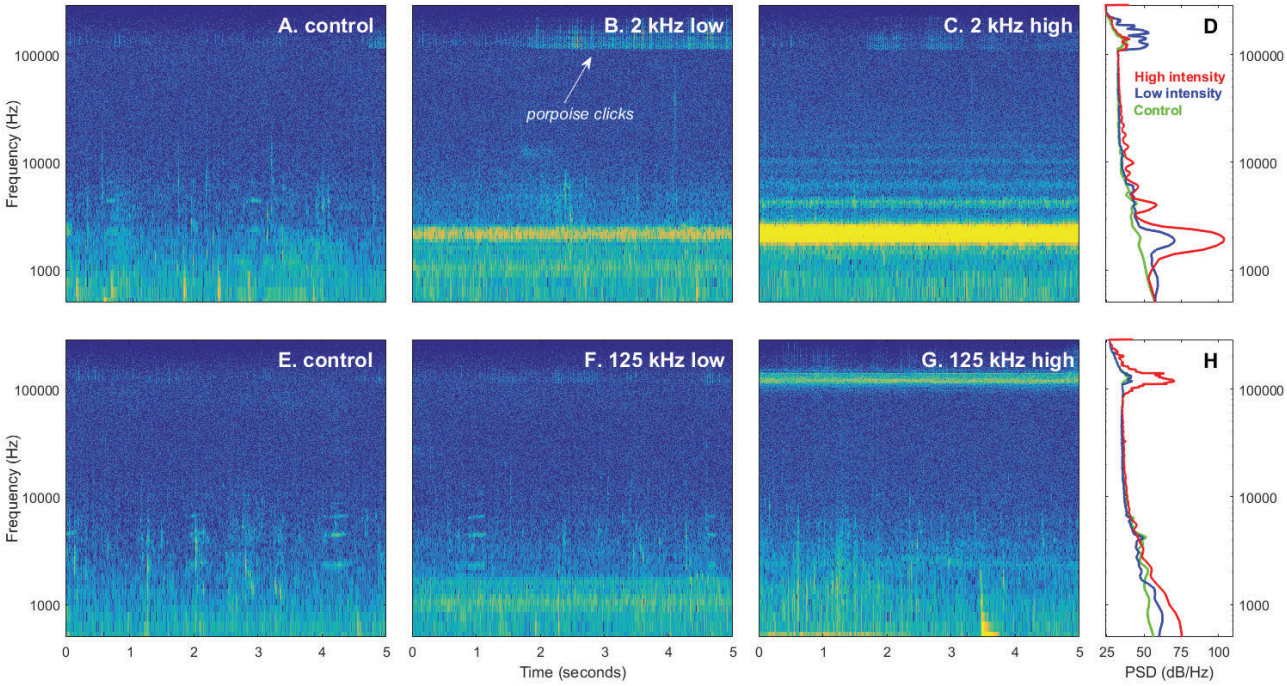

Figure 2. The five different types of noise exposures, as recorded at the sending station, shown as spectrograms and power spectrum densities.

Experimental protocol

During experiments, the non-participating animal was stationed/occupied in a neighboring pool to avoid both the distraction of the study animal and the recording of clicks from the non-participating porpoise. Two types of sessions were conducted. In the first session type, noise was only transmitted from behind the targets, in line with the porpoise swim path, and it contained at least ten trials with ten different combinations of targets, noise types, and noise levels (Fig. 1C). In the second session type, noise was either played in line with the target of perpendicular to the swim path, and was either a control with the easy alternative target (PVC) or a trial with a high level of 125 kHz noise with the difficult alternative target (steel). Before each session, the trial combinations and presentation order were generated using a pseudo-random Gellermann schedule (Gellermann, 1933). The position of the rewarded and non-rewarded target was randomly switched within a session between the right and left position, and was not deployed in the same place more than three times in succession to avoid the animal basing its decision on the previous trials. The following two criteria to maintain animal motivation; 1) a session always started with one of the combinations expected to be easy (control without noise, or PVC comparison target with low noise) and 2) never ended with an unsuccessful trial. In cases where the final trial resulted in an unsuccessful target discrimination, the session was extended with an easy trial condition.

A trial started with the trainer stationing the animal before sending it towards the targets to perform the discrimination task (Fig 1). The trial and noise exposure started when the DTAG on the animal was first submerged, where the animal was no more than a body length from the sending station (Fig. 1). The blindfolded animal swam towards the targets while echolocating and made a choice between targets by touching the selected target with the tip of its rostrum. The trainer whistled to bridge a correct answer (of selecting the aluminium target) and the animal was rewarded with fish, if the rewarded target was selected. Between trials, targets were lifted out of the water, regardless of

whether targets were to be changed or not. The noise exposure was stopped 5 s after the trainer's whistle to avoid the animal making a rash discrimination decision in an attempt to switch off the noise. If the animal chose the non-rewarded target in a trial, the trainer did not whistle, the targets were lifted out of the water and the animal was sent back to the station without a reward. Trials where the animal did not choose a target were noted as a failure to solve the task, and noise was stopped 5 s after the animal either left the path towards the spheres or passed by them without choosing.

Throughout trials, a HTI-96 hydrophone (frequency response 20 Hz – 32 kHz) coupled to an in-air loudspeaker was used to detect whether considerable construction or boat noise from the neighboring harbour was present. If anthropogenic noise was audible to the person controlling the noise exposure, a session was postponed until the noise was no longer audible.

Noise recordings

Noise levels, as recorded on the DTAG, were quantified by third octave band levels in the bands from 2 to 203 kHz (Fig. 3). For lower frequency bands (below 50 kHz), a 22 ms analysis window (no overlap) was used which ensured a minimum of 10 samples for the 2 kHz centered third octave band. Band levels above 50 kHz were computed with a 1 ms analysis window (no overlap), which was chosen to ensure that only a minor fraction of the analysis windows contained echolocation clicks and that it was still long enough to provide at least 10 samples in the frequency domain per third octave band. Percentiles of noise were then computed for the pooled TOLs and grouped based on noise playback level and sphere combination (Fig. 3).

Quantification of porpoise echolocation behaviour

The recordings on the DTAG and the two target hydrophones were synchronized on a trial basis using the sync sweeps projected at the beginning and end of a trial. Porpoise clicks on the DTAG recordings and the target hydrophones were detected with a supervised click detector as in Wisniewska et al. (2012). Based on observations that the porpoises were scanning across the targets, a subset of clicks were selected and categorized as presumed on-axis clicks during the approach phase. On-axis clicks were selected manually using plots of RL versus time for each trial with the selected on-axis clicks being the clicks with the highest RL within distinct click sequences of increasing and decreasing RL.

In all trials where the porpoises made contact with the standard target and where buzz clicks were detected on both the DTAG and standard target hydrophone, the shortest detection time delay served as a 0 m range reference. In trials where the porpoise never placed its rostrum on the target, the shortest time-of-arrival difference between clicks recorded on the target and DTAG could not simply be assumed to represent 0 m target range, thus an echogram (Johnson et al. 2004) was made using the DTAG recordings to manually identify the animal-to-target range for a specific click. This specific click was then also identified in the target sphere recordings by comparing ICI patterns. Using the time delay between the detections of this click in the DTAG and target recordings coupled with the echogram-based range estimate, this delay and range point then served as a reference to which all other delay-based range estimates were adjusted in a given trial.

The ability of the animals to correctly discriminate and select the standard target was quantified as a *success rate* (%), and hypothesized to decrease for exposures to high levels of 125 kHz noise. To investigate how the different noise types affected the echolocation performance of the animals, three different parameters were extracted: *trial duration*, *buzz duration* and the *number of scans*; all hypothesized to increase if the task was difficult. *Trial duration* was estimated as the duration between the synchronization sweeps emitted in the beginning and end of each trial. Porpoise clicks were detected on both the DTAG and the target hydrophones with a supervised automated detector. The inter-click intervals (ICIs) were measured for each pair of successive clicks detected in the DTAG recordings. ICIs above 13 ms were categorized as approach-phase, and below as buzz phase, in accordance with Wisniewska et al. (2012). The total *buzz duration* was measured trial-by-trial as the sum of all buzz-phase ICIs. The *number of scans* across the aluminium target was taken to be the number of on-axis clicks (with ICIs >13 ms) in the aluminium sphere recordings.

For each click, parameters were computed after first extracting a 100 ms window centred on the detection time and filtering with a 4 pole 50 kHz high pass Butterworth filter before extracting a 500 µs analysis window centred on the detection time. The 500 µs window prior to each click analysis window was saved and used later for signal-to-noise ratio (SNR) estimation. The click received levels (RL) were quantified either as peak-to-peak (pp) or RMS level after interpolating the waveform by a factor of 10 using the MATLAB ‘interp’ function to slightly improve estimates of peak levels. The RMS level was estimated within the duration between the -10 dB points on either side of the peak (normalized to 0 dB) of the amplitude envelope (Madsen and Wahlberg, 2007). The SNR was then computed by subtracting the RMS level within the noise analysis window from the click RMS level and then dividing by the noise RMS level.

Source levels (RMS) of echolocation clicks were calculated for on-axis clicks assuming a spherical spreading loss over the animal-to-target range. The animal-to-target range was measured using the time delay between the same click recorded on the DTAG and the SoundTrap, assuming a sound speed

of 1500 m/s. In order to estimate the ENR for the on-axis clicks in control, and low and high level 125 kHz noise conditions, we used the noise-limited active sonar equation (equation 1; Au, 1988; Au, 1990) with the SL_{RMS} 2 x TL of $20\log_{10}$(range), and the TS for the standard target (-38 dB). In control trials, where self-noise limitations (Ladegaard et al., 2019) prevented reliable noise level estimation, we used a 125 kHz TOL estimate of 60 dB re 1 µPa based on thermal noise at 125 kHz (Mellen, 1952) and corrected for the energy within the 125 kHz third octave bandwidth and assumed a receiving DI of 11.7 dB for porpoises (Kastelein et al., 2005). In the 125 kHz low-noise level trials, self-noise of the DTAG also limited the reporting of noise level estimations at the porpoise station, and we therefore calculated a TOL of 75 dB re µPa based on the transmitting sensitivity of the transducer and its voltage input, assuming linearity. For the 125 kHz high-noise level trials, we used the 50th percentile TOLs computed as a pooled estimate for each experimental condition (107-110 dB re 1µPa RMS). It is only appropriate to subtract the receiving DI (DI_R) from the NL for an isotropic noise field. Because noise was transmitted from specific locations in this study, we did not correct for DI when noise was played from the front, but instead subtracted 13 dB from NL when noise came from the side (~70 degrees) according to the receiving beam pattern estimated by Kastelein et al. (2005).

Statistical Analysis

Linear mixed-effects models tested the significance of porpoise echolocation behaviour (trial duration, success rate, buzz duration, number of scans) across treatments and animals using the functions "lmer" and "glmer" from the statistical model package "lme4" (Bates et al., 2015) in *R* software (version 3.5.1, R Core Team, 2019). SL, buzz duration, trial duration and ENR were classified as continuous variables. The number of target scans was classified as Poisson-distributed and tested with a generalized linear model. The model inputs in all models were 'Noise' (categorical, five levels: control, 2 kHz low intensity, 2 kHz high intensity, 125 kHz low intensity or 125 kHz high intensity) and 'Alternative Target' (categorical, two levels: steel or PVC). 'Animal' (categorical, two levels: Sif or Freja) was added as a random effect in all models. In the models for SL, which were based on multiple on-axis clicks per trial, 'Trial Number' was also added as a random effect.

Results

The two porpoises, Freja and Sif, performed 197 and 190 trials (Fig. 4A), respectively. In most trials (89 and 97%, respectively; Fig. 4A), the animals correctly selected the rewarded target. As expected, the experimental condition that proved most difficult for the porpoises was with high intensity 125 kHz noise (median received level 106 dB re 1µPa RMS, 75% confidence interval [103, 108]; Fig. 3C and supplementary Table S1) and the steel sphere as the alternative target, where the success rate sof Freja and Sif were only 54% and 85%, respectively. For Freja, the success rate was only slightly higher (58%) when faced with the high intensity 125 kHz noise with the PVC target as the alternative, whereas Sif made no errors for that condition. Both animals made a few errors (2 or 3 in total per animal) in different trials setups that did not include high levels of 125 kHz noise, but that were all with the steel target.

The parameters *trial duration*, *buzz duration* and *number of target scans* were estimated for each trial (Fig. 4B-D) and tested statistically (see supplementary Table S2). Trial duration and buzz duration across both animals were significantly longer, by 10.6% (1.18 s, 95% confidence interval, CI [0.65, 1.71]) and by 9.1% (0.22 s, 95% CI [0.04, 0.39]), respectively, in trials where porpoises were exposed to high levels of 125 kHz noise. The difficulty of the discrimination task also affected porpoise

performance, with trials using steel as the alternative target (*i.e*. a difficult task) had longer trial durations (0.41 s, 95% CI [0.04, 0.78]) and buzz durations (0.19 s, 95% CI [0.6 0.31]). During trials that had the high contrast discrimination task (with steel as the alternative target) and had exposure to high intensity 125 kHz noise, the porpoises on average increased trial duration by 14.2% (1.59 s) and buzz duration by 17% (0.41 s). The number of target scans did not differ significantly between different trial combinations.

While absolute SLs differed between the individual porpoises, both individuals each emitted clicks with similar SLs across the control conditions, all 2 kHz noise conditions, and the trials with low intensity 125 kHz noise conditions (Fig. 5A). In contrast, both animals significantly increased their click SLs, Freja by 17 dB (95% CI [14.8, 18.6]) and Sif by 9 dB (95% CI of [7.0, 10.8]), when they were exposed to high levels of 125 kHz noise (Fig. 5A and supplementary Table S3). Sif produced clicks at higher baseline levels (median SLs of 160-163 dB re 1µPa pp) than Freja (median SLs of 152-155 dB re 1µPa pp), but increased the SL to similar absolute levels for the high intensity 125 kHz noise conditions where noise was arriving from the front (median SLs of 167-169 dB re 1µPa pp). Freja increased SLs regardless of whether 125 kHz noise was emitted from the direction of the targets or from the side relative to the swim path, with only slightly lower SLs by 0.6 dB for trials with noise played from the side (95% CI [-1.9, 3.1]). For Sif, click SLs during trials with similar settings (125 kHz high noise from side) were significantly lower by an average -6.1 dB (95% CI [-8.5, -3.7]) compared to when Sif was exposed to 125 kHz from in front, thereby approximating the SLs that this animal used during the remaining trial conditions (Fig. 5A).

Despite the fact that both porpoises increased their click SLs for the presumed most challenging trial conditions, the ENR estimations (Fig. 5B) show that the SL adjustments were inadequate to fully compensate for the effects of the masking noise, thus leading to lower ENRs during these conditions. In trials where both levels of high intensity 125 kHz noise conditions where noise arrived from the front, medians of ENRs were at or below 0 dB for both animals, except for when Freja was presented with the PVC alternative target (median ENR of 5 dB). The ENRs were improved for trials where noise was played from the side and stayed above 0 dB, but were still below the ENRs for trials with control or low 125 kHz noise, which had median ENRs of 12-34 dB.

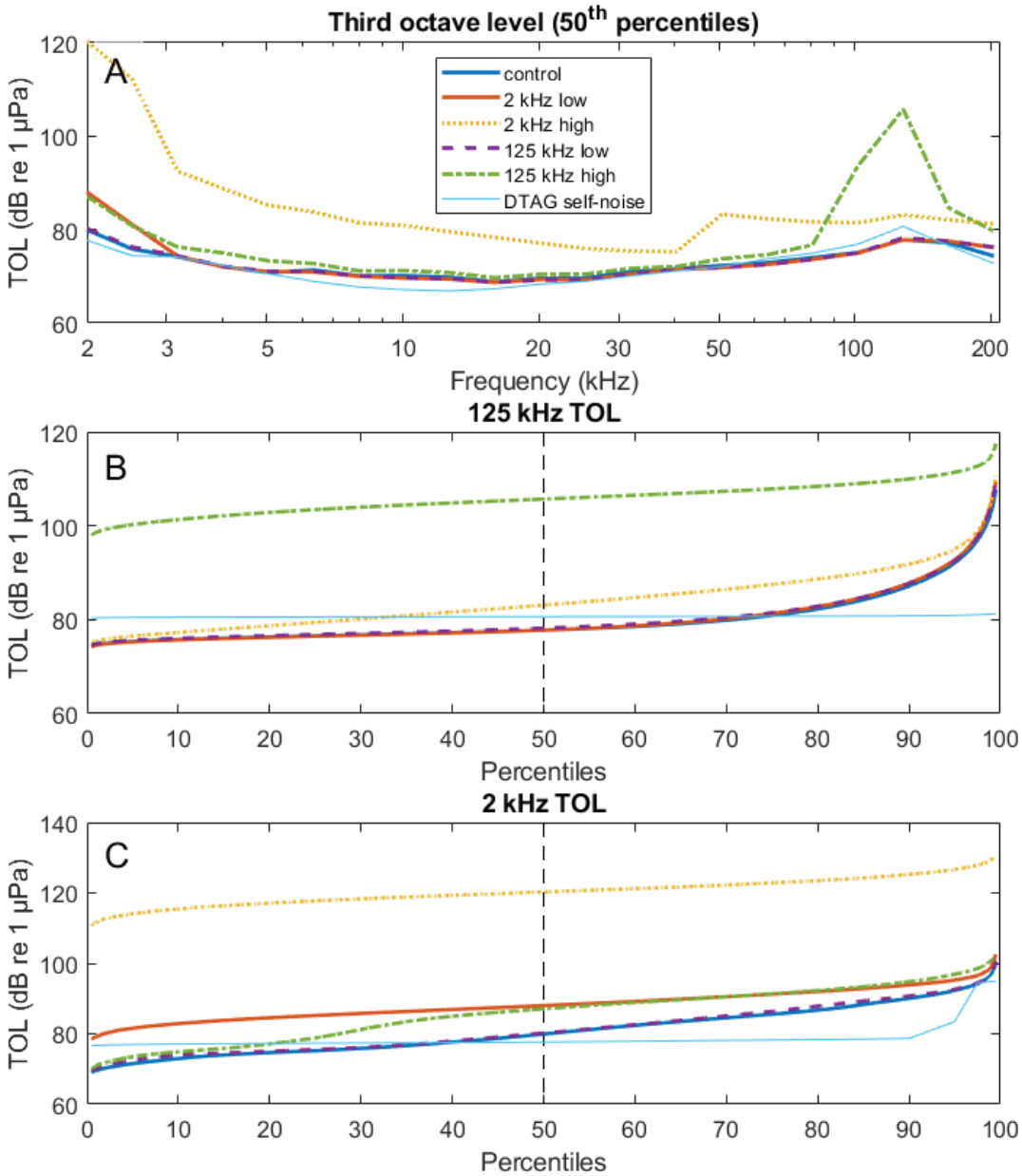

Figure 3. Third octave noise levels (TOL) under the different noise conditions recorded on the approaching animal with a DTAG (i.e. 10-18 m from the noise source). **A)** Median TOL estimated for the third octave bands from 2 to 203 kHz. **B)** Percentiles of the estimated TOL for the 125 kHz third octave band. **C)** Percentiles of the estimated TOL for the 2 kHz third octave band. Vertical dashed lines in plot B and C mark the median.

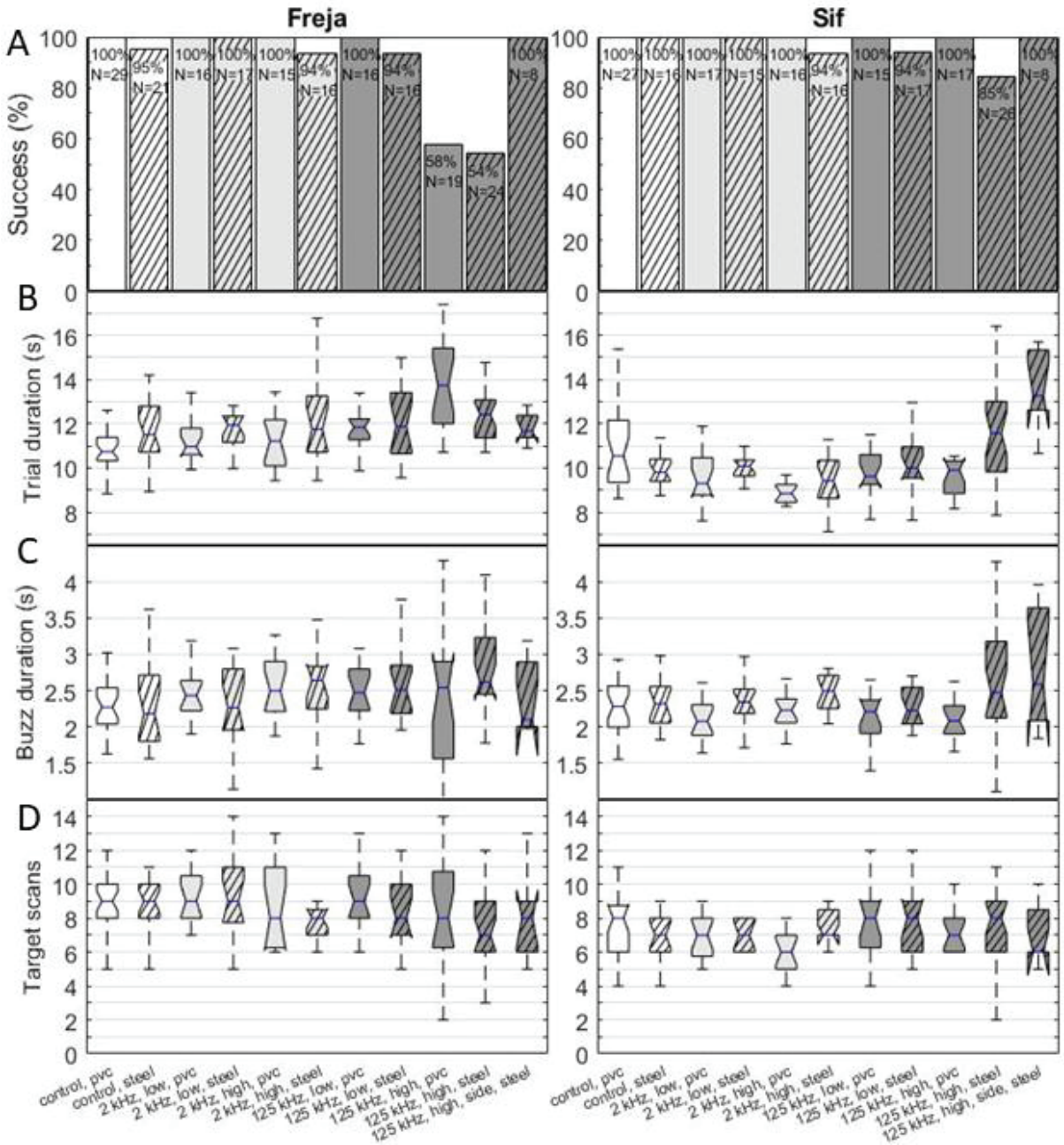

Figure 4. Measures of echolocation performance in two porpoises (left and right) during ten different trial combinations (bottom). **A)** success rate in target discrimination, **B)** trial duration, **C)** total echolocation buzz duration, and **D)** number of target scans. For boxplots (**B-D**), horizontal middle lines are the medians, while the whiskers show the 25th and 75th percentiles within each trial combination.

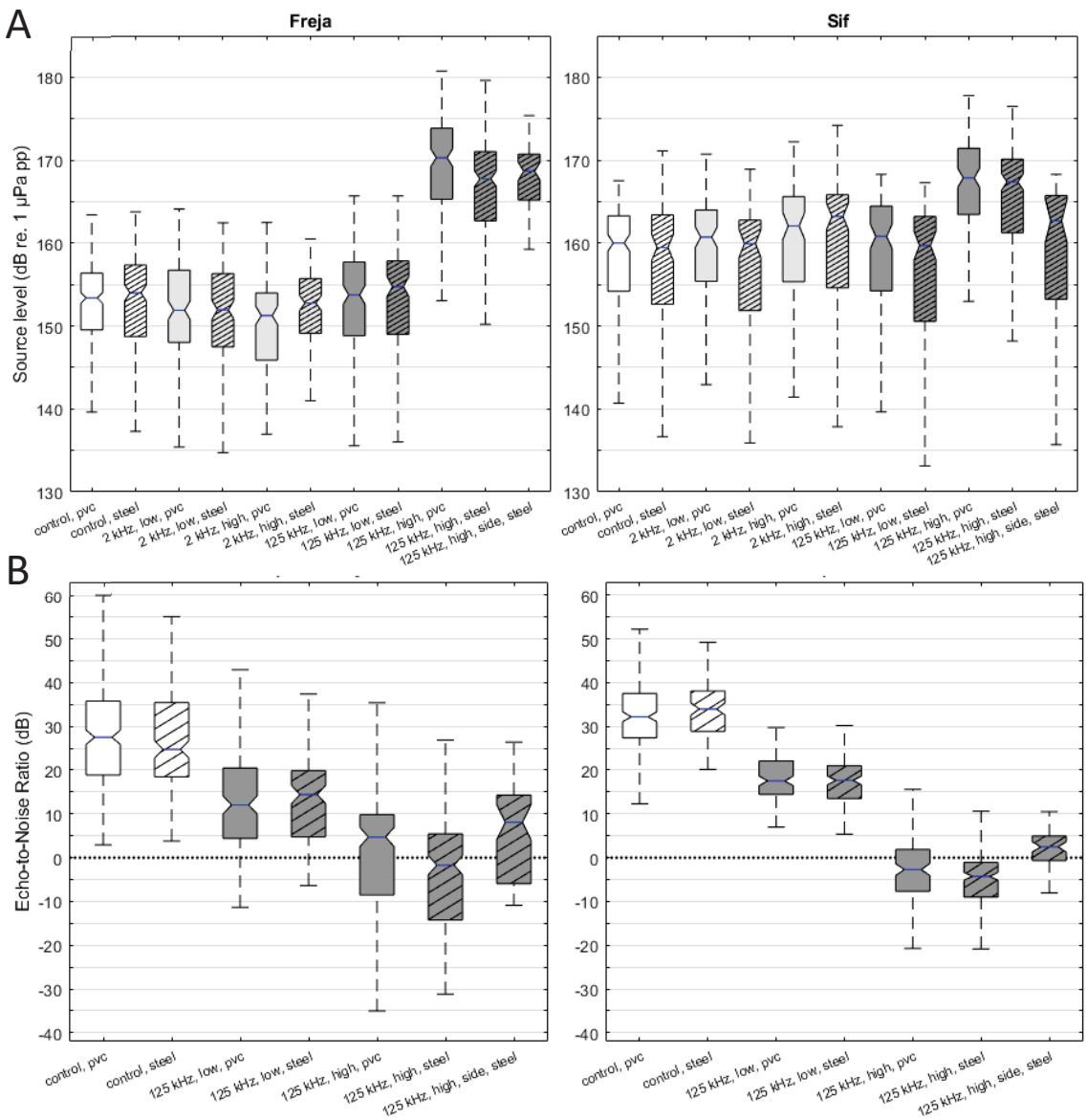

Figure 5. A) The back-calculated source levels and **B)** estimated echo-to-noise ratios (bottom) of on-axis echolocation clicks of two porpoises (left and right) during different trial combinations. Medians are shown as blue horizontal lines in each boxplot, and whiskers show the 25th and 75th percentiles within each trial combination. The horizontal lines in the bottom plots equal an ENR of 0 dB.

Discussion

Here, we investigated the masking impacts of high-frequency noise that overlaps in frequency with echolocation signals of porpoises. Specifically, we used setup where two trained harbour porpoises were engaged in a two-alternative-forced choice task involving active target interception. We did so in control and noise trials to examine whether weak high frequency noise can mask biosonar-based target discrimination. Specifically, we hypothesized that: i) a drop in sonar performance would be due to masking in the same frequency band as the biosonar signals, ii) masking impacts on biosonar performance would be smaller if there was spatial release from masking, and iii) the porpoises would compensate for masking by increasing the intensity of their biosonar signals. To promote the ecological validity in addressing masking effects of vessel noise in the wild, we used realistic vessel noise levels as measured on wild harbor porpoises (Wisniewska et al., 2018). To decouple masking effects and behavioural responses to high-intensity noise, we also tested how the trained porpoises performed and responded to a distractor noise at 2 kHz. The porpoises were tasked with discriminating between two targets of different materials to simulate a foraging decision, as echolocating animals engage in selective foraging on the basis of echo information (Arranz et al., 2011). Furthermore, by allowing the study animals to move freely and to use their echolocation in solving the task, they had the opportunity to invoke compensatory mechanisms to cope with the noise, as wild animals do.

In most trials, the two porpoises performed very well in the echolocation discrimination task and made very few errors in selecting the rewarded (aluminium) target over the non-rewarded target (PVC or stainless steel). Only when the noise level was high, overlapped in frequency with the echo, and was presented from a point behind the targets (offering no spatial release from masking), did the rate of errors increase (Figure 4A). This is in agreement with out first hypothesis that echolocation performance would be most impacted when the frequency of the noise overlapped with the frequency of the echolocation signals. The fact that neither the low-level of the high frequency noise, nor either level of the low frequency noise had any effect on the performance and source level supports that masking is what drives the deteriorated echolocation performance. When the noise source was moved to a point perpendicular to the swimming path so that spatial release from masking could be possible, porpoise echolocation performance was restored; this gives credence to our second hypothesis that the impact of masking on biosonar performance would be smaller when spatial release from masking was possible.

Concurrent with the increase in errors was an increase in source level of the clicks (Figure 5A). Both animals increased their SLs, only in the presence of the high level, high frequency noise, but irrespective of whether the non-rewarded target was PVC (the “easy” task) or stainless steel (the “difficult” task) and whether the noise came from behind the targets or perpendicular to the swim path. This seems to indicate that the compensatory increase in source level of a true Lombard response, coupled directly to the received level of noise. This is in agreement with out third hypothesis that the porpoises compensate for masking by increasing the intensity of their biosonar signals.

The less that complete compensation (with a slope of 0.1 to 0.5 dB/1 dB noise increase) is consistent with the general pattern seen in terrestrial animals, about 0.4 dB/1dB compensation (*e.g.* Brumm and Todt, 2002; Brumm and Slabbekoorn, 2005). A similar Lombard response has been reported for the same two porpoises in Ladegaard et al., (*in prep.*, **Chapter IX**) during an interception experiment with a single target. In that experiment, no deterioration in performance was seen despite significantly

higher noise levels of up 127 dB re 1µPa (TOL, 125 kHz). These different results probably relate to the more difficult task of discriminating between two targets as opposed to intercepting a single target in noise, highlighting that assessment of noise impacts on echolocation requires a suite different experiments. Further, a porpoise that echolocates louder during noise exposure to mitigate masking could, lead to the erroneous interpretations in passive acoustic monitoring data. For example, a time-varying acoustic detection range for the monitoring instruments would be needed to account for the relationship between click source level and noise level, as not doing so could skew acoustic density estimations.

Instead of compensating by biosonar adjustments to maintain/improve ENR, an echolocating animal may also alter other parameters to increase the echolocation effort (*i.e*. more time spent echolocating, longer buzz durations, and a greater number of scans) to successfully acquire prey and make optimal foraging decisions. Here, we found that trial duration was increased significantly by 14.2% (Figure 4B), while buzz duration was increased by 17% (Figure 4C; supplementary Table S2) during difficult tasks with steel as the alternative target and exposure to noise that spectrally overlapped with their echolocation. These compensations are also indicative of the task being more challenging for the animals in the presence of the high level, high frequency noise.

The highest median noise TOL at 125 kHz was 108 dB re 1µPa RMS (Fig. 3A and Table S1) corresponds, if based on vessel noise recordings from Hermannsen et al. (2014), to potential masking of porpoises within a range of ~100-300 m from a vessel travelling at a high speed (43-78 km/h) in front on the animal. As longer echolocation ranges and small targets (such as the preferred prey of Inner Danish water porpoises, Wisniewska et al., 2018), will lead to a similar level of masking at lower received noise levels, we propose that cavitating vessels can cause masking of porpoise biosonar at ranges of several hundred meters.

However, this is a worst case scenario of being subjected to high levels of high-frequency masking noise. Porpoises have a directional hearing that in passive hearing tests offers spatial release from masking (Kastelein et al., 2005). Consistent with that notion, we show that when 125 kHz noise was transmitted from the left side of the animals (~70 degrees from front), the both maintained their high success rate (Fig. 4A). Interestingly, Freja exhibited an equally high increase in SL, when noise was projected from the side compared to the front, suggesting that the ability to discriminate effectively during these trials was likely achieved through a combination of spatial release of masking and adjustment of biosonar behaviour. The generally higher SL of Sif (Fig. 5A), and therefore higher ENR, which remained above 0 dB in exposures to noise from the side (Fig. 5B), was likely the reason for why this animal did not have to increase SL to solve the discrimination task in these trials.

With the large spatial overlap between key habitats for porpoises and areas with high densities of cargo ships, fishing and recreational vessels (Erbe et al., 2014; Hermannsen et al., 2019), porpoises are frequently exposed to vessel noise. Wisniewska et al. (2018) estimated that porpoises were exposed to some forms of vessel noise 17-87% of the time, while Hermannsen et al. (2019) estimated that motorized vessels were within 2 km of a shallow coastal study area, with a known population of porpoises, for 62% of the daylight hours. Most negative impacts of such vessel noise exposures likely pertain to behavioural effects, but our findings in this paper shows that a subset of these exposures with high frequency noise ahead of echolocating porpoises will lead to a deterioration in biosonar performance. Given that anthropogenic noise levels are predicted to continue rising in the future (Hildebrand, 2009), we see a need for more studies of when and how toothed whales are affected by, react to, and seek to compensate for noise levels that can be encountered in the wild.

Abbreviations

DI_R	directivity index (receiving)
ENR	echo-to-noise ratio
NL	noise level
SL	sonar output level, source level
SNR	signal-to-noise ratio
TOL	third octave level
TL	transmission loss
TS	target strength

Author contributions

LH, JT and PTM designed the study. LH and PT collected data, with help from CEM. KB made the LabVIEW program. LH, PT, ML and CEM processed the data. LH and ML analyzed the data and made the figures. LH conducted the statistical analysis. All authors helped to interpret the results. LH, ML, CEM, JT and PTM wrote the manuscript. All authors reviewed the final manuscript and gave approval for publication.

Ethical statement

The animals are kept at the Fjord & Belt Centre, Kerteminde, Denmark, under permit numbers SN 343/FY-0014 and 1996-3446-0021 from the Danish Nature Agency under the Ministry of Environment and Food of Denmark.

Acknowledgements

Thanks to A. Bøttcher, P. M. Sørensen, J. Kaczmarek and M. Wahlberg for help with the experimental work, N. U. Svane for building the metal frame and target spheres, and M. Johnson for developing the tags and accompanying DTAG toolbox for analysis. Thanks to Laia Rojano-Doñate for providing statistical advice. A special thanks to trainers and staff at the Fjord & Belt Centre, Kerteminde: Josefin Larsson, Fredrik Johansson, Mathilde Kjølby and Jakob Højer Kristensen. This work was funded by FNU and Carlsberg Semper Ardens grants to PTM.

References

Aguilar Soto, N., Johnson, M., Madsen, P. T., Tyack, P. L., Bocconcelli, A. and Borsani, J. F. (2006). "Does intense ship noise disrupt foraging in deep-diving Cuvier's beaked whales (*Ziphius Cavirostris*)?," Mar. Mamm. Sci., 22, 690-699. doi: 10.1111/j.1748-7692.2006.00044.x

Arranz, P., Aguilar de Soto, N., Madsen, P. T., Brito, A., Bordes, F. and Johnson, M. P. (2011). "Following a foraging fish-finder: diel habitat use of Blainville's beaked whales revealed by echolocation," PLoS ONE 6(12): e28353. doi: 10.1371/journal.pone.0028353.

Arveson, P. T., and Vendittis, D. J. (2000). "Radiated noise characteristics of a modern cargo ship," J. Acoust. Soc. Am., 107, 118–129.

Au, W. W. L., and Moore, P. W. B. (1984). "Receiving beam patterns and directivity indicies of the Atlantic bottlenose dolphin (Tursiops truncatus)," J. Acoust. Soc. Am., 75, 255–262.

Au, W. W. L., Carder, D. A., Penner, R. H., and Scronce, B. L. (1985). "Demonstration of adaptation in beluga whale echolocation signals," J. Acoust. Soc. Am., 77, 726–730. doi:10.1121/1.392341

Au, W. W. L., Moore, P. W. B., and Pawloski, D. A. (1988). "Detection of complex echoes in noise by an echolocating dolphin," J. Acoust. Soc. Am., 83, 662–668. doi:10.1121/1.396161

Au, W. W. L., and Moore, P. W. B. (1990). "Critical ratio and critical bandwidth for the Atlantic bottlenose dolphin," J. Acoust. Soc. Am., 88, 1635–1638. doi:10.1121/1.400323

Au, W. W. L., Kastelein, R. A., Rippe, T., and Schooneman, N. M. (1999). "Transmission beam pattern and echolocation signals of a harbor porpoise (Phocoena phocoena)," J. Acoust. Soc. Am., 106, 3699–3705. doi:10.1121/1.428221

Au, W. W. L., Branstetter, B. K., Benoit-Bird, K. J., and Kastelein, R. A. (2009). "Acoustic basis for fish prey discrimination by echolocating dolphins and porpoises," J. Acoust. Soc. Am., 126, 460–467. doi:10.1121/1.3147497

Bates, D., Mächler, M., Bolker, B., and Walker, S. (2015). "Fitting linear mixed-effects models using lme4," J. Stat. Software. 67(1): 1-48. doi: 10.18637/jss.v067.i01

Branstetter, B. K., Trickey, J. S., Bakhtiari, K., Black, A., Aihara, H., and Finneran, J. J. (2013). "Auditory masking patterns in bottlenose dolphins (*Tursiops truncatus*) with natural, anthropogenic, and synthesized noise." J. Acoust. Soc. Am., 133(3), 1811-1818. doi:10.1121/1.4789939

Brumm, H. and Slabbekoorn, H. (2005). "Acoustic Communication in Noise". Adv. Study Behav., 35, 151-209.

Brumm, H., and Todt, D. (2002). "Noise-dependent song amplitude regulation in a territorial songbird," Anim. Behav., 63, 891–897. doi:10.1006/anbe.2001.1968

Clark, C. W., Ellison, W. T., Southall, B. L., Hatch, L., Parijs, S. M. Van, Frankel, A., and Ponirakis, D. (2009). "Acoustic masking in marine ecosystems: intuitions, analysis, and implication," Mar. Ecol. Prog. Ser., 395, 201–222. doi:10.3354/meps08402

Erbe, C., Williams, R., Sandilands, D., and Ashe, E. (2014). "Identifying Modeled Ship Noise Hotspots for Marine Mammals of Canada's Pacific Region," PLoS ONE 9(3), 1–10. doi:10.1371/journal.pone.0089820

Erbe, C., Reichmuth, C., Cunningham, K., Lucke, K., and Dooling, R. (2015). "Communication masking in marine mammals: A review and research strategy," Mar. Pollut. Bull., 103, 15–38. doi:10.1016/j.marpolbul.2015.12.007

Gellermann, L. W. (1933). "Chance orders of alternating stimuli in visual discrimination experiments," Pedagog. Semin. J. Genet. Psychol., 42, 206–208.

Hermannsen, L., Beedholm, K., Tougaard, J., and Madsen, P. T. (2014). "High-frequency components of ship noise in shallow water with a discussion of implications for harbor porpoises (*Phocoena phocoena*)," J. Acoust. Soc. Am., 136, 1640–1653. doi:10.1121/1.4893908

Hermannsen, L., Mikkelsen, L., Tougaard, J., Beedholm, K., Johnson, M., and Madsen, P. T. (2019). "Recreational vessels without Automatic Identification System (AIS) dominate anthropogenic noise contributions to a shallow water soundscape," Sci. Rep., 9(1), 1-10. doi: 10.1038/s41598-019-51222-9

Hildebrand, J. A. (2009). "Anthropogenic and natural sources of ambient noise in the ocean," Mar. Ecol. Prog. Ser., 395, 5-20. doi:10.3354/meps08353.

Jensen, F. H., Bejder, L., Wahlberg, M., Aguilar Soto, N., Johnson, M., and Madsen, P. T. (2009). "Vessel

noise effects on delphinid communication," Mar. Ecol. Prog. Ser., 395, 161–175. doi:10.3354/meps08204

Jensen, F. H., Johnson, M., Ladegaard, M., Wisniewska, D., and Madsen, P. T. (2018). "Narrow acoustic field of view drives frequency scaling in toothed whale biosonar," Curr. Biol., 28, 1-8. doi: 10.1016/j.cub.2018.10.037

Johnson, M. P., and Tyack, P. L. (2003). "A digital acoustic recording tag for measuring the response of wild marine mammals to sound," IEEE J. Ocean. Eng., 28, 3–12. doi:10.1109/JOE.2002.808212

Johnson, M., Madsen, P. T., Zimmer, W. M., De Soto, N. A., and Tyack, P. L. (2004). "Beaked whales echolocate on prey," Proc. R. Soc. Lond., Ser. B: Biol. Sci. 271, S383-S386.

Kastelein, R. A., Bunskoek, P., Hagedoorn, M., Au, W. W. L., and de Haan, D. (2002). "Audiogram of a harbor porpoise (*Phocoena phocoena*) measured with narrow-band frequency-modulated signals," J. Acoust. Soc. Am., 112, 334–344.

Kastelein, R. A., Janssen, M., Verboom, W. C., and Haan, D. De (2005). "Receiving beam patterns in the horizontal plane of a harbor porpoise (*Phocoena phocoena*)," J. Acoust. Soc. Am., 118(2), 1172-1179. doi: 10.1121/1.1945565. doi:10.1121/1.1945565

Kastelein, R. A., Wensveen, P. J., Hoek, L., Au, W. W. L., Terhune, J. M., and de Jong, C. A. F. (2009). "Critical ratios in harbor porpoises (*Phocoena phocoena*) for tonal signals between 0315 and 150 kHz in random Gaussian white noise," J. Acoust. Soc. Am., 126, 1588–1597. doi:10.1121/1.3177274

Kastelein, R. A., Hoek, L., and Wensveen, P. J. (2010). "The effect of signal duration on the underwater detection thresholds of a harbor porpoise (*Phocoena phocoena*) for single frequency-modulated tonal signals between 0 25 and 160 kHz," J. Acoust. Soc. Am., 128(5), 3211-3222. doi: 10.1121/1.3493435. doi:10.1121/1.3493435

Koblitz, J. C., Wahlberg, M., Stilz, P., Madsen, P. T., Beedholm, K., and Schnitzler, H.-U. (2012). "Asymmetry and dynamics of a narrow sonar beam in an echolocating harbor porpoise," J. Acoust. Soc. Am., 131, 2315–2324. doi:10.1121/1.3683254

Kyhn, L. A., Tougaard, J., Beedholm, K., Jensen, F. H., Ashe, E., Williams, R., and Madsen, P. T. (2013). "Clicking in a Killer Whale Habitat : Narrow-Band , High- Frequency Biosonar Clicks of Harbour Porpoise (Phocoena phocoena) and Dall ' s Porpoise (Phocoenoides dalli)," PLoS ONE, 8(5): e637763. doi: 10.1371/journal.pone.0063763. doi:10.1371/journal.pone.0063763

Ladegaard, M., Beedholm, K., Johnson, M., Malinka C. E., and Madsen, P. T. (*In prep*.) "Sensory-motor control of output levels as a function of range and target strength in echolocating harbour porpoises."

Madsen, P. T., and Wahlberg, M. (2007). "Recording and quantification of ultrasonic echolocation clicks from free-ranging toothed whales," Deep-sea Research I 54, 1421–1444. doi:10.1016/j.dsr.2007.04.020

Mellen, R. H. (1952). "The thermal-noise limit in the detection of underwater acoustic signals," J. Acoust. Soc. Am. 24, 478-480.

Møhl, B., and Andersen, S. M. (1973). "Echolocation: high-frequency component in the click of the Harbour Porpoise (*Phocoena ph* L)," J. Acoust. Soc. Am., 54, 1368–1372. doi:10.1121/1.1914435

Møhl, B. (1981). "Masking effects of noise: their distribution in time and space," Proc. from a Work. Quest. sound from icebreaker Oper. Feb 23-24, 1981.

Møhl, B. (1988). "Target detection by echolocating bats," Anim. Sonar Process. Perform., Springer, Boston, MA, pp. 435–450.

Rojano-Doñate, L., McDonald, B. I., Wisniewska, D. M., Johnson, M., Teilmann, J., Wahlberg, M., Højer-

Kristensen, J., et al. (2018). “High field metabolic rates of wild harbour porpoises,” J. Exp. Biol., 221, jeb185827. doi:10.1242/jeb.185827

Ross, D. (1976). *Mechanics of underwater noise*, Pergamon Press, New York.

Schusterman, R. J. (1980). “Behavioral methodology in echolocation by marine mammals”. In *Animal Sonar Systems*. Editors: R. G. Busnel and J. F. Fish. Plenum Press, New York, pp. 11–41.

Williams, R., Lusseau, D. and Hammond, P. S. (2006). “Estimating relative energetic costs of human disturbance to killer whales (*Orcinus orca*),” Biol. Cons. 133, 301-311. doi: 10.1016/j.biocon.2006.06.010

Wisniewska, D. M., Johnson, M., Beedholm, K., Wahlberg, M., and Madsen, P. T. (2012). “Acoustic gaze adjustments during active target selection in echolocating porpoises,” J. Exp. Biol., 215, 4358–4373. doi:10.1242/jeb.074013

Wisniewska, D. M., Ratcliffe, J. M., Beedholm, K., Christensen, C. B., Johnson, M., Koblitz, J. C., Wahlberg, M. and Madsen, P. T. (2015). “Range-dependent flexibility in the acoustic field of view of echolocating porpoises (*Phocoena phocoena*): Short title: Flexible field of view in echolocating porpoises,” Elife, 2015, 1–29. doi:10.7554/eLife.05651

Wisniewska, D. M. M., Johnson, M., Teilmann, J., Rojano-Doñate, L., Shearer, J., Sveegaard, S., Miller, L. A. A., Siebert, U. and Madsen, P. T. (2016). “Ultra-High Foraging Rates of Harbor Porpoises Make Them Vulnerable to Anthropogenic Disturbance,” Curr. Biol., 26, 1441–1446. doi:10.1016/j.cub.2016.03.069

Supplementary Material

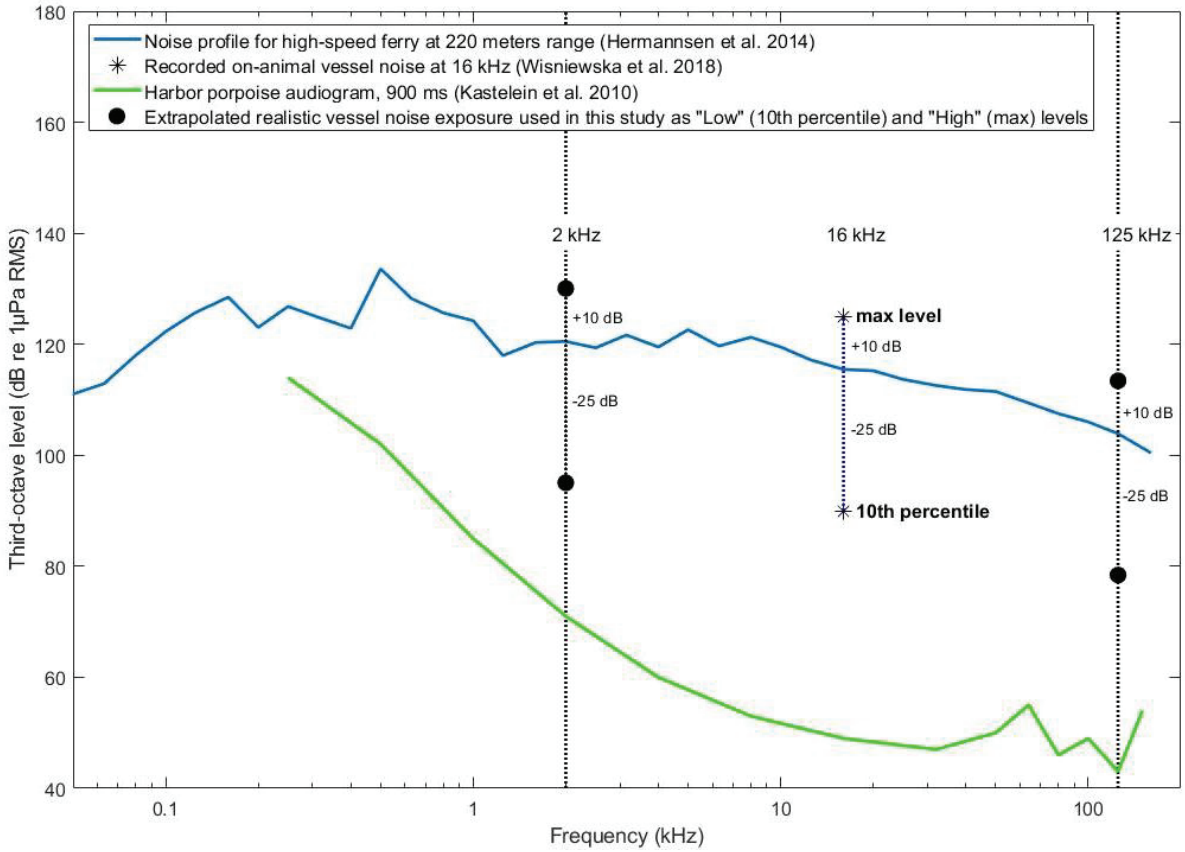

Figure S1. The method for choosing realistic vessel noise levels to transmit in the experimental setup. By use of the difference between the noise level at 16 kHz of a high-speed ferry (Hermannsen et al., 2014) and the noise levels reported from on-animal digital tags on wild porpoises (Wisniewska et al., 2018), noise exposures at 2 and 125 kHz were extrapolated using the same relationship to get realistic maximum levels and 10th percentile vessel noise.

Table S1: The five noise levels transmitted during experimental sessions, given as 25th, 50th and 75th percentiles.

Recorded noise levels	**Noise in a third-octave band centred at 2 kHz (dB re 1uPa RMS)**			**Noise in a third-octave band centred at 125 kHz (dB re 1uPa RMS)**		
	Control	*Low level*	*High level*	*Control*	*Low level**	*High level*
25th percentile	75	85	118	77	77	103
50th percentile	80	88	120	78	78	106
75th percentile	86	91	123	81	81	108

Table S2. Model results estimated with generalized linear models in *R* for three trial parameters; 1) trial duration, 2) buzz duration and 3) the number of target scans. Estimates (Est.), 95% confidence intervals (CI) and standard errors (SE) of trial parameters are shown. The baseline trial condition is the control (*i.e.* without transmission of noise) with the PVC sphere as the alternative target. Deviations from the baseline are shown for the four noise conditions and for the other alternative target 'steel'. Treatments that are significantly different from the baseline treatment are marked with blue background.

Other trial parameters rel. to control trials	Trial duration (seconds)			Buzz duration (seconds)			Target scans (count)		
Trial settings	**Estimate**	**SE**	**95% CI**	**Estimate**	**SE**	**95% CI**	**Estimate**	**SE**	**95% CI**
Intercept	10.72	0.88	[8.99, 12.45]	2.21	0.09	[2.04, 2.37]	2.68	0.07	[2.55, 2.81]
NoiseHH	1.18	0.27	[0.65, 1.71]	0.22	0.09	[0.04, 0.39]	-0.03	0.04	[-0.10, 0.05]
NoiseHL	0.05	0.29	[-0.53, 0.61]	0.10	0.10	[-0.10, 0.29]	0.04	0.04	[-0.04, 0.12]
NoiseLH	-0.45	0.29	[-1.02, 0.13]	0.19	0.10	[0.00, 0.39]	-0.06	0.04	[-0.14, 0.03]
NoiseLL	-0.23	0.29	[-0.80, 0.34]	0.02	0.10	[-0.17, 0.22]	-0.01	0.04	[-0.09, 0.08]
targetaltsteel	0.41	0.19	[0.04, 0.78]	0.19	0.06	[0.06, 0.31]	0.02	0.03	[-0.03, 0.07]

Table S3. Model results estimated with generalized linear models in *R* for porpoise click source levels in different trial settings. Estimates (Est.), 95% confidence intervals (CI) and standard errors (SE) of porpoise click SLs are shown. The baseline trial condition is the control (*i.e.* without transmission of noise) with the PVC sphere as the alternative target. Deviations from the baseline are shown for the four noise conditions and for the other alternative target 'steel', as well as the interactions of noise conditions and the steel target. Treatments that are significantly different from the baseline treatment are marked with blue background. At the bottom of the table, the effect of transmitting the noise from the side rather than in front of the study animal is estimated. All values are in dB re 1µPa pp.

Porpoise click SLs rel. to control trials	*Both animals*			*Only Freja*			*Only Sif*		
Trial settings	**Est.**	**SE**	**95% CI**	**Est.**	**SE**	**95% CI**	**Est.**	**SE**	**95% CI**
Intercept	154.6	1.4	[151.7, 157.4]	151.9	0.6	[150.7, 153.1]	157.4	0.6	[156.2, 158.6]
NoiseHH (125 kHz high)	**13.2**	0.8	[11.6, 14.8]	**16.7**	1.0	[14.8, 18.6]	**8.9**	1.0	[7.0, 10.8]
NoiseHL (125 kHz low)	0.6	0.8	[-1.0, 2.3]	0.5	1.0	[-1.4, 2.5]	0.8	1.0	[-1.1, 2.7]
NoiseLH (2 kHz low)	-0.2	0.9	[-1.9, 1.5]	-2.5	1.0	[-4.5, -0.4]	2.2	1.0	[0.2, 4.3]
NoiseLL (2 kHz high)	0.2	0.8	[-1.4, 1.9]	-0.3	1.0	[-2.3, 1.6]	0.7	1.0	[-1.2, 2.6]
Targetaltsteel (steel)	0.1	0.8	[-1.4, 1.7]	0.7	0.9	[-1.1, 2.5]	-0.5	1.0	[-2.5, 1.5]
NoiseHH:targetAltsteel	**-2.9**	1.1	[-5.1, -0.6]	**-2.8**	1.3	[-5.4, -0.1]	**-2.2**	1.4	[-4.9, 0.5]
NoiseHL:target Altsteel	-0.9	1.2	[-3.3, 1.5]	-0.7	1.5	[-3.5, 2.2]	-1.5	1.5	[-4.3, 1.4]
NoiseLH:target Altsteel	1.2	1.3	[-1.2, 3.7]	1.8	1.5	[-1.1, 4.7]	0.5	1.5	[-2.5, 3.4]
NoiseLL:target Altsteel	-1.1	1.2	[-3.5, 1.3]	-1.5	1.4	[-4.3, 1.4]	-0.4	1.5	[-3.3, 2.6]
Intercept	165.7	1.1	[163.6, 167.8]	166.3	0.7	[165, 167.8]	165.0	0.6	[163.8, 166.2]
noisePosside (noise transmission from side rel. to front)	**-2.6**	1.0	[-4.6, -0.6]	**0.6**	1.3	[-4.6, -0.6]	**-6.1**	1.2	[-8.5, -3.7]

Chapter IX.

Revisiting Automatic Gain Control

Ladegaard, M., Beedholm, K., Johnson, M., **Malinka, C. E.**, & P. T. Madsen. (2021). "Sensory-motor control of biosonar output levels as a function of target range, target strength, and masking noise in harbour porpoises (*Phocoena phocoena*)," (*Manuscript draft*).

Sensory-motor control of biosonar output levels as a function of target range, target strength, and masking noise in harbour porpoises (*Phocoena phocoena*)

Michael Ladegaard[1*], Kristian Beedholm[1], Mark Johnson[2], Chloe E. Malinka[1], and Peter Teglberg Madsen[1]

1) Zoophysiology, Department of Biology, Aarhus University, Denmark
2) Aarhus Institute of Advanced Studies, Aarhus University, Denmark
*Corresponding author: Michael Ladegaard
Email: michael.ladegaard@bio.au.dk

Keywords: Echolocation, sensory flow, gain control, Lombard effect, toothed whales

Author Contributions: PTM conceptualised the project. ML led the data collection. KB developed data collection software. MJ developed on-animal recording tag. ML, KB, and MJ developed analysis tools and methods. ML and KB analysed the data. ML and KB visualized the data. PTM secured funding for the project. ML, CEM and PTM drafted the manuscript. All authors revised and approved the manuscript before submission.

Competing Interest Statement: The authors declare no competing interests.

Abstract

For echolocating toothed whales the combination of varying target ranges and sizes means that received echo levels for a constant source level may fluctuate by more than 100 decibel. This greatly exceeds the functional dynamic range of the auditory system, impeding acute echo processing required for successful biosonar-guided prey interception. Toothed whales have been proposed to solve that problem by employing range-dependent $20\log_{10}(R)$ automatic gain control (AGC) on both the transmitting and receiving-side, apparently to stabilize perceived echo levels, but the sensory motor drivers for AGC are not understood. To investigate drivers of transmitting-side AGC, we trained two harbour porpoises to actively intercept targets of different sizes and the same target in different noise levels to test the hypotheses that i) porpoises employ closed-loop vocal motor control where click outputs are adjusted to stabilize perceived echo levels from the target, and that ii) porpoise defend a certain echo-to-noise ratio when masked. We show that SLs are reduced with range in a manner that is independent of target size, and that porpoises therefore do not seek to stabilize echo levels in the auditory system. We demonstrate that porpoises exposed to masking noise employ a Lombard response of ~0.4 dB increase in output per 1 dB noise increase to render positive echo-to-noise ratios. We conclude that output level adjustments in the porpoise biosonar system are adjusted to target range and noise levels in order to reduce echo level fluctuations to a functional dynamic range that allows for extraction of information on size of prey targets.

Introduction

Echolocating toothed whales probe their environment actively with powerful clicks and perform auditory processing of weak echoes returning milliseconds later to locate, approach and capture mobile small prey under conditions of poor lighting (Au, 1993). Inherently, echolocating whales only receive information when they emit sound, meaning that they control the information flow by the rate, type and direction of the sounds they produce as well as by adjusting the sensitivity of their hearing. These parameters directly influence the temporal resolution and spatial extent of their acoustic field of view, enabling dynamic control of attention in response to environmental complexity and behavioural objectives (Wisniewska et al., 2016). Extraction of such complex information from echo cues is challenged by a high transmission loss, and that small prey targets with poor backscattering properties must be detected and tracked in a constantly changing actively generated auditory scene as the echolocating whale swims through and ensonifies heterogeneous underwater habitats with fluctuating noise levels. Because toothed whales can echolocate prey targets over tens to hundreds of meters (Au et al., 1974; Madsen et al., 2007) and yet end up with very short target ranges for bio-sonar guided capture of their food, the returning echo levels may, for the same source level, vary by more than a 100 dB depending on the range and the target strength of the ensonified prey (Supin and Nachtigall, 2013). Such fluctuations in echo level may exceed the functional dynamic range of the auditory system, calling for mechanisms to reduce such fluctuations in sensory input (Supin et al., 2010).

In human-made sonars the problem of a limited dynamic range is solved by employing a time-varying gain control on the receiving-side in which the receiving gain is increased as a function of temporal delay after pulse emission. Depending on whether targets are point-targets or distributed targets, the resulting automatic gain control (AGC) may then either compensate by $40\log_{10}(R)$ or $20\log_{10}(R)$ over the range, R, to the target (MacLennan, 1986; Urick, 1983). Similar mechanisms have been suggested for both echolocating bats and toothed whales that not only seem to adjust on the receiving-side but also on the transmitting-side of their biosonar systems. Bats employ receiving-side AGC (Kick and Simmons, 1984; Suga and Jen, 1975) via a stapedial reflex (Henson, 1965) and more central mechanisms to render either partial (Hartley, 1992) or full compensation for the transmission loss(Simmons et al., 1992). On the transmitting-side, the studied echolocating bat species use a 10 to $40\log_{10}(R)$ reduction in source levels (SLs) (Boonman and Jones, 2002; Hiryu et al., 2007; Stidsholt et al., 2020; Stidsholt et al., 2021) that in concert with the receiving-side AGC serve to stabilize perceived echo levels in a much smaller dynamic range presumably facilitating high fidelity auditory processing (Moss and Schnitzler, 1995; Neuweiler, 1990; Stidsholt et al., 2020; Stidsholt et al., 2021) perhaps via cortical auditory neurons that are tuned to target distance and optimized for managing echo-level compensation (Macías et al., 2016).

The last decades of research have revealed that toothed whales employ different mechanisms to seemingly achieve the same effect of stabilizing perceived echo levels when echolocating. On the receiving-side, they employ a $20\log_{10}(R)$ AGC, not via a stapedial reflex (Schrøder et al., 2017), but via forward masking evoked by the loud outgoing clicks (Finneran et al., 2013;

Finneran et al., 2016; Supin and Nachtigall, 2013) that may be augmented by efferent auditory feedback under cognitive control (Supin and Nachtigall, 2013). This improvement in hearing sensitivity takes place over the first 30 ms after click emission, corresponding to a target range of some 20 meters in water. After this, the hearing threshold seems to be stable in porpoises (Linnenschmidt et al., 2012a), and in delphinids, it seems to decrease at a slower rate out to a range of some 80 meters (Finneran et al., 2013). The concept of transmitting-side AGC was first reported by Rasmussen et al. (Rasmussen et al., 2002) and has since been elaborated on by Au and Benoit-Bird (2003)(Au and Benoit-Bird, 2003)(Au and Benoit-Bird, 2003)(Au and Benoit-Bird, 2003)(Au and Benoit-Bird, 2003)(Au and Benoit-Bird, 2003)(Au and Benoit-Bird, 2003)(Au and Benoit-Bird, 2003), where they reported that several toothed whales in the wild adjust their biosonar SLs in a $20\log_{10}(R)$ fashion to hydrophone arrays. Such transmitting-side AGC has since been reported by a large number of field studies (see Fenton et al. (Fenton et al., 2014) for a review) suggesting that range-dependent adjustments in output levels is common at least among smaller toothed whales. However, some field studies suffer from the potential problems of thresholding and clipping that both tend to bias the calculated SLs as a function of range towards a $20\log_{10}(R)$ dependence (Ladegaard et al., 2017), and it remains unclear if the animals indeed are adjusting to the hydrophone arrays or merely just happen to scan across them. Nevertheless, when accounting for such errors and potential confounds, both recent field and lab studies suggest that smaller toothed whales rapidly adjust their biosonar outputs to the actual or expected echo delays to form a transmitting-side AGC (Finneran et al., 2013; Jensen et al., 2009; Kloepper et al., 2014; Ladegaard et al., 2015; Linnenschmidt et al., 2012b; Wisniewska et al., 2012).

The current understanding therefore is that echolocating toothed whales, like bats, employ a combination of receiving- and transmitting-side AGC that serves to stabilize perceived echo levels by each providing around 6 dB reduction per distance halved (Supin and Nachtigall, 2013). At first glance, this dual AGC model is attractive in that it ensures the maximum number of recruitable auditory neurons to be available for echo processing, irrespective of target range, allowing the whale to extract the greatest amount of possible information concerning target properties. Such closed-loop feedback where outputs are constantly adjusted according to each incoming echo level is difficult to reconcile with the pneumatic capacitor model, which proposes that SL changes are due to changes in interclick interval (ICI) adjusted to target range (Au and Benoit-Bird, 2003; Beedholm and Miller, 2007). Under this theory, adjustments in ICI to the two-way travel time to the target of interest not only drives SL and thereby the transmitting-side AGC, but also the degree of forward masking and hence the receiving-side AGC; under this theory gain adjustments are driven only by echo delays and not by echo levels. If so, this would result in perceived echo levels that are indeed stable over the ranges where AGC takes place, but only for objects of the same target strength (TS). Recent data suggest that echolocating dolphins have cognitive control over SL in anticipation of target range (Kloepper et al., 2014), but as the ICI is also adjusted to the anticipated range, the SL control could again just be a passive consequence of ICI choice. Thus there is ambiguity in the underlying mechanism for SL control that raises questions regarding the objective and function of this control.

Echolocating toothed whales ensonify a large number of targets that may vary in TS by several orders of magnitude. If their AGC is only driven by echo delay, the perceived echo levels will not be constant but rather be offset by the difference in TS of the targets of interest and will thereby vary by orders of magnitude. Alternatively, toothed whales may be hypothesized to stabilize perceived echo levels completely by adjusting both their hearing sensitivity and SLs not only to echo delays, but also to echo levels in what may be called closed-loop vocal motor control. However, the complexity of such echo stabilization may further be compounded by fluctuating noise levels that may give rise to an objective of defending or stabilizing the echo-to-noise ratio, rather than adjusting SL to render stable echo levels. These adjustment scenarios have not been addressed experimentally, and it remains to be tested how and to what cues echolocating toothed whales adjust their output levels.

In an attempt to do that and to understand the drivers of SL adjustment in echolocating toothed whales, we here designed an experiment using two blindfolded harbour porpoises trained to actively approach targets of different sizes while echolocating either in a background of low ambient noise or in different levels of high frequency masking noise. Specifically we sought to test the hypotheses that they: i) employ closed-loop vocal motor control where click outputs are adjusted to the level and delay of preceding target echoes, and ii) defend an echo-to-noise ratio above a certain threshold when masked by using higher SL in noise for the same range and target size.

Results

The porpoises Freja and Sif each completed 185 and 170 target approaches, respectively. In these trials, a total of 87,926 clicks were produced during approaches up until the buzz phase (defined by ICIs <10 ms) and 46,451 of those approach clicks were produced at target ranges exceeding 1 m. From those clicks, a total of 2,290 on-axis clicks were selected with a mean±SD of 6.5±1.9 on-axis clicks selected per trial. The number of on-axis clicks for each porpoise, target size and noise treatment are listed in Table 1. An example of the on-animal and on-target recordings obtained during a target approach are shown in Figure 1.

SL adjustments to range and target size

The biosonar adjustments of SL to target range for different target sizes show that adjustments are highly similar between the small and medium targets (Figure 2A-C). The GLMM comparison (results not shown) indicated that the best model for describing the SL adjustments included the fixed effects of $\log_{10}(R)$, target size, and their interaction (Suppl. Table 1, Suppl. Info can be accessed here: http://www.marinebioacoustics.com/sharing/Ladegaard_et_al_Porpoise_Biosonar_Suppl_Info.zip). The model showed that the SL at the intercept (i.e. 1 m target range) was 164 dB re µPa (pp) for the medium target and that there was no significant difference between the intercepts for the medium and small targets. The porpoises used slightly lower SLs on average when approaching the large target, whereby the model found a 4 dB lower intercept than for the medium target. The range-dependent SL adjustments to the medium target followed $11\log_{10}(R)$, and again there was no significant difference between the adjustments

to the medium and small targets. For the large target, the range-dependent adjustment had a slope of $16\log_{10}(R)$, which was significantly different from the adjustment to the medium target (**Error! Reference source not found.** Table 1).

EL adjustments to range and target size

The changes of EL with target range for different target sizes show that adjustments are highly similar between the small and medium targets (Figure 2D-F). For allowing comparison of echo levels measured either as EFD or pp, we computed the median difference which was found to be 54 dB (1 dB IQR). Using this conversion factor, the ABR threshold was estimated as 50 dB re $\mu Pa^2 \cdot s$ (EFD) from a mean reported ABR threshold of 104 dB re µPa (pp) (Smith et al. in review). The GLMM comparison (results not shown) indicated that the best model for describing the SL adjustments included the fixed effects of $\log_{10}(R)$, target size, and their interaction (**Error! Reference source not found.** Table 2). The model showed that the EL at the intercept was 76 dB re $\mu Pa^2 \cdot s$ (EFD) for the medium target. There were significant differences between intercepts for the medium and the other target sizes with the intercept being 67 dB re $\mu Pa^2 \cdot s$ (EFD) for the small target and 79 dB re $\mu Pa^2 \cdot s$ (EFD) for the large target. The ELs changed in a range-dependent manner following $-28\log_{10}(R)$ for the medium target, and this was not significantly different compared to the adjustments to the small target. For the large target, the range-dependent adjustments were significantly different and followed $-23\log_{10}(R)$ (**Error! Reference source not found.** Table 2). Because the EL estimates are based on the SLs, the relative differences between the range-dependent adjustments are likely to be similar for the SL and EL models.

SL adjustments to range and masking noise

The biosonar adjustments of SL to target range for the medium target in different noise conditions show an overall increase in biosonar SL with increasing noise (Figure 3A-C). The GLMM comparison (results not shown) indicated that the best model for describing the SL adjustments included the fixed effects of $\log_{10}(R)$ and noise level without an interaction term (**Error! Reference source not found.** Table 3), i.e. the $\log_{10}(R)$ adjustments were not significantly different between noise treatments. This model had an intercept at 168 dB re µPa (pp) for the approaches with medium noise. This intercept was significantly different from the low and high noise treatments where intercepts differed by -4 and 7 dB, respectively. The porpoises used an average range-dependent SL adjustment of $11\log_{10}(R)$ during noise trials.

EL adjustments to range and masking noise

The EL increased considerably for increasing masking noise as a result of the higher SLs used by the porpoises (Figure 3D-F). The GLMM comparison (results not shown) indicated that the best model for describing the EL adjustments included the fixed effects of $\log_{10}(R)$ and noise level without an interaction term (**Error! Reference source not found.** Table 4), i.e. the $\log_{10}(R)$ adjustments were not significantly different between noise treatments. For medium noise treatments, the intercept was 81 dB re $\mu Pa^2 \cdot s$ (EFD). For low and high noise, the

intercepts differed by -5 and 7 dB, respectively, which are similar differences as for the intercepts in the SL model. The range-dependent EL changes followed -29$\log_{10}$(R).

ENR adjustments to range and masking noise

ENR estimates were only computed for the three noise treatments (Figure 4), as the background noise measured during no-noise trials was very similar (~4 dB higher) compared to the DTAG-3's self-noise, strongly implying that we could not reliably measure ambient noise at 125 kHz. The best GLMM model included the fixed effects of noise treatment and $\log_{10}$(R) including their interaction (**Error! Reference source not found.** Table 5). This model had an intercept for the trials with medium masking noise (SL of 117 dB re µPa, RMS) of 19 dB. This was significantly different from the ENR intercepts for low and high masking noise, which differed by 2.9 and -3.6 dB from the medium noise intercept, respectively. The range-dependent ENR adjustments followed -23$\log_{10}$(R) for the medium masking noise treatment, and this was not significantly different from other noise treatments.

ICI adjustments to range and target size

The ICI adjustments were relatively similar regardless of target size (Figure 5A-C). The best GLMM model included the fixed effects for target size and $\log_{10}$(R) without their interaction (**Error! Reference source not found.** Table 6). The intercept (i.e. the ICI at 1 m target range) was an ICI of 26 ms for the medium target and this was not significantly different for the small target, but differed from the 22 ms intercept estimate for the large target. The range-dependent ICI adjustments followed 38$\log_{10}$(R) (slope unit in ms).

ICI adjustments to range and masking noise

The ICI adjustments were also relatively similar for the different noise treatments, except that Sif seemed to click slightly faster during high masking noise (Figure 5D-F). The best GLMM model included the fixed effects for target size and $\log_{10}$(R) including an interaction term (**Error! Reference source not found.** Table 7). The intercept was 24 ms for the medium noise treatment and 20 ms for low noise, which was a significant difference, whereas the high noise intercept of 21 ms was not significantly different from the medium noise intercept at the 5% level. The range-dependent ICI adjustments followed 34$\log_{10}$(R) (slope unit in ms) for the medium noise treatment, which differed by 7 and 1 relative to the $\log_{10}$(R) adjustments for low and high noise, respectively, but only for low noise was the difference significant.

SL adjustments in relation to ICI and masking noise

The relationship between SL and ICI was tested for different masking noise levels, including controls with no masking noise, to address the hypothesis that biosonar SL is driven by ICI (Figure 6). The best GLMM model included the fixed effects for noise treatment and $\log_{10}$(R) including an interaction term (**Error! Reference source not found.** Table 8). The intercept was 146 dB re µPa (pp) for the controls (i.e. approaches to the medium target without noise transmission), and the intercepts for low and medium noise treatments were not significantly different from this. The intercept for the high noise treatment was 18 dB higher compared to

the control. The model found a slope of $16\log_{10}$(ICI) for the control approaches which was not significantly different for the slopes during the three masking noise treatments.

Discussion

Here we sought to investigate the drivers of range-dependent adjustments in SL for echolocating porpoises by testing the hypothesis that transmitting-side AGC in concert with receiving-side AGC serve to provide a constant perceived echo level independent of range and targets (sensu (Kloepper et al., 2014; Supin and Nachtigall, 2013)). Specifically we asked whether transmitting-side AGC is determined passively by ICI adjustments to range or is adjusted actively to the received echo levels. Previous experiments both on stationed porpoises (Linnenschmidt et al., 2012b) and dolphins (Finneran et al., 2013; Kloepper et al., 2014) have shown that they reduce their SL in an approximate $20\log_{10}$(R) manner when a same sized target is moved between different ranges, and that the animals adjust their SL in anticipation of a particular range, suggesting some form of cognitive control (Kloepper et al., 2014). While these experiments are highly instructive due to the degree of experimental control, they suffer from the problem that they do not address the situation faced by toothed whales echolocating in the context in which their biosonars evolved; to guide motor behaviours during active target interception. That problem was somewhat handled by Wisniewska et al. (2012) who studied echolocation outputs of porpoises during active two-forced choice tasks. SLs collected as a function of range over 5 m target approaches also rendered a transmitting-side AGC close to $20\log_{10}$(R) (Wisniewska et al., 2012).

None of these studies suffer from the many pitfalls that may erroneously lead to conclusions of $20\log_{10}$(R) transmitting-side AGC in field studies (see (Ladegaard et al., 2017)); porpoises and dolphins do reduce SL with range to the target. However, currently it is unknown if the observed transmitting-side AGC is a passive consequence of ICIs adjusted to reducing echo delays with range, or if it in fact actually serves to stabilize echo levels by also adjusting the SL to the returning echo levels. Here we conducted an experiment to alleviate that pertinent data gap by having two echolocating porpoises actively approach different sized targets with targets strength differing by up to 16 dB over the course of an approach range of 13 m which renders two-way transmission loss dynamics of ~44 dB from 13 to 1m. We confirm that porpoises do employ a transmitting-side time-varying gain control by reducing their SL with range which on average follows 11 to $16\log_{10}$(R) (Figure 2A-C), giving rise to a growth in received echo levels for decreasing ranges by -23 to $-28\log_{10}$(R) on average (Figure 2D-F). Thus, with a $20\log_{10}$(R) receiving-side AGC (Linnenschmidt et al., 2012a), the perceived echo levels will for the same target not be stable but change by an average 3 to 9 dB over the course of a 13 meter approach.

If the porpoises, as hypothesized in a closed-loop fashion, seek to stabilize perceived echo levels they must not only employ a combined $40\log_{10}$(R) AGC on the receiving- and transmitting-sides, but also modulate either or both according to the TS of the target of interest. Given that hearing AGC seems to be mostly explained by forward masking (Finneran

et al., 2013; Supin and Nachtigall, 2013) and therefore is related to both the echo delay to and the SL of the outgoing click, we posit that the stabilization of perceived echo level should mainly manifest itself in the SL distribution according to changes in TS over the 16 dB range used here. We find that the SL distributions are quite similar for the different sized targets (Figure 2) and only for the large 18 cm target do the porpoises significantly change SLs by lowering outputs. The statistical EL model shows that intercepts, at 1 m range, for the small and large targets differ by -9 and 3 dB relative to the intercept for the medium target, and the differences for median ELs of the EL distributions for each target size show similar differences of -11 and 3 dB, respectively. This is close to the TS differences of -10 and 6 dB, which means that that the received echo level distributions are offset closely by the difference in TS of the ensonified targets. Accordingly, we reject the closed-loop vocal motor hypothesis that proposes that echolocating porpoises adjust their SLs to the TS of the target they ensonify to keep perceived echo levels constant. For the same range, an echolocating porpoise will thus get a louder echo from a larger target than a smaller target, perhaps offering potential cues for target size estimation.

The full dynamic range of the received ELs over the approaches to all three targets span a 40 dB range (90% of the data) from 35 to 75 dB re 1μPa^2·s. While hearing-side AGC may accommodate up to 20 dB of that for the ranges considered here (Linnenschmidt et al., 2012a), it still means that perceived echo levels varied by at least two orders of magnitude in the present experiment. This effect is then further compounded by the fact that the animals very likely also use the echo information from some of the many clicks pointed slightly off-axis (Beedholm et al., 2021), resulting in lower ELs for the same range and TS, and hence more scatter in perceived echo levels. We therefore conclude that transmission and hearing side AGC mechanisms do not in combination achieve a stabilization of perceived echo levels (Supin and Nachtigall, 2013), but they do bring them into a dynamic range of around 20 dB that likely facilitates high fidelity auditory processing in the auditory system (Moss and Schnitzler, 1995; Neuweiler, 1990) where we speculate that a large number of auditory neurons are dedicated to allow for encoding of spectral and level changes in echoes from ensonified targets. We note that the dynamic range of received ELs starts right around the likely detection threshold for echolocating porpoises (if they have echo detection thresholds comparable to bottlenose dolphins), and extends upwards by 40 dB. As porpoises exposed to high masking noise (Figure 3C) can produce SLs 10 to 15 dB louder than the maximum levels around 185 dB re 1μPa (pp) in the no-noise target approaches (Figure 2), and as they reduce their SLs as they approach the targets, it follows that they actively seek to produce fairly weak echoes to guide their target interception. In fact, 60% of our estimated echo levels for the small target (Figure 2D) are below the hearing thresholds inferred from click-based ABR experiments (figure 2, Schmidt et al., in review) and do not stay consistently above this threshold until target range is less than 4 m. This shows that ABR-based inferences about hearing AGC are made from the very high end of the echo level distribution employed by echolocating toothed whales, raising the question about whether a similar receiving-side AGC is at play at low echo levels? Our experiments also highlight why experiments on ABR responses to target echoes must invariably happen with high TS of phantom or real targets (Linnenschmidt et al., 2012a; Mulsow et al., 2018) as smaller targets do not render useful

ABR responses despite that we in the present study show that toothed whales may routinely use such ELs

In our experiment, the blindfolded porpoises were very familiar with the approach to the targets that were always placed in the same position with respect to the starting point of the porpoises. It is therefore likely that the transmitting-side AGC observed here is the result of the porpoises knowing the task and as proposed by Kloepper et al. (2014), they may execute a vocal-motor program in accordance with such spatial memory and/or focal expectancy (Vandenberghe et al., 2001) and known swimming speeds. In that sense, the observed TS-independent transmitting-side AGC may be explained by a simple open-loop sensory-motor system. On the other hand, the porpoises do scan other parts of the pool while approaching the targets and yet they quickly redial their ICIs and SLs to the range in question when scanning back at the target where they update on target range. This argument is further strengthened by the observation that stationed dolphins quickly adjust their biosonar to changing target ranges (Kadane and Penner, 1983; Penner, 1988). This shows that they do employ some form of closed-loop motor-control based on the echo delay. A prevailing theory in that context is that it is only the ICIs that are adjusted to range as gauged by click-echo delays, and that the SL of echolocating toothed whales is a passive consequence of different actuation rates of a sound production system operating as a pneumatic capacitor (Au and Benoit-Bird, 2003; Beedholm and Miller, 2007). Here we find a correlation between ICI and range (Figure 5***Figure 2***) similar to those in previous studies of porpoises (DeRuiter et al., 2009; Verfuß et al., 2009; Wisniewska et al., 2012). However, the ICI variation explains some 6 to 33% of the variation in SL for the control and different noise treatments (Figure 6A-D***Figure 2***), and there is substantial scatter of up to ~30 dB in SL for the same ICI values showing that the SL is not hardwired to the actuation rate. Thus, while a pneumatic capacitor may account for some of the SL variation with range via ICI in the transmitting-side AGC of echolocating porpoises, the SLs are, *sensu* Finneran et al. (2013) for dolphins, not merely passive consequences of ICI adjustments to range as previously proposed (Au and Benoit-Bird, 2003; Beedholm and Miller, 2007).

The demonstration that echolocating porpoises actively adjust their output levels to render fairly low received levels over a 40 dB span up from their presumed detection threshold prompted us to explore the consequences of masking noise on that regulation. In low noise and clutter-free conditions, the detection threshold is limited by the auditory sensitivity of the echolocator, but when the ambient noise corrected for the receiving DI exceeds the hearing threshold, the masking noise will define the detection performance. To ensure that the porpoises were offered no spatial, spectral or temporal release from masking, we played back 80-150 kHz noise from a small transducer mounted just below our medium target with a TS of -34 dB at SLs of 107, 117, and 127 dB re μPa (RMS). The advantage of that setup is that the noise will always be on the same range axis as the target echo, whereas the potential disadvantage of a co-located target and noise source is that the animals may use the noise as a homing cue to the target. We excluded that possibility by running control trials where the noise source was moved away from the target, and observed that the porpoises invariably

went for the sphere and always employed an approach phase and a terminal buzz in their echolocation no matter the noise treatment or the spatial relationship between the noise source and the target.

Even the lowest noise source level of 107 dB re 1µPa (RMS) did at 13 meters give rise to a noise level (~85 dB re 1µPa, RMS) at the porpoises in the beginning of the trial that is well above the very low ambient noise levels in the echolocation band around 125 kHz, and also some 40 dB above their hearing threshold at that frequency (Kastelein et al., 2002). Thus, the porpoises were masked to various degrees during all three noise treatments, leading us to hypothesize that they i) would actively shift up their EL distribution by using higher SLs for the same ranges compared to the control trials, and ii) dispense with their output AGC to improve ENR as they swam closer to the noise source and the target. In support of our first hypothesis, we find that both porpoises produced higher source levels in the noise trials and that the SL adjustments were higher for the higher noise treatments. In the high noise trials we recorded maximum SLs close to 200 dB re 1µPa (pp), which is 10-20 dB higher than the maximum SLs used by these porpoises in no-noise tasks of target interception (Ladegaard and Madsen, 2019), and on par with the highest SLs ever reported for wild porpoises (Villadsgaard et al., 2007). There was no significant difference between the SL adjustments in the low noise trials (Figure 3A) and the control trials (Figure 2B), implying that the porpoises could solve the target interception task in low noise even at broad-band ENRs close to zero out at 10 meters, and that they did not do much to defend their ENRs from the control trials in the low noise treatment. The medium noise treatment caused an increase in the median SL of 4 dB compared to the low noise trials, whereas the high noise treatment induced a median SL increase of 10 dB compared to the low noise trials to render positive ENRs between 0 and 30 dB for a sufficient number of on-axis clicks to solve the task. This 10 dB median increase in SL over the 20 dB increase in noise level suggests a Lombard response of 0.5 dB/1dB noise (or 0.3 dB/1 dB noise if estimated using the 6.5 dB intercept difference from the GLMM), which is comparable to the typical mammalian Lombard response, but higher than seen for echolocating bats of 0.15 dB/dB in a very similar experiment (Foskolos et al., *in prep.*). Thus, higher levels of masking noise induce a strong Lombard response in echolocating porpoises to partly off-set the compromised ENR. This suggests that echolocating porpoises may be able to somewhat mitigate masking effects from for example fast moving vessels (Hermannsen et al., 2014) on their biosonar based target interception. However, observations of trained porpoises show that masking noise can decrease target discrimination performance (**Chapter VIII**, Hermannsen et al., *in prep.*) and wild porpoises exposed to vessel noise may temporarily abort normal foraging behaviour (Wisniewska et al., 2018). A similar response has been reported for a beluga whale that was moved to a noisier environment and there produced higher source levels during a long range target detection task (Au et al., 1985), showing that echolocating toothed whales can evoke a Lombard response to partially offset masking noise in their echolocation bands.

By playing the noise from the target, the approaching porpoises faced a situation where the noise level would double for every halving of the range to the sphere. With a $20\log_{10}(R)$ AGC on their SLs, they would thus maintain the same ENR, whereas a complete dispense of SL

reduction with range would give rise to a doubling in ENR per halving in range. Thus, we hypothesized that the porpoises would seek to improve their ENR during noise trials by relaxing their transmitting-side AGC. During control trials with the medium sized target, we found an $11\log_{10}(R)$ AGC that in turn lead to increases in ELs for decreasing target ranges by $-28\log_{10}(R)$. To our surprise, we reject our second hypothesis of AGC omission in noise trials by finding that the porpoises used range adjustments in SL during the noise trials very similar to the control trials, so that the ENRs changed by $23\log_{10}(R)$ on average, which is not as much as they could have increased it by if the AGC had been fully dispensed with. We find that the porpoises, in keeping with a range of previous studies on the same individuals (Ladegaard and Madsen, 2019; Verfuß et al., 2009; Wisniewska et al., 2012), clicked faster the closer they got to the target in no noise trials, but that they maintained very similar ICI adjustments with range across the different noise trials. From the pneumatic capacitor model of AGC (Au and Benoit-Bird, 2003), such faster clicking would be predicted to be the driver of lower source levels closer to the target. However, our data are not consistent with that hypothesis: we show that the porpoises can produce higher SLs for the same ICIs in noise (Figure 6), demonstrating that SL is not just a passive mechanistic consequence of faster rates of pressure release in their pneumatic sound production system. It therefore seems that both ICI and SL are adjusted with range, but the range-dependent SL adjustments might not be a consequence of the range-dependent ICI adjustments despite that SL adjustments have somewhat similar slopes whether modelled as $\log_{10}(R)$ or $\log_{10}(ICI)$. Similar observations have been made for bottlenose dolphins producing click packets, where short click bursts are produced with short ICIs and high SLs (Finneran, 2013; Ivanov, 2004; Ladegaard et al., 2019). Under the pneumatic capacitor scheme, it may of course be that the maximum SL possible will be affected if the ICI gets short enough, perhaps explaining why we record few SLs of more than 180 dB re 1μPa (pp) at some of the shortest ICIs around 20 ms during the approach. If that is the case, it is implied that sensory redundancy via faster sampling at close target ranges is more important for the porpoises to solve the target interception task than to get ENRs higher than around 20 dB (Figure 4). In concert with the low ELs during the small sphere trials (Figure 2D), it is clear that porpoises can operate their biosonars efficiently with echo levels very close to their ABR-inferred echo detection thresholds (Smith et al. in review), and that they, in noisy conditions, do not actively work to ensure an ENR of more than 0 to 25 dB even at short range (Figure 4) when target interception is imminent.

In conclusion, we find that echolocating porpoises do adjust their SLs to range, but that they do not adjust their SLs to the TS of their targets. We therefore conclude that receiving- and transmitting-side AGC do not render stable perceived echo levels, but rather perceived levels that are proportional to target strength for a given delay window. These findings are in line with the limited evidence available from echolocating bats suggesting that echolocating animals use AGC mechanisms to bring perceived echo levels into a dynamic range of the auditory system that allow for high fidelity echo processing (Moss and Schnitzler, 1995). The porpoises therefore do not seem to adjust their SLs in relation to target strength to keep perceived echo levels constant, but rather to compress the dynamic range of the returning echoes. ICI is tightly related to range, but is not a strong driver of SL adjustments, and we

therefore conclude that transmitting-side AGC in toothed whales is not governed by a pneumatic capacitor, but rather by a form of closed-loop sensory-motor feedback primarily based on echo delays or echo-to-noise ratios. By masking the porpoises we demonstrate that they can partially compensate for reduced ENRs by a Lombard response, and find that porpoises can solve target interception tasks in noise with very low errors rates even at ENRs close to 0 dB.

Materials and Methods

Data collection, equipment, and animals

The experiments were conducted at Fjord&Bælt, Kerteminde, Denmark, in an enclosure (approximately 34×17 m, sandy bottom, 2-3 m water depth) that offers semi-natural conditions including natural tide movements, natural temperature fluctuations, and the presence of wild fish and other marine life. Two harbour porpoises (Freja, 21 years old female, Sif, 14 years old female) were trained to approach a single target over a range of 13 meters (**Figure 1**). In the first set of experiments, the target size varied between three sizes and in a second phase, the porpoises were tasked with approaching only the medium-sized target in the presence of masking noise. During each trial, the animals were bridged with a whistle when they touched the target with their rostrum and then received a fish reward after returning to the starting point. For trials with no target contact, no fish reward was given.

The porpoises wore a DTAG-3 (https://www.soundtags.org) positioned behind their blowhole to record outgoing echolocation clicks and returning echoes. They were also equipped with opaque suction cups over their eyes to prevent them from using visual cues. The targets were three aluminium spheres with diameters of 2.54, 7.62, 18.0 cm, rendering target strengths (TS_E) of -44, -34 and -28 dB, respectively. Only a single target was used in each trial. Each target was suspended from a 1 mm monofilament line, with a receiving hydrophone positioned directly above the target. For trials with masking noise, a second hydrophone was attached directly below the medium-sized target with the hydrophone cable running through a small vertical hole in the target. These hydrophones were custom-built from small cylindrical piezo-ceramic elements having a calibrated receiving sensitivity of -211 (±2dB) dB re 1V/µPa and a calibrated transmitting sensitivity of 130 dB (±4dB) re µPa/1V in the frequency range from 100 to 150 kHz. Masking noise was transmitted at fixed SL in each masking trial with SL options being 107, 117, and 127 dB re µPa (RMS) and spectrally consisting of white noise across the range of 80 to 150 kHz. The analog signal from the receiving hydrophone was amplified by 40 dB (or by 30 dB in some trials with high masking noise) and band-pass filtered between 1 and 180 kHz (1 and 4 pole respectively) before being digitized at 500 kHz, 16 bit, using one ADC channel of an National Instruments (NI, Houston, Texas, USA) multifunction device, (NI USB-6356) and custom LabVIEW software. The clipping level of the entire recording chain was 177 (or in some cases, 187) dB re. µPa (peak). Receiving and transmitting data were stored together within the same multi-channel wav-files, along with time-stamps of the start and ending of each trial (durations of ~10 seconds each), using a battery-powered laptop. The DTAG-3 sampled stereo sound at 500 kHz, 16 bit, with a flat (±2 dB) frequency response from 0.5 to 150 kHz, and recorded

continuously for the duration of each session, which generally consisted of 5-12 trials per animal tested. The DTAG-3 clipping level (179 dB re. µPa, peak) was determined relative to a RESON TC-4034 hydrophone (Teledyne RESON, Slangerup, Denmark) in an anechoic water tank using porpoise-like clicks (130 kHz, 5-cycle transients), which were generated using a waveform generator (model 33220A, Agilent Technologies, Santa Clara, CA, USA) and transmitted from one of the custom-built hydrophones.

Click detection, recorder synchronization and target range estimation

All analysis were done in MATLAB (version 2017a or higher, MathWorks, Natick, MA, USA) using custom-written scripts. The click detection and target range estimation was performed with similar methods as (Ladegaard and Madsen, 2019; Ladegaard et al., 2019). First, clicks were detected in the DTAG-3 recordings after applying a 180 kHz high pass Butterworth filter (4-pole) to reduce the amplitude of possible clicks from non-focal animals, as on-animal click recordings contain energy at much higher frequencies than would be found in on-axis click recordings. The majority of clicks were detected in the DTAG-3 recordings using an automated click detector (detection thresholds were varied between trials depending on click amplitudes and noise), which was followed by a supervised step that allowed for both the manual removal of false detections and the addition of missed clicks below the detection threshold. The supervised step involved plots of intensity, ICI and spectrograms for visual identification of click trains.

Click detection in the target recordings relied on DTAG-3 click detection times and synchronization between the recorders. Initial synchronization between the DTAG-3 and target recordings was performed by identification of specific clicks in each trial: ICIs were compared for clicks recorded in the late-approach phase immediately before the buzz, where the ICIs are generally continuously decreasing thus producing a series of unique ICIs that are easily compared between recordings of each trial. Because the buzz phase generally starts at target ranges of <1 m and because the sound speed is ~1500 m/s, this method ensured device synchronisation accuracy to within ~1 ms, which was sufficient for the subsequent analysis. Clicks were then detected in the target recordings by first extracting a time window (with a duration larger than the one-way travel time for a 13 m target range, i.e. >9 ms) in these recordings around the time of each DTAG-3 click detection. These recording snippets were then colour-coded for intensity and stacked to produce echogram-like plots, where incoming clicks recorded on the target could be seen as distinct traces with decreasing delays between the DTAG-3 and target recordings as the porpoise approached the target. The visually identified clicks were then manually selected in the plots using a supervised peak-detection tool allowing for selection of up to 200 clicks at a time and the information was saved together with information of time-of-arrival-difference (TOAD) for each click between the DTAG-3 and target. The TOAD estimates could then be converted to a range estimate using an assumed sound speed of 1,500 m/s. To smooth out occasional physically unrealistic outlier distances resulting from false detections, the range estimates were filtered using a two-stage (speed and range) Kalman filter (Kalman, 1960) followed by a Rauch smoother (Bar-Shalom et al., 2004). Given the noted visual observations that the porpoises touched the target at the end

of each trial, the range estimates were shifted slightly for each trial so that the shortest range estimate was set to exactly 0 m to match the precise timing of when the porpoise touched the target (Figure 1).

On-axis click selection

The porpoises would generally move their head to scan across the target during target approach, and thus received levels (RLs) at the target would invariably increase and decrease as the directional biosonar beam moved across the target. For most clicks, the centre of the beam would therefore be pointed more or less off-axis relative to the target and only few clicks would point directly on the target. In each of these scanning events, the click with the highest received amplitude was selected as the most likely on-axis candidate following (Kyhn et al., 2010; Kyhn et al., 2013; Wisniewska et al., 2012).

Biosonar parameter estimation

To estimate click parameters, a 100-ms time window was centred on each click detection time and extracted from the raw recordings and was then filtered using a 50 kHz Butterworth high-pass filter (4-pole). A 0.5-ms time window centred on the click detection in the filtered recordings was then used for computation of signal parameters. The signal duration was computed as the −10 dB points on either side of the peak of the amplitude envelope following (Madsen and Wahlberg, 2007). To estimate the signal-to-noise (SNR) ratio, the 0.5-ms window preceding each signal window was used for noise estimation. Each SNR was computed as the standard deviation within the signal duration window minus the standard deviation of the 0.5-ms noise window and then divided by the standard deviation of the noise window before converting this SNR to a decibel scale by taking $10\log_{10}(SNR)$.

RLs were computed as peak-to-peak (pp) level, as RMS level within the -10 dB signal duration window, and as energy flux density (EFD) within the -10 dB signal duration window(Madsen and Wahlberg, 2007). For the target recordings, apparent SLs were back-calculated from the RLs by adding geometric transmission loss (TL) assumed to be $20\log_{10}(R)$. SLs were only estimated for clicks where estimated target range exceeded 1 m, because slight errors in range estimation can have large effects on the TL estimates for short ranges. The echo level (EL) was estimated for each click as the RL on the target plus the TS_E minus a one-way TL.

For estimating echo-to-noise ratio (ENR), we first computed the received RMS level on the target (in the 50 kHz high pass filtered recordings) for a 260 µs time window centred on each click detection time to reflect the reported auditory integration time in toothed whales, as the integration time in bottlenose dolphins have been measured to be ~260 µs (Au et al., 1988; Moore et al., 1984; Vel'min and Dubrovskii, 1976). The EL was then estimated from these received RMS levels by adding TS_E and subtracting TL from target to porpoise. The noise level at the porpoise was estimated as the third octave level centred at 128 kHz measured in the 0.5 ms noise window recorded before each click on the DTAG-3, as this third octave band (ranging from 114-144 kHz) has a suitable overlap with the bandwidth of porpoise clicks.. The echo-to-noise ratio (ENR) was then estimated by subtracting NL from EL.

Statistical analysis

Only on-axis clicks were included in the statistical analysis following the assumption that these clicks would best represent any biosonar adjustments made relative to the target. To account for possible adjustment variation between the two porpoises, the biosonar adjustments were analysed using a generalized linear mixed-effects model (GLMM, MATLAB function fitglme). Model selection involved comparisons using theoretical likelihood ratio tests (5% significance level, MATLAB function compare) of increasingly complex models with the possible fixed effects being $\log_{10}(R)$, target size, and noise SL and interactions thereof. As random effects, all tested and selected models had intercepts for porpoise (Freja and Sif) as well as by-porpoise random slopes for the effect of $\log_{10}(R)$. In these models, target range was $\log_{10}$-transformed to reflect that geometric spreading loss changes logarithmically with range, therefore so might the possible biosonar adjustments, and because we wanted to compare our results with $\log_{10}(R)$ slopes from other studies. Residual plots for all selected models were visually inspected and did not reveal any obvious deviations from homoscedasticity or normality.

Acknowledgments

We thank the trainers at Fjord&Bælt for their dedicated and professional assistance during data collection. We further thank D. Wisniewska and J. Tougaard for helpful discussions. This work was funded by frame grants from the Danish National Research Foundation (http://www.dg.dk/) to PTM. MJ was supported by the Marine Alliance for Science and Technology, Scotland. The animals are maintained by Fjord&Bælt, Kerteminde, Denmark, under permit no. SN 343/FY-0014 and 1996-3446-0021 from the Danish Forest and Nature Agency, Danish Ministry of Environment.

References

Au, W. W. L. (1993). *The Sonar of Dolphins*. New York: Springer-Verlag, New York.

Au, W. W. L. and Benoit-Bird, K. J. (2003). Automatic gain control in the echolocation system of dolphins. *Nature* **423**, 861–863.

Au, W. W. L., Floyd, R. W., Penner, R. H. and Murchison, A. E. (1974). Measurement of echolocation signals of the Atlantic bottlenose dolphin, Tursiops truncatus Montagu, in open waters. *J. Acoust. Soc. Am.* **56**, 1280–1290.

Au, W. W. L., Carder, D. A., Penner, R. H. and Scronce, B. L. (1985). Demonstration of adaptation in beluga whale echolocation signals. *J. Acoust. Soc. Am.* **77**, 726–730.

Au, W. W. L., Moore, P. W. B. and Pawloski, D. A. (1988). Detection of complex echoes in noise by an echolocating dolphin. *J. Acoust. Soc. Am.* **83**, 662–668.

Au, W. W. L., Lemonds, D. W., Vlachos, S., Nachtigall, P. E. and Roitblat, H. L. (2002). Atlantic bottlenose dolphin (Tursiops truncatus) hearing threshold for brief broadband signals. *J. Comp. Psychol.* **116**, 151–157.

Bar-Shalom, Y., Li, X. R. and Kirubarajan, T. (2004). *Estimation with applications to tracking and*

navigation: theory algorithms and software. John Wiley & Sons.

Beedholm, K. and Miller, L. a. (2007). Automatic Gain Control in Harbor Porpoises (Phocoena phocoena)? Central Versus Peripheral Mechanisms. *Aquat. Mamm.* **33**, 69–75.

Beedholm, K., Malinka, C., Ladegaard, M. and Madsen, P. T. (2021). Do echolocating toothed whales direct their acoustic gaze on- or off-target in a static detection task? *J. Acoust. Soc. Am.* **149**, 581–590.

Boonman, A. and Jones, G. (2002). Intensity control during target approach in echolocating bats; stereotypical sensori-motor behaviour in Daubenton's bats, Myotis daubentonii. *J. Exp. Biol.* **205**, 2865–2874.

DeRuiter, S. L., Bahr, A., Blanchet, M.-A., Hansen, S. F., Kristensen, J. H., Madsen, P. T., Tyack, P. L. and Wahlberg, M. (2009). Acoustic behaviour of echolocating porpoises during prey capture. *J. Exp. Biol.* **212**, 3100–3107.

Fenton, B. M. B., Jensen, F. H., Kalko, E. K. V and Tyack, P. L. (2014). Sonar Signals of Bats and Toothed Whales. In *Biosonar*, pp. 11–59. Springer.

Finneran, J. J. (2013). Dolphin "packet" use during long-range echolocation tasks. *J. Acoust. Soc. Am.* **133**, 1796–1810.

Finneran, J. J., Mulsow, J. and Houser, D. S. (2013). Auditory evoked potentials in a bottlenose dolphin during moderate-range echolocation tasks. *J. Acoust. Soc. Am.* **134**, 4532–4547.

Finneran, J. J., Echon, R., Mulsow, J. and Houser, D. S. (2016). Short-term enhancement and suppression of dolphin auditory evoked responses following echolocation click emission. *J. Acoust. Soc. Am.* **140**, 296–307.

Foskolos, I., Pedersen, M.B., Beedholm, K., Uebel, A.S., Macaulay, J., Stidsholt, L., Brinkløv, S., Madsen P.T. Echolocating Daubenton's bats show high resilience to broadband, ultrasonic masking noise during active target approaches. (*In prep.*)

Hartley, D. J. (1992). Stabilization of perceived echo amplitudes in echolocating bats. I. Echo detection and automatic gain control in the big brown bat, E ptesicusfuscus, and the fishing bat, N octilioleporinus. *J. Acoust. Soc. Am.* **91**, 1120–1132.

Henson, O. W. (1965). The activity and function of the middle-ear muscles in echo-locating bats. *J. Physiol.* **180**, 871–887.

Hermannsen, L., Beedholm, K., Tougaard, J. and Madsen, P. T. (2014). High frequency components of ship noise in shallow water with a discussion of implications for harbor porpoises (Phocoena phocoena). *J. Acoust. Soc. Am.* **136**, 1640–1653.

Hiryu, S., Hagino, T., Riquimaroux, H. and Watanabe, Y. (2007). Echo-intensity compensation in echolocating bats (Pipistrellus abramus) during flight measured by a telemetry microphone. *J. Acoust. Soc. Am.* **121**, 1749–1757.

Ivanov, M. P. (2004). Dolphin's echolocation signals in a complicated acoustic environment. *Acoust. Phys.* **50**, 469–479.

Jensen, F. H., Bejder, L., Wahlberg, M. and Madsen, P. T. (2009). Biosonar adjustments to target range of echolocating bottlenose dolphins (Tursiops sp.) in the wild. *J. Exp. Biol.* **212**, 1078–1086.

Kadane, J. and Penner, R. (1983). Range ambiguity and pulse interval jitter in the bottlenose

dolphin. *J. Acoust. Soc. Am.* **74**, 1059–1061.

Kalman, R. E. (1960). A new approach to linear filtering and prediction problems. *J. Fluids Eng. Trans. ASME* **82**, 35–45.

Kastelein, R. A., Bunskoek, P., Hagedoorn, M., Au, W. W. L. and de Haan, D. (2002). Audiogram of a harbor porpoise (Phocoena phocoena) measured with narrow-band frequency-modulated signals. *J. Acoust. Soc. Am.* **112**, 334–344.

Kick, S. A. and Simmons, J. A. (1984). Automatic gain control in the bat's sonar receiver and the neuroethology of echolocation. *J. Neurosci.* **4**, 2725–2737.

Kloepper, L. N., Smith, A. B., Nachtigall, P. E., Buck, J. R., Simmons, J. A. and Pacini, A. F. (2014). Cognitive Adaptation of Sonar Gain Control in the Bottlenose Dolphin. *PLoS One* **9**, e105938.

Kyhn, L. A., Jensen, F. H., Beedholm, K., Tougaard, J., Hansen, M. and Madsen, P. T. (2010). Echolocation in sympatric Peale's dolphins (Lagenorhynchus australis) and Commerson's dolphins (Cephalorhynchus commersonii) producing narrow-band high-frequency clicks. *J. Exp. Biol.* **213**, 1940–1949.

Kyhn, L. A., Tougaard, J., Beedholm, K., Jensen, F. H., Ashe, E., Williams, R. and Madsen, P. T. (2013). Clicking in a Killer Whale Habitat: Narrow-Band, High-Frequency Biosonar Clicks of Harbour Porpoise (Phocoena phocoena) and Dall's Porpoise (Phocoenoides dalli). *PLoS One* **8**, e63763.

Ladegaard, M. and Madsen, P. T. (2019). Context-dependent biosonar adjustments during active target approaches in echolocating harbour porpoises. *J. Exp. Biol.* **222**,.

Ladegaard, M., Jensen, F. H., de Freitas, M., da Silva, V. M. F., Madsen, P. T., Ferreira da Silva, V. M. and Madsen, P. T. (2015). Amazon river dolphins (Inia geoffrensis) use a high-frequency short-range biosonar. *J. Exp. Biol.* **218**, 3091–3101.

Ladegaard, M., Jensen, F. H., Beedholm, K., da Silva, V. M. F. and Madsen, P. T. (2017). Amazon river dolphins (*Inia geoffrensis*) modify biosonar output level and directivity during prey interception in the wild. *J. Exp. Biol.* **220**, 2654–2665.

Ladegaard, M., Mulsow, J., Houser, D. S., Jensen, F. H., Johnson, M., Madsen, P. T. and Finneran, J. J. (2019). Dolphin echolocation behaviour during active long-range target approaches. *J. Exp. Biol.* **222**, jeb189217.

Linnenschmidt, M., Beedholm, K., Wahlberg, M., Hojer-Kristensen, J. and Nachtigall, P. E. (2012a). Keeping returns optimal: gain control exerted through sensitivity adjustments in the harbour porpoise auditory system. *Proc. R. Soc. B Biol. Sci.* **279**, 2237–2245.

Linnenschmidt, M., Kloepper, L. N., Wahlberg, M. and Nachtigall, P. E. (2012b). Stereotypical rapid source level regulation in the harbour porpoise biosonar. *Naturwissenschaften* **99**, 767–771.

Macías, S., Mora, E. C., Hechavarría, J. C. and Kössl, M. (2016). Echo-level compensation and delay tuning in the auditory cortex of the mustached bat. *Eur. J. Neurosci.* **43**, 1647–1660.

MacLennan, D. N. (1986). Time varied gain functions for pulsed sonars. *J. Sound Vib.* **110**, 511–522.

Madsen, P. T. and Wahlberg, M. (2007). Recording and quantification of ultrasonic echolocation clicks from free-ranging toothed whales. *Deep Sea Res. Part I Oceanogr. Res. Pap.* **54**, 1421–1444.

Madsen, P. T., Wilson, M., Johnson, M. P., Hanlon, R. T., Bocconcelli, A., Aguilar De Soto, N. and Tyack, P. L. (2007). Clicking for calamari: toothed whales can echolocate squid Loligo pealeii.

Moore, P. W. B., Hall, R. W., Friedl, W. A. and Nachtigall, P. E. (1984). The critical interval in dolphin echolocation: What is it? *J. Acoust. Soc. Am.* **76**, 314–317.

Moss, C. F. and Schnitzler, H.-U. (1995). Behavioral Studies of Auditory Information Processing. In *Hearing by Bats. Springer Handbook of Auditory Research, vol 5* (ed. Popper, A. N.) and Fay, R. R.), pp. 87–145. Springer, New York, NY.

Mulsow, J., Finneran, J. J., Houser, D. S., Nordstrom, C. A., Barrett-Lennard, L. G. and Burkard, R. F. (2018). Click reception in the harbor porpoise (Phocoena phocoena): Effects of electrode and contact transducer location on the auditory brainstem response. *J. Acoust. Soc. Am.* **143**, 2076–2084.

Neuweiler, G. (1990). Auditory adaptations for prey capture in echolocating bats. *Physiol. Rev.* **70**, 615–641.

Penner, R. H. (1988). Attention and detection in dolphin echolocation. In *Animal Sonar*, pp. 707–713. Springer.

Rasmussen, M. H., Miller, L. A. and Au, W. W. L. (2002). Source levels of clicks from free-ranging white-beaked dolphins (Lagenorhynchus albirostris Gray 1846) recorded in Icelandic waters. *J. Acoust. Soc. Am.* **111**, 1122–1125.

Schrøder, A. E. M., Beedholm, K. and Madsen, P. T. (2017). Time varying auditory gain control in response to double pulse stimuli in harbour porpoises is not mediated by a stapedial reflex. *Biol. Open* bio. 021469.

Simmons, J. A., Moffat, A. J. M. and Masters, W. M. (1992). Sonar gain control and echo detection thresholds in the echolocating bat, Eptesicus fuscus. *J. Acoust. Soc. Am.* **91**, 1150–1163.

Smith, A. B., Madsen, P. T., Johnson, M., Tyack, P. L. and Wahlberg, M. (In review). Toothed whale auditory evoked potentials measured with a non-invasive, on-animal tag. *J. Acoust. Soc. Am.*

Stidsholt, L., Müller, R., Beedholm, K., Ma, H., Johnson, M. and Madsen, P. T. (2020). Energy compensation and received echo level dynamics in constant-frequency bats during active target approaches. *J. Exp. Biol.* **223**,.

Stidsholt, L., Greif, S., Goerlitz, H. R., Beedholm, K., Macaulay, J., Johnson, M. and Madsen, P. T. (2021). Hunting bats adjust their echolocation to receive weak prey echoes for clutter reduction. *Sci. Adv.* **7**, eabf1367.

Suga, N. and Jen, P. H. (1975). Peripheral control of acoustic signals in the auditory system of echolocating bats. *J. Exp. Biol.* **62**, 277–311.

Supin, A. Y. and Nachtigall, P. E. (2013). Gain control in the sonar of odontocetes. *J. Comp. Physiol. A* **199**, 471–478.

Supin, A. Y., Nachtigall, P. E. and Breese, M. (2010). Target distance-dependent variation of hearing sensitivity during echolocation in a false killer whale. *J. Acoust. Soc. Am.* **127**, 3830–3836.

Urick, R. J. (1983). *Principles of Underwater Sound*. 3rd ed. (ed. Heiberg, D.) and Davis, J.) Los Altos, California: Peninsula Pub.

Vandenberghe, R., Gitelman, D. R., Parrish, T. B. and Mesulam, M. M. (2001). Location- or feature-based targeting of peripheral attention. *Neuroimage* **14**, 37–47.

Vel'min, V. A. and Dubrovskii, N. A. (1976). Critical interval of active hearing in dolphins. In *Soviet Physics Acoustics-USSR*, pp. 351–352. Amer. Inst. Physics Circulation Fulfillment Div., 500 Sunnyside Blvd, Woodbury, NY 11797-2999.

Verfuß, U. K., Miller, L. A., Pilz, P. K. D. and Schnitzler, H.-U. (2009). Echolocation by two foraging harbour porpoises (Phocoena phocoena). *J. Exp. Biol.* **212**, 823–834.

Villadsgaard, A., Wahlberg, M. and Tougaard, J. (2007). Echolocation signals of wild harbour porpoises, Phocoena phocoena. *J. Exp. Biol.* **210**, 56–64.

Wisniewska, D. M., Johnson, M., Beedholm, K., Wahlberg, M. and Madsen, P. T. (2012). Acoustic gaze adjustments during active target selection in echolocating porpoises. *J. Exp. Biol.* **215**, 4358–4373.

Wisniewska, D. M. M., Johnson, M., Teilmann, J., Rojano-Doñate, L., Shearer, J., Sveegaard, S., Miller, L. A. A., Siebert, U. and Madsen, P. T. T. (2016). Ultra-High Foraging Rates of Harbor Porpoises Make Them Vulnerable to Anthropogenic Disturbance. *Curr. Biol.* **26**,.

Wisniewska, D. M., Johnson, M., Teilmann, J., Siebert, U., Galatius, A., Dietz, R. and Madsen, P. T. (2018). High rates of vessel noise disrupt foraging in wild harbour porpoises (Phocoena phocoena). *Proc. R. Soc. B Biol. Sci.* **285**,.

Figures and Tables

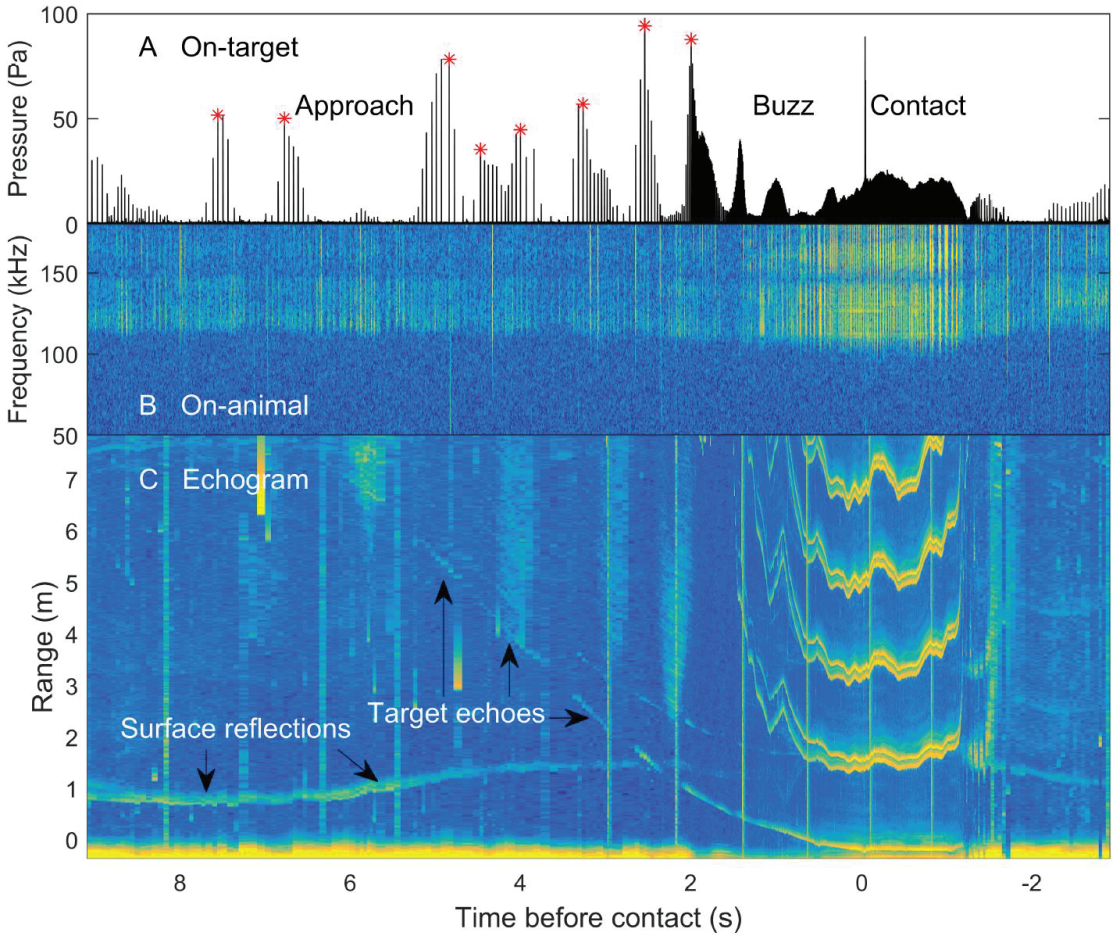

Figure 1. Example of approach to the medium-sized target by the porpoise Sif. **A** Amplitude envelope of the clicks recorded on the target. Biosonar scanning can be inferred from the fluctuations in received level. Selected on-axis clicks are marked with red asterisks. Note how on-axis click levels stay within ~6 dB of each other despite a one-way transmission difference of 18 dB, showing that the animal reduced SL with range. Note also the distinct spike at time zero caused by the porpoise touching the target. **B** Spectrogram of clicks during the same approach as recorded on the back of the porpoise, showing that the energy is centred between 110-150 kHz. **C** Echogram showing returning echoes at the porpoise following each click out to a range of 8 m. Note how target echo levels increase when the animal scans across the target as seen by the received level fluctuations in panel **A**. In this approach, the buzz phase (defined as ICIs <10 ms) begins at a target range of 0.7 m.

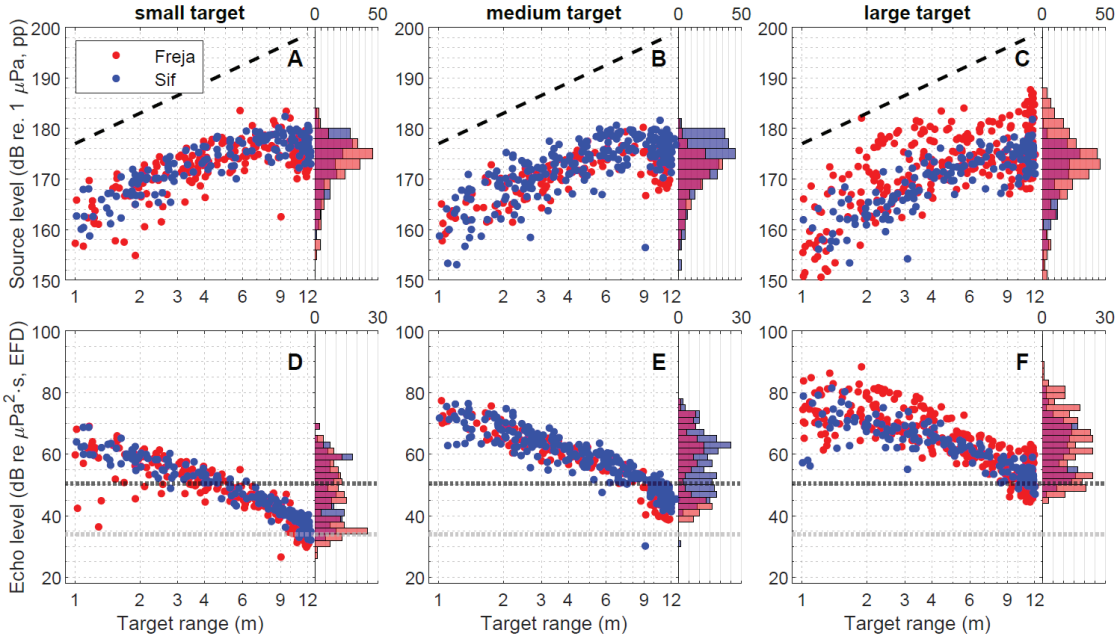

Figure 2. Biosonar adjustments of SL and EL to target range (on a log scale) for different target sizes. **A** SL plotted against target range for approaches to the small target (TS_E of -44 dB) for the porpoises Freja (red) and Sif (blue). The histogram on the right shows the overall distribution of SLs (bin width of 2 dB). The data contain 201 on-axis clicks for Freja and 150 for Sif. The black dashed line shows the 177 dB re μPa (peak) clipping level of the target recording chain plus $20\log_{10}(R)$ to illustrate that on-axis click amplitudes were recorded below the clipping level. **B** and **C** show similar plots for the medium (TS_E of -34 dB) and large (TS_E of -28 dB) targets, respectively. **B** The data contain 144 on-axis clicks for Freja and 245 for Sif. **C** The data contain 301 on-axis clicks for Freja and 167 for Sif. **D-F** show estimated echo levels for the same clicks as in **A-C**. The black dotted horizontal line at 50 dB re μPa²·s shows the mean of five auditory brainstem response (ABR) thresholds reported by (Smith et al. in review), The grey dotted horizontal line at 34 dB re μPa²·s show the auditory threshold reported for bottlenose dolphins during psychophysical experiments for comparison (Au et al., 2002).

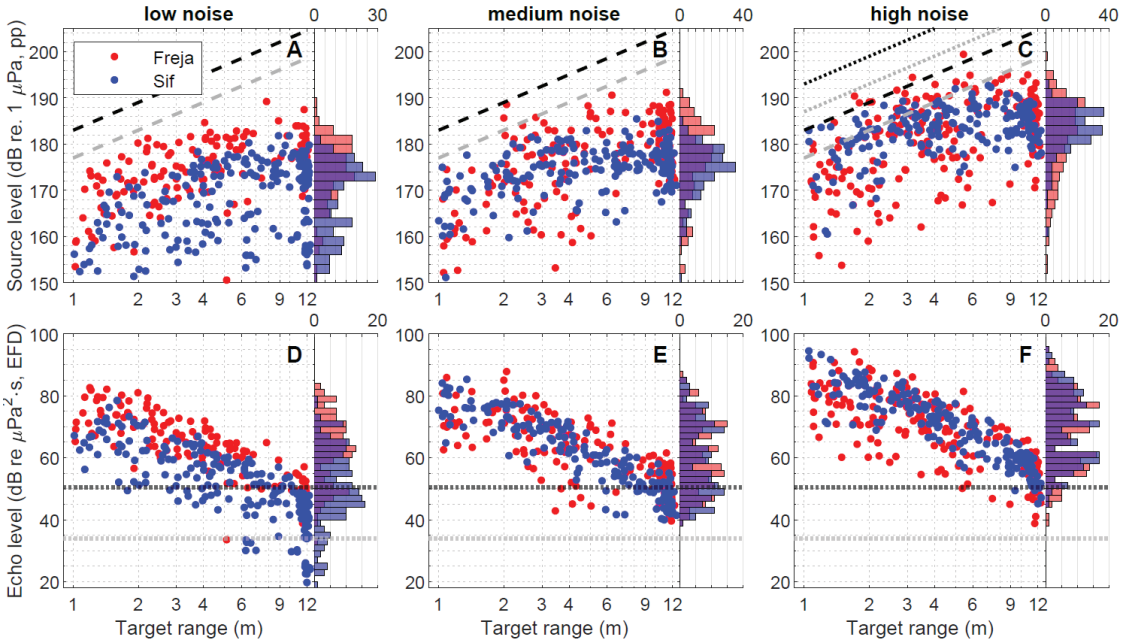

Figure 3. Biosonar SL and EL adjustments to target range (log-scaled) for different noise levels during approaches to the medium-sized target. **A** SL as a function of target range for target approaches during low noise (SL of 107 dB re µPa, RMS) for the porpoises Freja (red) and Sif (blue). The histogram on the right shows the overall distribution of SLs (bin width of 2 dB). The data contain 140 on-axis clicks for Freja and 196 for Sif. The grey dashed line shows the 177 dB re µPa (peak) clipping level of the target recording chain plus $20\log_{10}(R)$ to illustrate that on-axis click amplitudes were recorded below the clipping level. The black dashed line shows the 183 dB re µPa peak-to-peak clipping level, i.e. the highest possible level that can be recorded without clipping. **B** and **C** show similar plots for the medium (SL of 117 dB re µPa, RMS) and high (SL of 127 dB re µPa, RMS) noise treatments, respectively. **B** The data contain 171 on-axis clicks for Freja and 181 for Sif. **C** The data contain 202 on-axis clicks for Freja and 192 for Sif. In several trials with high level noise, the clipping level was set 10 dB higher by reducing the gain in the target-mounted recording chain to avoid clipping, which is illustrated with black dotted lines. **D-F** show estimated echo levels for the same clicks as in **A-C**. The horizontal dotted lines show auditory threshold estimates for porpoises (black) and bottlenose dolphins (grey) as in Figure 2.

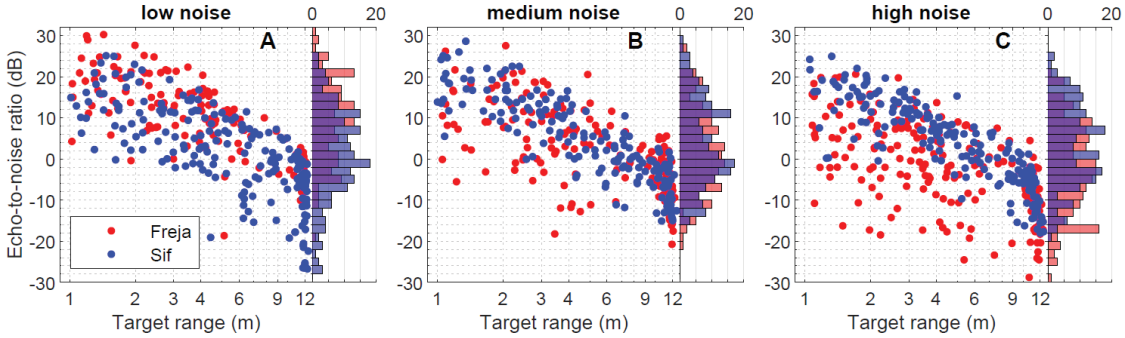

Figure 4. ENR changes with target range (log scaled) for different noise levels during approaches to the medium target. **A** plot showing changes of estimated ENR with target range (log scaled) for target approaches during low masking noise (SL of 107 dB re µPa) for the porpoises Freja (red) and Sif (blue). The histogram on the right shows the overall distribution of ENRs (bin width of 2 dB). The data contain 140 ENR estimates for Freja and 196 for Sif. **B** and **C** show similar plots for the medium (SL of 117 dB re µPa) and high (SL of 127 dB re µPa) level noise exposures, respectively. **B** The data contain 171 ENR estimates for Freja and 181 for Sif. **C** The data contain 202 ENR estimates for Freja and 192 for Sif.

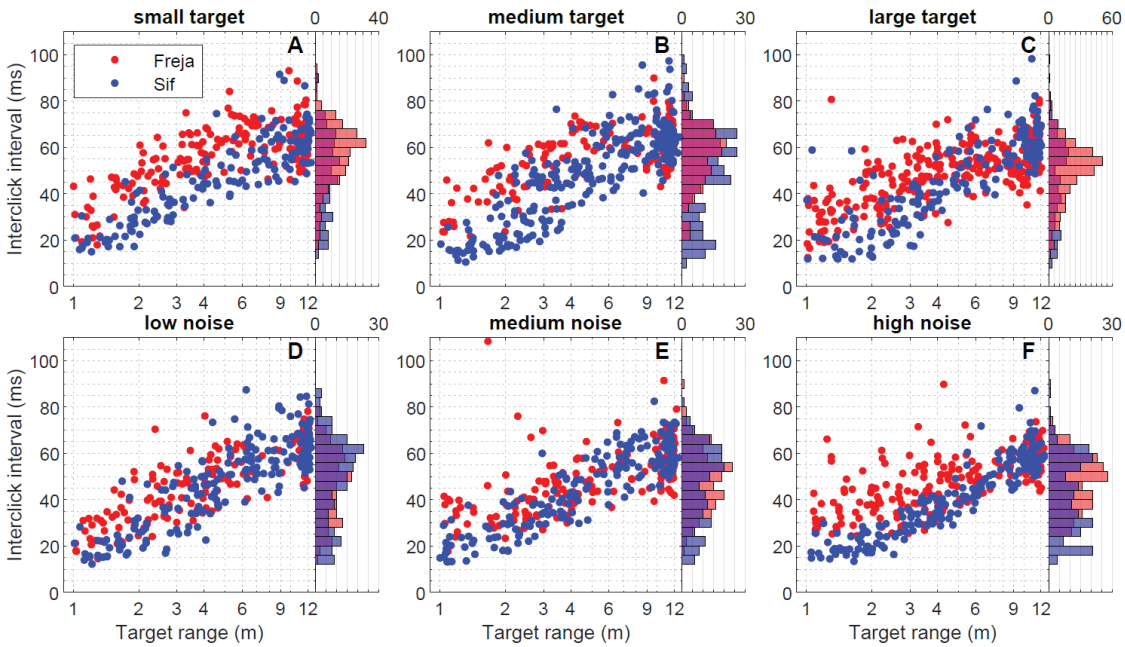

Figure 5. ICI adjustments to target range (log scaled) for different target sizes and noise levels. **A-C** ICIs to target range for small, medium and large targets, without any noise. **A** ICI adjustments to target range for approaches to the small target for the porpoises Freja (red) and Sif (blue). The histogram on the right shows the overall distribution of ICIs (bin width of 4 ms). The data contain 201 ICIs for Freja and 150 for Sif. **B** and **C** show similar plots for the

medium and large targets, respectively. **B** The data contain 144 ICIs for Freja and 245 for Sif. **C** The data contain 301 ICIs for Freja and 167 for Sif. **D-F** ICI adjustments to target range for different noise levels during approaches to the medium target. **D** plot showing how ICI changes with target range (log scaled) for target approaches with low noise for the porpoises Freja (red) and Sif (blue). The histogram on the right shows the overall distribution of ICIs (bin width of 4 ms). The data contain 140 ICIs for Freja and 196 for Sif. **E** and **F** show similar plots as **D** for the medium and high level noise treatments, respectively. **E** The data contain 171 ICIs for Freja and 181 for Sif. **F** The data contain 202 ICIs for Freja and 192 for Sif.

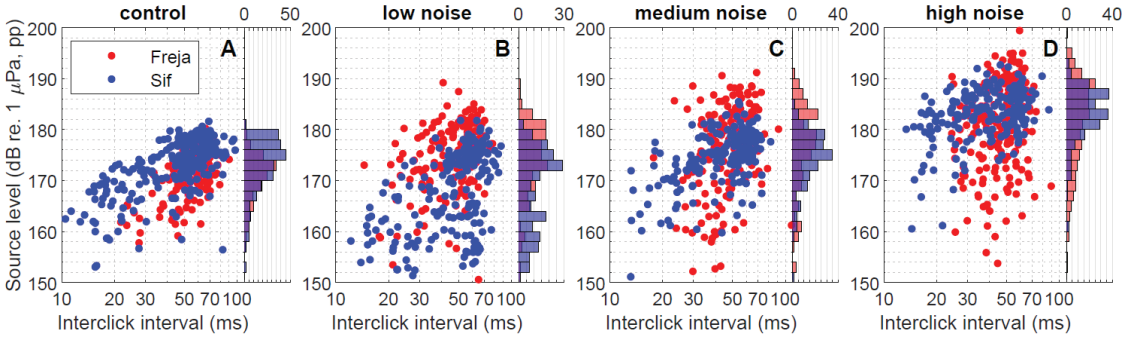

Figure 6. SL as a function of ICI (log scaled) for target approaches in background noise and different masking noise treatments. **A** SLs and ICIs of on-axis clicks for Freja (red) and Sif (blue) when approaching the medium target in trials without masking noise transmission. The data contain 144 on-axis clicks for Freja and 245 for Sif. Histograms on the right show overall SL distribution (2 dB bin width). **B-D** show similar plot for low, medium and high noise treatments. **B** The data contain 201 ICIs for Freja and 150 for Sif. **C** The data contain 144 ICIs for Freja and 245 for Sif. **D** The data contain 301 ICIs for Freja and 167 for Sif.

Table 1. Overview of on-axis clicks per treatment for each porpoise.

Porpoise	Target strength (dB)	Noise SL (dB re µPa, RMS)	On-axis clicks
Freja	-44	control	201
	-34	control	144
		107	140
		117	171
		127	202
	-28	control	301
Sif	-44	control	150
	-34	control	245
		107	196
		117	181
		127	192
	-28	control	167